Investigating the substrate binding mechanism of the mitochondrial ADP/ATP carrier

Vasiliki Mavridou

Murray Edwards College

December 2021

This thesis is submitted for the degree of Doctor of Philosophy

Declaration

This thesis is the result of my own work and includes nothing which is the outcome of work done in collaboration, except as declared in the Preface and specified in the text. I further state that no substantial part of my thesis has already been submitted, or, is being concurrently submitted for any such degree, diploma or other qualification at the University of Cambridge or any other University or similar institution, except as declared in the Preface and specified in the text. It does not exceed the prescribed word limit for the Clinical Medicine Degree Committee.

Summary

Mitochondrial ADP/ATP carriers catalyse the equimolar exchange of ADP and ATP across the mitochondrial inner membrane, providing metabolic energy for the cell. Crystal structures of the inhibited cytoplasmic-open and matrix-open states support an alternating access mechanism, involving a cytoplasmic and a matrix gate. However, the molecular nature of substrate binding remains unresolved. Substrate binding is concomitant with the structural movements required for translocation, because substrate binding and release provides the free energy changes for the disruption and formation of the gates. The aim of this project was to provide experimental evidence for the residues that are involved in the substrate binding process. For this purpose, all conserved, solvent-accessible residues between the boundaries of the two gates were mutated to alanine, creating a set of 36 variants. A combination of functional complementation, thermostability and transport assays consistently identified five residues (K30, R88, R197, R246 and R287) to be critical for substrate binding. The Ala variants of these residues did not complement growth of an Aac-deficient strain, abolished the concentration-dependent response to substrate, that is observed for the wild-type protein, and had no transport activity. These residues are located roughly in the middle of the central cavity. Around them, another six residues (N85, N96, L135, V138, G192 and Y196) were found to contribute to the binding process. The variants of these residues did not or partially complement growth of the Aac-deficient strain, presented with significantly reduced substrate-induced thermostability shifts compared to the wild-type protein and were either inactive or had altered transport properties. Residues K30, R88, L135, V138, G192, Y196 and R287 cluster together and are accessible with similar conformers in both conformational states, thus forming the main binding site. Residues N96/R197 and N85/R246 form two pairs located on the cytoplasmic and matrix side of the main site and have conformers that change in a state-dependent manner. Hence, they may be involved in the initial binding and guiding of the substrates to the main site and then in their release to the other side of the membrane, inducing conformational changes. The obtained results provide a plausible mechanism for substrate binding, demonstrate that there is a single binding site for ADP and ATP, explain the reversibility of transport and the importance of charge neutralisation in presence of a membrane potential. Results also show that the size and hydrophobicity of the binding pocket are key for the nucleotide base selection.

Acknowledgements

“Setting out for Ithaka, wish for the journey to be long; full of adventures, full of learning…’’, the Alexandrian poet wrote. In my journey the last four years I wanted to “stop in many Phoenician trading markets, to acquire fine merchandise’’ and “go to many Egyptian cities, to learn and keep learning from the erudite’’, as he advises. The journey is still at the beginning and I have long to go, but I would like to thank all the people that helped me to fight the Laistrygonians and the Cyclops until now.

Firstly, I would like to express my gratitude to Edmund, my supervisor, initially for giving me the opportunity to join his laboratory and then for providing constant support and guidance throughout my PhD. His enthusiasm, continuous encouragement and patience have been instrumental and his freedom of spirit has made the experience very pleasant.

Then I would like to thank all members of the Kunji laboratory, present and past, for their support, nice discussions and for creating a nice environment to work in. Especial thank you go to Martin, Roula, Jonathan and Gonçalo for their advice about my project and their invaluable help in writing a manuscript. To Martin again, for his help and all the little things he does around the lab, e.g. adding scintillant to the plates and even weighing bio beads many times! Also, for reading my thesis and making great suggestions and comments. Moreover, to Roula for introducing me to the world of membrane proteins, as an Erasmus student, and teaching me fundamental principles.

I would like to thank also Shane for the many fermenter runs and harvesting kilograms of yeast. Furthermore, all people that work in the media kitchen, IT support, administrative and technical matters. A special thank you for Penny, who has been there to answer all sorts of questions, even during Christmas. Additionally, I must acknowledge the Medical Research Council for funding my research project.

Moreover, I am grateful to all people that made life in Cambridge enjoyable, especially the friends I made here: Katerina, Niki, Mariagrazia, Dea and my trainer Fronzie.

Most importantly, I would like to thank my family and Chancie for always being here for me. My parents, Yiorgos and Dina, for their love and support, always and especially during the covid-19 pandemic. My brother, Prokopis, for providing a 1 hour away home, with all the meanings this word can have. My sister, Zoi, always present

and available to listen, to encourage, give advice and make arrangements for Greek-way celebrations. Lastly and very specially, I would like to thank Chancie, for making these years unique and for being an endless source of support.

Abbreviations

Å	angstrom
Ala	alanine
AAC	ADP/ATP carrier
ABC	ATP-binding cassette
ADP	adenosine diphosphate
AMP	adenosine monophosphate
ATP	adenosine triphosphate
BCA	bicinchoninic acid
BKA	bongkrekic acid
BSA	bovine serum albumin
Bt	*Bos taurus*
$C_{10}E_5$	pentaethylene glycol monodecyl ether
CATR	carboxyatractyloside
CDP	cytosine diphosphate
CL	cardiolipin
Cp	*Cryptosporidium parvum*
CPM	N-[4-(7-diethylamino-4-methyl-3-coumarinyl)phenyl]-maleimide
CTP	cytosine triphosphate
Cys	cysteine
DDM	dodecyl-β-D-maltoside
DNA	deoxyribonucleic acid
DTT	dithiothreitol
ECL	enhanced chemiluminescence
EDTA	ethylenediaminetetraacetic acid
ETF	electron transfer flavoprotein
ETF-QO	electron transfer flavoprotein-ubiquinone oxidoreductase
FAD	flavin dinucleotide
FMN	flavin mononucleotide
FPLC	fast protein liquid chromatography
g	gram
GDP	guanosine diphosphate
Gly	glycine
GTP	guanosine triphosphate
HRP	horseradish peroxidase
Hs	*Homo sapiens*
IDP	inosine diphosphate
Ile	isoleucine
ITP	inosine triphosphate
K_d	dissociation constant
K_m	Michaelis constant
L	litre
LB	Luria Bertani broth
Leu	leucine
M	molar
MWCO	molecular weight cut-off

N	asparagine
NAD	nicotinamide adenine dinucleotide
OD	optical density
PC	phosphatidyl choline
PCR	polymerase chain reaction
PDB	Protein Data Bank
PMSF	phenylmethylsulphonylfluoride
PVDF	polyvinylidene difluoride
R	arginine
RFU	relative fluorescence units
Sc	*Saccharomyces cerevisiae*
SDS-PAGE	sodium dodecyl sulphate-polyacrylamide gel electrophoresis
SOC	super optimal broth with catabolite repression
TBG	Tris buffer glycerol
TCA	tricarboxylic acid
TDP	thymine diphosphate
Thr	threonine
TIM	translocase of the inner membrane
Tm	apparent melting temperature
TOCL	tetraoleoyl cardiolipin
Trp	tryptophan
Tt	*Thermothelomyces thermophila*
TTP	thymine triphosphate
UDP	uracil diphosphate
UTP	uracil triphosphate
Val	valine
VDAC	voltage-dependent anion channel
YPD	yeast peptone dextrose
YPG	yeast peptone glycerol
V_{max}	maximal velocity
Δp	proton motive force
Δψ	membrane potential

Contents

1. Introduction

1.1. The mitochondrion

Mitochondria are subcellular organelles, the main function of which is the conversion of the chemical energy stored in macromolecules to the “energy currency’’ of the cell, adenosine triphosphate (ATP) via oxidative phosphorylation. They also serve other functions, for example calcium signalling (Bravo-Sagua et al., 2017) and apoptosis (Estaquier et al., 2012). They are involved in many metabolic pathways, such as the tricarboxylic acid (TCA) cycle, the β-oxidation of fatty acids, the amino acid metabolism and iron-sulphur cluster synthesis. They are proposed to have evolved from the endosymbiosis of an alpha proteobacterium with an archaeal-derived host cell (Roger et al., 2017). They contain their own genome, which in humans and the other animals encodes 13 proteins of the respiratory chain (three subunits of cytochrome c oxidase, two subunits of the ATP synthase, one subunit of ubiquinol: cytochrome c oxidoreductase and seven subunits of the NADH: ubiquinone oxidoreductase), 22 tRNAs and 2 rRNAs (Anderson et al., 1981). Slightly different gene content has been found in nematodes, bivalves and cnidarians (Boore, 1999). The yeast mitochondrial genome contains 30 or 40 genes (Freel et al., 2015), which in *Saccharomyces cerevisiae* encode eight proteins of the respiratory chain (three subunits of cytochrome c oxidase, three subunits of the ATP synthase, one subunit of ubiquinol: cytochrome c oxidoreductase and a ribosomal protein), 24 tRNAs, 7 to 8 replication origin-like elements, 2 rRNAs and the 9S RNA component of RNase P (Foury et al., 1998). In addition to those, in other yeasts the mitochondrial genome might encode seven proteins of the NADH: ubiquinone oxidoreductase and an additional ribosomal protein var1 (Freel *et al.*, 2015). The majority of mitochondrial proteins in all species are encoded by the nuclear genome and are imported into mitochondria.

1.2. Structure of mitochondria

Mitochondria are divided in two aqueous compartments, the mitochondrial matrix and the intermembrane space, surrounded by the mitochondrial inner and outer membranes, respectively. The outer membrane is largely permeable, as it contains voltage-dependent anion channels (VDAC), which allow the diffusion of metabolites and ions (Benz R, 1995). Its lipid composition is similar to that of other eukaryotic membranes (Sperka-Gottlieb et al., 1988).

In contrast, the mitochondrial inner membrane has a distinct lipid composition, containing high amount (10-15%) of cardiolipin (Horvath and Daum, 2013; Schenkel and Bakovic, 2014). It is impermeable for solutes and ions, which are present at the intermembrane space and the mitochondrial matrix. The inner membrane forms invaginations, called cristae, which significantly increase the surface area of this membrane. Numerous proteins localise in the inner membrane, including the complexes of the respiratory chain, the ATP synthase and many transport proteins, the most abundant being the members of the SLC25 family. These transport proteins are responsible for the selective exchange of metabolites and ions (**section 1.6**). The cristae form tubular networks, which create micro-compartments. They are highly dynamic, undergoing fission and fusion, in response to the metabolic needs of the cell and other processes, such as mitophagy (Giacomello et al., 2020). The curvature of cristae has been shown to be influenced by the arrangement of ATP synthase dimers into rows (Davies et al., 2012; Paumard et al., 2002) and can change during these processes. The dynamic interface shown to exist between ATP synthase monomers allows the enzyme to operate at this changing environment (Spikes et al., 2021).

The mitochondrial matrix hosts the enzymes participating in key metabolic processes, many copies of the mitochondrial genome and the proteins required for replication, transcription and translation of the mitochondrial genome.

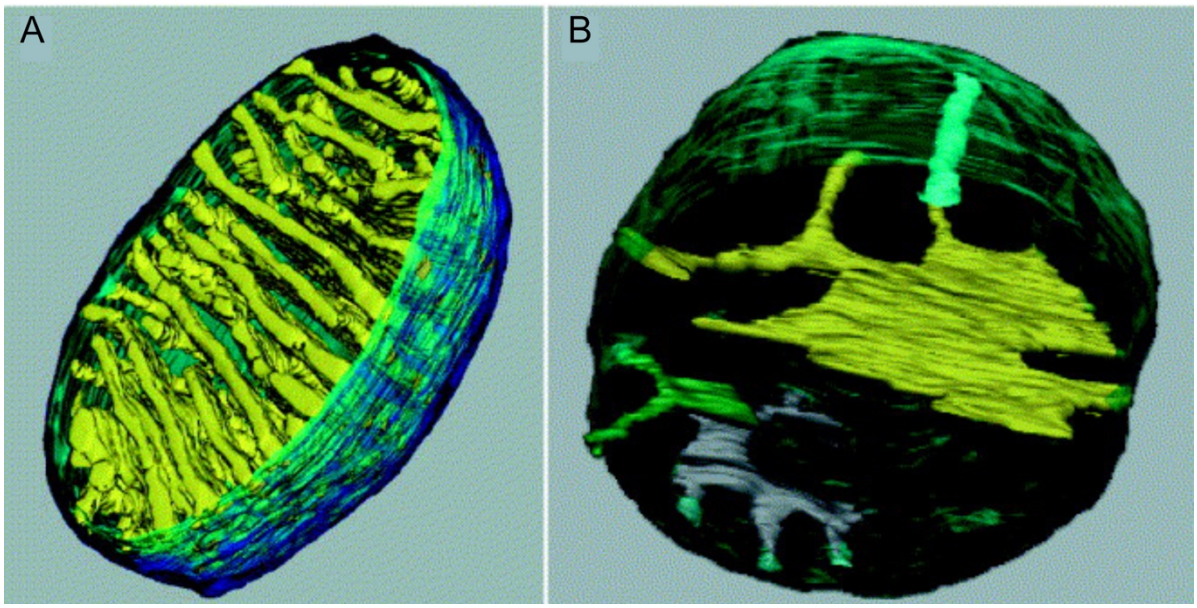

Figure 1.1: The structure of mitochondria. (A) Three-dimensional model of a segmented tomogram of a mitochondrion in chick cerebellum. The outer membrane is displayed in dark blue and the cristae in yellow. (B) Four cristae segmented separately

and depicted in different colours (yellow, grey, green and highlight green) to indicate the range of crista morphologies that can be observed. Figure taken from (Frey et al., 2002).

1.3. Function of mitochondria

The mitochondria are best known for their participation in cellular bioenergetics and the synthesis of ATP. In mitochondria, electron carriers interact with protein complexes that contain redox centres. The transfer of electrons is coupled to the translocation of protons across the mitochondrial inner membrane, building the proton motive force, which is used for the synthesis of ATP.

1.3.1. The chemiosmotic theory

Mitochondria harness energy from the oxidation of metabolites to catalyse the synthesis of ATP. This is achieved by 'chemiosmotic coupling', first proposed by Peter Mitchell (Mitchell, 1961). The four postulates regarding the necessary 'components' for chemiosmosis are the following:

1. A reversible, proton-translocating ATPase,
2. Oxidoreduction centres capable of generating electrochemical gradients,
3. Transporters that facilitate the exchange of solutes and maintain an osmotic equilibrium,
4. A permeability barrier (membrane) where all these components reside that has low proton conductance.

These principles form the basis of energy conversion and the generation of proton motive force (Δp), that drives the synthesis of ATP. The proton motive force is composed of the membrane potential (Δψ) and the pH gradient (ΔpH), related according to the following equation:

$$\Delta p = \Delta \psi - 2.303RT\Delta pH/F$$

Equation 1.1: Proton motive force. The proton motive force (Δp, mV) is composed of the membrane potential (Δψ) and a pH gradient (ΔpH). R, molar gas constant (8.31 J mol^{-1} K^{-1}); T, temperature (K); F, Faraday constant (9.65 x 10^{-2} kJ mol^{-1} mV^{-1}).

1.3.2. Oxidative phosphorylation

Electrons released during the oxidation of macromolecules supplied from nutrition reduce electron carriers and are transferred through the complexes of the respiratory

chain to O_2, the terminal electron acceptor. The flow of electrons is concomitant with the translocation of protons by complexes I, III and IV across the mitochondrial inner membrane to the intermembrane space, generating the proton motive force (**Equation 1.1**) which is used by the mitochondrial ATP synthase for the synthesis of ATP from ADP and phosphate (**section 1.3.4**).

1.3.3. The components of the respiratory chain

The electrons from NADH, generated by the oxidation of sugars and fatty acids, are transferred to the primary electron acceptor, flavin mononucleotide (FMN), which is non-covalently bound to complex I (NADH: ubiquinone oxidoreductase) (Hirst, 2013). Mammalian complex I is composed of 45 subunits (Zhu *et al.*, 2016), 14 of which, named the 'core subunits', are sufficient to catalyse the redox reactions and can constitute the full enzyme in bacteria (Baradaran et al., 2013). The remaining 31 subunits are accessory, can be present in different numbers in different orthologues and are believed to contribute to the assembly and stability of the complex (Sousa et al., 2018). Complex I oxidises NADH to NAD+ and by transferring the two electrons to ubiquinone, it reduces it to ubiquinol, while translocating four protons across the mitochondrial inner membrane, contributing to the proton motive force (Agip et al., 2019).

There are four additional enzymes, all membrane-bound flavoproteins, that contribute electrons to the ubiquinone pool, but they do not pump protons. The first one is complex II (succinate: ubiquinone oxidoreductase), which catalyses the oxidation of succinate to fumarate during the TCA cycle. Electrons from the covalently bound flavin adenine dinucleotide (FAD) are transferred via three iron-sulphur clusters to ubiquinone (Sun *et al.*, 2005). The other three enzymes are the electron-transferring flavoprotein-ubiquinone oxidoreductase (ETF-QO), the mitochondrial glycerol-3-phosphate dehydrogenase and the dihydroorotate dehydrogenase. ETF-QO contributes electrons to the ubiquinone pool from several dehydrogenases that are involved in β-oxidation of fatty acids (Watmough and Frerman, 2010). Mitochondrial glycerol-3-phosphate dehydrogenase oxidises glycerol-3-phosphate to dihydroxyacetone phosphate transferring the electrons to the ubiquinone pool (Mracek et al., 2013). Dihydroorotate dehydrogenase catalyses the oxidation of dihydroorotate coupled to the reduction of FMN and the subsequent transfer of electrons to the ubiquinone pool (Walse et al., 2008).

Ubiquinol is oxidised by complex III (ubiquinol: cytochrome c oxidoreductase), which is composed of 11 subunits (three core subunits that are highly conserved from bacteria to mammals and up to eight accessory subunits) and forms dimers (Iwata *et al.*, 1998). Electrons are passed to cytochrome c via a Q cycle mechanism (Xia et al., 2013) and the enzyme concomitantly pumps four protons (per two electrons transferred by two ubiquinol molecules) to the intermembrane space, contributing to the Δp.

Complex IV (cytochrome c oxidase) comprises 13 subunits in mammals (three core subunits) (Tsukihara *et al.*, 1995). Four electrons are sequentially transferred from cytochrome c to O_2, reducing it to water. Complex IV takes eight protons from the mitochondrial matrix, from which four are used for water formation and the other four are pumped to the intermembrane space, contributing to the Δp (Wikstrom, 1977).

In summary, for every two electrons passed from NADH to ubiquinone, Complex I pumps four protons to the intermembrane space. For every four electrons passed from two ubiquinol molecules to two cytochrome c and one ubiquinone in Complex III, it pumps four protons to the intermembrane space. Complex IV pumps four protons per catalytic cycle, so for every four electrons transferred by four cytochrome c, it pumps four protons to the intermembrane space. In a simplified way, it could be summarised that for every two electrons harvested from the oxidation of NADH, four protons are pumped by Complex I, four protons are pumped by Complex III (noting though that two ubiquinols are used from the pool) and two protons are pumped by Complex IV (**Figure 1.2**).

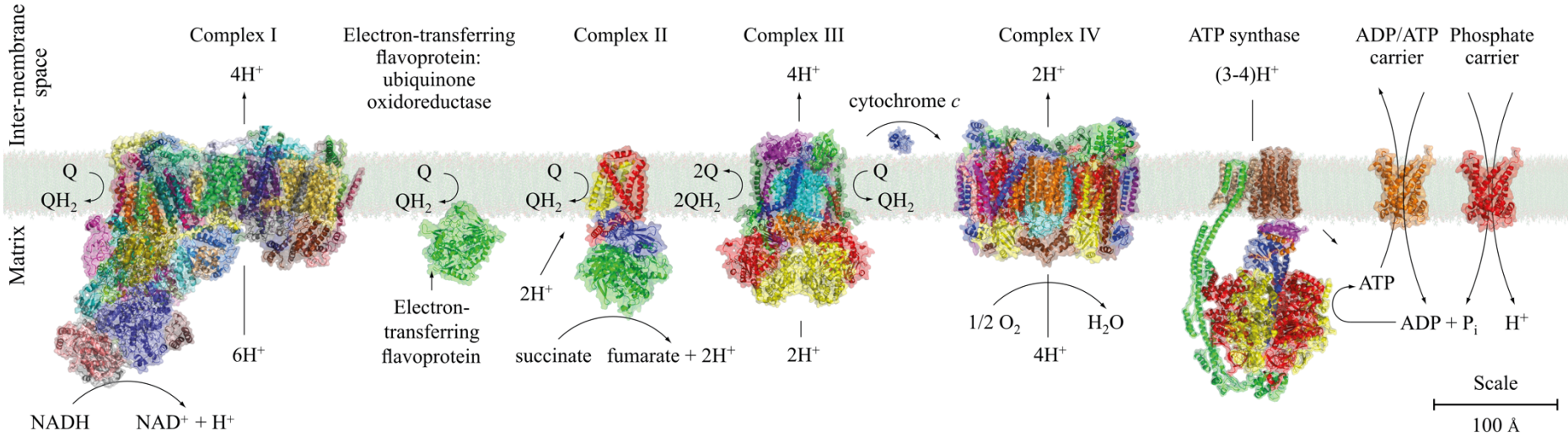

Figure 1.2: The major proteins involved in mitochondrial energy conversion. From left to right Complex I (PDB 5ldw) (Zhu et al., 2016), electron transferring flavoprotein: ubiquinone oxidoreductase (PDB 2gmh) (Zhang et al., 2006), Complex II (PDB 1zoy) (Sun et al., 2005), Complex III (pdb 1be3) (Iwata et al., 1998), cytochrome c (soluble) (PDB 1cxa) (Axelrod et al., 1994), Complex IV (PDB 1occ) (Tsukihara et al., 1995), ATP synthase (PDB 5ara) (Zhou et al., 2015), ADP/ATP carrier (PDB 1okc) (Pebay-Peyroula et al., 2003) and a homology model of the phosphate carrier, based on the ADP/ATP carrier. Figure prepared by Dr Martin King.

1.3.4. ATP synthesis

The Δp generated and sustained by respiratory complexes I, III and IV is used by the ATP synthase (F_1F_o-ATP synthase) as a source of energy to synthesise ATP from ADP and phosphate via a rotary catalysis mechanism (Walker, 1998). The ATP synthase is composed of two domains, the hydrophilic F_1 domain, which protrudes into the mitochondrial matrix and the membrane F_o domain. The two domains are connected by central and peripheral stalks (Walker, 2013). The F_1 domain contains the catalytic site of the enzyme, where ATP is formed (Abrahams et al., 1994), whilst the F_o domain contains a motor that uses the potential energy stored in Δp to generate rotation. The rotational energy is transmitted by the central stalk to the catalytic domain, inducing conformational changes that are necessary for the catalytic action. In addition to the central stalk, the F_1 and F_o domains are linked by the peripheral stalk, which, importantly, prevents the dissociation of the catalytic part from the central stalk during catalysis and resists the rotational torque of the central stalk, thus preventing the catalytic part from adopting the same rotational movement (Rees et al., 2009).

The F_1 domain is composed of $\alpha_3\beta_3\gamma_1\delta_1\varepsilon_1$ subunits. Part of the γ subunit and the δ and ε subunits are firmly attached to the F_o domain and constitute the central stalk. The F_o domain is composed of a ring made up of c subunits (the number of which differs between species and has biological importance) (Watt et al., 2010), the a subunit, which includes two half proton channels, and the e, f, g, A6L (or ATP8), k (or DAPIT) and j (or 6.8 kDa proteolipid) subunits. The peripheral stalk is composed of the OSCP, b, d F6 and the membrane extrinsic region of the A6L subunit (Walker, 2013) (**Figure 1.3**).

Rotation of the c ring occurs as protons from the intermembrane space move through a half channel in the a subunit via a Grotthus mechanism (Spikes et al., 2020) and protonate a glutamate residue in a c subunit, which then, by Brownian motion, moves to a hydrophobic environment generating rotation of the c ring. The glutamate residue subsequently re-ionises, returning the proton to the mitochondrial matrix (Zhou *et al.*, 2015), potentially through a similar mechanism as in the inlet (Spikes *et al.*, 2020). Catalysis occurs as the rotation of the asymmetric central stalk induces conformational changes in the α and β subunits (Walker, 2013). A full rotation of the c ring leads to the synthesis of three ATP molecules. In humans the c ring is composed

of eight c subunits, hence eight protons are required for formation of three ATP molecules, or 2.7 protons per ATP molecule (Watt *et al.*, 2010).

The function of the ATP synthase for the generation of ATP relies on the generation of Δp by the respiratory complexes, as explained in **section 1.3.3**, but also on the function of two transporters, the mitochondrial ADP/ATP carrier and the mitochondrial phosphate carrier. These two carriers import ADP and phosphate respectively, which are the substrates of the ATP synthase. The ADP/ATP carrier subsequently exports the ATP produced by the ATP synthase, to fuel the energy requiring processes of the cell (**Figure 1.3**).

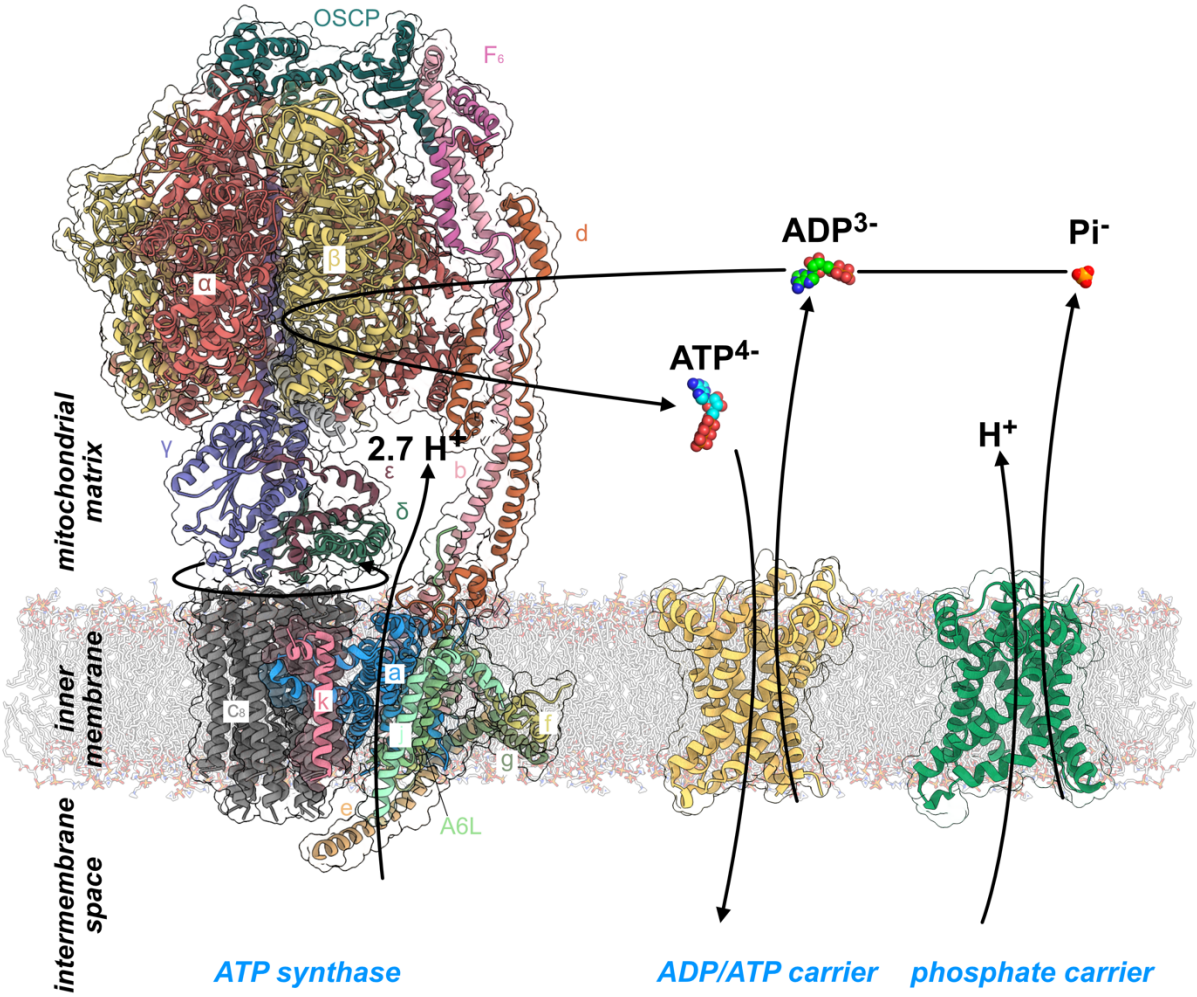

Figure 1.3: Generation of ATP and the necessary transport steps for the process. The mitochondrial ADP/ATP carrier (yellow) (PDB entry 6gci chain A) (Ruprecht et al., 2019) and a homology model of the phosphate carrier (green) based on PDB entry 4c9h (Ruprecht et al., 2014) provide key transport steps (indicated by arrows) for the synthesis of ATP, catalysed by the ATP synthase (coloured by subunit) (PDB 6zqn) (Spikes *et al.*, 2020) via a rotary mechanism. Eight proton translocation steps are required for the synthesis of three ATP molecules. Figure adapted from (Kunji et al., 2016) by Dr Chancievan Thangaratnarajah.

1.3.5. Other functions of mitochondria

In addition to oxidative phosphorylation and ATP synthesis, the mitochondria are crucial for other processes and metabolic pathways (**Figure 1.4**). They are involved in calcium homeostasis (Bravo-Sagua *et al.*, 2017), apoptosis (Estaquier *et al.*, 2012), thermogenesis (Bertholet and Kirichok, 2021), permeability transition (Baines and Gutierrez-Aguilar, 2018; Halestrap, 2009) and the biogenesis of haem and iron sulphur clusters (Lill, 2009).

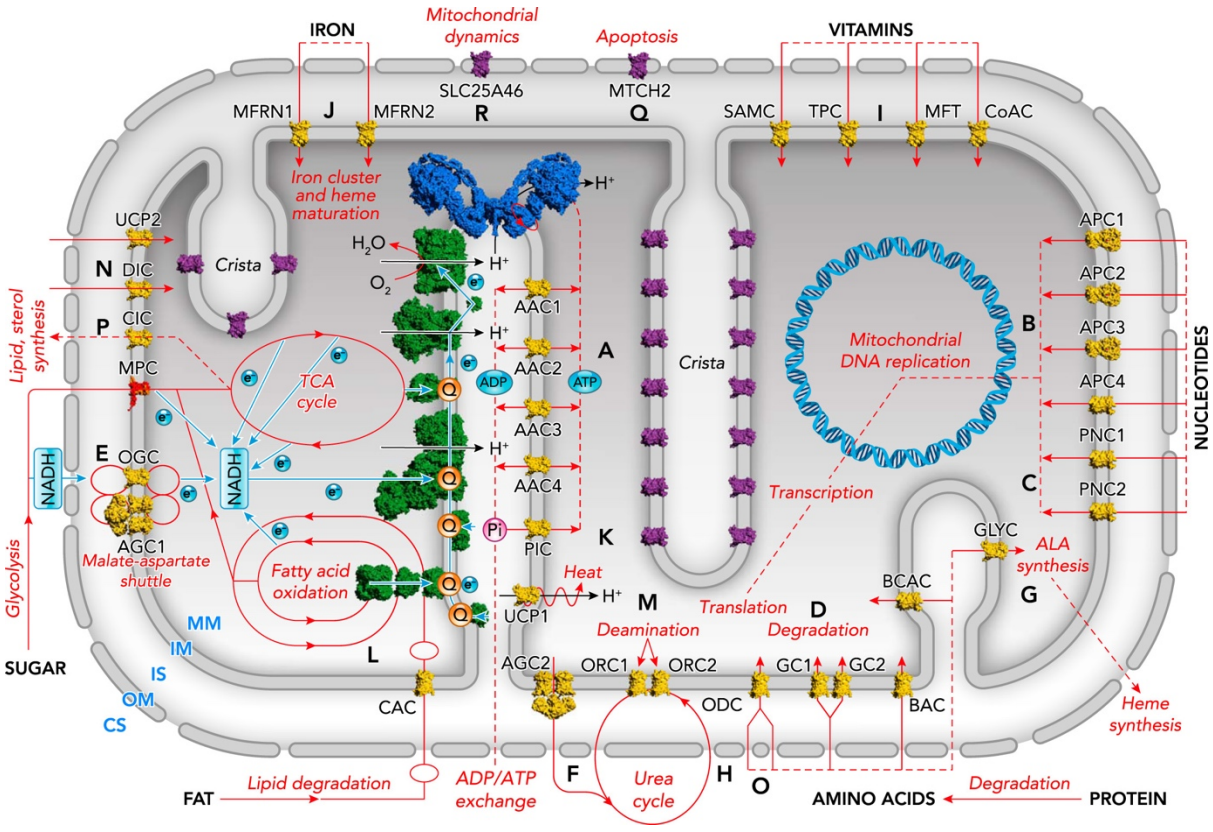

Figure 1.4: The functions of mitochondria. Schematic representation of the mammalian mitochondrion. Shown in green are the electron transfer chain complexes, in blue the ATP synthase dimer, in red the mitochondrial pyruvate carrier, in yellow characterised mitochondrial carriers and in purple mitochondrial carriers of unknown function (a detailed list is provided in **Table 1.1**). Arrows indicate important metabolic processes and transport steps. Figure taken from (Kunji et al., 2020).

1.4. Mitochondrial transport proteins and the SLC25 family

Since the mitochondrial inner membrane imposes a barrier to solutes, several transport proteins are situated in the mitochondrial inner membrane to allow or catalyse the transport of molecules selectively. These proteins include the pyruvate

carrier (Bricker et al., 2012; Herzig et al., 2012; Tavoulari et al., 2019), ATP binding cassette transporters (Schaedler et al., 2015), the calcium uniporter (Alevriadou et al., 2021; Baughman et al., 2011; De Stefani et al., 2011) and the sideroflexins (Kory et al., 2018). However, the majority of solutes are transported by members of the SLC25 family, called the mitochondrial carriers.

The mitochondrial carriers constitute the largest solute carrier family in humans, counting 53 members (**Table 1.1**). They have key roles in many metabolic pathways, including oxidative phosphorylation, the β-oxidation of fatty acids, the aspartate-malate shuttle, the urea cycle and the catabolism of amino acids. They are also implicated in numerous other functions, such as thermogenesis, mitochondrial dynamics, signalling, development and cell death (Kunji *et al.*, 2020; Palmieri and Monne, 2016). Although they have been studied extensively, the function of approximately one third has not been identified.

The vast majority of mitochondrial carriers are targeted to the mitochondrial inner membrane, but there is a member that has been found in the peroxisomal membrane (SLC25A17) (Visser et al., 2002) and three members in the mitochondrial outer membrane (SLC25A46, SLC25A49 and SLC25A50) (Abrams et al., 2015; Zaltsman et al., 2010). Furthermore, members of the family have been identified in mitochondria-related organelles, such as the mitosomes (Chan et al., 2005; King et al., 2020; Tsaousis et al., 2008) and the hydrogenosomes (van der Giezen et al., 2002).

The members of the family display characteristic features in their sequences that have structural, functional and mechanistic importance (**sections 1.5.3** and **1.6**). Their sequences consist of three homologous tandem repeats of approximately 100 amino acids each (Saraste and Walker, 1982) and can be easily aligned, as they contain conserved motifs, including the ‘signature motif’ ([PS]x[DE]xx[KR]), the ([FY][DE]xx[RK]) motif, the GxxxG and πxxxπ motifs (Kunji *et al.*, 2020; Ruprecht and Kunji, 2020; 2021).

Table 1.1: Function of the 53 members of the SLC25 family.

Protein	Name	Substrate	Comments	References
SLC25A1	Citrate carrier	Citrate, malate, isocitrate , phosphoenolpyruvate		(Kaplan et al., 1990)
SLC25A2	Ornithine carrier 2	L/D-Orn, L/D-Lys, L/D -Arg, L/D-citrulline, L-His, H-Arg		(Fiermonte et al., 2003)
SLC25A3	Phosphate carrier	Phosphate/ H^+		(Runswick et al., 1987)
SLC25A4	ADP/ATP carrier 1	ADP/ ATP		(Cozens et al., 1989) (Neckelmann et al., 1987)
SLC25A5	ADP/ATP carrier 2	ADP/ ATP		(Ku et al., 1990)
SLC25A6	ADP/ATP carrier 3	ADP/ ATP		(Cozens *et al.*, 1989)
SLC25A7	Uncoupling protein 1	H^+		(Rial et al., 1983)
SLC25A8	Uncoupling protein 2	Asp		(Raho et al., 2020)
SLC25A9	Uncoupling protein 3	Not assigned		
SLC25A10	Dicarboxylate carrier	Malonate, malate, succinate, sulphate, trisulphate, phosphate		(Johnson and Chappell, 1973)
SLC25A11	Oxoglutarate carrier	2-oxoglutarate/ malate		(Iacobazzi et al., 1992)
SLC25A12	Aspartate/glutamate carrier 1	Asp/ Glu + H^+		(Palmieri et al., 2001)
SLC25A13	Aspartate/glutamate carrier 2	Asp/ Glu + H^+		(Palmieri *et al.*, 2001)
SLC25A14	Uncoupling protein 5	Not assigned		
SLC25A15	Ornithine carrier 1	L-Orn, L-lysine, L-Arg, L-citrulline		(Fiermonte *et al.*, 2003)
SLC25A16		Not assigned	Grave's disease, onychodystrophy	(Zarrilli et al., 1989) (Khan et al., 2018)
SLC25A17	Peroxisomal membrane protein 34	ATP, ADP, AMP	peroxisomal membrane	(Visser *et al.*, 2002)
SLC25A18	Glutamate carrier 2	Glu + H^+		(Fiermonte et al., 2002)
SLC25A19	Thiamine pyrophosphate carrier	Thiamine pyrophosphate		(Lindhurst et al., 2006)
SLC25A20	Carnitine/acyl-carnitine carrier	Carnitine/ acyl-carnitine		(Indiveri et al., 1990)

SLC25A21	Oxodicarboxylate carrier	2-oxoadipate/ 2-oxoglutarate		(Fiermonte et al., 2001)
SLC25A22	Glutamate carrier 1	Glu + H^+		(Fiermonte *et al.*, 2002)
SLC25A23	ATP-Mg/phosphate carrier 2	ATP-Mg/ phosphate		(Fiermonte et al., 2004)
SLC25A24	ATP-Mg/phosphate carrier 1	ATP-Mg/ phosphate		(Fiermonte *et al.*, 2004)
SLC25A25	ATP-Mg/phosphate carrier 3	ATP-Mg/ phosphate		(Fiermonte *et al.*, 2004) (Jabalameli et al., 2021)
SLC25A26	S-adenosyl methionine	S-adenosyl Met/ S-adenosyl HomoCys		(Agrimi et al., 2004)
SLC25A27	Uncoupling protein 4	Asp		(Lunetti et al., 2022)
SLC25A28	Mitoferrin 2	Fe		(Shaw et al., 2006)
SLC25A29	Basic amino acid carrier	Arg, Lys, H-Arg, M-Arg, Orn, His		(Porcelli et al., 2014)
SLC25A30	Uncoupling protein 6	Not assigned		
SLC25A31	ADP/ATP carrier 4	ADP/ ATP		(Dolce et al., 2005)
SLC25A32	Folate or flavin carrier	Folate or flavin		(Titus and Moran, 2000) (Spaan et al., 2005)
SLC25A33	Pyrimidine nucleotide carrier 1	Uracil, thymine, cytosine (deoxy)nucleoside di- and tri-phosphates		(Di Noia et al., 2014)
SLC25A34		Not assigned		
SLC25A35		Not assigned		
SLC25A36	Pyrimidine nucleotide carrier 2	Cytosine, uracil (deoxy)nucleoside mono-, di-, tri-phosphates		(Di Noia *et al.*, 2014)
SLC25A37	Mitoferrin 1	Fe		(Shaw *et al.*, 2006)
SLC25A38	Glycine carrier	Gly		(Lunetti et al., 2016)
SLC25A39	Glutathione carrier	Glutathione		(Wang et al., 2021) (Shi et al., 2021)
SLC25A40		Not assigned		
SLC25A41	ATP-Mg/phosphate carrier 4	ATP-Mg/ phosphate		(Traba et al., 2009)
SLC25A42	CoA transporter	CoA, dephospho-CoA, ADP, adenosine 3', 5' diphosphate		(Fiermonte et al., 2009)

SLC25A43		Not assigned		
SLC25A44	Branch chain amino acid carrier	Val, Leu, Ile		(Yoneshiro et al., 2019)
SLC25A45		Not assigned		
SLC25A46		Not assigned	mt outer membrane, mt dynamics	(Abrams *et al.*, 2015)
SLC25A47		Not assigned		
SLC25A48		Not assigned		
SLC25A49		Not assigned		
SLC25A50	Mitochondrial carrier homologue 2/ Met-induced mt protein	Not assigned	mt outer membrane, role in apoptosis	(Zaltsman *et al.*, 2010)
SLC25A51	MCART1	NAD^+		(Kory et al., 2020) (Girardi et al., 2020) (Luongo et al., 2020)
SLC25A52	MCART2	Not assigned		
SLC25A53	MCART6	Not assigned		

1.5. The mitochondrial ADP/ATP carrier

The mitochondrial ADP/ATP carrier (AAC) catalyses the equimolar exchange of ADP for ATP across the mitochondrial inner membrane. It is the archetypal member of the SLC25 family and the most well studied member (Klingenberg, 2008; Kunji *et al.*, 2016). It is the only carrier protein for which complete structures are available. Studies of the carrier were facilitated because, indicative of its vital function, it is highly abundant in the mitochondrial inner membrane (Riccio et al., 1975). Furthermore, there are two classes of specific and potent inhibitors that can lock the transporter in two distinct conformational states: one in which the substrate binding site is accessible from the mitochondrial matrix (matrix-open state) and one in which it is open towards the intermembrane space (cytoplasmic-open state).

1.5.1. State specific inhibitors and mode of inhibition

Two classes of compounds were identified to inhibit oxidative phosphorylation, but not acting on ATP synthase or the electron transfer chain. Atractyloside (ATR) and carboxy-atractyloside (CATR) are toxic diterpene glycosides produced by plants of the

Asteracea family, such as the species *Atractylis gummifera*. Bongkrekic acid (BKA) is a toxic compound produced by the bacterium *Pseudomonas cocovenans*, which can be found in fermented food. It was later shown that these poisons inhibit the ADP/ATP carrier in a state-dependent way. ATR (Bruni et al., 1964) and CATR (Luciani et al., 1971; Vignais et al., 1971) trap the transporter in a cytoplasmic-open state, while BKA in a matrix-open state (Erdelt et al., 1972; Henderson and Lardy, 1970; Klingenberg and Buchholz, 1973). Both of these states were shown to be abortive (Klingenberg, 2008; Ruprecht *et al.*, 2019), because the larger molecular volume of the inhibitors compared to the substrates forces the carrier to adopt a conformation in which the substrates can no more bind. The inhibitors bind deep in the carrier cavity and make multiple interactions, increasing their affinity compared to the substrates.

1.5.2. Structural determination

1.5.2.1. Structure of the cytoplasmic-open state

Structural information became available firstly for the yeast Aac3 protein, in complex with ATR by electron crystallography of 2D crystals (Kunji and Harding, 2003). The projection map showed that the carrier displays three-fold pseudosymmetry, is monomeric and has a central translocation pathway for the substrates. The first atomic structure was obtained by X-ray crystallography of the bovine ADP/ATP carrier inhibited by CATR (Pebay-Peyroula *et al.*, 2003). The structure showed that each sequence repeat folds into a domain consisting of an odd-numbered transmembrane α-helix (H1, H3, H5), a loop containing a short helix running parallel to the membrane (h12, h34, h56) and an even-numbered transmembrane α-helix (H2, H4, H6) (**Figure 1.5**). The three domains are related by three-fold pseudosymmetry. This structural fold was confirmed by structures of the yeast carriers Aac2 and Aac3 in complex with CATR (Ruprecht *et al.*, 2014).

The proline residues of the signature motif ([PS]x[DE]xx[KR]) induce kinks in the odd numbered helices, giving them an L-shape (Pebay-Peyroula *et al.*, 2003; Ruprecht *et al.*, 2014). In over 40% of AAC sequences, including the yeast Aac2 and Aac3 sequences, as well as the sequence of the thermotolerant fungus *Thermothelomyces thermophila*, the proline residue of the second domain (helix H3) is substituted by serine (Babot et al., 2012). It was shown that in these cases, the serine residue adopts an unusual arrangement, as a hydrogen bond is formed

between the side chain and the backbone amide group. This arrangement mimics the structure of proline and results in disruption of the α-helical backbone hydrogen bonding in a similar way as when proline is present (Ruprecht *et al.*, 2014). Furthermore, three cardiolipin molecules are tightly bound to the carrier, occupying three pockets with positive electrostatic potential due to the N-terminal dipoles of the matrix helices and the even numbered transmembrane helices. They also interact via hydrogen bonds with the amide groups of the N-terminal ends of the matrix helices and the even numbered transmembrane helices and via hydrophobic contacts (Nury et al., 2005; Pebay-Peyroula *et al.*, 2003; Ruprecht *et al.*, 2014). Their binding is crucial for the protein stability and function (Klingenberg, 2009; Kunji and Ruprecht, 2020).

The charged residues of the signature motif form a salt bridge network at the bottom of the cavity (Pebay-Peyroula *et al.*, 2003; Ruprecht *et al.*, 2014) (**Figures 1.5** and **1.6**), as had been proposed on the basis of sequence analysis and mutagenesis (Nelson et al., 1998). These inter-domain salt bridge interactions, now called the 'matrix network', make the carrier cavity inaccessible from the matrix side (Pebay-Peyroula *et al.*, 2003; Ruprecht *et al.*, 2014). A proximal glutamine residue forms hydrogen bonds with both of the charged residues of the H1-H5 pair, providing additional stabilisation of the matrix network (Ruprecht *et al.*, 2014) (**Figure 1.6**). This interaction is called 'glutamine brace'. These glutamine residues are conserved in the SLC25 family and other carriers have one to three. The matrix network together with the glutamine braces are part of a 15 Å thick gate (Ruprecht *et al.*, 2019), which seals the protein from the matrix side and is called the matrix gate. The matrix network and glutamine brace interactions create an energy barrier that prevents the carrier from changing conformation, unless energy is provided by substrate binding (Robinson et al., 2008; Springett et al., 2017).

1.5.2.2. Structure of the matrix-open state

The matrix-open state was known to be unstable (Crichton et al., 2015), impeding the structure determination for a long time. Recently, the structure of the carrier inhibited by BKA in a matrix-open state was determined by X-ray crystallography (Ruprecht *et al.*, 2019), making a great step towards the elucidation of the transport mechanism. The general three-domain architecture is apparent in the matrix-open state, but the helices are rotated compared to the cytoplasmic-open state, opening the carrier cavity to the matrix side and closing it to the intermembrane space.

In this conformational state, the residues of the matrix network and braces are far apart and they do not interact. However, the charged residues of the conserved motif ([FY][DE]xx[RK]) (Robinson *et al.*, 2008), found in the even-numbered helices, come together in the cytoplasmic side of the protein and form salt bridge interactions, similar to the matrix network in the cytoplasmic-open state. These interactions are called the 'cytoplasmic network' (**Figures 1.5** and **1.6**). Existence of these interactions had been proposed based on sequence and pseudosymmetry analysis (Robinson *et al.*, 2008) and was shown experimentally by biophysical studies (King et al., 2016), until visualised in the crystal structure (Ruprecht *et al.*, 2019). Proximal tyrosine residues form hydrogen bonds with the residues of the cytoplasmic network, bracing the network with additional inter-domain interactions. These are now called 'tyrosine braces' (**Figure 1.6**). They are conserved among the SLC25 members, but in the ADP/ATP carriers the tyrosine of the first domain (helix 2) is substituted by a lysine residue, which though serves the same purpose (Ruprecht *et al.*, 2019). The cytoplasmic network and tyrosine braces are surrounded by bulky, hydrophobic residues, which create a 15 Å thick insulation layer (hydrophobic plug), closing the carrier cavity to the intermembrane space and together they constitute the cytoplasmic gate. The strength of the cytoplasmic network and tyrosine braces are important, as they impose an energy barrier which prevents the carrier from changing conformation in the absence of substrate, unless energy is provided (Springett *et al.*, 2017).

In order to form the cytoplasmic gate, the transmembrane helices in the cytoplasmic side of the carrier are packed close together. To allow for this to happen, small amino acids are found in the intra-domain interfaces, such as the residues of the GxxxG motif on the odd-numbered helices and of the πxxxπ motif on the even-numbered helices (Ruprecht *et al.*, 2019) (**Figure 1.6**). Furthermore, tightly bound cardiolipins are observed in the three positively charged pockets formed between the even-numbered and matrix helices (Ruprecht *et al.*, 2019).

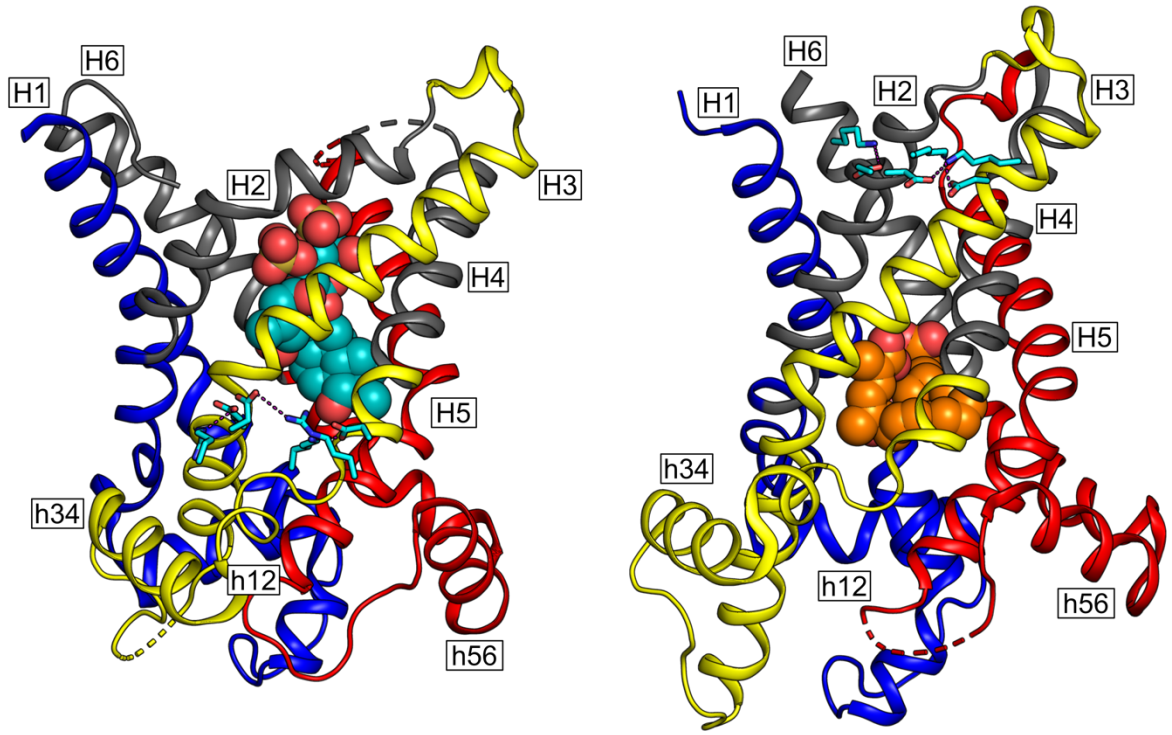

Figure 1.5: Structures of the inhibited cytoplasmic-open and matrix-open states. Membrane view of the cytoplasmic-open state structure (PDB entry 4c9h) locked by CATR (shown in teal spheres) (left) and of the matrix-open state (right) (PDB entry 6gci chain A) lock by BKA (shown in orange spheres). The core elements of domains 1, 2 and 3 are shown in blue, yellow and red, respectively and the gate elements in grey (**section 1.5.3**). The matrix network is engaged in the cytoplasmic-open state and the cytoplasmic network in the matrix-open state (networks shown in cyan stick representation and the interactions indicted as magenta dashes). Transmembrane and matrix helices are labelled.

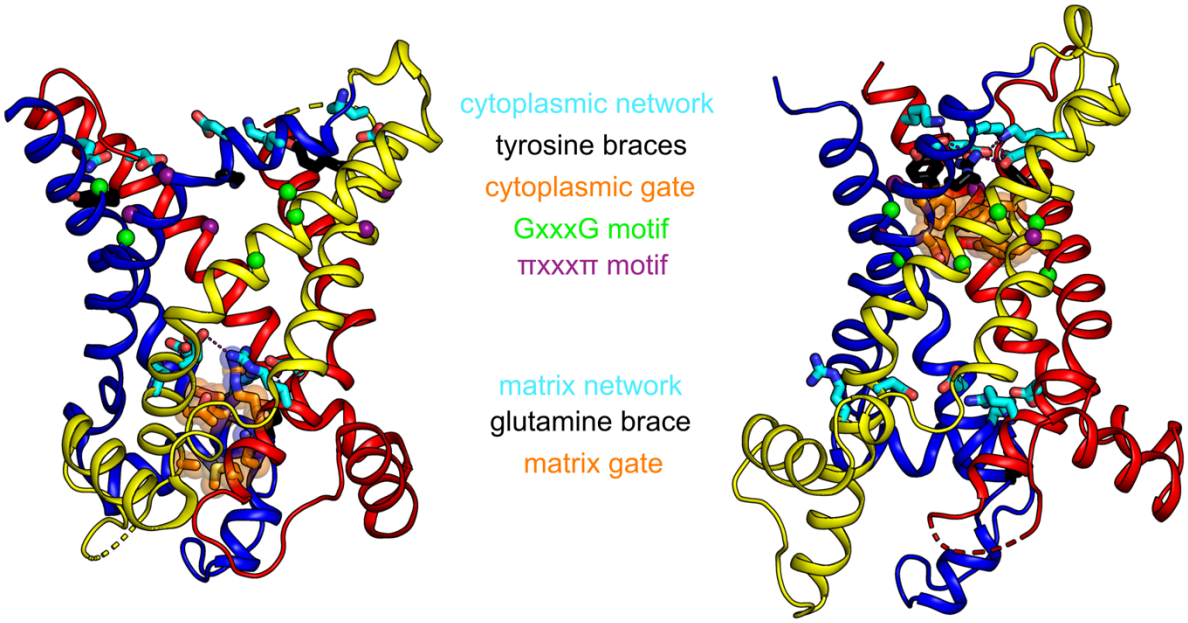

Figure 1.6: Characteristic structural features of mitochondrial carriers. Cytoplasmic-open state (PDB entry 4c9h) (left) and matrix-open state (right) (PDB entry 6gci chain A) structures. The cytoplasmic and matrix networks are shown in cyan sticks, the tyrosine and glutamine braces in black sticks and interactions are indicated by magenta dashes. Residues of the cytoplasmic and matrix insulation layers are shown in orange sticks and transparent spheres and the small amino acid residues of the GxxxG and πxxxπ motifs are shown in green and purple spheres respectively.

1.5.3. Structural mechanism

Comparing the structures of the two conformational states, the three domains contain a region that is structurally conserved between the two states and one that changes. In each domain, the odd-numbered helix, matrix helix and the first one third of the even-numbered helix are structurally conserved and make up the so called 'core element'. The second part of the even-numbered helix is significantly different between the two states and forms the 'gate element' (Ruprecht *et al.*, 2019) (**Figures 1.5 and 1.7**).

Interconversion between the two states was proposed to occur in an alternating way, by breaking and forming the matrix and cytoplasmic networks and braces, overcoming the energy barriers of the ground states by substrate binding (Klingenberg, 2007; Springett *et al.*, 2017). The study of the two structures reveals that the interconversion requires extensive movements of all six structural elements around the central cavity. A direct morph between the two structures did not provide plausible solutions, because of the distortions the inhibitors impose, creating abortive states (Ruprecht *et al.*, 2019; Ruprecht and Kunji, 2019). After correcting for the deviation of pseudosymmetry induced by inhibitor binding, a model was obtained that traversed through an occluded state, as required for an alternating access mechanism (Ruprecht *et al.*, 2019; Ruprecht and Kunji, 2019) (**Figure 1.7**).

The three core elements of the protein domains have to perform rigid-body movements, rocking outwards to open and inwards to close the carrier on the matrix side. Concomitantly, the gate elements move in reverse. They rotate inwards to bring the cytoplasmic gate together and close the cavity to the intermembrane space in the transition from the cytoplasmic- to the matrix-open state, while in the transition from the matrix-open to cytoplasmic-open state, they move outwards to make the translocation pathway accessible from the intermembrane space (Ruprecht *et al.*, 2019; Ruprecht and Kunji, 2019) (**Figure 1.7**). The coordinated movement of these

six structural elements makes the ADP/ATP carrier the most dynamic transporter identified in nature so far (Ruprecht and Kunji, 2019).

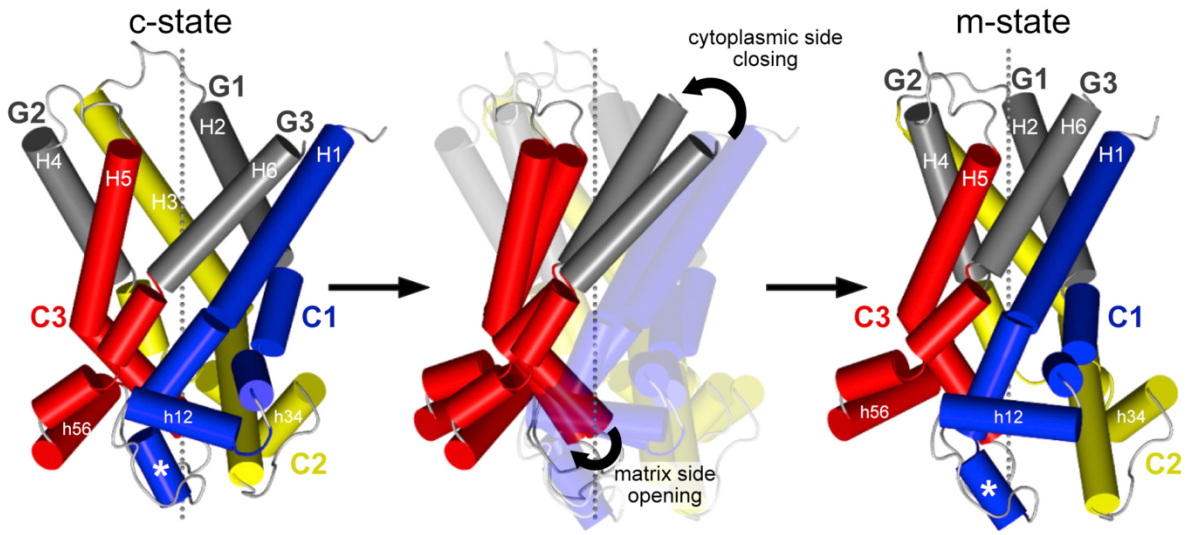

Figure 1.7: Structural movements required for the interconversion between the cytoplasmic-open and the matrix-open state. Models of the uninhibited cytoplasmic-open (left) and matrix-open states (right), with helices shown as cylinders. The three domains are colour-coded as in **Figures 1.5** and **1.6** and the three-fold pseudosymmetry axis is indicated as a grey dotted line. Conformational changes between the two states can be described as rigid-body rotations of the three core elements (indicated as C1, C2, C3 respectively), coupled with inward movement of the three gate elements (indicated as G1, G2, G3 respectively). Figure taken from (Ruprecht *et al.*, 2019).

1.5.4. The substrate binding site and specificity

Several studies have addressed the question of where the substrates, ADP and ATP, bind. Prior to the determination of structures, studies that used labelled, non-transportable nucleotide analogues proposed that substrate binding occurs in the matrix loops (Dalbon et al., 1988; Dianoux et al., 2000; Majima et al., 1998; Mayinger et al., 1989) and the C-terminal region of the protein (Dianoux *et al.*, 2000). The determined structures do not support this idea, since these regions are outside of the central carrier cavity. Furthermore, this notion is inconsistent with biochemical data (e.g. competition experiments with ADP, ATP and ATR and BKA), given that the binding sites of the inhibitor molecules have been shown to be in the central cavity.

Furthermore, not all residues that were predominantly labelled are conserved among ADP/ATP carriers (**section 4.1**).

After the topology and general fold of the protein were elucidated by the structure determination (Kunji and Harding, 2003; Pebay-Peyroula *et al.*, 2003), extensive *in silico* studies have been performed. In the first study, sequence analyses that applied chemical and distance constraints identified three 'contact points' that are universal to all mitochondrial carriers and depend on the specificity of the transporters (Kunji and Robinson, 2006; Robinson and Kunji, 2006). Carriers that transport chemically related substrates share common features in their binding sites. The three contact points are located on the even-numbered helices and roughly in the middle of the translocation pathway (Kunji and Robinson, 2006; Robinson and Kunji, 2006). Another study used the deviation of pseudosymmetry as a defining principle, considering that the carriers must have evolved an asymmetric site for the binding of substrates, as these molecules are not symmetrical. This study identified asymmetrical residues mainly in a central region which overlapped with the three 'contact points' identified earlier (Robinson *et al.*, 2008). Moreover, multiple molecular dynamic simulations have been performed (Dehez et al., 2008; Mifsud et al., 2013; Pietropaolo et al., 2016; Tamura and Hayashi, 2017; Wang and Tajkhorshid, 2008), giving variable results, some of which are consistent with the rest of the bioinformatic studies and some are not. The aforementioned approaches are discussed in more detail in **Chapter 4**, **section 4.1**.

Regarding the substrate specificity, there are many studies that have shown that AAC has a strict specificity for ADP, ATP and their deoxy- forms (Dolce *et al.*, 2005; Duee and Vignais, 1969; King *et al.*, 2020; Mifsud *et al.*, 2013; Pfaff and Klingenberg, 1968). Moreover, it has been shown that the nucleotides not in complex with Mg^{2+} are being transported (Klingenberg, 2008), but currently there is no molecular explanation for these observations.

1.5.5. The kinetic mechanism of AAC

Kinetic studies on AAC had concluded that it operates via a simultaneous mechanism, implying that there are two substrate binding sites, one for ADP and one for ATP and that these two molecules must form a ternary complex with the carrier, either simultaneously or sequentially, for the translocation to occur (Chan and Barbour, 1983; Duyckaerts et al., 1980). These studies were conducted in rat liver/liver

hepatoma and rat heart mitochondria, respectively, and it is possible that the results were affected by technical issues (e.g. not correcting for leak of internal substrate), as reviewed in (Klingenberg, 2008). Furthermore, these models were favoured by the notion that AAC was dimeric. This idea has been proven to be wrong in multiple studies (**section 1.5.6**). However, proposals for the existence of two substrate binding sites have been made for the monomer as well (Yao et al., 2021).

Alternatively, a ping pong mechanism has been proposed, in which the carrier alternatingly exposes a single substrate binding site on the two sides of the mitochondrial inner membrane. This mechanism is supported by the structural analyses (Ruprecht *et al.*, 2019; Ruprecht and Kunji, 2019; Ruprecht and Kunji, 2021), competition experiments between substrate and inhibitors, reviewed in (Klingenberg, 2008), bioinformatical studies (Robinson *et al.*, 2008) and theoretical studies (Klingenberg, 2005; Springett *et al.*, 2017). This topic remains an active research area, until the transport mechanism is fully elucidated.

1.5.6. The oligomeric state of AAC

For many years, the general consensus was that mitochondrial carriers, including AAC, are dimeric. After the sequence of bovine AAC was determined (Aquila et al., 1982), it was thought at that time that it is not possible for a protein of just six transmembrane helices to transport large substrates. This notion was initially supported by many techniques, reviewed in (Kunji and Crichton, 2010), including size-exclusion chromatography, analytical ultracentrifugation, small-angle neutron scattering, native gel electrophoresis and differential affinity purification. However, after structures were determined, it was shown that the protein was monomeric (Kunji and Harding, 2003; Pebay-Peyroula *et al.*, 2003; Ruprecht *et al.*, 2014; Ruprecht *et al.*, 2019). A thorough revisit of the results of previous studies identified technical errors and misinterpretations of the data (Kunji and Crichton, 2010). The factors that led to a dimer interpretation were investigated in each study and it was shown that if certain critical factors were taken into account, the monomer was the only option. The common unaccounted factor was the size of the detergent/lipid micelle associated with the transporter (Kunji and Crichton, 2010). Studies with the yeast ADP/ATP carrier using size-exclusion chromatography, blue native gel electrophoresis and analytical ultracentrifugation, taking into account the size of the detergent/lipid micelle, and also differential affinity chromatography, binding studies and atomic force microscopy

showed that it exists and functions as a monomer, both in detergents and in the membrane (Bamber et al., 2006; Bamber et al., 2007a; Bamber et al., 2007b; Crichton et al., 2013; Kedrov et al., 2010; Kunji et al., 2008). Recently, results from native mass spectrometry indicated that the bovine carrier can exist either as a dimer or monomer in the membrane (Chorev et al., 2018). However, the data of this study were proven to be misinterpreted (Hirst et al., 2019). The mass of the bovine carrier had been determined before and was consistent with a monomer (Smith et al., 2003). Subsequent analysis attributed the observed mass to the presence of extensive post-translational modifications (Chorev and Robinson, 2019), which though are incompatible with the function of the carrier and have not been observed in the crystal structures, as reviewed in (Kunji and Ruprecht, 2020). To conclude, data from multiple biophysical and biochemical techniques have shown that the ADP/ATP carrier is a monomer; functional and structural studies have proven that the monomeric carrier contains all the functional and mechanistic features required for transport of ADP and ATP, as reviewed in (Kunji and Ruprecht, 2020) and described in **section 1.5.3**.

1.5.7. Implication in disease

There are four ADP/ATP carrier paralogues expressed in humans, that display different expression levels and tissue specificity. Disease mutations have been associated with AAC1 (*SLC25A4* gene), which is predominantly expressed in the heart and the skeletal muscle (Kunji *et al.*, 2020; Palmieri et al., 2020). There are three different pathologies associated with this protein: adult-onset autosomal-dominant progressive external ophthalmoplegia 2 (AdPEO2) with mitochondrial DNA deletions (Kaukonen et al., 2000), late-onset recessive mitochondrial DNA depletion syndrome (MTDPS) (Fontanesi et al., 2004; Palmieri et al., 2005) and early-onset dominant *de novo* mutations leading to mitochondrial disease (King et al., 2018; Thompson et al., 2016).

They are all characterised by multiple deletions in the mitochondrial DNA and reduced respiratory chain and oxidative phosphorylation capacity. The symptoms of the first syndrome include ragged-red fibers in muscle biopsies, progressive muscle weakness, mainly of the external eye muscle and ptosis (Palmieri et al., 2020). The symptoms of the second disease are muscle ragged-red fibers, mild myopathy with exercise intolerance and lactic acidosis, but no ophthalmoplegia (Palmieri et al., 2020). In a more recent case (von Renesse et al., 2019), elevated L-2-hydroxyglutarate urine

levels were also reported and no mitochondrial DNA deletions. Finally, the symptoms of the third pathology are similar to those of the second, but more severe, because the hypotonia is apparent immediately after birth and the infants display respiratory insufficiency and impaired motor development, often resulting in death (Palmieri et al., 2020).

The first syndrome is caused by point mutations in residues outside the translocation pathway, while the second by deletion, frame shift and point mutations close to the computationally identified substrate binding site and the matrix gate. Responsible for the third pathology are mutations in contact point I (**sections 1.5.4** and **4.1**) or in the matrix network (**sections 1.5.2** and **1.5.3**) (Kunji et al., 2020; Palmieri et al., 2020). Therefore, the type of mutations and their location seem to justify the milder symptoms of the first syndrome, in which the reported mutations have no obvious role in the transport mechanism. In the other two syndromes, key areas of the protein are affected.

Higher eukaryotes cannot survive without ADP/ATP carrier activity, as the lethal poisons CATR and BKA demonstrate. The survival of these patients and the range of the symptoms is probably dependent on the functional compensation provided by the other three AAC paralogues (Kunji *et al.*, 2020). In addition, humans possess four paralogues of the ATP-Mg/phosphate carrier, which catalyse the electro-neutral exchange of phosphate for adenine nucleotides (AMP, ADP, ATP) coupled with magnesium or protons (Austin and Aprille, 1984; del Arco and Satrustegui, 2004; Fiermonte *et al.*, 2004). In addition, the Co-A transporter (SLC25A42) and the thiamine pyrophosphate transporter (SLC25A19) can transport adenine nucleotides, in addition to their canonical substrates (Kunji *et al.*, 2020). Therefore, there are many proteins implicated in adenine nucleotide transport in mitochondria and further investigation is required to understand better the mechanism, onset and difference in severity of these diseases.

1.5.8. Other proposed functions of AAC

In addition to its role on ADP and ATP transport, AAC has been reported to have other functions, including the transport of protons (dissipating the proton motive force) and the participation in the permeability transition pore. Furthermore, it has been proposed to interact with plethora of proteins in the mitochondrial inner membranes, thus

participating in several pathways, for example the protein import machinery TIM complex.

AAC has been shown in electrophysiology experiments to mediate proton transport, as a ‘second function’ in a CATR insensitive way, contributing to ‘basal’ uncoupling (Brand et al., 2005). Alternatively, it has been shown to transport protons in a regulated way, similar to the uncoupling protein 1. Fatty acids are necessary to bind in the carrier cavity, in order for the proton transport function to be induced (Bertholet et al., 2019; Brustovetsky and Klingenberg, 1994). However, these functions are inhibited when ADP and ATP are present, potentially limiting physiological relevance. During transport, proton leak can be prevented since AAC contains a 15 Å thick insulation layer on each side, composed of hydrophobic and aromatic amino acids (Ruprecht and Kunji, 2021).

Moreover, it has been proposed in many studies, but also rejected in others (as reviewed in (Baines and Gutierrez-Aguilar, 2018; Carrer et al., 2021; Halestrap, 2009)) that AAC is a central component of the pore formed in the mitochondrial inner membrane during the non-specific permeabilisation of the mitochondrial inner membrane, induced by high calcium and oxidative stress, called the permeability transition pore. However, it has been shown in mouse liver that this process can take place even when the *Aac* genes have been inactivated, thus demonstrating that AAC is not essential, even though it might have a regulatory role (Kokoszka et al., 2004). The protein constituents of the permeability transition pore still have not been identified and the topic remains an active area of research (Brustovetsky, 2020).

Finally, AAC has been proposed to interact with many other proteins, including the TIM23 translocase, respiratory supercomplexes, the ATP synthase and other carriers (Claypool, 2009; Clemencon, 2012). These interactions are claimed to be largely mediated by cardiolipin molecules, except for the TIM23 complex (Claypool, 2009; Dienhart and Stuart, 2008). However, it has not been explained how these interactions can be maintained during substrate translocation, during which AAC undergoes profound conformational changes (Ruprecht and Kunji, 2019; Ruprecht and Kunji, 2021).

In conclusion, apart from the ADP/ATP transport function, which is well established, further investigations are required to confirm any of the other proposed functions.

1.6. Mitochondrial carriers share key features and have a common transport mechanism

Sequence analysis has shown that the mitochondrial carriers have conserved motifs and features that are important for function, as has been described for the ADP/ATP carrier **(section 1.5.2, 1.5.3** and **1.5.4**). For example, there are the [PS]x[DE]xx[KR] and [FY][DE]xx[RK] motifs, the charged residues of which form the matrix and cytoplasmic networks, respectively. These two motifs are overall conserved, with few small deviations in certain carriers, that are specific adaptations, as mentioned in the text below and shown in **Figure 1.8**. Furthermore, all carriers contain one to three glutamine and tyrosine braces. The conservation of these features supports the notion that mitochondrial carriers operate via a common mechanism (Robinson *et al.*, 2008). Furthermore, there is high level of symmetry between the members of the family, meaning that amino acids that have an important mechanistic function are either conserved or symmetrical between the members (Robinson *et al.*, 2008). The AAC has largely served as a model for the study of the whole family and the mechanism presented in **section 1.5.3**, as well as the properties explained in **sections 1.5.4** (substrate binding) and **1.5.6** (oligomeric state, with the only exception being the aspartate/glutamate carrier, which is a structural dimer (Thangaratnarajah et al., 2014)), represent the current view of the mechanism of all SLC25 members.

Differences of course exist in the substrate binding site areas, since the members transport very diverse substrates. Additionally, some members are proton-coupled, some members catalyse electroneutral exchange and others electrogenic, so differences are present in the ion coupling sites, when they exist (Robinson *et al.*, 2008). Also, there are differences in regulation; for example, the aspartate/glutamate and the ATP-Mg/phosphate carriers are calcium regulated (del Arco and Satrustegui, 2004; Harborne et al., 2017; Harborne et al., 2015; Palmieri *et al.*, 2001; Thangaratnarajah *et al.*, 2014). Finally, small differences exist in the conserved features as well, which can explain the different modes of transport. For example, the strength of the gates (networks and braces) may explain why some carriers can present some uniport activity and not others (Robinson *et al.*, 2008). A semi-quantitative measure of the strength of the gates has been calculated by assigning one unit for a salt bridge and half unit for a hydrogen bond (Ruprecht and Kunji, 2020) (**Figure 1.8**). If one of the two gates is weaker than the other, the carrier might be able

to break that gate stochastically and transition to the other state in absence of substrate. These carriers can have both exchange and uniport activity, dependent on if the substrates are present on both sides or not (e.g. the aspartate/glutamate carrier, the carnitine/ acyl-carnitine carrier and the oxoglutarate carrier). If both gates are weak, the carrier can have uniport activity, equilibrating the substrate concentrations on both sides of the membrane, whereas when both gates are strong and equal, the carrier performs strict equimolar exchange (e.g. the ADP/ATP carrier) (**Figure 1.8**).

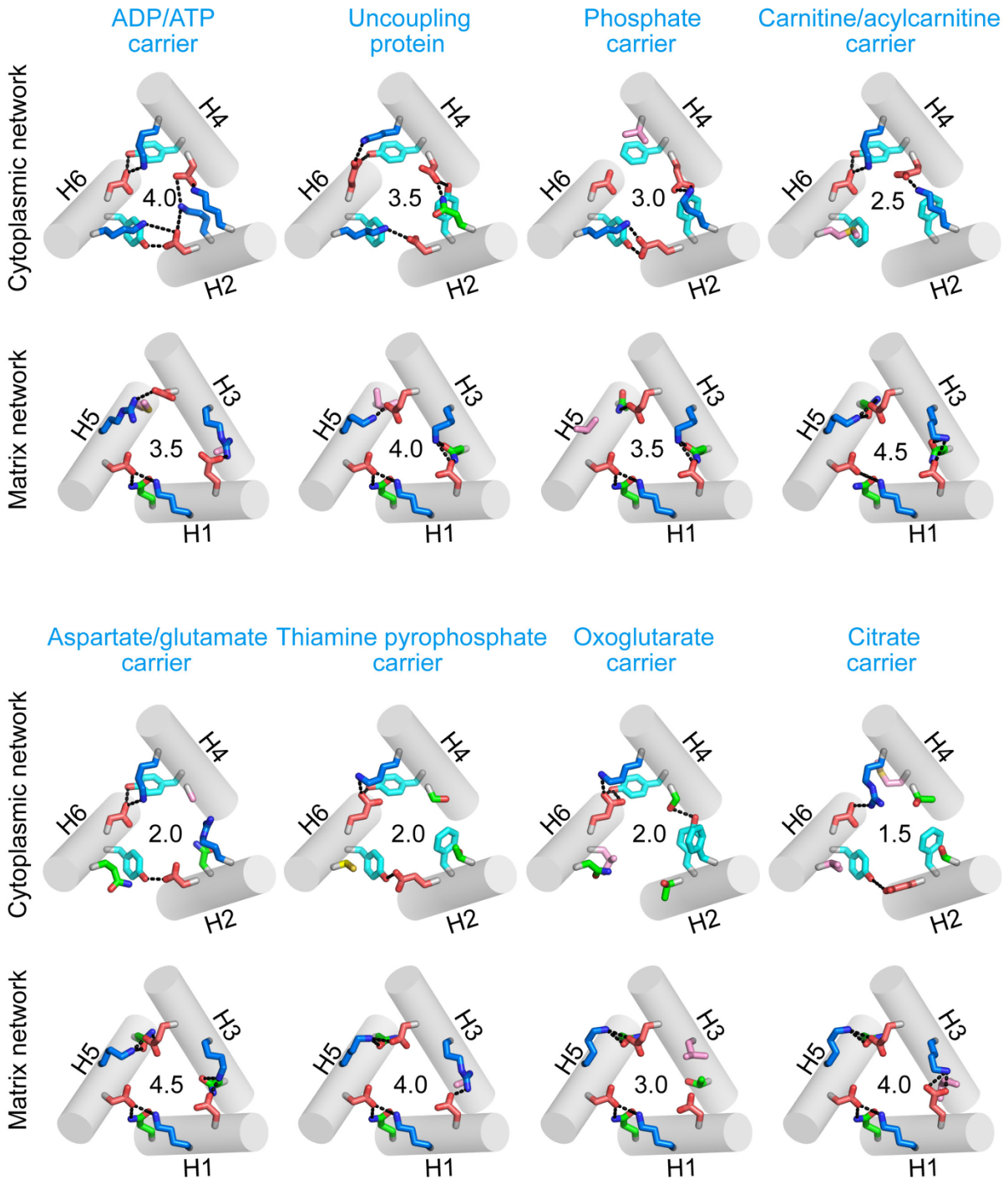

Figure 1.8: Cytoplasmic and matrix gate strength of different SLC25 carriers. Helices are shown as cylinders and are models of the respective carriers, for the cytoplasmic-open state based on PDB entry 1okc and for the matrix-open state on PDB entry 6gci, chain A. Positively charged, negatively charged, polar, aliphatic and aromatic residues are shown in blue, red, green, pink and cyan sticks respectively. The bonds are shown as black dashes. The number indicated is the total interaction energy of the gate, where salt bridge interactions and hydrogen bonds are accounted as 1.0 and 0.5 respectively. Figure taken from (Ruprecht and Kunji, 2020).

1.6.1. Substrate specificity of mitochondrial carriers

The differences found in the binding site areas can explain the big diversity of substrates transported by the different carriers. These include amino acids, nucleotides, vitamins, inorganic ions, fatty acids and di- and tri- carboxylates (Kunji *et al.*, 2020) (**Figure 1.9**). For example, the amino acid transporters include the aspartate/glutamate carrier, which has key roles in the aspartate/malate shuttle, gluconeogenesis and the urea cycle and the ornithine carriers, which are important for the urea cycle. The nucleotide carriers include the ADP/ATP carrier, which is essential for oxidative phosphorylation (**sections 1.3.2, 1.3.4** and **1.5**) and the ATP-Mg/phosphate carrier, which can change the adenine nucleotide pool, in response to changes in energetic demand and after mitochondrial division. Vitamin carriers include the S-adenosylmethionine carrier, which is required for methylation reactions of DNA, RNA and proteins in the mitochondrial matrix and the thiamine pyrophosphate carrier, whose substrate is important for dehydrogenase reactions. Inorganic ion transporters include the phosphate carrier, which is critical for oxidative phosphorylation and fatty acid transporters include the carnitine/ acyl-carnitine carrier, which is involved in the β-oxidation of fatty acids. Di- and tri- carboxylate carriers include the oxoglutarate carrier, involved in aspartate/malate shuttle and gluconeogenesis and the citrate carrier, whose function is important for acetyl CoA in the cytosol, among others (Kunji *et al.*, 2020).

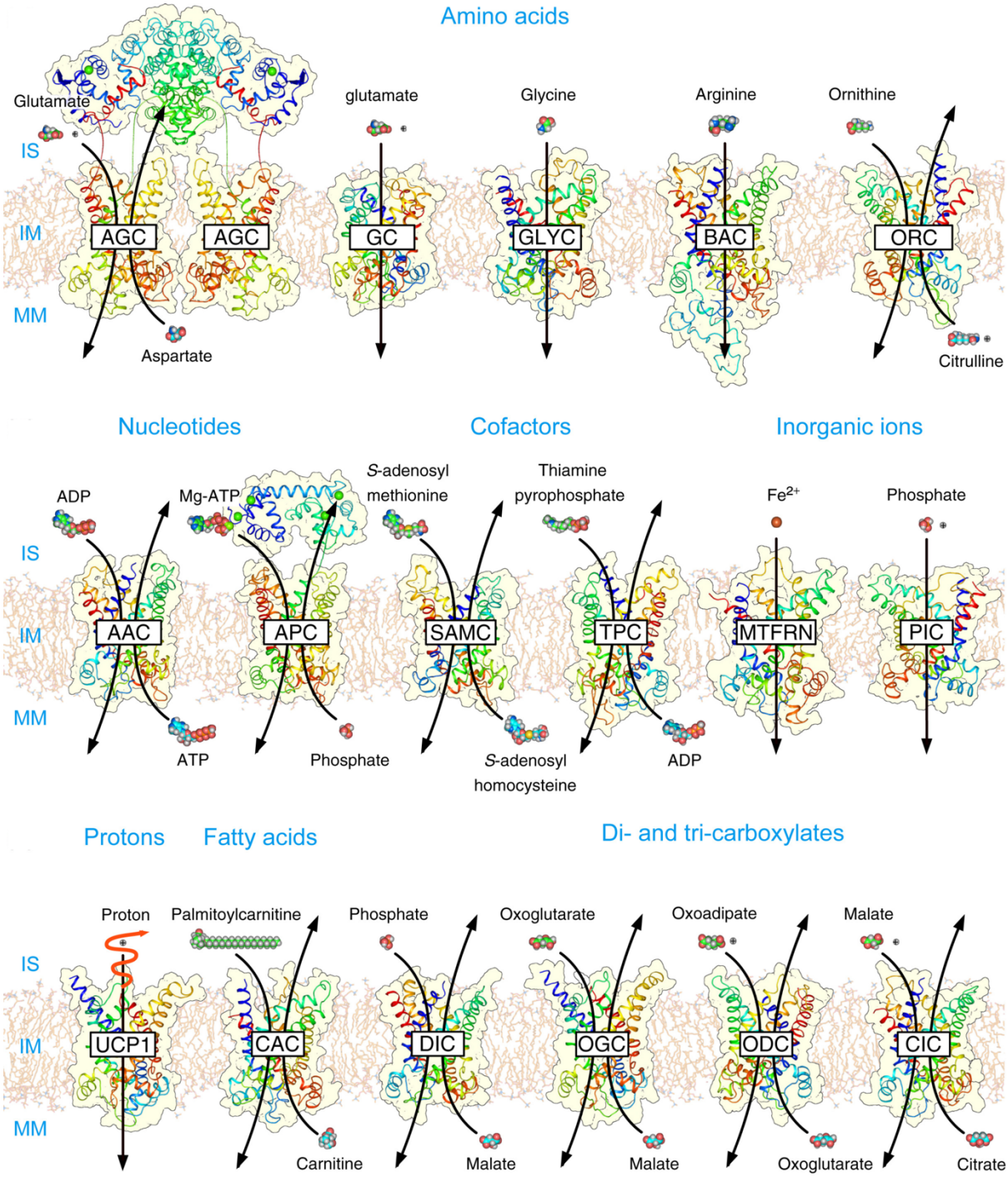

Figure 1.9: The diversity of substrates transported by the mitochondrial carrier family and the different modes of transport. The structures are homology models based upon PDB entries 1okc and 4c9h chain A. The regulatory domains of AGC and APC are from the PDB entries 4P5W and 4ZCU, respectively and the links to the carrier domains are not modelled. Abbreviations: AAC, ADP/ATP carrier (SLC25A4, SLC25A5, SLC25A6, SLC25A31); AGC, aspartate glutamate carrier (SLC25A12, SLC25A13); APC, ATP-Mg/Pi carrier (SLC25A23, SLC25A24, SLC25A25); BAC, basic amino acid carrier (SLC25A29); CAC, carnitine-acylcarnitine carrier (SLC25A20); CIC, citrate (tricarboxylate) carrier (SLC25A1); DIC, dicarboxylate carrier (SLC25A10); GC, glutamate carrier (SLC25A18, SLC25A22); GLYC: glycine carrier

(SLC25A38); IM, inner membrane; IS, intermembrane space; MM mitochondrial matrix; MTFRN mitoferrin (SLC25A28, SLC25A37); ODC, oxoadipate carrier (SLC25A21); OGC, oxoglutarate carrier (SLC25A11); ORC, ornithine carrier (SLC25A2, SLC25A15); PIC, phosphate carrier (SLC25A3); SAMC, S-adenosylmethionine carrier (SLC25A26); TPC, thiamine pyrophosphate carrier (SLC25A19); UCP1, uncoupling protein (SLC25A7). Figure taken from (Ruprecht and Kunji, 2020).

1.6.2. Mitochondrial carriers and pathology

Considering the central role the mitochondrial carriers play in cell and mitochondrial metabolism, it is not surprising that their dysfunction leads to severe human diseases (Kunji *et al.*, 2020; Palmieri *et al.*, 2020). Most of the reported pathologies have neuromuscular, metabolic or developmental disease phenotypes. To date, mutations in 18 carriers have been reported to cause disease (Palmieri *et al.*, 2020). These include missense mutations, nonsense and silent mutations, insertions, deletions and insertions/deletions. Point mutations can affect residues that face inside the translocation pathway, the lipid bilayer or can be buried within the protein structure. The most frequent are the ones occurring in the translocation pathway: approximately 65 % of the residues facing inside the translocation pathway have at least one pathogenic mutation (Kunji *et al.*, 2020; Palmieri *et al.*, 2020). In all cases, the pathology can arise from structural defects or instability of the transporter, reduction or elimination of its activity, but also issues in the biogenesis and targeting (Kunji *et al.*, 2020). All these defects can result in accumulation of the relevant metabolites in either the mitochondrial matrix or the cytosol, with obvious consequences for metabolism and cellular function.

The symptoms of the different diseases can vary a lot, dependent on the metabolic pathway that the affected carrier participates in, the expression pattern of the carrier and the relevance for specific tissues/organs, as well as the presence of other paralogues or other transporters that can potentially compensate to different extent for the loss of function. Therefore, large differences can exist among individuals suffering from the same syndrome (Kunji *et al.*, 2020; Palmieri *et al.*, 2020). It becomes, hence, evident that the study of the mechanism, structure, regulation, expression and targeting of the wild-type carriers is of great importance, in order to understand the cause of the pathologies and to assist therapeutic studies.

1.7. Project aims

The mitochondrial ADP/ATP carrier is the most well studied member of the SLC25 family. Structures in two conformational states have been resolved and there are many studies regarding its function (Klingenberg, 2008; Kunji *et al.*, 2016; Kunji and Ruprecht, 2020; Ruprecht and Kunji, 2021). Based on these studies, an alternating access mechanism has been described (**section 1.5.3**). However, unresolved aspects concern the experimental investigation of the substrate binding site and of the mechanism by which substrate binding induces the conformational changes required for translocation. Addressing these questions was the major aim of this thesis. Since all mitochondrial carriers are thought to operate via a common mechanism, the insights gained from this study may advance the understanding of all members of the SLC25 family, many of which are uncharacterised and about a third have been reported to play a role in mitochondrial diseases.

The selected approach for studying the substrate binding process was mutagenesis. In **Chapter 3**, the preparatory work is described: the criteria for selection of the target-residues, the generation of constructs, their expression, as well as the evaluation of protein function, assessed by a complementation assay. Additionally, the purification of the wild-type protein and variants is described, as well as their biophysical characterisation, using a thermostability assay. Moreover, the principle applied to identify substrate binding residues is tested by mapping the binding sites of the inhibitors CATR and BKA, which are known from the crystal structures.

In **Chapter 4** the response of the wild-type protein to substrate is characterised, using the thermostability shift assay and the differences in the responses of the variants are used to identify residues with critical and contributing roles to substrate binding.

In **Chapter 5** the transport properties of the proteins are studied to provide supporting evidence for the thermostability analysis. Firstly, the optimisation of the transport assays for the wild-type carrier is described, as well as its transport kinetics. Subsequently, the variants are tested using the established conditions.

In **Chapter 6** the study of a mitosomal transporter which shares sequence features with the mitochondrial ADP/ATP carriers, but displays a broader nucleotide specificity, provides the opportunity to investigate the molecular determinants of substrate specificity. It is shown that through point mutations on a single residue of the

mitochondrial ADP/ATP carrier, it is possible to expand its specificity. These data provide information on the factors that contribute to the selection of the nucleotide base in the ADP/ATP carrier.

In **Chapter 7** the results are recapitulated and a mechanism for the interdependent processes of substrate binding and structural changes is proposed. Finally, some preliminary results obtained with native mass spectrometry and solid supported membrane electrophysiology give directions for future studies.

Chapter 2: Materials and Methods

2.1. Chemicals, reagents and enzymes

Unless otherwise stated, general laboratory chemicals, primers, pre-cast sodium dodecyl sulphate-polyacrylamide gel electrophoresis (SDS-PAGE) gels, N-[4-(7-diethylamino-4-methyl-3-coumarinyl)phenyl] maleimide (CPM), bongkrekic acid (BKA), carboxyatractyloside (CATR) and nucleotides were obtained from Merck (Gillingham, UK). Ultra-pure water was prepared using the Milli-Q purification system (Merck-Millipore, Billerica, MA, USA) followed by autoclaving. Chloramphenicol and lysozyme were obtained from BDH Chemicals (Poole, UK). All enzymes (restriction endonucleases, T4 DNA ligase and factor Xa) were purchased from New England Biolabs (Ipswich, MA, USA). Complete Mini EDTA-free protease inhibitor tablets and nickel Sepharose High Performance were purchased from Roche (Basel, Switzerland) and Cytiva (Hatfield, UK), respectively. The detergents N-dodecyl β-D-maltoside (DDM) and pentaethylene glycol monodecyl ether ($C_{10}E_5$) were purchased from Glycon (Luckenwalde, Germany) and Merck (Gillingham, UK), respectively. All lipids, tetraoleoyl cardiolipin (18:1) (TOCL), egg L-α-phosphatidylcholine (Egg PC), *E. coli* polar lipid extract, bovine heart total extract and bovine heart polar extract were purchased from Avanti Polar Lipids (Alabaster, AL, USA). Radiolabelled substrates were purchased either from Perkin Elmer (Waltham, MA, USA: [^{14}C]-adenosine 5'-diphosphate), Moravek (Brea, CA, USA: [^{14}C]-adenosine 5-triphosphate, [^{14}C]-cytidine 5'- triphosphate, [^{14}C]-guanosine 5'-triphosphate, [^{14}C]-thymidine 5'-triphosphate and [^{14}C]-uridine 5'-triphosphate) or Hartmann Analytic (Braunschweig, Germany: [^{33}P]-adenosine 5-triphosphate). Media and plates for growth of bacteria and yeast were prepared at the MRC/Wellcome Trust Building (Cambridge, UK) (**Table 2.1**). All chemicals involved in the preparation of growth media were purchased from ForMedium (Hunstanton, Norfolk, UK).

Table 2.1: Bacterial and yeast growth media composition

Media	Components	Use
Escherichia coli		
LB medium + ampicillin pH 7.4	0.5 % (w/v) yeast extract 1 % (w/v) tryptone 140 mM NaCl 50 µg mL^{-1} ampicillin	Liquid culture
LB agar plates + ampicillin pH 7.4	0.5 % (w/v) yeast extract, 1 % (w/v) tryptone 140 mM NaCl 50 µg mL^{-1} ampicillin 1.5 % (w/v) agar	Transformation, selection
SOC pH 7.4	0.5 % (w/v) yeast extract 2 % (w/v) tryptone 10 mM NaCl 20 mM glucose 10 mM $MgCl_2$ 2.5 mM KCl	Transformation, recovery medium
2x TY pH 7.0	1 % (w/v) yeast extract 1.6 % (w/v) tryptone 0.1 mM NaCl	Liquid culture
Saccharomyces cerevisiae		
Synthetic dropout media, Sc-Trp (medium)	0.67 % (w/v) Yeast Nitrogen Base 2 % (w/v) D-glucose, 1 X complete synthetic medium (CSM) -Trp	Liquid culture, selection medium
Sc-Trp agar plates	0.67 % (w/v) Yeast Nitrogen Base 2 % (w/v) D-glucose 1 X complete synthetic medium (CSM) -Trp 1.5 % (w/v) agar	Transformation, selection
YPD	1 % (w/v) yeast extract 2 % (w/v) peptone 2 % (w/v) D-glucose	Liquid culture, rich medium
YPD agar plates	1 % (w/v) yeast extract 2 % (w/v) peptone 2 % (w/v) D-glucose 1.5 % (w/v) agar	Non-selection plates, rich medium
YPG + 0.2 % glucose	1 % (w/v) yeast extract 2 % (w/v) peptone 3 % (v/v) glycerol	Liquid culture rich medium

	0.2 % (w/v) D-glucose	
Lactococcus lactis		
M17 medium	19 % (w/v) disodium-β-glycerophosphate 5 % (w/v) pancreatic digest of casein 5 % (w/v) beef extract 5 % (w/v) soy peptone 2.5 % (w/v) yeast extract 0.5 % (w/v) ascorbic acid 0.25 % (w/v) magnesium sulphate	Liquid culture
M17 agar plates + chloramphenicol	19 % (w/v) disodium-β-glycerophosphate 5 % (w/v) pancreatic digest of casein 5 % (w/v) beef extract 5 % (w/v) soy peptone 2.5 % (w/v) yeast extract 0.5 % (w/v) ascorbic acid 0.25 % (w/v) magnesium sulphate 1.5 % (w/v) agar 5 µg ml^{-1} chloramphenicol	Growth plates
SM17 medium	19 % (w/v) disodium-β-glycerophosphate 5 % (w/v) pancreatic digest of casein 5 % (w/v) beef extract 5 % (w/v) soy peptone 2.5 % (w/v) yeast extract 0.5 % (w/v) ascorbic acid 0.25 % (w/v) magnesium sulphate 500 mM sucrose	Liquid culture recovery medium
SM17 agar plates	19 % (w/v) disodium-β-glycerophosphate 5 % (w/v) pancreatic digest of casein 5 % (w/v) beef extract 5 % (w/v) soy peptone 2.5 % (w/v) yeast extract 0.5 % (w/v) ascorbic acid	Transformation selection

	0.25 % (w/v) magnesium sulphate 500 mM sucrose 1.5 % (w/v) agar

2.2. Strains, vectors and genes

2.2.1. Strains

Electro-competent *E. coli* XL1 blue cells[1] were used as an intermediate host in cloning for propagating expression vectors and ligation products. They were obtained from Stratagene (La Jolla, USA). The *S. cerevisiae* strain W303-1B[2] (Ralser et al., 2012) was used for protein expression. The *S. cerevisiae* strain WB-12[3], in which the genes *aac1* and *aac2* have been disrupted (Hashimoto et al., 1999), was used for complementation assays and was a gift from Prof H. Terada. The *Lactococcus lactis* strain NZ9000[4] (Mierau and Kleerebezem, 2005), which has the genes for NisK and NisR integrated in its genome, was used for protein expression and was donated by Dr. O. P. Kuipers (National Institute for Diary Research, Ede, the Netherlands)

[1] Genotype: *endA1 gyrA96(nal^R) thi-1 recA1 relA1 lac glnV44 F'[::Tn10 proAB$^+$ lacI^{q}Δ(lacZ)M15] hsdR17(rK$^-$mK$^+$)*
[2] Genotype: MATα *leu2-3, 112 trp1-1 can1-100 ura3-1 ade2-1 his3-11,15*
[3] Genotype: MATα ade2-1 trp1-1 ura3-1 can1-100 aac1::LEU2 aac2::HIS3
[4] Genotype: *pepN*::*nisRnisK*

2.2.2. Expression vectors

For protein expression in *S. cerevisiae*, the gene encoding *Aac* from *Thermothelomyces thermophila* (TtAac) was cloned in the pPIC2 vector, which is a derivative of the pYES3/CT vector, generated by Marylin Harding, MRC Mitochondrial Biology Unit, containing the constitutively active promoter of the phosphate carrier isoform 2 (PIC2) from *S. cerevisiae* (Bamber *et al.*, 2007a) (**Figure 2.1A**). For protein expression in *L. lactis* the gene was cloned in the pNZ8048 vector (de Ruyter et al., 1996) containing a nisin A inducible promoter nisA (**Figure 2.1B**).

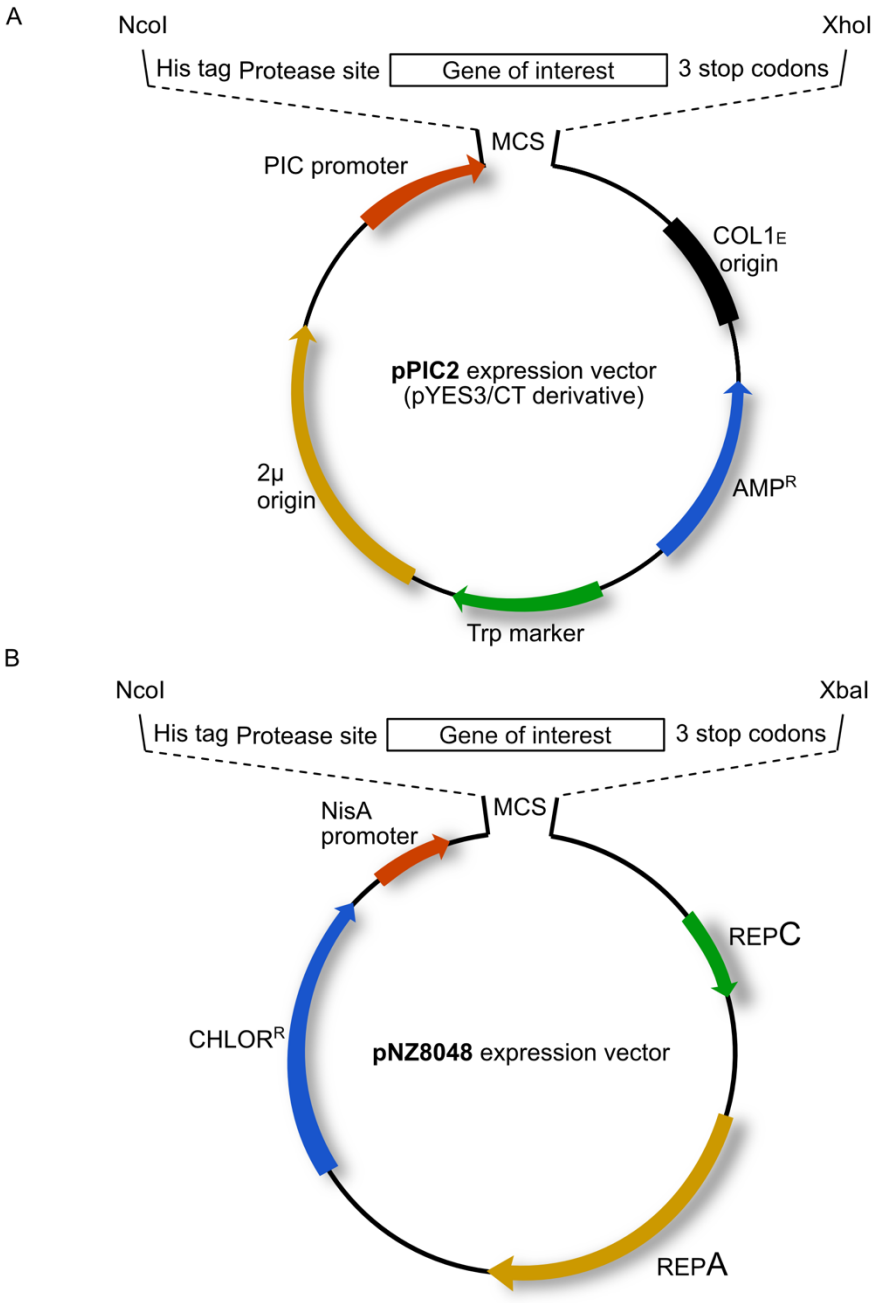

Figure 2.1: Schematic representation of the pPIC2 (*S. cerevisiae*) and pNZ (*L. lactis*) expression vectors. (A) pPIC2 vector (B) pNZ8048 vector. Functional elements are represented as arrows. The target gene, containing an octa-histidine tag, a protease site at the N-terminus and three stop codons, was cloned into the multiple cloning site (MCS) with NcoI and XhoI or XbaI restriction sites. Promoter regions are shown as orange arrows, antibiotic resistance genes as blue arrows, the auxotrophic selection marker and the origin of replication in the pPIC2 vector as green and yellow arrows, respectively. The green and yellow arrows in the pNZ vector represent replication proteins. Figure adapted from (Thangaratnarajah, 2014).

2.2.3. Construct design

The gene encoding the residues 8 – 308 of Aac from *Thermothelomyces thermophila* (TtAac), codon optimised for expression in *S. cerevisiae*, was synthesised by GenScript (Piscataway, NJ, USA). The construct was designed with an octa-histidine tag and a factor Xa protease recognition site 'IEGR' at the N-terminus (**Figure 2.2**) by Marilyn Harding (MRC Mitochondrial Biology Unit). Linker sequences 'SDRA' and 'TATSE', which mimic the factor Xa recognition site in prothrombin, were added before and after the factor Xa recognition site for improving the binding and cleavage efficiency.

The thirty-six point mutations in the gene were introduced by overlap extension PCR (**section 2.3.3**), by replacing the equivalent codon at the desired position with GCT (most frequently occurring codon for alanine in *S. cerevisiae*). The mutagenesis for 10 variants, K30A, R88A, R100A, G192A, I193A, Y196A, R197A, S238A, R246A and R287A, was performed by Dr Martin King.

A

B

MAHHHHHHHHSDRAIEGRTATSEKILGMPPFVVDFLMGGVSAAV**SK**TAAAPIERIK**L**LV**Q**
NQDEMIKAGRLDRRYNGIIDCFRRTTADEGLMALWRGNTA**N**VI**RY**FP**TQ**AL**NF**AF**R**DK
FKAMFGYKKDKDGYAKWMAG**N**LASGGAAGAT**SL**LF**V**YSLDYAR**T**RLANDAKSAKGGG
ARQFNGLIDVYRKTLASDGIAGLYRGFGP**S**VA**GI**VV**YR**GL**Y**FGM**Y**DSIKPVVLVGPLANN
FLASFLLGWC**VT**TGA**G**IA**SY**PLDTVR**R**RMMMTSGEAVKYKSSIDAFRQIIAKEGVKSLFK
GAGA**N**IL**RG**VA**G**AG**VL**SIYDQLQILLFGK

Figure 2.2: TtAac construct and position of introduced alanine mutations. (A) Sequence of affinity tag (green), linker regions (blue) and factor Xa recognition site (red), cloned at the N-terminus of the gene. The arrow indicates the position where

Factor Xa protease cleaves. (B) Sequence of TtAac gene with the positions where single Ala mutations were introduced indicated with bold letters. The first 18 amino acids of the construct (shown in grey) are cleaved during protein purification.

2.3. Molecular biology methods: DNA based

2.3.1. Agarose gel electrophoresis

DNA fragments were separated and visualised on agarose gels. Gels were cast with 1 % (w/v) agarose (BioGene Ltd., Kimbolton, UK) in TBE buffer (89 mM Tris-borate, 100 mM boric acid, 2 mM EDTA) and contained 16 x 10^{-5} % (v/v) Sypro Safe DNA gel stain (Thermo Fischer Scientific, Carlsbad, CA, USA). Electrophoresis was performed at 100 mA in TBE buffer. Separated DNA fragments were visualised with the ChemiDoc XRS+ (Bio-Rad, Watford, Hertfordshire, UK) imaging system. DNA concentrations (260 nm) and purity (260/280nm) were determined using the NanoDrop ND-8000 spectrophotometer (Thermo Scientific, Wilmington, DE, USA).

2.3.2. PCR amplification

PCR amplification reactions were performed using the KOD Hot Start DNA polymerase kit, according to manufacturer's instructions. In all cases the cloning vector containing the original target gene was used as template DNA (**Appendix 1.1**). All oligonucleotides were designed to have a complementary region binding to the template DNA with an annealing temperature > 60°C. Oligonucleotides used for PCR amplifications are listed in **Appendix 1.2**. Components and parameters for PCR amplification reactions are described in **Table 2.2**. The reactions were performed using a thermocycler (Techne TouchGene, Stone, UK). PCR products were analysed by agarose gel electrophoresis and then treated with *Dpn*I (NEB, Ipswich, MA, USA) according to the manufacturer's instructions, in order to remove methylated template DNA.

Table 2.2: Standard PCR amplification components using the KOD Hot Start polymerase kit

Reagent	Volume (µL)
KOD DNA polymerase kit buffer (10x)	5
25 mM $MgSO_4$	3
2 mM deoxynucleotide triphosphates (dNTPs)	5
10 µM forward oligonucleotide	1.5
10 µM reverse oligonucleotide	1.5
Template DNA (approximately 100 ng mL^{-1})	1
Ultra-pure sterile water	Adjust total volume to 49
KOD DNA polymerase	1

Table 2.3: PCR amplification reaction parameters

Procedure state	Temperature (°C)	Time	Cycle(s)
Initial denaturation	95	5 minutes	1
Denaturation	95	20 seconds	35
Annealing	60	20 seconds	35
Elongation	70	1 minutes	35
Final elongation	70	1 minutes	1

2.3.3. Site-directed mutagenesis

Overlap extension PCR was used to introduce site-directed point mutations into the sequence of the gene in three steps (four reactions) (**Figure 2.3**) (Ho et al., 1989). Initially, two DNA fragments with overlapping ends were generated in two separate reactions. Fragment 1 was generated using a 'generic' forward oligonucleotide, complementary to the 5' region of the gene and a mutagenic reverse oligonucleotide (reaction 1). Fragment 2 was generated using a mutagenic forward oligonucleotide and a 'generic' reverse oligonucleotide, complementary to the 3' region of the gene (reaction 2). In the third reaction, fragments 1 and 2 were combined due to their overlapping ends, hence no oligonucleotides were required. In the fourth reaction, the full gene was amplified using the 'generic' forward and reverse oligonucleotides (**Figure 2.3**).

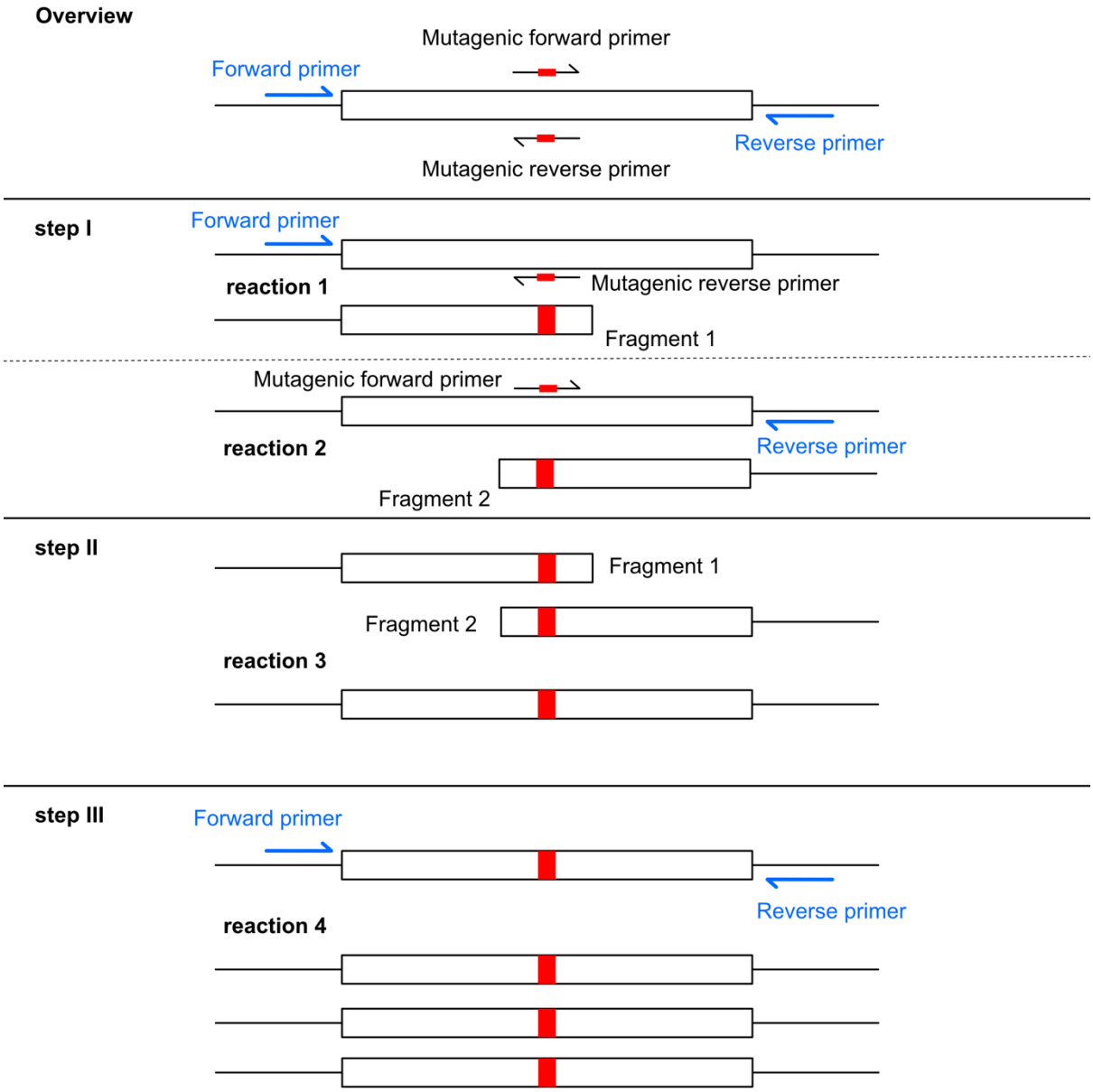

Figure 2.3: Schematic representation of site directed mutagenesis for introduction of point mutations using overlap extension PCR.

2.3.4. Restriction digestion

The gene inserts and vectors were digested with either NcoI and XhoI restriction enzymes for cloning into the pPIC2 vector or NcoI and XbaI for cloning into the pNZ vector, according to the manufacturer's instructions. The digested vector was separated on a 1 % (w/v) agarose gel and the relevant fragment was isolated by gel extraction, using the Qiagen QIAquick gel extraction kit (Venlo, the Netherlands) according to manufacturer's instructions, with a minor modification: Bound DNA fragments were recovered with 30 µL pre-warmed elution buffer (provided in the kit). For inserts, 25 µL PCR amplified DNA were used. Typically, the digestion reaction

volume was 50 µL and the mixtures were incubated at 37°C for 3 hours, followed by 20 minutes at 80°C for inactivation of the enzymes.

2.3.5. Ligation of target gene into the expression vector

NcoI-XhoI/XbaI restricted genes were cloned into the appropriate expression vectors using T4 DNA ligase, according to the manufacturer's instructions. The reaction contained 50 ng of vector and the amount of insert was calculated according to the following equation:

$$\text{Amount of insert} = \frac{3}{1} \times \frac{\text{length of insert in bp}}{\text{length of vector in bp}} \times 50 \text{ ng vector}$$

The amount of insert for the pPIC2 vector was 25 ng and for pNZ8048 40 ng. Typically, the ligation reaction volume was 30 µL and the mixtures were incubated at room temperature for 90 minutes, followed by 10 minutes at 65°C for inactivation of the enzyme.

2.3.6. DNA sequencing

All clones were verified by Sanger sequencing (Source Bioscience UK Ltd., Nottingham, UK) and analysed by sequence alignment using the Clustal Omega online server (Madeira et al., 2019), accessible through https://www.ebi.ac.uk/Tools/msa/clustalo/. Oligonucleotides for sequencing were specific for the vectors and are listed in **Appendix 1.2**.

2.4. Strain specific methods

2.4.1. Preparation of *L. lactis* competent cells

Overnight cultures of the *L. lactis* strain NZ9000 were grown in SM17 medium (**Table 2.1**) supplemented with 0.8 % (w/v) glucose and 1.5 % (w/v) glycine, at 30°C without aeration. SM17 medium supplemented with glucose and glycine as above was inoculated with the overnight culture at a twenty-fold dilution and incubated at 30°C, until an OD_{600nm} of 0.5–0.7 was reached (typically 2-3 h). Cells were pelleted by centrifugation at 5,500 x g, for 5 minutes at 4°C and resuspended in 50 mL sterile wash buffer (0.5 M sucrose, 10 % (v/v) glycerol). Repeat of the wash steps was carried

out another three times. The final pellet was resuspended in 3 mL wash buffer. Cells were aliquoted, flash-frozen in liquid nitrogen, and stored at -70°C.

2.4.2. DNA precipitation and transformation into *L. lactis*

Ligation reactions were supplemented with 0.1 volumes (typically 3 µL) of Pellet Paint Co-Precipitant (Merck, Gillingham, UK), 0.1 volumes of 3 M sodium acetate pH 5.2 and 2 volumes of 100 % (v/v) ethanol. The mixture was briefly vortexed and incubated for 5 minutes at room temperature. Precipitated DNA was pelleted by centrifugation at 13,800 x g for 10 minutes, at room temperature and washed twice with 70 % (v/v) and 100 % (v/v) ethanol respectively. The final pellet was dried for 20 minutes at 90°C, then resuspended in 20 µL ultra-pure sterile water and stored at -20°C.

Electroporation cuvettes (Flowgen, Nottingham, UK) were pre-chilled on ice. The transformation mixture was composed of 50 µL electrocompetent *L. lactis* cells and the whole ligation product (~30 µL). *L. lactis* cells were transformed using an electroporation system (Bio-Rad GenePulser II and Pulse Controller Plus, Hercules, CA, USA) at 25 µF capacitance, 2.5 kV voltage and resistance above 200 Ω. Cells were recovered with 2 mL *L. lactis* recovery medium (**Table 2.1**) at 30°C for 3 hours, without shaking and subsequently plated 100 µL on SM17 agar plates supplemented with 0.5 % (w/v) glucose and 5 µg/mL chloramphenicol and incubated at 30°C for 48 hours.

2.4.3. Preparation of electrocompetent XL1 blue cells

E. coli XL-1 blue cells were streaked onto LB agar plates (**Table 2.1**), without ampicillin, and incubated at 37°C overnight. The next day, 5 mL of 2xTY medium (**Table 2.1**) was inoculated with a single colony and incubated overnight, at 37°C, 225 rpm. 2xTY medium was inoculated with the overnight culture at a 200-fold dilution and incubated at 37°C, 225 rpm until an OD_{600nm} of approximately 0.6 was reached. The cultures were cooled on ice for 30 minutes and cells were pelleted by centrifugation at 8,000 x g, 10 minutes, 4°C. Cell pellets were washed twice in 20 mL sterile 10 % (v/v) glycerol and pelleted at 5000 x g, 10 minutes, 4°C. The final pellet was resuspended in 6 mL sterile 10 % (v/v) glycerol. Cells were aliquoted, flash-frozen in liquid nitrogen, and stored at -70°C.

2.4.4. Transformation of electrocompetent XL1 blue cells

Electroporation cuvettes (Flowgen, Nottingham, UK) were pre-chilled on ice. The transformation mixture contained 70 µL electrocompetent *E. coli* cells and 3 µL of the ligation product. The cells were transformed by electroporation as described in **section 2.4.2.** Cells were recovered with 1 mL SOC medium, incubated at 37°C for 1 hour and subsequently 70 µL were plated on LB+Amp agar plates (**Table 2.1**) and incubated at 37°C for 24 hours.

2.4.5. Transformation of *S. cerevisiae* competent cells

Expression vectors isolated from *E. coli* cells were used to transform the *S. cerevisiae* strains W303-1B or WB-12, using the Li/Ac method (Gietz and Schiestl, 2007). The strains were streaked out on YPD agar plates (**Table 2.1**) and incubated at 30°C for 48 hours. A single colony was selected and used to inoculate 8 mL of YPD medium. The culture was grown overnight at 30°C, 225 rpm. The next day, 25 mL of pre-warmed YPD medium was inoculated with 1.2 mL for strain W303-1B or 1.7 mL for WB-12 of the starting culture and incubated at 30°C, 225 rpm until an optical density (OD_{600nm}) of approximately 1 was reached. Cells were pelleted by centrifugation at 1,250 x g, 10 minutes, at 4°C and resuspended in 25 mL cold ultra-pure sterile water. Cells were pelleted as before and resuspended in 500 µL cold sterile TE/LiAc solution (10 mM Tris-HCl, pH 8.0, 1 mM EDTA, 100 mM lithium acetate). The transformation mixture contained 4 µL of plasmid, 20 µL of 2 mg mL^{-1} (single-stranded) boiled salmon sperm carrier DNA and 100 µL of competent yeast cells. The mixture was incubated for 10 minutes at room temperature. 500 µL sterile PEG/TE/LiAc solution (TE/LiAC solution supplemented with 50 % (w/v) PEG 4000) was added to each mixture and mixed by gentle pipetting. The mixture was initially incubated at 30°C for 30 minutes and then heat shocked at 42°C for 20 minutes. Cells were pelleted at 500 x g, for 3 minutes, at 4°C and resuspended in 200 µL sterile water. 50 µL of cells were plated out onto Sc-Trp agar plates (**Table 2.1**). Plates were incubated at 30°C for 72 hours. Overnight cultures from single colonies were grown in 5 mL SC-Trp medium supplemented with 2 % (w/v) glucose, at 30°C, 225 rpm. Glycerol stocks were prepared by mixing overnight culture and 30 % (w/v) glycerol in a 1:1 ratio. Glycerol stocks were stored at -70°C.

2.5. Protein based methods

2.5.1. General methods

2.5.1.1. Protein concentration determination

Protein concentration was determined using the NanoDrop ND-8000 Spectrophotometer (Thermo Scientific, Wilmington, DE, USA) with the absorbance measured at 280 nm and indicating that the extinction coefficient of the protein (ε) is 37,485 M^{-1} cm^{-1} and that the molecular weight is 33.07 kDa, as calculated based on the protein sequence, using the expasy ProtParam tool, available at https://web.expasy.org/cgi-bin/protparam/protparam. These values are used in the Lambert-Beer equation to calculate the concentration. Alternatively, the bicinchoninic acid (BCA) assay was used, according to the manufacturer's instructions. A standard curve with bovine serum albumin (0-1.5 mg mL^{-1}) was prepared to assist protein quantification. Absorbance of the protein standards and samples was measured at 562 nm on a SpectraMax Plus^{384} plate reader (Molecular Devices, Sunnyvale, CA, USA).

2.5.1.2. SDS-PAGE

Protein samples were mixed with 5x loading buffer (250 mM Tris-HCl pH 6.8, 10 % (w/v) sodium dodecyl sulphate (SDS), 10 % (w/v) dithiothreitol (DTT), 50 % (v/v) glycerol and 0.05 % (w/v) bromophenol blue) and then separated on a pre-cast TruPAGE 4-20 % SDS-PAGE gel at 130 mV for 1 hour, with TruPAGE TEA-Tricine SDS Running Buffer supplied by the manufacturer. Alternatively, mPAGE 4-12 % Bis-Tris pre-cast gels were used, with the same settings and MES SDS Running Buffer (0.6 % w/v Tris-base, 1% w/v MES, 0.1 % w/v SDS, 0.03 % w/v EDTA). Proteins bands were visualised with InstantBlue Coomassie stain (Abcam, Cambridge, UK).

2.5.1.3. Western blotting

SDS-PAGE gels were blotted onto polyvinylidene difluoride (PVDF) membranes either by semi-dry or wet transfer. For semi-dry transfer, a PVDF membrane was activated

in 100 % methanol for 30 seconds and stored in transfer buffer (25 mM Tris-HCl pH 8.3, 192 mM glycine, 10 % (v/v) methanol). The SDS-PAGE gel was transferred using a TE-77 semi-dry transfer unit (Amersham Biosciences, Piscataway, NJ, USA) at 120 mA, 16 V, for one hour. For wet transfer the Trans-Blot Electrophoretic Transfer Cell (Bio-Rad, Watford, Hertfordshire, UK) was used, applying 350 mA, 100 mV for 1h on ice. The transfer buffer was composed of 12.5 mM Tris-base, 96 mM glycine, and 10 % (v/v) methanol and the PVDF membrane was activated in 100 % methanol prior to the transfer. Dependent on the properties of the antibodies used for protein detection (fluorescent or horseradish peroxidase conjugate), the membranes were blocked in blocking buffer containing either 10 mM Tris-HCl, pH 8.0, 150 mM NaCl, 0.4 % (v/v) Tween 20 and 5 % (v/v) Marvell skimmed milk powder (for horseradish peroxidase conjugate antibodies), or in a 1:1 Odyssey blocking buffer (LI-COR Biosciences, Lincoln, NE, USA) mixed with TBS (25 mM Tris-HCl pH 8, 150 mM NaCl, 1.6 mM KCl) for fluorescent antibodies. Blocking solution was left overnight at 4°C. Details of probing with primary and secondary antibodies are summarised in **Table 2.4**. Proteins were detected either using the Enhanced Chemiluminescence (ECL) detection kit (GE Healthcare, Chalfont St Giles, UK), according to the manufacturer's instructions and visualised on X-ray films (Fujifilm, Tokyo, Japan), or using an Odyssey Clx Imaging System (LI-COR Biosciences, Lincoln, NE, USA).

Table 2.4: Antibody information

Target	Epitope	Provider	Dilution	Time
AAC (chicken)	YPLDTVRRRMMMT	Agrisera	1:20,000	1 hour
Anti-His (mouse)	HHHHHH	Roche	1:25,000	2 hours
Anti-His (rabbit)	HHHHHH	Abcam	1:5,000	4 hours
Fluorescent anti-mouse (donkey)		LI-COR	1:20,000	1 hour
Fluorescent anti-rabbit (donkey)		LI-COR	1:20,000	1 hour
HRP-conjugate Anti-mouse (goat)		Thermo Fischer Scientific	1:25,000	1 hour
HRP-conjugate Anti-chicken		Agrisera	1:20,000	1 hour

2.5.2. *S. cerevisiae* specific methods

2.5.2.1. Small scale expression trials in *S. cerevisiae*

Cells from glycerol stocks were streaked out on Sc-Trp agar plates (**Table 2.1**) and incubated at 30°C for 72 hours. A starter culture was grown from a single colony in Sc-Trp at 30°C, 225 rpm overnight and was used to inoculate YPG medium containing 0.1 % (w/v) D-glucose. The cells were left to grow at 30°C, 225 rpm for approximately 20 hours. Cells were pelleted and washed once in ice-cold ultra-pure sterile water (6,000 x g, for 15 minutes, 4°C) and then harvested by centrifugation (same settings).

2.5.2.2. Small scale isolation of crude yeast mitochondria

All steps were carried out at 4°C. Cells were homogenised in Breaking buffer (0.65 M sorbitol, 0.1 M Tris, pH 8.0, 5 mM EDTA, 0.2 % (w/v) fatty acid free BSA, EDTA-free protease inhibitor cocktail tablets and disrupted using 0.5 – 0.75 mm glass beads (Willy A. Bachofen AG, Muttenz, Switzerland) by vortexing. Cell debris was removed by centrifugation at 3,000 x g, 10 minutes, 4°C. Subsequently, isolation of crude mitochondria was performed by centrifugation at 25,000 x g, 30 minutes, 4°C. Crude mitochondria were resuspended in a buffer containing 0.1 M Tris-HCl buffer pH 7.5 and 10 % (v/v) glycerol and were stored at -20°C.

2.5.2.3. Large scale isolation of crude yeast mitochondria

All steps were carried out at 4°C. Cells were resuspended in 3 L per kg of cells Breaking buffer (0.65 M sorbitol, 0.1 M Tris pH 7.5, 5 mM EDTA pH 8.0, 5 mM aminohexanoic acid, 5 mM benzamidine, 0.2 % (w/v) fatty acid free BSA) and supplemented with 4.5 % (w/v) phenylmethylsulphonylfluoride (PMSF) in ethanol. The cell suspension was passed through a bead mill (Dyno-Mill, Willy A. Bachofen AG, Muttenz, Switzerland) with 0.5 – 0.75 mm glass beads at a constant current of 4.2 A and a constant flow-rate of 3 L per hour, using a peristaltic pump (Watson-Marlow 520S, Wilmington, MA, USA). The broken cells were collected on ice. 1 mL of PMSF was added and the pH was adjusted to 8.0 with 2 M Tris-HCl pH 8 every 10 minutes to limit protease activity. Unbroken cells and cell debris were removed by a low-speed centrifugation at 3000 x g for 45 minutes, 4°C. The mitochondria enriched fraction was

isolated by two high-speed centrifugations at 25,500 x g for 1 hour each. After the first spin, the pellets were homogenised in Wash buffer (0.65 M sorbitol, 0.1 M Tris pH 7.5, 5 mM aminohexanoic acid, 5 mM benzamidine). After the second spin the pellets were homogenised in TBG buffer (0.1 M Tris-HCl pH 7.5, 10 % (v/v) glycerol). Protein concentration was measured with BCA assay and the sample was aliquoted according to the upcoming experiments in amounts between 200-500 mg. Crude mitochondria were then flash-frozen in liquid nitrogen and stored at -70°C.

2.5.3. Protein purification with on-column digestion

Isolated crude mitochondria (approximately 300 mg total protein) were solubilised (at approximately 10 mg mL^{-1} final protein) by resuspension in a buffer containing 20 mM Tris–HCl pH 7.5, 10 % (v/v) glycerol, 150 mM NaCl, 20 mM imidazole pH 7.5, one Complete EDTA-free protease inhibitor cocktail tablet and 1 % (w/v) dodecyl-β-maltoside followed by gentle agitation at 4°C for 1 hour. Particulate material was removed by ultracentrifugation (235,000 x g, 45 minutes, 4°C) and the soluble fraction was incubated with previously washed and equilibrated (20 mM Tris-HCl pH 7.5, 150 mM NaCl) nickel Sepharose High Performance beads for 2 hours, at 4°C, under gentle agitation. Unbound proteins were removed by centrifugation (200 x g, 5 minutes, 4°C) and the bound fraction was transferred to an empty Econo-Pac chromatography column (Bio-Rad, Watford, Hertfordshire, UK), where it was washed with 40 column volumes of Buffer A (20 mM HEPES-NaOH pH 7.5, 150 mM NaCl, 20 mM imidazole pH 7.5, 0.1 % (w/v) dodecyl-β-maltoside, 0.1 mg/mL tetraoleoyl cardiolipin), followed by 25 column volumes of Buffer B (20 mM HEPES-NaOH pH 7.5, 150 mM NaCl, 0.1 % (w/v) dodecyl-β-maltoside, 0.1 mg/mL tetraoleoyl cardiolipin). Alternatively, the soluble fraction was applied to the nickel Sepharose High Performance resin at 1 mL min^{-1}, using an ÄKTA prime fast protein liquid chromatography (FPLC) purification system (GE Healthcare, Chalfont St Giles, UK) at 4°C. The resin was washed with 60 column volumes Buffer A (as above) and 40 column volumes Buffer B (as above). The column material in both cases was then recovered with 500 µL Buffer B and supplemented with 5 mM $CaCl_2$ and 10 µg factor Xa protease for on-column digestion, overnight at 10°C, with gentle agitation. Following factor Xa treatment, the cleaved protein was separated from the nickel Sepharose resin with an empty Proteus Midi spin column (Generon, Maidenhead, UK) (200 × g, 5 minutes, 4°C).

The same purification strategy was used for the wild type and all variants except for N123A, G192A, I193A, R197A and R246A. In these cases, due to protein instability, the on-column digestion step was reduced to 2 hours with 30 µg factor Xa protease. This modification was applied to variants L41A, Q44A, T146A, Y239A and N284A as well, which however did not yield folded protein.

2.5.4. Protein reconstitution into liposomes for radioactive uptake assays

Egg L-α-phosphatidylcholine and tetraoleoyl cardiolipin (18:1) were mixed in a 20:1 (w/w) ratio and dried under a stream of nitrogen. In the experiments indicated in text the mixture was composed of *E. coli* polar lipid extract or bovine total/polar extract and egg L-α-phosphatidylcholine/ tetraoleoyl cardiolipin (18:1) in a ratio 15:1:1 (w/w). Dried lipids were kept on ice. The lipids were rehydrated (final concentration 10 mg mL^{-1}) in buffer containing 20 mM HEPES-NaOH pH 7.5, 50 mM NaCl and when indicated, 1 mM ATP. Solubilisation was performed with pentaethylene glycol monodecyl ether ($C_{10}E_5$) at a final concentration of 1.5 % (v/v) by vortexing. Approximately 15 µg (for the wild type) or 20 µg (for the variants) of purified protein was added to the mixture (lipid-to-protein ratio 600-800:1 w/w) and incubated for 5 minutes on ice. Liposomes were formed by step-wise removal of the $C_{10}E_5$ using additions of SM-2 bio-beads (Bio-Rad, Watford, Hertfordshire, UK). Four additions of 60 mg followed by one addition of 480 mg were made every 20 minutes, while the samples were inverting at 4°C. The samples were incubated overnight at 4°C with inversion. Bio-beads were removed the next day by passage through empty micro-bio spin columns (Bio-Rad, Watford, Hertfordshire, UK). The external substrate was removed by gel filtration, shortly before the initiation of the transport reaction, using a PD10 desalting column (Cytiva, Hatfield, UK)).

2.5.5. Protein reconstitution into liposomes for SSM-based electrophysiology

Egg L-α-phosphatidylcholine and tetraoleoyl cardiolipin (18:1) were mixed in a 20:1 (w/w) ratio and dried under a stream of nitrogen. The lipids were rehydrated in a final concentration of 5 mg mL^{-1} in a buffer containing 20 mM HEPES-NaOH pH 7.5, 50 mM NaCl and when indicated, 1 mM ATP. Solubilisation was performed with $C_{10}E_5$ at

a final concentration of 0.25 % (v/v) by vortexing. Purified proteins concentrated up to 2-3 mg mL^{-1} (using a 50 kDa MWCO concentrator) were added at a lipid-to-protein ratio of 5:1 (w/w) or 10:1 (w/w) and incubated for 5 minutes on ice. Liposomes were formed by step-wise removal of the $C_{10}E_5$ using additions of SM-2 bio-beads (Bio-Rad, Watford, Hertfordshire, UK). Five additions of 20 mg followed by one addition of 160 mg were made every 20 minutes, while the samples were inverting at 4°C. The samples were incubated overnight at 4°C with inversion. Bio-beads were removed the next day by passage through empty Micro Bio-spin chromatography columns (Bio-Rad, Watford, Hertfordshire, UK) and the samples were frozen in liquid nitrogen.

2.5.6. *L. lactis* specific methods

2.5.6.1. Protein expression in *L. lactis* and isolation of *L. lactis* membranes

A starter culture was grown from glycerol stocks in M17 medium (**Table 2.1**) supplemented with 1 % (w/v) glucose and 5 µg mL^{-1} chloramphenicol, at 30°C overnight, with no aeration. Cells were diluted to an OD_{600nm} of 0.1 with fresh medium and grown until an OD_{600nm} of 0.5 was reached. Expression of the protein was induced by addition of 1:10,000 nisin A of spent M17 medium from nisin A-excreting *L. lactis* strain NZ9700. The cells were grown for 2 hours and then were harvested by centrifugation (6000 x g, 10 minutes, 4°C), washed with PIPES/NaCl buffer pH 7 (10 mM PIPES pH 7, 50 mM NaCl) and collected by centrifugation (same settings). Cells were subsequently resuspended in 50 mL PIPES/NaCl buffer and disrupted mechanically with a cell disruptor (Constant Cell Disruption Systems, Daventry, UK) at 33 kpsi. Undisrupted cells and debris were removed by centrifugation (11,000× *g*, 20 minutes, 4°C) and the membranes were collected by ultracentrifugation (138,000× *g*, 1 hour, 4°C). The membranes were resuspended in PIPES/NaCl buffer and stored in liquid nitrogen.

2.5.6.2. Fusion of *L. lactis* membranes with vesicles

For preparation of the liposomes, *E. coli* polar lipid extract and egg L-α-phosphatidylcholine were mixed at a mass ratio of 3:1 (w/w) and dried under a stream of nitrogen. The lipids were rehydrated in PIPES/NaCl buffer pH 7 (as above) to a final

concentration of 20 mg mL^{-1}. For the fusions, 1 mg of lactococcal membranes was mixed with 5 mg of liposomes, diluted to 900 µL and fused by seven cycles of freezing in liquid nitrogen and thawing at room temperature. The fused membranes were stored at liquid nitrogen.

2.6. Biophysical characterisation

2.6.1. Functional complementation assays

2.6.1.1. Spot tests

The WB-12 strain expressing the wild-type or mutant proteins or the empty vector was grown overnight in Sc-Trp medium supplemented with 2 % (w/v) glucose (**Table 2.1**). Cells were washed three times with ultra-pure sterile water, so that glucose was completely removed and diluted to an OD_{600} of 1. Four serial dilutions (1:10) were made and 3.5 µL of the starting culture and each dilution were dispensed on a YPG plate and incubated at 30°C for 72 hours. Only the second and third dilutions (10^{-2}, 10^{-3}) were used in the analysis presented. Each plate contained the wild type and empty vector control.

2.6.1.2. Densitometry and quantification of growth

Growth of the wild type and alanine replacement mutants was quantified by densitometry. Scanned images or photographs of the plates were analysed using the Fiji software (Schindelin et al., 2012). The density of the colonies was measured and expressed as a percentage of the density of the wild type of the same plate and dilution, after subtracting the density of the empty vector from both. The growth percentages calculated from the second and third dilutions (10^{-2}, 10^{-3}) were being averaged and this value was constituting one biological repeat. The experiment was conducted with four biological repeats.

2.6.2. Thermostability assays

2.6.2.1. The CPM thermostability assay

The assessment of protein population stability for the wild type and the variants in presence and absence of effectors (substrates or inhibitors) was performed via thermal unfolding, induced by a temperature ramp, and reaction with the thiol-reactive fluorophore N-[4-(7-diethylamino-4-methyl-3-coumarinyl)phenyl]-maleimide (CPM), as described previously (Alexandrov et al., 2008; Crichton *et al.*, 2015). For each experiment, 5 mg mL^{-1} CPM stock solution in dimethyl sulfoxide was diluted to 0.1 mg mL^{-1} in purification Buffer B (20 mM HEPES–NaOH pH 7.5, 150 mM NaCl, 0.1 % (w/v) dodecyl-β-maltoside, 0.1 mg/mL tetraoleoyl cardiolipin) and was equilibrated in the dark, for 10 minutes, at room temperature. Typically, 3 µg of purified protein were mixed with the relevant effector (where indicated, **sections 2.6.2.2** and **2.6.2.3**) and diluted into Buffer B to a final volume of 45 µL, to which 5 µL of CPM solution of 0.1 mg mL^{-1} were added. The mixture was vortexed very briefly and was incubated in the dark, for 10 minutes, at 4°C, before being placed in rotary quantitative PCR (qPCR) instrument (Rotor-Gene Q 2plex HRM Platform, Qiagen, Venlo, the Netherlands). Subsequently, the protein population was assayed in a temperature gradient from 25 to 90°C, corresponding to a rate of approximately 4°C per minute. The increasing fluorescence emitted by the protein-fluorophore adduct was measured in the HRM channel of the machine (excitation at 440–480 nm and emission at 505–515 nm). Unfolding profiles were analysed with the Rotor-Gene Q software 2.3, where the inflection point of the unfolding curves was used to determine the apparent melting temperature (Tm) of the protein population in the different conditions tested. A ΔTm value was obtained, where indicated, by subtracting the apparent Tm of the protein in absence of effectors from the apparent Tm at each concentration of the effectors.

For the experiments where the stability of the protein population was assessed over time the same procedure was followed, with one modification: The initial temperature was set to the value indicated in each experiment and the rate of temperature increase was set to 0.04°C per minute, leading to an increase of 1°C during the assay.

2.6.2.2. Thermostability shift in presence of inhibitors

The inhibitor CATR was added at 20 µM final concentration and BKA at 20 µM plus 5 µM ADP, which was necessary in order to allow the carriers to cycle between states and bind the inhibitor (King *et al.*, 2016). The procedure followed for thermal denaturation and reaction with the thiol-reactive probe as in **section 2.6.2.1**.

2.6.2.3. Thermostability shift in presence of substrate

The effectors ADP and ATP were added at final concentrations of 0.1, 0.5, 1, 5, and 10 mM (**paragraphs 4.3-4.6**) or for ADP titration (**paragraph 4.2**) at final concentrations of 0, 0.1, 0.2, 0.4, 0.8, 1.6, 3.1, 6.3, 12.5, 25 and 50 mM and 0, 0.01, 0.05, 0.1, 0.5, 1, 5 and 10 mM. The procedure followed for thermal denaturation and reaction with the thiol-reactive probe as in **section 2.6.2.1**.

2.7. Uptake assays

2.7.1. Radioactive uptake assays in *L. lactis* fused membranes

On the day of the experiment, 1 mL of membrane vesicle fusions (**section 2.5.6.2**) were thawed and a ten-fold stock of substrate was added. Vesicles were extruded 11 times through a 1 µm polycarbonate filter, passed through a pre-equilibrated PD10 column for removal of external substrate and collected in PIPES/NaCl buffer (as in **section 2.5.6.1**). Transport assays were carried out using a Hamilton MicroLab Star robot (Hamilton Robotics Ltd., Birmingham, UK). Transport of [^{14}C]-labelled ADP was initiated by the addition of 100 µL PIPES/NaCl buffer with 1.5 µM [^{14}C]-ADP to 5 µg vesicles in a MultiScreenHTS-HA 96-well filter plate (pore size 0.45 µm, Merck, Gillingham, UK). The uptake was stopped at 0, 10, 20, 30, 45, 60, 150 seconds, 5, 7.5, 10 and 15 minutes by the addition of 200 µL ice-cold PIPES/NaCl buffer and filtration with a vacuum manifold, followed by two additional wash steps with 200 µL ice-cold PIPES/NaCl buffer. Plates were dried overnight and the levels of radioactivity in the vesicles were measured by the addition of 200 µL MicroScint-20 (Perkin Elmer, Waltham, MA, USA) and by quantifying the amount of radioactivity with a TopCount scintillation counter (Perkin Elmer, Waltham, MA, USA).

2.7.2. Radioactive uptake assays in liposomes with reconstituted protein

Transport assays were carried out with a Hamilton MicroLab Star robot (Hamilton Robotics Ltd., Bermingham, UK). 100 µL of proteoliposomes in 20 mM HEPES-NaOH pH 7.5, 50 mM NaCl buffer were loaded per well in a MultiScreenHTS-HA 96-well filter plate (pore size = 0.45 µm, Merck, Gillingham, UK). Uptake assays of radiolabelled [^{33}P]-ATP, where indicated in the presence of inhibitors CATR, BKA, was initiated by the addition of 100 µL HEPES-NaOH buffer pH 7.5 with [^{33}P]-ATP at a concentration of 0.2, 0.5, 1, 2, 10, 50, 100 and 200 µM per well as indicated (the final concentration was hence half the above mentioned). The uptake of [^{33}P]-ATP was stopped after 0, 10, 20, 30, 45, 60, 150 seconds and 5, 7.5 and 10 minutes by addition of 200 µL ice-cold HEPES-NaOH buffer pH 7.5, 50 mM NaCl and the samples were filtered with a vacuum manifold, followed by two additional wash steps with 200 µL ice-cold buffer. Plates were dried overnight and subsequently, the radioactivity was measured by adding 200 µL MicroScint-20 (Perkin Elmer, Waltham, MA, USA) using a TopCount scintillation counter (Perkin Elmer, Waltham, MA, USA).

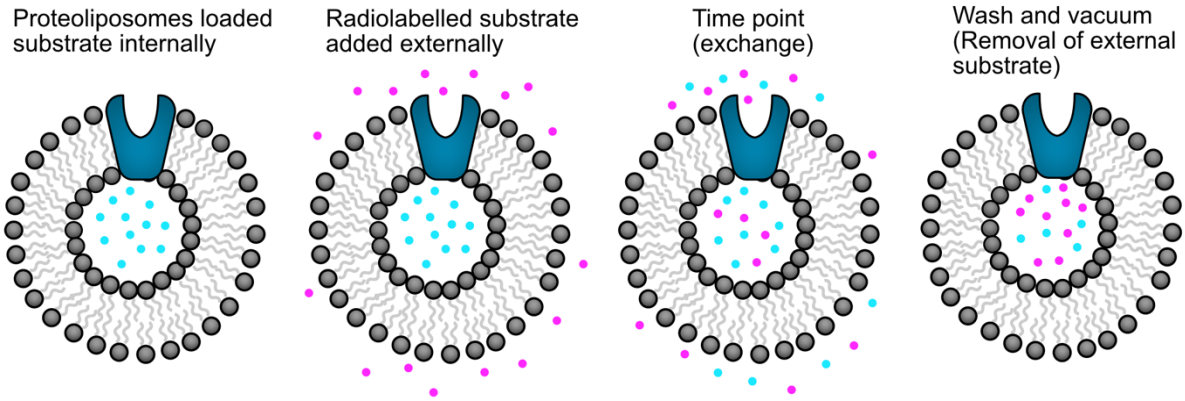

Figure 2.4: Schematic representation of radioactive uptake assays in liposomes. Proteoliposomes were loaded with non-radiolabelled substrate (1 mM ATP, cyan spheres) and substrate uptake was initiated by addition of radiolabelled substrate (magenta spheres) externally. The uptake was measured for 10 minutes with 10 time points. The reaction was stopped by wash with ice-cold buffer and filtration through 0.45 µm filters at 350 mbar vacuum for removal of the external substrate.

2.7.2.1. Protein quantification

Liposome samples were mixed with 5x loading buffer (as in **section 2.5.1.2**) and then separated on a pre-cast 4-20 % dodecyl sulphate-polyacrylamide gel electrophoresis

(SDS-PAGE) alongside pure TtAac protein standards (amounts used 0.025, 0.05, 0.1, 0.25 and 0.5 µg) to assist the protein quantification. The bands were visualised with InstantBlue Coomassie stain (Abcam, Cambridge, UK) and destained for 24 hours. Scanned images were analysed with Fiji software (Schindelin et al., 2012) using the gel analysis function.

2.8. SSM-based electrophysiology

The experiments for SSM-based electrophysiology were performed by Dr Andre Bazzone (Nanion Technologies GmbH, Munich, Germany).

2.9. Native mass spectrometry

The experiments for native mass spectrometry were performed by Dr Shahid Mehmood (Francis Crick Institute, London, UK).

The raw data of the functional complementation and the CPM assays will be available at doi: 10.17632/mrhnw45w5y.1. The statistical tests performed are shown in **Appendix 3**.

Chapter 3: The translocation pathway of the mitochondrial ADP/ATP carrier, selection of residues for mutagenesis and evaluation of protein function

3.1. Introduction

The mitochondrial ADP/ATP carrier is the archetypal member of the SLC25 family, the largest solute carrier family in humans (Ruprecht and Kunji, 2020). It has been used as a model to study the structural fold and transport mechanism of all members of the family (Kunji *et al.*, 2016; Ruprecht and Kunji, 2019). The carrier cycles between a cytoplasmic-open and a matrix-open state, alternately exposing the substrate binding site on the two sides of the mitochondrial inner membrane, in order to import ADP into mitochondria and export ATP, synthesised by the ATP synthase, to the cytosol (Klingenberg, 2008). Interconversion between the two states is triggered by substrate binding and release (Klingenberg, 2007; Robinson *et al.*, 2008), as this step provides the energy for disruption and formation of two gates, which contain one salt bridge network each, that seal the protein in a state-dependent way: In the cytoplasmic-open state, the matrix gate is formed and makes the carrier cavity inaccessible from the mitochondrial matrix, due to the formation of the matrix salt bridge network (Nelson *et al.*, 1998; Pebay-Peyroula *et al.*, 2003; Ruprecht *et al.*, 2014). Similarly, in the matrix-open state, the cytoplasmic gate forms and achieves the same via the formation of the cytoplasmic network (King *et al.*, 2016; Robinson *et al.*, 2008; Ruprecht *et al.*, 2019).

The multiple studies of this carrier have been facilitated by the availability of two high-affinity inhibitors, which bind in the two distinct conformational states and put the carrier in abortive states, so that it can no longer bind ADP and ATP (Klingenberg, 2008). ATR and CATR bind in the cytoplasmic-open conformation (Bruni and Luciani, 1962; Luciani *et al.*, 1971; Vignais *et al.*, 1971), whereas BKA in the matrix-open conformation (Erdelt *et al.*, 1972; Henderson and Lardy, 1970; Klingenberg and Buchholz, 1973). Crystal structures of these two states have been determined at high resolution (Pebay-Peyroula *et al.*, 2003; Ruprecht *et al.*, 2014; Ruprecht *et al.*, 2019),

defining the structural movements required for substrate translocation and confirming an alternating access mechanism (Ruprecht and Kunji, 2019).

However, the big unresolved question is where exactly do the substrates bind and how do they trigger these complex structural movements. All residues facing the water-filled carrier cavity could potentially be interacting with the substrates and have a role in this process. The main aim of this project was to investigate this problem in order to provide some answers for the question above. Mutagenesis was the selected approach, as it can serve as a powerful tool to interfere with the mechanism (Wagner and Benkovic, 1990), in combination with functional, biophysical and biochemical assays. The ADP/ATP carrier from the thermotolerant fungus *Thermothelomyces thermophila* was used as the study subject. In this chapter the preparatory work for this specific analysis is described.

3.1.1. Aims

The aims of this chapter were: firstly to identify the residues that are potentially involved in the mechanism of substrate binding; secondly, to target these residues with single alanine replacement mutagenesis and to assess the effect on the overall protein function by functional complementation assays; and finally, to express and purify the variants in yeast for their biophysical characterisation, in order to investigate their role in the substrate binding process.

3.2. Target selection and generation of single alanine mutants

In order to identify residues that could potentially participate in substrate binding, three factors were considered. Firstly, the residues had to be solvent accessible in the cytoplasmic-open and the matrix-open state, in order to be able to interact with the substrate. Secondly, they should be conserved among AAC orthologues, as their role needs to be preserved through evolution to maintain the specificity, or not interfere with it (Robinson *et al.*, 2008). Thirdly, as discussed in **section 3.1**, the protein operates by an alternating access mechanism, in which formation and disruption of the matrix and cytoplasmic networks makes the substrate binding site alternately accessible to the intermembrane space or the mitochondrial matrix (Ruprecht and Kunji, 2020). Therefore, the substrate binding site should be located in a region between these two networks.

The structures of the two conformational states, as well as an alignment of 128 AAC sequences, part of which is shown in **Figure 3.1** (the UniProt accession codes used for the full alignment are listed in **Appendix 2**) were used to identify which residues in the protein cavity meet these criteria. For the matrix-open state, the experimentally-determined structure of the mitochondrial ADP/ATP carrier from the fungus *Thermothelomyces thermophila* (TtAac) inhibited with BKA (Ruprecht *et al.*, 2019) was used. For the cytoplasmic-open state, a comparative homology model was used, based on the four determined structures of the bovine and yeast orthologues in that state (Pebay-Peyroula *et al.*, 2003; Ruprecht *et al.*, 2014), built by Dr Jonathan Ruprecht. In total, 48 solvent-exposed residues were identified between the salt bridge networks, five of which were alanine residues. From the remaining 42, five were not well conserved and the final two were glycine residues of the GxxxG motif (**section 1.5.2.2**), which are important for dynamic aspects of the mechanism (Ruprecht *et al.*, 2019; Ruprecht and Kunji, 2019) and were excluded. Therefore, 36 residues were found to fulfil the posed criteria (**Figures 3.2** and **3.3**). Each of these residues was replaced by the small and neutral amino acid alanine, generating a set of 36 variants. The choice of alanine was based on the grounds that it would disrupt any putative interaction formed between a residue and the substrates. At the same time, the size of the introduced side-chain should not cause any steric effects in the protein cavity.

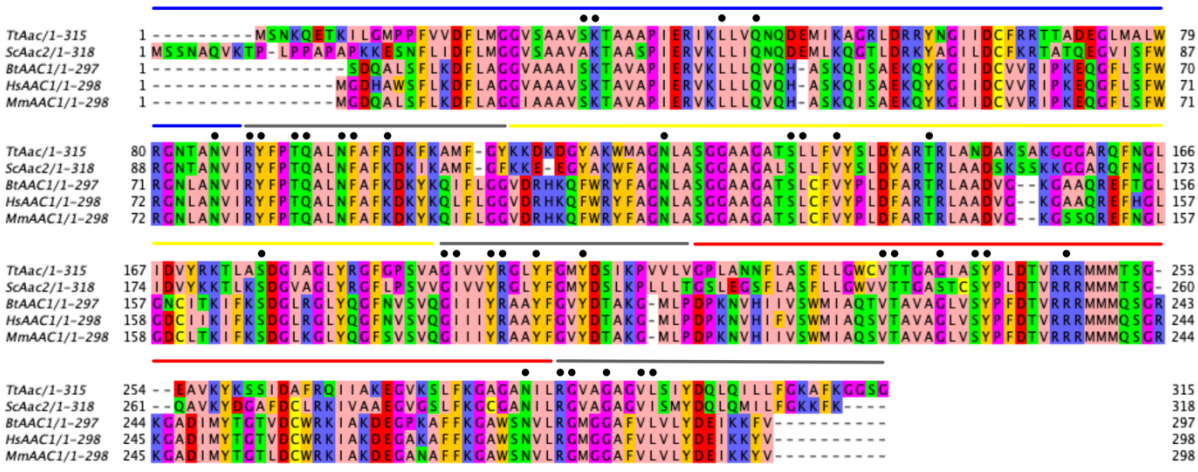

Figure 3.1: Alignment of AAC sequences showing the conservation of the selected target residues among different orthologues. The alignment was created with ClustalO and is part of a larger alignment composed of 128 sequences (**Appendix 2**). Blue, yellow and red bars indicate the core elements of the three domains and grey bars the gate elements (**Figure 1.5**). The target residues are indicated with a black sphere. Amino acids are coloured based on their properties (Zappo colour scheme):

Lys, Arg, His (basic) are blue; Asp, Glu (acidic) red; Asn, Gln, Ser and Thr (polar) green; Ala, Ile, Leu, Met, Val (aliphatic) pink; Phe, Tyr and Trp (aromatic) orange; Gly and Pro (structurally important) magenta and Cys yellow. Tt; *Thermothelomyces thermophila*, Sc; *Saccharomyces cerevisiae*, Bt; *Bos taurus*, Hs; *Homo sapiens,* Mm; *Mus musculus*.

The mutants were prepared using overlap extension PCR (Ho *et al.*, 1989), as described in **section 2.3.3**. The constructs for 10 variants, K30A, R88A, R100A, G192A, I193A, Y196A, R197A, S238A, R246A and R287A, were prepared by Dr Martin King.

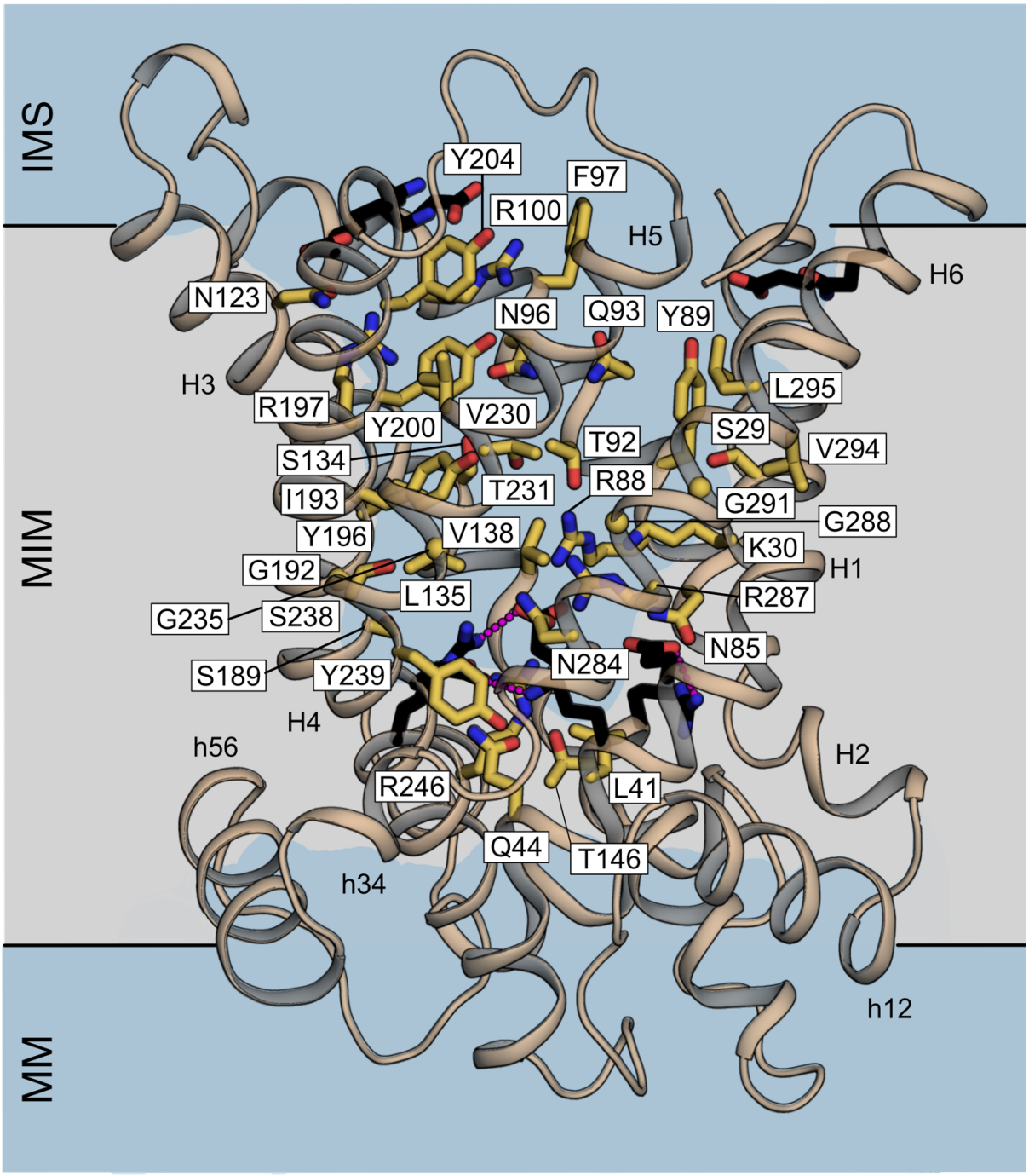

Figure 3.2: The amino acid residues analysed in this study mapped onto the cytoplasmic-open state. Membrane view of homology model of TtAac in the cytoplasmic-open state, generated with Modeller 9.22 based on PDB codes: 1okc, 4c9h, 4c9q and 4c9j. The residues analysed in this study are indicated as yellow sticks, whereas the residues of the matrix and cytoplasmic networks as black sticks, with ionic interactions shown as magenta dashes. The water-accessible surfaces are shown in blue.

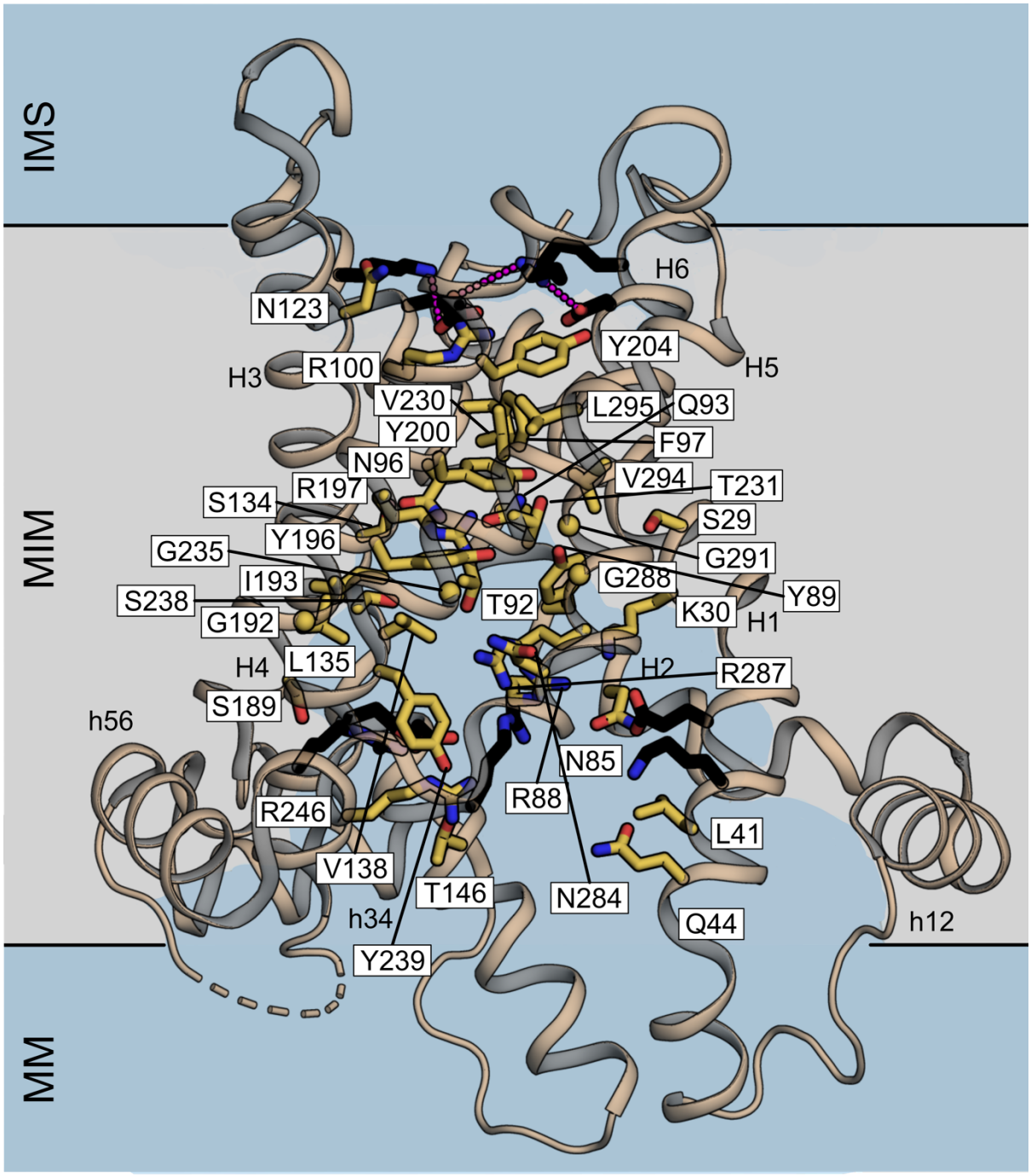

Figure 3.3: The amino acid residues analysed in this study mapped onto the matrix-open state. Membrane view of the matrix-open state (PDB code: 6gci chain A). The residues analysed in this study are indicated as yellow sticks, whereas the residues of the matrix and cytoplasmic networks as black sticks, with ionic interactions shown as magenta dashes. The water-accessible surfaces are shown in blue.

3.3. Functional complementation assays in strain WB-12

The first step was to use a functional complementation assay, to test the effect of each alanine mutation on the overall function of TtAac *in vivo*. Functional complementation

assays have been widely used to study protein function in many protein families, including the mitochondrial carrier family (SLC25). They have provided information on the physiological and pathological roles of different family members, including the ADP/ATP carrier (David et al., 2008; Heidkämper et al., 1996; Heimpel et al., 2001; Klingenberg and Nelson, 1994; Müller et al., 1996; Nelson et al., 1993; Ruprecht *et al.*, 2019; Thompson *et al.*, 2016; Zeman et al., 2003), the aspartate/glutamate carrier (Cavero et al., 2003; Wongkittichote et al., 2013), the Mg-ATP/phosphate carrier (Chen, 2004) and SLC25A42 (Fiermonte *et al.*, 2009). The advantage is that function is assessed in the mitochondrial membrane, hence the results are not affected by the isolation of mitochondria and protein purification procedures.

In the present study, an Aac deletion strain of *Saccharomyces cerevisiae*, the WB-12 strain (Hashimoto *et al.*, 1999) was used. *Saccharomyces cerevisiae* contains three Aac paralogues (Kolarov et al., 1990; Lawson and Douglas, 1988; O'Malley et al., 1982). Aac2 is the dominant paralogue in aerobic conditions, whereas Aac1 is expressed at low levels (Gawaz et al., 1990; Lawson et al., 1990). Aac3 is expressed under strictly anaerobic conditions (Kolarov *et al.*, 1990; Visser et al., 1994). In the WB-12 strain, *aac1* and *aac2* genes are disrupted (Hashimoto *et al.*, 1999). As a result, growth of this strain on non-fermentable carbon sources, such as glycerol, can be achieved only upon introduction of a functional ADP/ATP carrier in an expression vector. Therefore, growth tests of this strain on media containing a non-fermentable carbon source can be used to assess the activity of ADP/ATP carrier variants.

For this purpose, the WB-12 strain was transformed with the wild-type TtAac, an empty pYES3/CT derivative vector or each alanine variant and complementation assays on glycerol were performed. Introduction of the wild-type TtAac in WB-12 could fully restore growth on glycerol (**Figure 3.4**) and was defined as 100% complementation. The empty pYES3/CT derivative vector was used as a negative control to evaluate the background growth, which was negligible (**Figure 3.4**). Complementation of the mutant variants was expressed as a percentage of the wild-type growth after subtracting the background from both (as described in **section 2.6.1.2**).

From the 36 variants analysed, only 5 complemented growth to a similar extent as the wild type, whereas 19 did not grow at all (< 2.6 % of wild-type growth) and 12 complemented significantly less (18-76 % of wild type growth) (**Figures 3.4** and **3.5**). The five variants that grew similar to the wild type were S29A, V230A, G288A, G291A

and V294A (**Figures 3.4** and **3.5A**). These residues are located on H1, H5 and H6 (**Figure 3.5B**). Consistent with the results presented here, it was shown that a G291S mutant of the equivalent residue in ScAac2 could also grow on glycerol (Zeman *et al.*, 2003). The 12 variants that complemented growth, but to a significantly lesser extent than the wild type, were N85A, Y89A, T92A, Q93A, N96A, R100A, N123, S134A, V138A, Y200A, T231A and S238A. In agreement with the results of this study, a cysteine mutant of the equivalent residue of Y89 in ScAac2 has been shown to grow on glycerol as well (Zeman *et al.*, 2003), while variants R100A and S238A have been previously shown to complement growth of WB-12 (Ruprecht *et al.*, 2019). Additionally, the equivalent mutation of Y200A in ScAac2 has been shown able to grow on lactate as well (David *et al.*, 2008).

The 19 residues where alanine mutation yielded a non-functional protein (K30, L41, Q44, R88, F97, L135, T146, S189, G192, I193, Y196, R197, Y204, G235, Y239, R246, N284, R287 and L295), were dispersed throughout the translocation pathway (**Figure 3.5B**). The importance of some of these residues, particularly of the positively charged ones (K30, R88, R197, R246 and R287), has been reported in other studies as well, using yeast, bovine or human orthologues. It has been shown that alanine mutants of these five residues could not complement growth on glycerol (Heimpel *et al.*, 2001; Klingenberg and Nelson, 1994; Nelson *et al.*, 1993; Ruprecht *et al.*, 2019). Additionally, different substitutions have been tested with similar outcomes. Specifically, mutants equivalent to R88D/H/L/P (Heidkämper *et al.*, 1996; Heimpel *et al.*, 2001; Müller *et al.*, 1996; Nelson *et al.*, 1993), R197L (Heidkämper *et al.*, 1996; Klingenberg and Nelson, 1994; Müller *et al.*, 1996; Nelson *et al.*, 1993), R246I (Heidkämper *et al.*, 1996; Klingenberg and Nelson, 1994; Müller *et al.*, 1996; Nelson *et al.*, 1993) and R246G (Thompson *et al.*, 2016) were also shown not to grow on glycerol. For the remaining 14 variants that did not complement growth, there is relevant information for G192, I193, Y196 and Y204. Alanine mutants of these residues have been previously shown not to grow on glycerol (Ruprecht *et al.*, 2019) and for Y196 the equivalent mutation in ScAac2 (Y203A) has been shown not to grow on lactate either (David *et al.*, 2008). However, the equivalent mutation of Y204A in ScAac2 (Y211A) has been shown to complement growth on lactate, albeit with reduced phenotype compared to the wild type after 6 days (David *et al.*, 2008), in contrast with the results presented here. This difference could be related either to the differences in the used carbon source or the duration of incubation.

These results suggested that the majority of the residues in the translocation pathway are critical for efficient ADP/ATP exchange. However, cell growth is the resultant of many parameters and the functional complementation assay could provide limited information on which aspect of the ADP/ATP carrier function was affected. Biogenesis and targeting issues could prevent the mutant protein from being inserted correctly into the mitochondrial membrane. Even if correctly inserted, this assay could not discriminate between mutations affecting the folding of the protein, the structure or the transport mechanism and which aspect of it (e.g. substrate binding, dynamic movements or formation of the gates). Therefore, additional assays were needed to complement these results and to confirm whether the variants were expressed and folded and to evaluate their properties at the protein level.

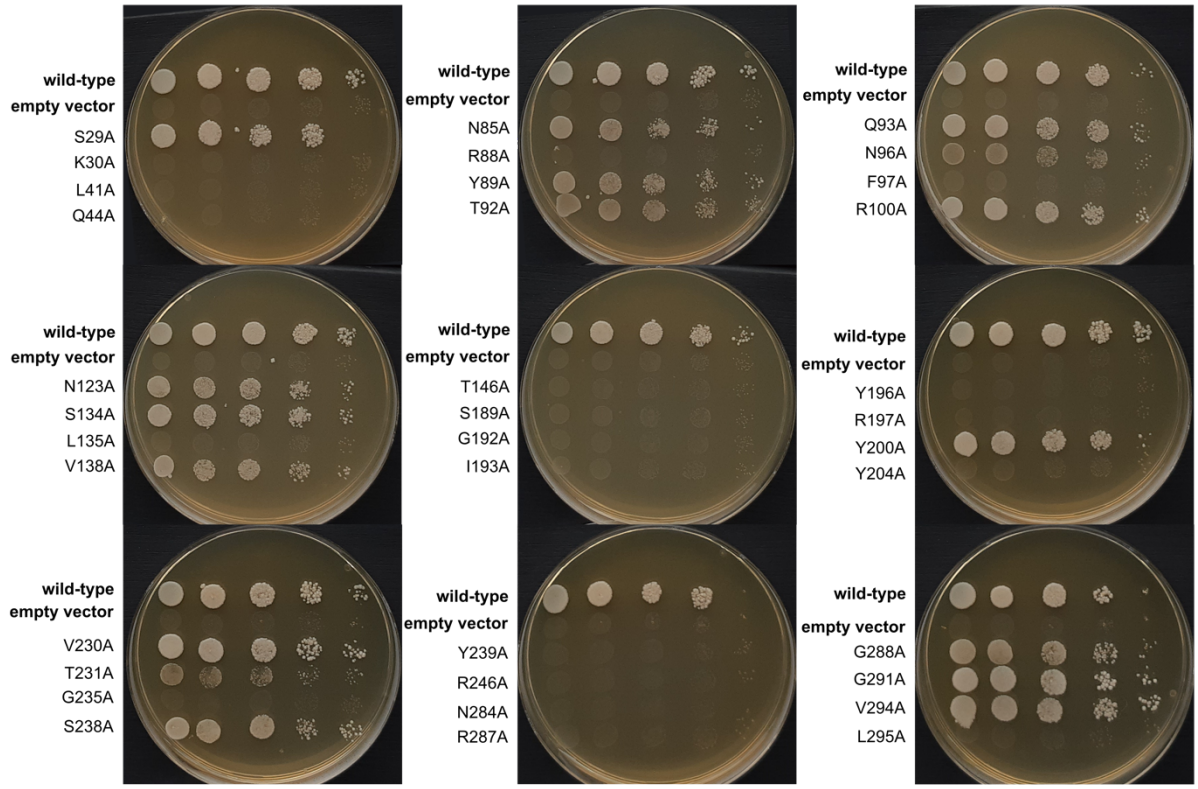

Figure 3.4: Functional complementation assay of the WB-12 strain expressing wild-type or variant TtAac. The images depict one representative experiment (performed 4 times) for each variant. Wild type and empty vector controls are included in each plate as reference. From OD_{600}=1, four serial (1/10) dilutions were made and cells were grown on YPG medium, 30°C for 72 h.

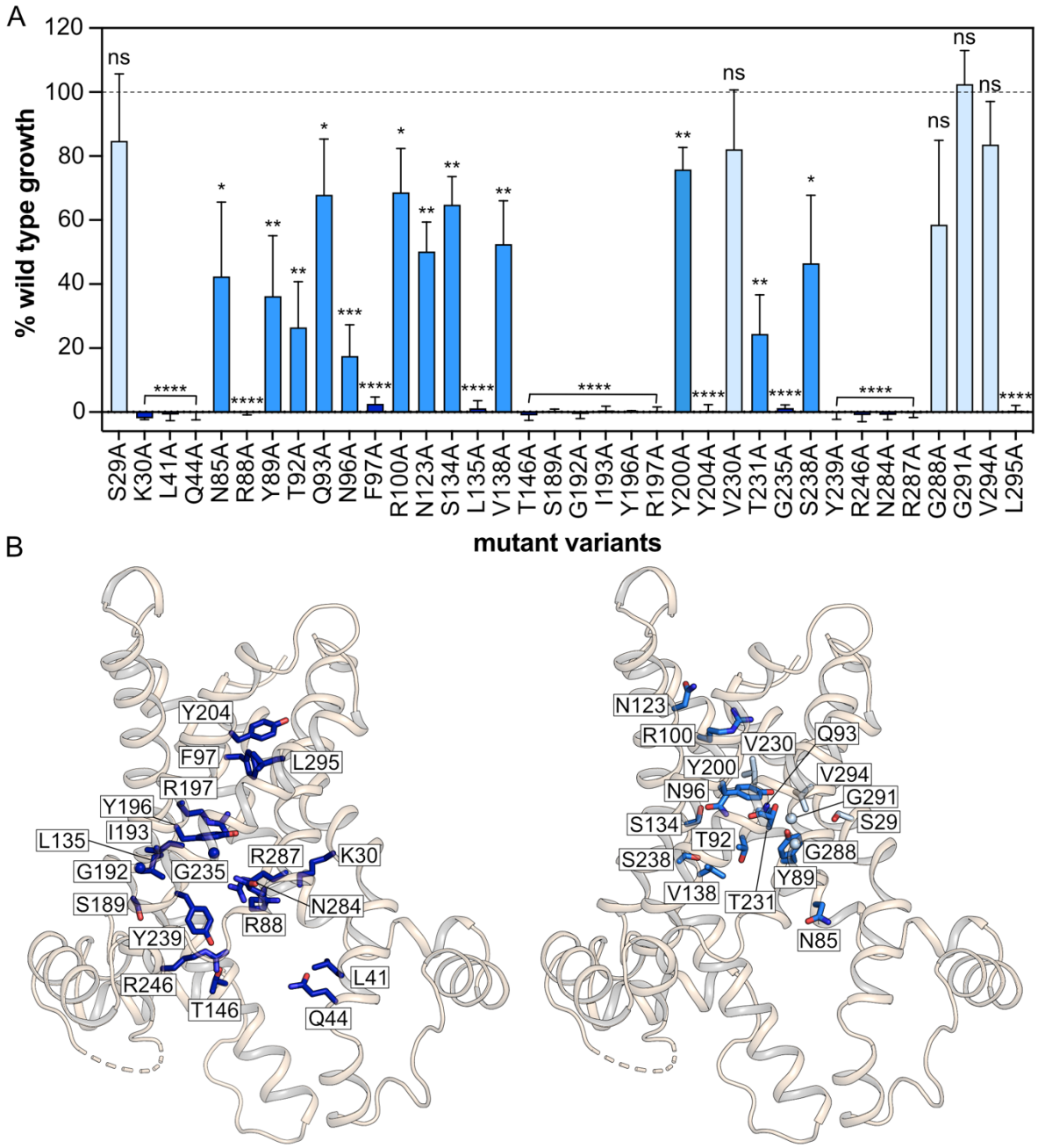

Figure 3.5: Most residues of the substrate translocation pathway are critical for function of TtAac (A) Percentage of functional complementation of the WB-12 strain expressing TtAac variants compared to expressing the wild-type carrier (100 % complementation), as determined by densitometry (**section 2.6.1.2**) of serial dilution spot tests on YPG medium (**Figure 3.4**). The bars and error bars represent mean and standard deviation of four independent experiments. Significance analysis was performed with two-tailed one sample t-tests, shown in **Appendix 3**, comparing the growth percentage of the variants to the mean percentage growth of the wild type. Differences were considered significant at the 5% level. ($p > 0.05$, ns; $p \leq 0.05$, *; $p \leq 0.01$, **; $p \leq 0.001$, ***; $p \leq 0.0001$, ****). Colours represent the three observed growth phenotypes: growth not affected significantly (ns), light blue; growth significantly affected ($0.5 \geq p > 0.0001$), marine; no growth ($p \leq 0.0001$), dark blue. (B) Position of

the residues alanine replacement of which resulted in no complementation (left) or complementation (significantly reduced or not) (right) mapped onto the matrix-open TtAac structure (PDB code: 6gci chain A). The structure is shown as cartoon representation and the residues as sticks or sphere for Gly and are color-coded as in (A).

Due to the aforementioned limitations of the complementation assay, it was necessary to use purified proteins, in order to gather information at the protein level for each variant and to be able to identify the ones in which the substrate binding step had been affected. Many assays have been used to evaluate binding of a ligand or substrate to membrane proteins and estimate affinity. These include thermostability assays, for example differential scanning fluorimetry (Niesen et al., 2007) and thermofluor-based thermal-shift assays, like the CPM thermostability assay (Alexandrov *et al.*, 2008) and the fluorescence-detection size-exclusion chromatography based thermostability assay (Hattori et al., 2012). Furthermore, affinity assays, for example scintillation proximity assays (Quick and Javitch, 2007), assays with radioactive ligands and other biophysical assays, for example microscale thermophoresis (Wienken et al., 2010), surface plasmon resonance (Patching, 2014) and isothermal titration calorimetry (Rajarathnam and Rosgen, 2014). The first step towards the use of those assays was to obtain purified proteins.

3.4. Small scale expression trials in strain W303-1B

In the complementation study, growth of most mutants was defective, hence this strain could not be used for protein expression and purification of the variants. To avoid this problem, the W303-1B strain of *Saccharomyces cerevisiae* was used, which contains all three Aac paralogues (Kolarov *et al.*, 1990; Lawson and Douglas, 1988; O'Malley *et al.*, 1982) and thus would allow the overexpression of all variants, irrespective of their functional state. The plasmids (containing the wild-type or mutated gene) were transformed into the W303-1B strain using the Li/Ac method (Gietz and Schiestl, 2007), as described in **section 2.4.5**. For small scale expression trials, mitochondria were isolated using a bead-beating procedure (**sections 2.5.2.1** and **2.5.2.2**) and expression was evaluated qualitatively by western blot analysis (**section 2.5.1.3**). All proteins could be expressed in those conditions (examples shown in **Figure 3.6**). Variants K30A, R88A, R100A, G192A, I193A, Y196A, R197A, S238A, R246A and R287A had been previously prepared by Dr Martin King and were not tested here.

These results indicated that the observed effects in the complementation assay (**Figures 3.4** and **3.5A)** were not due to expression and targeting issues, but a consequence of impaired protein function or structure. Therefore, the proteins were purified in order to further investigate their properties.

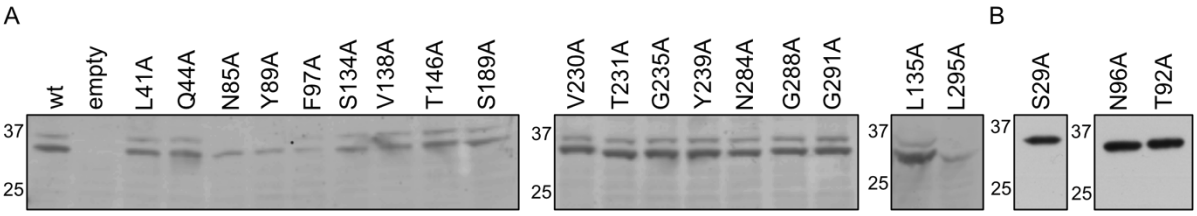

Figure 3.6: Examples of western blots for expression trials. The samples were separated on 4-20 % SDS-PAGE gels and transferred onto PVDF membranes. TtAac was detected with anti-His antibody (A) (Abcam, rabbit, 1:5,000/ secondary fluorescent Anti-rabbit antibody, Li-COR, 1:20,000) (B) (Roche, mouse, 1:25,000/ secondary HRP-conjugate Anti-mouse (Thermo Fischer Scientific 1:25,000).

3.5. Purification of the wild-type protein

The purification of TtAac by nickel-affinity chromatography was previously established (King *et al.*, 2016). The same protocol, with minor modifications, was used in this study, as described in **section 2.5.3**. Those conditions yielded sufficient levels of pure protein (**Figure 3.7**), approximately 2 mg TtAac per gram of crude mitochondria, as previously. Briefly, isolated crude mitochondria were solubilised with dodecyl-β-D-maltoside and after particulate material was removed, the soluble fraction was either incubated with nickel Sepharose beads (batch binding) or loaded onto a nickel Sepharose High Performance column connected to an ÄKTA prime FPLC (column binding). Bound proteins were released from the affinity chromatography beads/column by separating the His-tag from the protein by factor Xa protease treatment. The final untagged and pure protein sample was kept in a buffer containing HEPES/NaOH pH 7.5, NaCl, dodecyl-β-D-maltoside and tetraoleoyl cardiolipin.

Supplementation of buffers with cardiolipin is essential for the purification of unliganded mitochondrial carriers, because of their intrinsic instability in detergent solution (Crichton *et al.*, 2015). Cardiolipin is an abundant signature-lipid of the mitochondrial inner membrane (Horvath and Daum, 2013; Schenkel and Bakovic, 2014) and has been shown to significantly enhance stability of mitochondrial carriers (Crichton *et al.*, 2015; Klingenberg, 2009). Native cardiolipins are tightly bound to AAC

in three positively charged binding pockets at the N-terminal ends of the even-numbered and matrix helices (Nury *et al.*, 2005; Pebay-Peyroula *et al.*, 2003; Ruprecht *et al.*, 2014; Ruprecht *et al.*, 2019). Binding of these lipids has been proven essential for the structure and transport mechanism of the carrier, as reviewed in (Kunji and Ruprecht, 2020). Cardiolipin is believed to stabilise the detergent micelles additionally by introducing covalent bonds in the micelle. Since they are crosslinked lipid molecules via glycerol, they may follow a similar principle for stabilisation as the lauryl maltose neopentyl glycol detergents versus maltoside detergents.

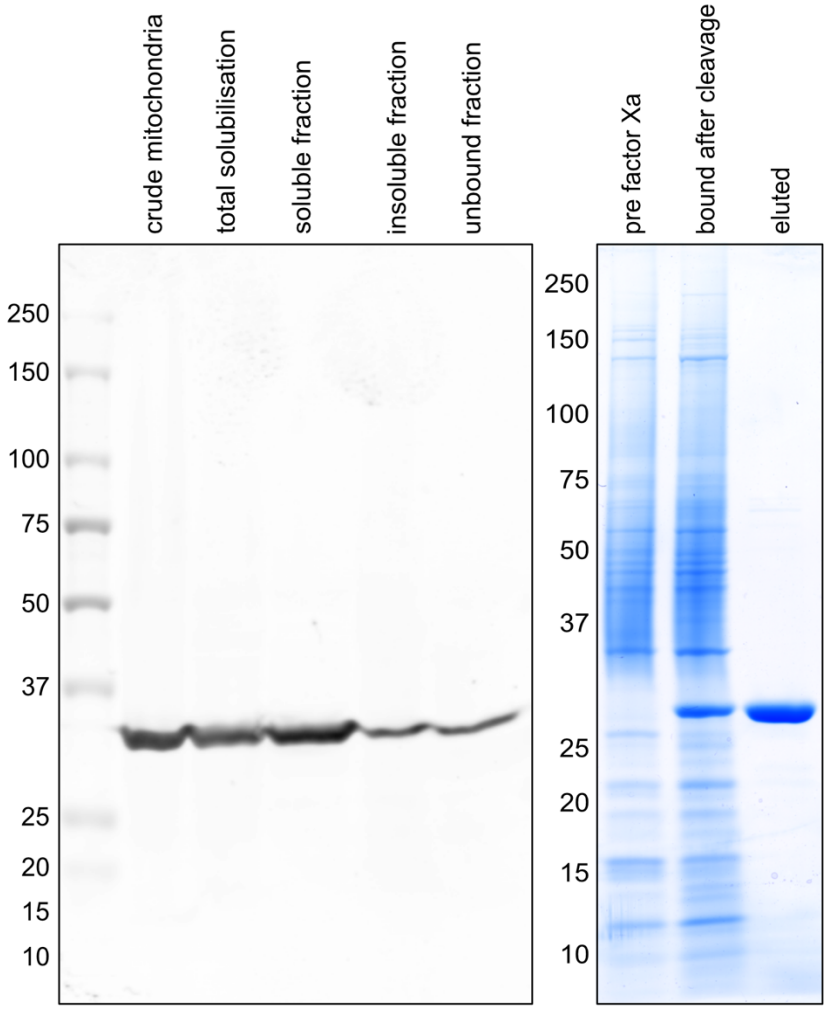

Figure 3.7: Purification of the wild-type protein. Western blot analysis was performed to detect His-tagged protein in the different steps of the purification procedure. 15 µL of each sample (volume of the original samples was made equal) were separated on a 4-20 % SDS-PAGE gel and transferred onto a PVDF membrane. TtAac was detected with an anti-His antibody (Roche, mouse, 1:25,000) and a fluorescent anti-mouse secondary antibody (Li-COR, 1:20,000). The steps after addition of factor Xa protease were analysed by SDS-PAGE. 5 µL of each sample (volume of the original samples was made equal) were separated on a 4-20 % SDS-

PAGE gel and the bands were visualised by Coomassie Blue staining. Molecular weight markers are indicated.

3.6. Purification of the variants

The same purification strategy was used for purification of the mutant variants. All of them were successfully purified (**Figure 3.8**). However, it was necessary to modify the purification protocol by reducing the cleavage time to two hours for mutants L41A, Q44A, N123A, L135A, T146A, G192A, I193A, R197A, Y239A, R246A, N284A, L295A, due to an increase in protein instability over time.

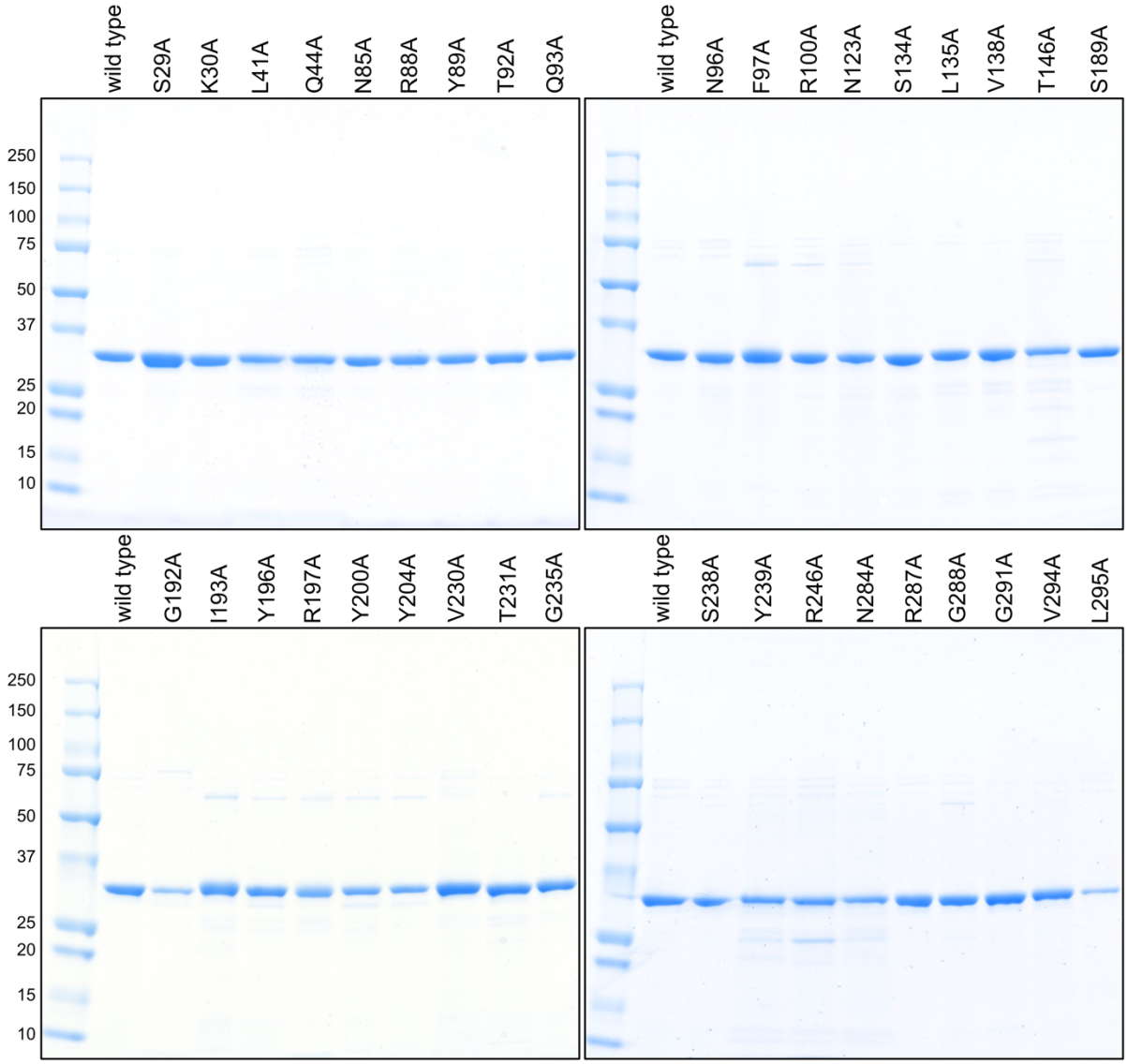

Figure 3.8: Purification of TtAac wild-type and variants. Approximately 2 µg of each protein were separated on 4-20 % SDS–PAGE gels and bands were visualised by Coomassie Blue staining. Molecular weight markers are indicated.

3.7. Assessment of protein stability and integrity of the binding pocket

In order to evaluate if the purified mutant proteins were folded and the mutations had not interfered with the structure and the integrity of the binding pocket, a thermostability assay which monitors the unfolding of a protein population with the thiol-reactive molecule 7-diethylamino-3-(4-maleimidophenyl)-4-methylcoumarin (CPM) in a temperature ramp (Alexandrov *et al.*, 2008) was used. As the protein population unfolds with the increase of temperature, the CPM reacts with initially buried cysteine residues that become solvent-exposed upon denaturation. The reaction yields a fluorescent adduct and hence measuring the fluorescence increase across the temperature ramp, an unfolding curve is obtained (**Figure 3.9**). The inflection point of this curve gives an apparent melting temperature (Tm) (Alexandrov *et al.*, 2008), which represents the temperature at which half of the protein population has reacted with the CPM molecule and the unfolding rate is maximal.

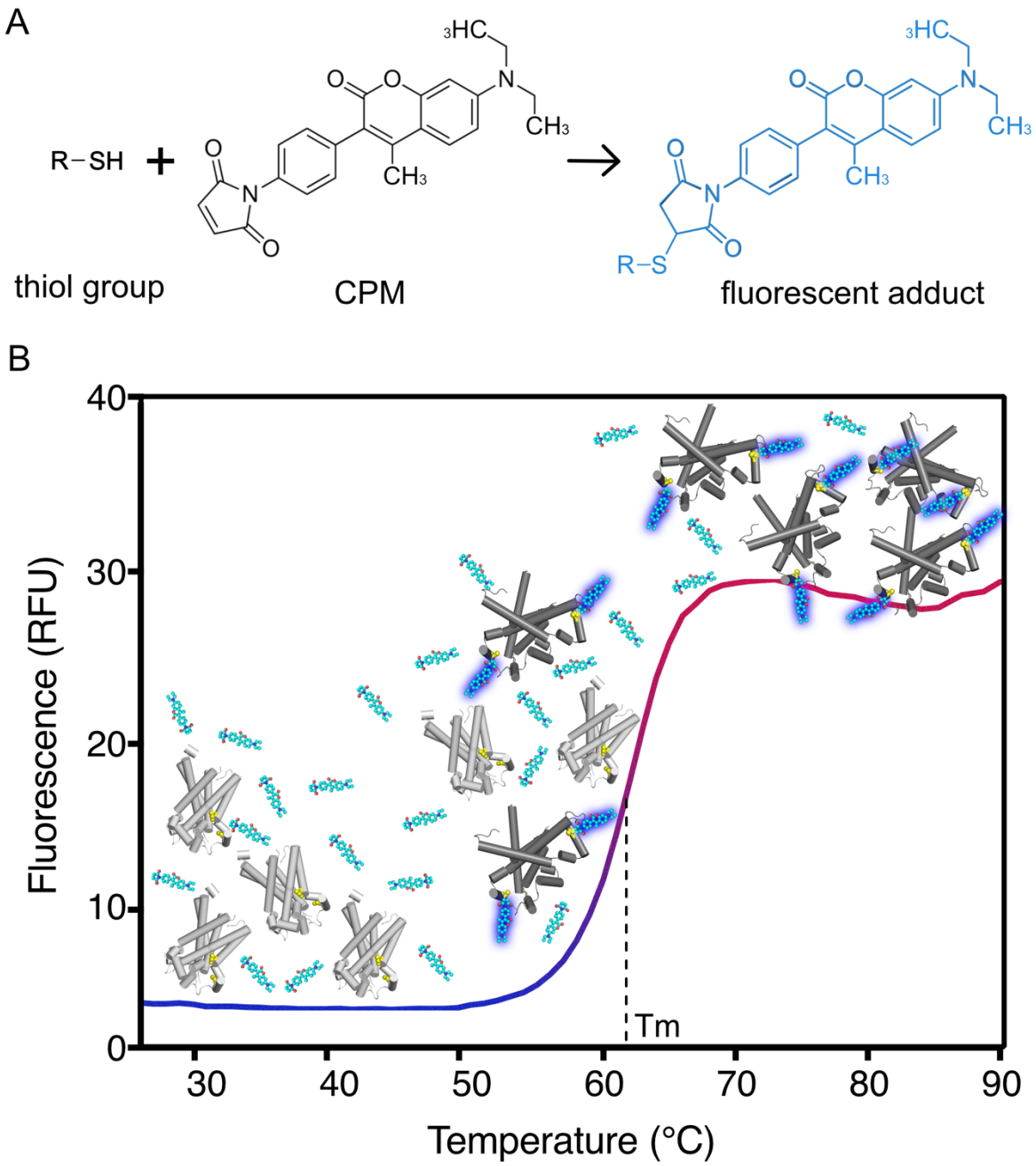

Figure 3.9: The CPM thermostability assay. (A) Chemical reaction of the CPM molecule with free thiols. The product is fluorescent. (B) Schematic representation of the unfolding of the protein population and the reaction with the CPM molecule that generates the protein-specific unfolding trace. The inflection point of this trace represents the apparent melting temperature (Tm).

The suitability of the assay is dependent on how many initially occluded cysteines are present within the protein. TtAac contains two cysteine residues, one in transmembrane helix H5 and one in the matrix helix h12 (**Figure 3.10**). It was shown previously that Cys229 is occluded in both the matrix-open and cytoplasmic-open

state, whereas Cys65 is occluded in the cytoplasmic-open state, but solvent-exposed in the matrix-open state, as observed in the presence of the state-specific inhibitor BKA (King *et al.*, 2016). This notion was later confirmed in the determined structure of TtAac in the matrix-open state (Ruprecht *et al.*, 2019).

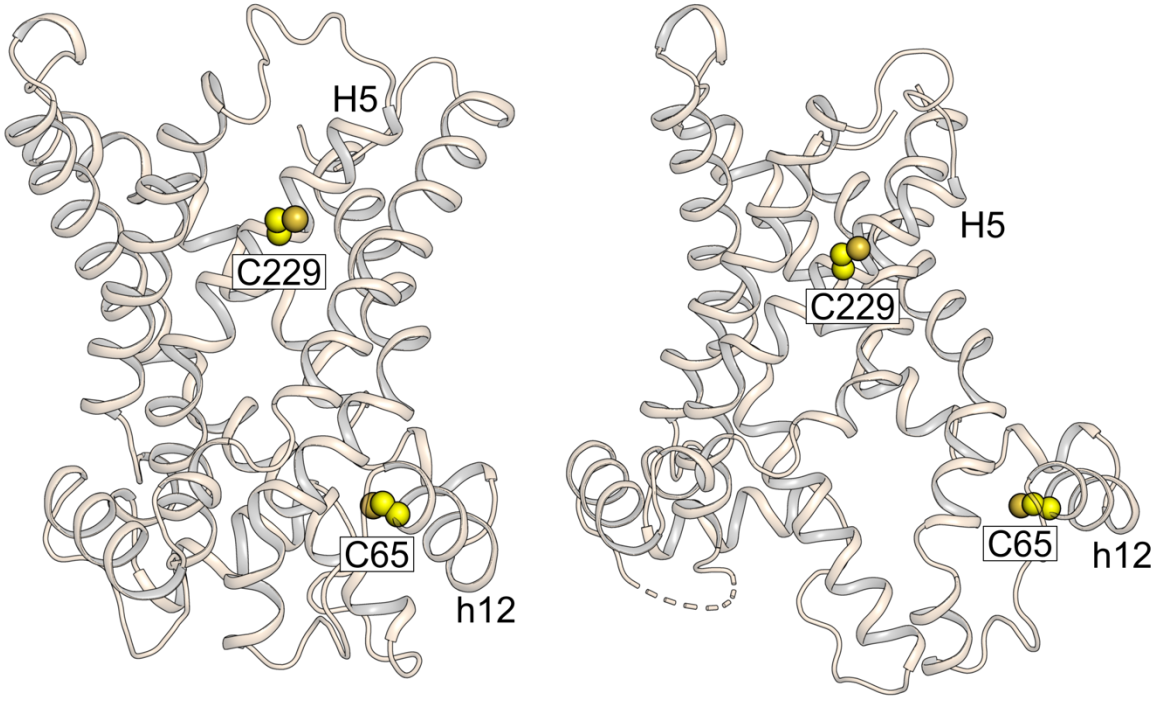

Figure 3.10: Location of cysteine residues in TtAac cytoplasmic-open and matrix-open state. Membrane view of homology model of TtAac in the cytoplasmic-open state (left), generated as in **Figure 3.2** and the experimentally determined structure of TtAac in the matrix-open state (right) (PDB code: 6gci chain A) shown as cartoon representations. Cysteine residues are represented with yellow spheres and the helices they are located in are labelled.

It has been established that the CPM thermostability assay can provide information on the folding state of membrane proteins and their stability under different purification and crystallisation conditions (Alexandrov *et al.*, 2008; Crichton *et al.*, 2015; Errey et al., 2015; Miljus et al., 2020). Additionally, shifts in the thermostability profile can reflect binding of inhibitors (Crichton *et al.*, 2015; Jaiquel Baron et al., 2021; King *et al.*, 2016; Ruprecht *et al.*, 2019; Tavoulari *et al.*, 2019) and other effectors (Harborne *et al.*, 2017; Heimpel *et al.*, 2001). These occur because specific interactions are forming between the protein and the ligand molecules (Crichton *et al.*, 2015), as explained in **section 3.7.3**. Binding of ligands indicates that the protein is well folded and that the binding pocket is intact.

Hence, such assays were used to evaluate the condition of the purified mutant proteins. The apparent Tm values of the proteins without the addition of any effector, as well as their apparent Tm in the presence of the inhibitors CATR and BKA+ADP were used as indicative measures. In the case of BKA, it is necessary to add a small amount of substrate (e.g. 5 μM ADP) to allow the carriers to cycle and transition to the matrix-open state, enabling the binding of BKA (King *et al.*, 2016) (**Figure 3.11**). The cytoplasmic-open conformation is probably more frequent in the protein population because of the mitochondrial isolation and purification procedures: after the carriers export all substrates that are present inside the mitochondria, they cannot transition back to the matrix-open state, because no substrate is present in the mitochondria-preparation buffers and the purification buffers (King *et al.*, 2016).

In the CPM assay, the wild-type protein presents a sigmoidal unfolding curve with the apparent Tm without addition of any effector to be 50.2 ± 0.6°C (average of eight biological repeats) (**Figure 3.11**). In presence of CATR and BKA, it was known that the apparent Tm is increased by ~30°C and ~10°C, respectively (King *et al.*, 2016). These results were reproduced in this analysis, with the apparent Tm in presence of CATR being 78.9 ± 1.0°C and in presence of BKA 60.3 ± 0.6°C (average from eight biological repeats, each with 3 technical replicates) (**Figure 3.11**). When most of the protein population is in the matrix-open conformation, e.g. in presence of BKA, there is a raised fluorescence baseline, because Cys65 contributes to the signal from the beginning of the assay, as it is directly accessible and thus cannot be used for monitoring the unfolding of the protein population. In contrast, when most of the protein population is in the cytoplasmic-open conformation, both cysteines contribute to the signal (**Figures 3.10** and **3.11**).

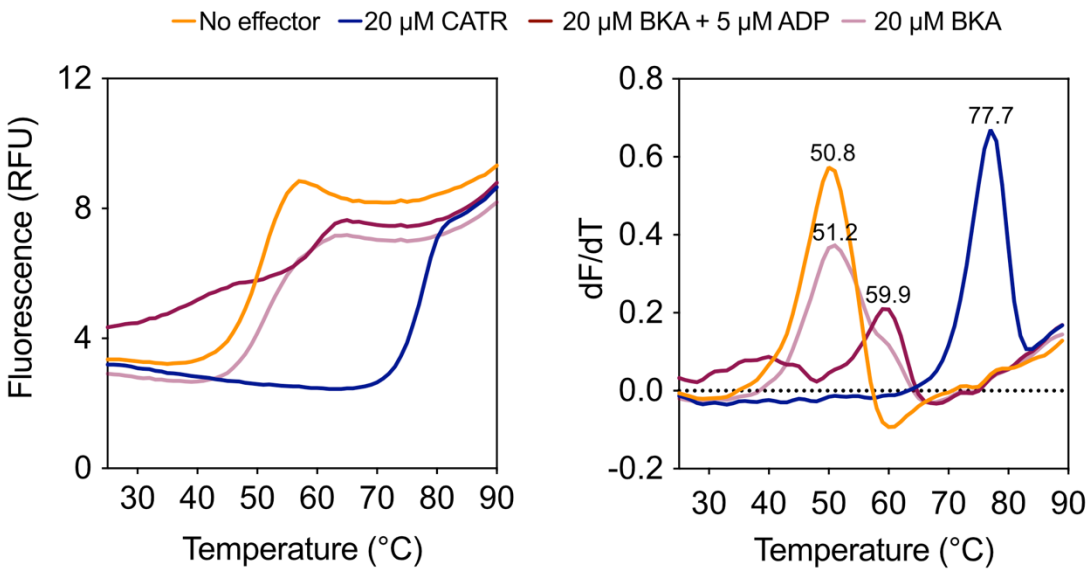

Figure 3.11: The thermostability profile of the wild-type TtAac. Typical thermal denaturation curves (left) and corresponding first derivatives (right) without addition of any effector and in the presence of the state-specific inhibitors CATR and BKA. Approximately 3 µg of protein were used in each condition and the assay was performed with three technical replicates.

The effect of the inhibitors on the wild-type protein was also evaluated in absence of a temperature ramp, but over time. The time experiments were performed at three different temperatures, 25°C, 35°C and 45°C (**Figure 3.12**). It can be observed that in absence of inhibitors, the higher the temperature the assay is performed at, the higher the fluorescence baseline. At 25°C, the unfolding trace started at around 6 RFU (relative fluorescence units), while at 35°C and 45°C at around 9 and 10 RFU, respectively. This result indicates that at higher temperatures, a bigger part of the protein population is initially unfolded. Over time, the fluorescence increased in all three experiments, showing that the population was gradually unfolding, but the unfolding rate was different. The highest unfolding rate was observed at 45°C. The fluorescence reached levels of around 16 RFU in the 25°C experiment, while at 35°C and 45°C it reached about 22 RFU. In presence of CATR, this profile was altered. The fluorescence baseline started lower than the ‘’no effector’’ condition in all three temperatures (around 6 or 7 RFU), indicating that the population had bound the inhibitor and was in a more stable state. The fluorescence remained nearly constant throughout the experiment at 25°C and at 35°C, while at 45°C it increased slightly, reaching levels around 11 RFU. This showed that CATR provides a protective effect against unfolding, which at lower temperatures can be translated

as almost no unfolding, while at higher temperatures as unfolding with much slower rates than in the absence of the inhibitor (**Figure 3.12**). In presence of BKA + ADP, for the 25°C and 35°C experiments, there was initially a small period of time (~250 s) during which there was an increase in fluorescence of about 2 RFU levels. This rise might reflect the time it takes until the majority of the population binds the inhibitor. Subsequently, the fluorescence level remained almost constant at these two temperatures at around 10 and 13 RFU respectively. At 45°C, there was a gradual increase in fluorescence, following a linear trend, which starting from about 10 RFU lead to fluorescence levels of around 16 RFU. In all three temperatures though, the fluorescence in presence of BKA was lower than in the absence of the inhibitor, demonstrating its protective effect (**Figure 3.12**). However, the fluorescence was higher than in presence of CATR, because in the matrix-open state Cys65 is exposed to solvent (**Figure 3.10**).

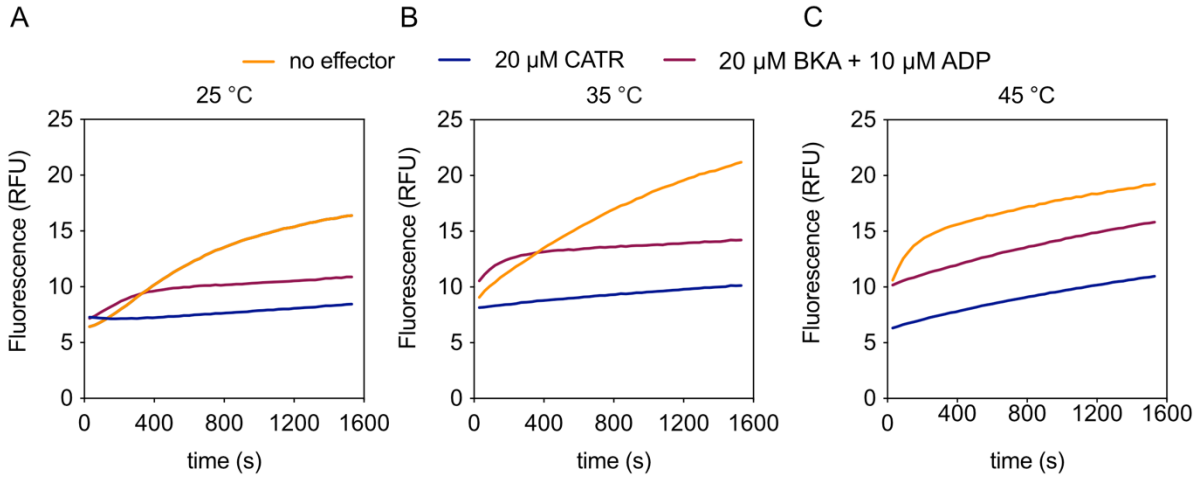

Figure 3.12: The stabilising effect of the inhibitors CATR and BKA evaluated over time. Unfolding traces of TtAac at 25°C (left), 35°C (middle) and 45°C (right) in absence of effectors and in presence of the inhibitors. Each trace is generated from three technical replicates and approximately 3 µg of protein were used for each condition.

3.7.1. Five variants were in an unfolded state

In order to assess the stability of the variants, the CPM thermostability assay (in presence of a temperature ramp) was used. Five variants, L41A, Q44A, T146A, Y239A and N284A, were found to be unfolded, as judged by the high initial fluorescence and the absence of a sigmoidal unfolding curve (**Figure 3.13A**). This effect could not be

rescued by inhibitor binding, as no unfolding trace could be obtained in the presence of inhibitors either (**Figure 3.13A**). Small modifications to the purification protocol (e.g. reducing the cleavage time from overnight to two hours), which helped purify other unstable variants (**section 2.5.3**), did not alter this result. This negative result was reproducible also between purifications performed from mitochondria isolated from different fermenter runs (**Table 4.2**).

Notably, all of these residues are located in the matrix gate (**Figure 3.13B**). The matrix gate provides an insulation layer, preventing the dissipation of the proton motive force through proton leak, when the carrier is in the cytoplasmic-open state (Ruprecht *et al.*, 2019). Residue Q44 is the glutamine brace between H1 and H5 in the cytoplasmic-open state (Ruprecht *et al.*, 2014), while residues T146 and Y239 have been shown to be important for the structural stability of the carrier in molecular dynamics simulations (Yi et al., 2019). Their important role was shown in the complementation assays as well, as all five mutants did not grow (>3 % complementation) (**Figures 3.4** and **3.5**), even though they were expressed, targeted to the mitochondrial inner membrane and could be purified (**Figures 3.6** and **3.8**). These five mutants were, hence, not included in any further analyses and their involvement in substrate binding could not be established.

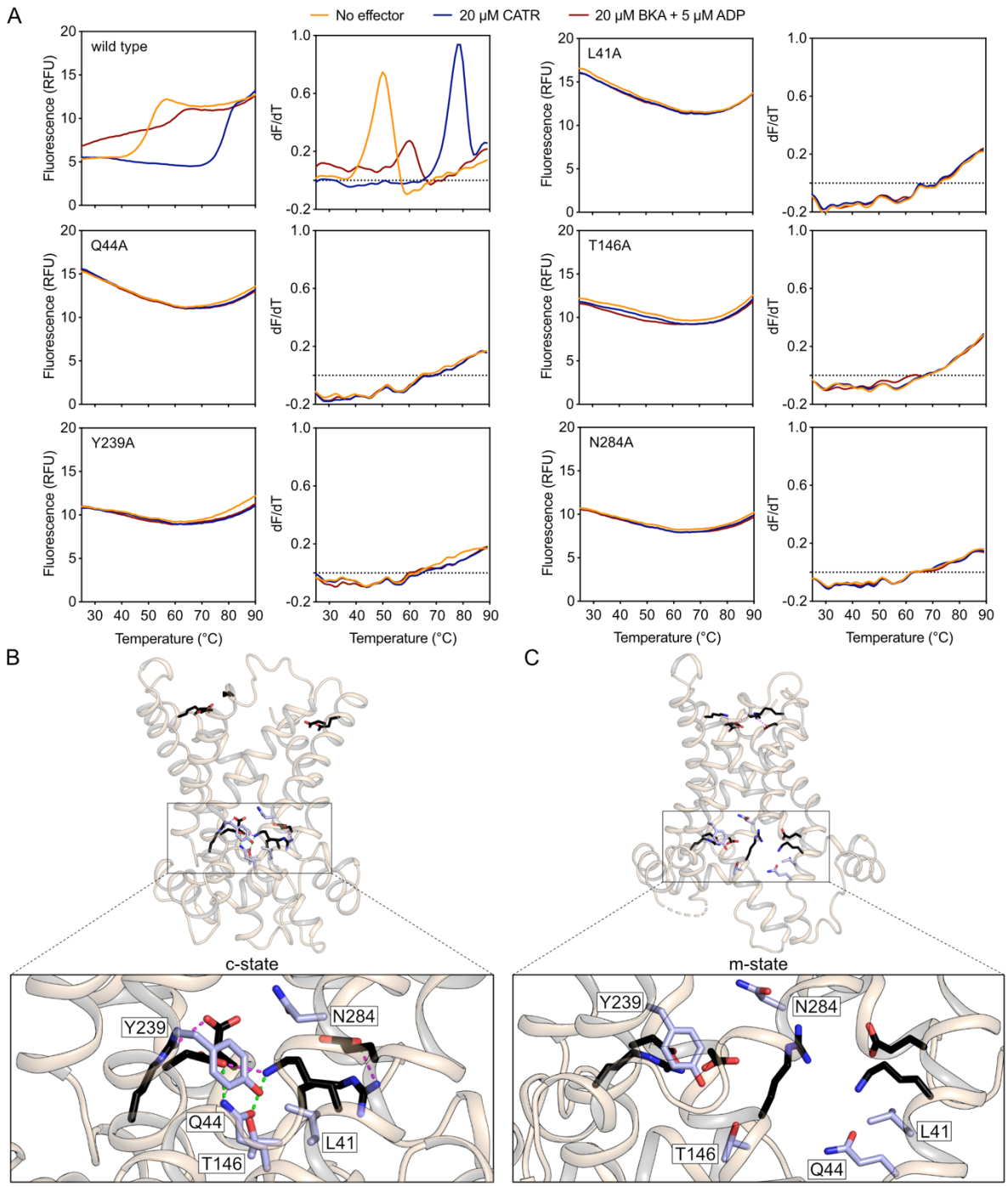

Figure 3.13: Thermostability profiles and residue positions of the five unfolded variants. (A) Typical thermal denaturation profile (left) and corresponding first derivative (right) of the wild type and the unfolded variants. The traces represent one representative experiment and are the average of three technical replicates. Approximately 3 µg of protein were used for each condition. Membrane view of (B) TtAac cytoplasmic-open model (generated as in **Figure 3.2**) and (C) of experimentally determined matrix-open structure (PDB 6gci chain A). The residues which yield unfolded proteins after replacement with alanine are shown in violet sticks. Residues of the matrix and cytoplasmic networks are shown as black sticks with salt bridges shown as magenta dashes. Green dashes represent the hydrogen bond interactions

bracing H1 with H5 in the cytoplasmic-open state. The insets show details of the matrix gate environment in the two different states.

3.7.2. Thirty-one variants were well folded and stable

Most variants (24 of the 36) had a similar apparent Tm value (48.2-52.8°C) as the wild-type TtAac (50.2 ± 0.6°C) (**Figure 3.14**), suggesting that the alanine mutation could be tolerated in the corresponding positions. Interestingly, variants K30A (57.3 ± 1.2°C), R88A (53.1 ± 1.0°C), R100A (53 ± 0.8°C), R287A (64.4 ± 0.2°C), G291A (55.9 ± 0.3°C) and V294A (53.7 ± 0.5°C) were significantly more stable than the wild type. As an exception, I193A was significantly less stable (45.2 ± 4.6°C) (**Figure 3.14**) and presented with a variable stability between experiments, as shown in **Chapter 4**. However, in each independent repeat, it did show a sigmoidal unfolding trace, similar to the one obtained for the wild type, but the values of the apparent Tm were variable between experiments. Since it was possible to obtain an unfolding trace in all conditions tested, this mutant was included in all analyses.

Furthermore, all 31 folded mutants were responsive to both inhibitors (**Figure 3.15**), unless the mutated residue was participating in a specific interaction with the inhibitor. In this case, the thermal shift to higher Tm value was reduced or abolished and these results could be used to map the binding sites of the inhibitors, as analysed in **section 3.7.3**. Taken together, the CPM thermostability data showed that with the exception of the five unfolded variants, all were well folded and stable, hence suitable for biophysical characterisation and evaluation of their role in substrate binding.

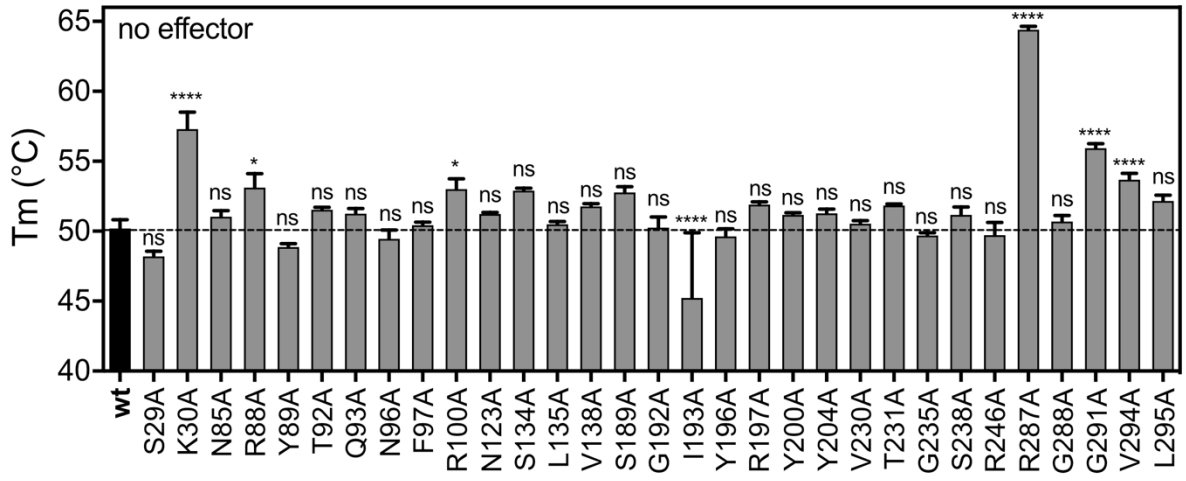

Figure 3.14: CPM thermostability data of each protein in absence of effectors. The bars and error bars represent the mean and sample standard deviation of 8 independent experiments for the wild type and 2-7 for the variants. Differences

between the variant-specific Tm values vs the wild-type Tm value were evaluated with one-way ANOVA, followed by Dunnett post hoc test to correct for multiple comparisons. Differences were considered significant at the 1% level ($p > 0.01$, ns; $p \leq 0.01$, *; $p \leq 0.001$, **; $p \leq 0.0001$, ***; $p \leq 0.00001$, ****).

3.7.3. The binding sites of CATR and BKA

As previously reported (King *et al.*, 2016) and noted in **section 3.7.2**, the inhibitors CATR and BKA induce a thermal shift to the wild-type TtAac, which can be monitored with the CPM assay. This shift occurs because of the specific interactions forming between the inhibitor and the protein. It has been shown, by comparing proteins from thermophilic organisms with their mesophilic homologues, that the existence of salt bridges (Kumar et al., 2000; Panja et al., 2015; Sadeghi et al., 2006) and hydrogen bonds between side chains (Kumar *et al.*, 2000) or main chains (Sadeghi *et al.*, 2006) increase protein stability. It is possible that the interactions forming upon binding of an inhibitor affect stability in a similar way. In addition, it has been demonstrated that ligands can stabilise membrane proteins in a concentration-dependent and affinity-dependent manner, increasing the stability when applied in concentrations higher than the dissociation constant (K_d) (DeSantis et al., 2012). These properties for CATR and BKA were evaluated in presence of a temperature ramp (**Figures 3.11** and **3.15**) and also in absence, but over time (**Figure 3.12**).

CATR forms four salt bridges with the protein and two hydrogen bonds, as well as multiple van der Waals interactions (Pebay-Peyroula *et al.*, 2003; Ruprecht *et al.*, 2014). Three salt bridges are formed between the sulphate groups of CATR and two positively charged residues ($R204_{ScAac2}$/$R197_{TtAac}$ and $K108_{ScAac2}$ /$R100_{TtAac}$) and one between the carboxyl group of CATR and a positively charged residue ($R96_{ScAac2}$/$R88_{TtAac}$). The interaction with residue $K108_{ScAac2}$ /$R100_{TtAac}$ is observed in one of the crystal packing arrangements for ScAac2 (PDB entry 4c9h chain B), in all ScAac3 crystals (PDB entries 4c9q and 4c9j) and in one of the bovine structures (PDB entries 1okc). The two hydrogen bonds involve one of the sulphate groups of CATR and a polar residue ($N104_{ScAac2}$/$N96_{TtAac}$) and the second the hydroxyl group and a positively charged residue ($R252_{ScAac2}$/$R245_{TtAac}$). The van der Waals interactions are not completely conserved between the solved structures (See Table S3 in (Ruprecht *et al.*, 2014)). TtAac is closely related to ScAac2, sharing 74% sequence identity, hence the residues participating in CATR binding are expected to be highly conserved. The existence of these interactions lead to a thermal shift of ~30°C for the wild-type

TtAac (**Figure 3.11**) (King *et al.*, 2016). Notably, mutation of the residues interacting with the inhibitor resulted in significantly reduced shift compared to the wild type (**Figure 3.15**) (Ruprecht *et al.*, 2019). Residues R100, S134 and S238 were observed to interact with CATR in the structure of ScAac2 PDB entry 4c9h (and are indicated in **Figure 3.15**) but were not consistently observed in all structures, hence it is not possible to confidently predict if they would interact in the case of TtAac. Furthermore, the equivalent of residues K30 and R246 were shown in the bovine structure to form interactions with the inhibitor mediated via water (Nury et al., 2006; Pebay-Peyroula *et al.*, 2003). It is possible that these interactions are formed in the case of TtAac too, hence a reduced shift is observed for these two variants (**Figure 3.15**).

BKA interacts through seven salt bridges, three hydrogen bonds and multiple non-bonded interactions with the protein (Ruprecht *et al.*, 2019). Four salt bridges are formed between two carboxyl groups of BKA and residue R197 and the other three between the other carboxyl group and residues R88 and K30. The hydrogen bonds involve residues Y89, N96 and Y196. These interactions enhanced the stability of the protein by ~10°C (**Figure 3.11**) (King *et al.*, 2016). Similar to the residues participating in CATR binding, mutation of the residues involved in BKA binding also resulted in significantly reduced shifts, in presence of BKA, compared to the wild type (**Figure 3.15**) (Ruprecht *et al.*, 2019).

It is interesting to note that apart from the residues involved in predominant interactions with the inhibitors, e.g. salt bridges and hydrogen bonds, mutation of residues contributing to the binding site with non-bonded interactions had a very significant effect too, in many cases (e.g. G192, I193, Y196 for CATR and Q93, S134, L135, V138, I193, Y200, R287 and G291 for BKA). This indicates that the CPM assay can be reliably used to detect both strong and weak interactions, making it a powerful tool to study protein-ligand interactions and in this way, all residues involved in inhibitor binding could be identified.

Furthermore, in the case of BKA, mutants F97A, R100A, N123A, Y204A and L295A presented a significantly reduced shift in presence of the inhibitor, even though they do not participate in its binding site. However, all these residues are part of the hydrophobic plug of the matrix-open state (Ruprecht *et al.*, 2019). Specifically, Y204 and R100 act as braces for the cytoplasmic network (Ruprecht *et al.*, 2019). Therefore, these residues might be critical for the formation or stability of the matrix-open state, so the observed effect is not directly related to BKA binding, but to the instability of the

matrix-open state. A similar finding was reported for alanine substitution of the residues of the cytoplasmic salt bridge network. The weaker the network (hence more unstable matrix-open state), the smaller the BKA-induced increase in the apparent Tm (King *et al.*, 2016).

Importantly, the thermostability data obtained upon addition of the inhibitors to the mutant proteins provided two pieces of information. Firstly, they showed that the mutants were well folded and suitable for further analysis, with regards to substrate binding, as presented in **Chapters 4** and **5**. Secondly, it was possible to map the binding sites of the inhibitors, which were defined by the crystal structures (Pebay-Peyroula *et al.*, 2003; Ruprecht *et al.*, 2014; Ruprecht *et al.*, 2019). The approach identified a few cases where the response of the mutant was not affected directly by interaction with the inhibitor, but was an indirect effect (e.g. potentially affected stability of variants F97A, R100A, N123A, Y204A and L295A in the matrix-open state, thus showing a reduced shift compared to the wild type in presence of BKA). This gave the opportunity to consider some 'false positives', highlighting the need for additional validating assays. However, since the obtained functional data agreed overall with the structural analysis, this provided proof that the CPM assay can be used to identify residues involved in protein-ligand interactions, a principle which will be employed in **Chapter 4** for the determination of residues interacting with the substrate.

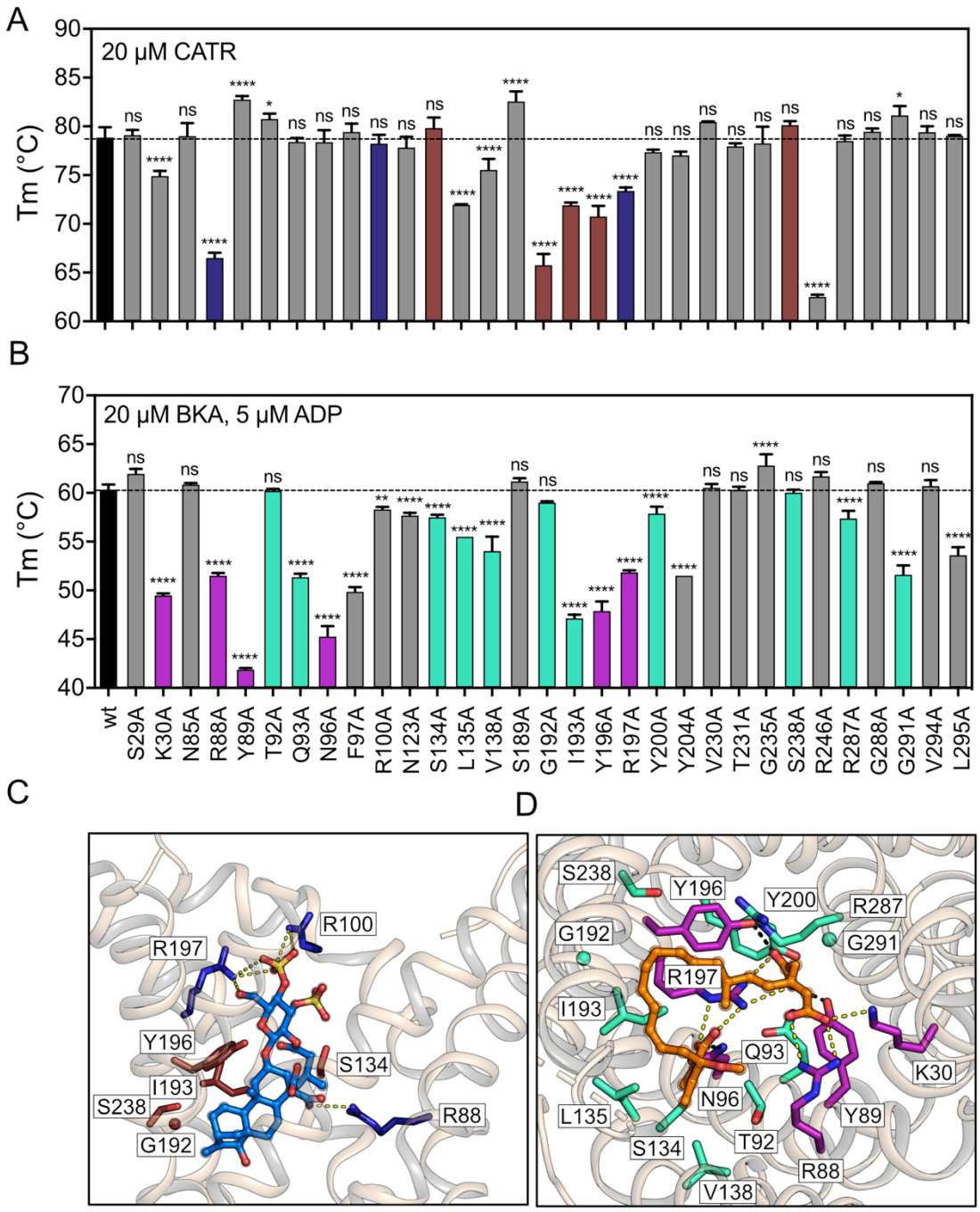

Figure 3.15: Mapping the binding sites of inhibitors CATR and BKA (A,B) CPM thermostability data of each protein in presence of CATR (A) or BKA (B). The bars and error bars represent the mean and sample standard deviation of 8 independent experiments for the wild type and 2-7 for the variants. Significance analysis for each condition was performed with one-way ANOVA, followed by Dunnett post hoc test to correct for multiple comparisons. Differences were considered significant at the 1% level ($p > 0.01$, ns; $p \leq 0.01$, *; $p \leq 0.001$, **; $p \leq 0.0001$, ***; $p \leq 0.00001$, ****). (C) Lateral view of ScAac2 cytoplasmic-open state structure in complex with CATR (PDB code: 4c9h chain A), indicating the position of equivalent residues of TtAac analysed in this study. Residues that form ionic interactions (yellow dashes) and hydrophobic contacts with CATR (marine) are shown in dark blue and brown, respectively. The

CATR binding site is highly conserved between the two fungal proteins, sharing 74% sequence identity. Residue K104 of ScAac2 has been modelled to Arg (R100) for TtAac. (D) Matrix view of the matrix-open structure of TtAac with BKA bound (PDB code: 6gci chain A). Residues that form ionic interactions (yellow dashes) or hydrogen bonds (black dashes) with BKA (orange) are shown in purple, while residues that form hydrophobic contacts are shown in cyan.

3.8. Discussion

The main goal of this chapter was first to identify all the residues that could be involved in the substrate binding mechanism of the mitochondrial ADP/ATP carrier. For this purpose, the translocation pathway of the ADP/ATP carrier from *Thermothelomyces thermophila* was examined for residues that could potentially be involved in substrate binding. The ADP/ATP carrier from this species was selected because a high resolution structure of this orthologue in an inhibited state is available (Ruprecht *et al.*, 2019) and also, functional studies (King *et al.*, 2016; Majd et al., 2018a), that would provide useful insights for the evaluation and interpretation of the obtained results.

All solvent-accessible residues that are conserved and located between the cytoplasmic and matrix salt bridge networks were the final candidates for the analysis, making a set of 36 single alanine replacement mutants. Alanine is a popular substitution when interactions are being probed, because of its aliphatic chemical nature and its relatively small size, which does not interfere with structural constraints (Cunningham and Wells, 1989).

Firstly, the overall function of the mutants was analysed in the native mitochondrial environment with complementation assays. It was shown that mutation of most of the target-residues affects a fundamental property of the protein or an essential step of the transport mechanism, because the majority of the mutants either did not complement growth of the Aac-deficient strain at all, or complemented significantly less. Other studies presented similar findings for 14 of the residues tested (David *et al.*, 2008; Heidkämper *et al.*, 1996; Heimpel *et al.*, 2001; Klingenberg and Nelson, 1994; Müller *et al.*, 1996; Nelson *et al.*, 1993; Ruprecht *et al.*, 2019; Thompson *et al.*, 2016; Zeman *et al.*, 2003). These results provided a good basis for the analysis, but it became apparent that it was necessary to perform additional analyses, in order to gain more specific information on the role of each residue.

Therefore, it was reasonable to use a simpler system, where the focus would be on the properties of the individual mutant proteins. In this way, biophysical and biochemical assays could be used to test which aspect of function or structure was affected in each case. Hence all the proteins were purified, using previously established methods, and a thermostability assay was selected to characterise their stability and response to the AAC-specific inhibitors CATR and BKA. The results showed that with an exception of five variants, all were well folded, stable and contained intact binding pockets for the inhibitors. The five unfolded variants (L41A, Q44A, T146A, Y239A and N284A) had to be excluded from further analysis. However, based on their position and information found in other studies (Ruprecht *et al.*, 2014; Yi *et al.*, 2019), they are most likely not involved in substrate binding, but may serve a role in preventing the dissipation of the proton motive force of the mitochondrial inner membrane.

The 31 variants that were stable will be further analysed with other methods in **Chapters 4, 5** and **6** to investigate their potential role in substrate binding. Importantly, the CPM thermostability assay, apart from confirming the folded status of the variants, was proven to be a valid technique to successfully detect protein-ligand interactions. This conclusion was obtained by mapping the binding sites of the inhibitors CATR and BKA, which are known from the determined crystal structures. The thermostability results were overall consistent with the structural analyses and some observations of indirect effects provided the opportunity to consider 'false positive' cases, indicating that additional assays should be considered for validating purposes. The results though provided a proof of the basic principle that will be extended to the substrates ADP and ATP, in **Chapter 4**.

Chapter 4: Mapping the substrate binding site of the mitochondrial ADP/ATP carrier

4.1. Introduction

In order for substrate translocation to happen, both the protein and the substrate have to undergo conformational changes. Because the energy required for these movements of the protein is provided by substrate binding and release, these processes are interdependent. Therefore, there must be a continuous series of substrate-bound states, which include all states from a cytoplasmic-open bound state, via an occluded state, to a matrix-open bound state and the reverse, upon binding of the counter substrate. During this highly dynamic process, ADP and ATP may also go through different conformers, as the carrier changes conformations. Studying this process is hence very challenging, especially with direct structural approaches. For crystallography a very stable state is needed and although it would be possible to trap a snapshot of this process, for example by artificially creating a halted state (e.g. using a substrate analogue), this would not represent the whole process. For cryo-electron microscopy, powerful algorithms that could probably classify the different intermediates have been developed and used (Hofmann et al., 2019), however, the small size and three-fold pseudo-symmetrical nature of the protein imposes a limit at present.

Biochemical studies, conducted prior to the availability of structures, used labelled, non-transportable nucleotide analogues and proposed substrate binding sites in the matrix loops (Dalbon *et al.*, 1988; Dianoux *et al.*, 2000; Majima *et al.*, 1998; Mayinger *et al.*, 1989) and C-terminal region (Dianoux *et al.*, 2000) (**Figure 4.1**). These experiments involved labelling followed by chemical cleavage of the protein and subsequent identification of the derived peptides with Edman degradation sequencing (Edman, 1949), and/or SDS-PAGE and/or mass spectrometry. When structures became available, it was shown that these regions are outside the substrate translocation pathway and could not enter the core of the structure, as it has been proposed (Nury *et al.*, 2006). It is possible that the results of these studies have been

affected by the extensive chemical treatment of the protein that could result in protein denaturation and non-specific labelling.

Later, bioinformatic studies that used sequence analyses, in combination with chemical and distance constraints (Kunji and Robinson, 2006; Robinson and Kunji, 2006) or deviation of pseudo-symmetry (Robinson *et al.*, 2008) pointed towards a location in the central part of the cavity (**Figure 4.2**). The first study identified three contact points for all mitochondrial carriers, that are related through three-fold pseudo-symmetry, like the rest of the structural features. The contact points are shared between carriers that transport similar substrates, but are distinct between the different classes of carriers. Specifically, contact point II can discriminate between the different groups of substrates. All amino acid carriers have in that position the sequence R-[DE], all nucleotide carriers have G-[IVLM] and all keto acid carriers have R-[QHNT]. Contact point I can discriminate between different substrates within the group of transporters. Carboxyl or phosphate groups interact with [RK], amino groups with [DE], aromatic moieties form stacking arrangements with [FY] and hydrophobic moieties, such as acyl or hydrophobic side chains, form van der Waals interactions with [ILV]. The residues at contact point III are usually [RK] and they bind either carboxyl or phosphate groups (Kunji and Robinson, 2006; Robinson and Kunji, 2006). It has been confirmed experimentally that the residues of the 'contact points' participate in substrate binding, as they can determine the substrate specificity (Monné et al., 2012). The second study used as concept the deviation of pseudo-symmetry between mitochondrial carriers expected to be found in the binding site and ion coupling site areas, as the these ligands are not symmetrical (Robinson *et al.*, 2008). This study identified asymmetric residues gathered in the central cavity, in an area that overlapped with the three 'contact points' that were identified by applying chemical and distance constraints (**Figure 4.2**).

In contrast, molecular dynamics simulations studies highlighted substrate interactions throughout the translocation pathway (Dehez *et al.*, 2008; Mifsud *et al.*, 2013; Pietropaolo *et al.*, 2016; Tamura and Hayashi, 2017; Wang and Tajkhorshid, 2008; Yao *et al.*, 2021). The various studies proposed multiple binding sites, but it was not clear whether they formed transient or more permanent interactions (**Table 4.1**).

Evidently, there are no systematic experimental data for the location of the binding site and the residues involved. Moreover, the different computational studies, including the sequence analyses and the molecular dynamic simulations, have not

pointed to a consistent location for the substrate binding site, neither have they agreed on the number of binding sites. Thus, the experimental determination of the substrate binding site is essential for resolving the complex transport mechanism of the mitochondrial ADP/ATP carrier and other members of the SLC25 family.

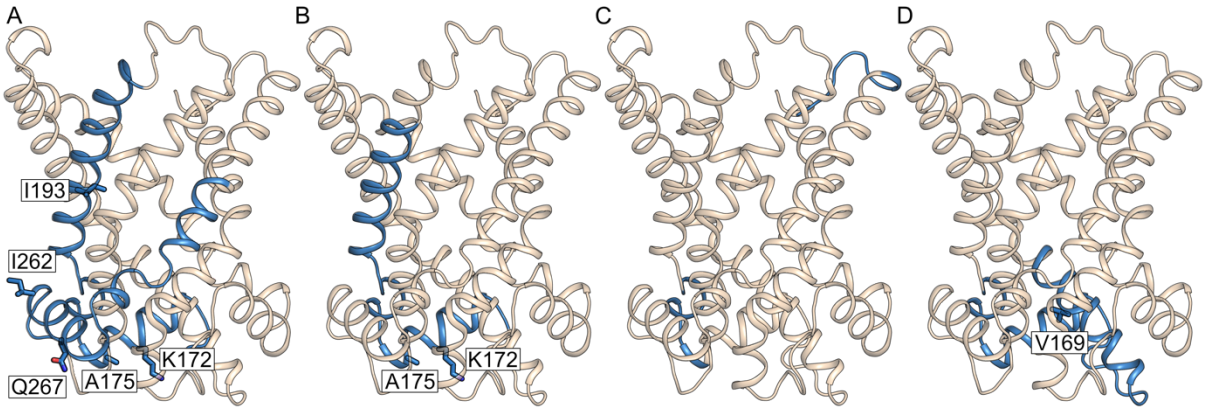

Figure 4.1: Proposed binding site region(s) identified with labelled, non-transportable substrate analogues. Membrane view of homology model of TtAac in the cytoplasmic-open state, generated with Modeller 9.22 based on PDB codes: 1okc, 4c9h, 4c9q and 4c9j showing in blue cartoon representation the proposed binding site(s) identified with (A) 2-azido[α- ^{32}P]-ADP (Dalbon *et al.*, 1988) (B) 2-azido[α- ^{32}P]-ATP and 8-azido-[γ- ^{32}P]-ATP (Mayinger *et al.*, 1989) (C) 2-azido-3'-O-naphtonyl-[β- ^{32P}]-ADP (Dianoux *et al.*, 2000) (D) fluorescein derivative eosin Y (Majima *et al.*, 1998). Blue sticks indicate the equivalent residues of TtAac that the label was predominantly found. (Apart from K172 and I193 the other labelled residues are not conserved between TtAac and the orthologue the study was conducted with. A175 is a lysine in BtAAC and ScAac2, Q267 is a lysine, I262 a valine and V169 a cysteine in BtAAC)

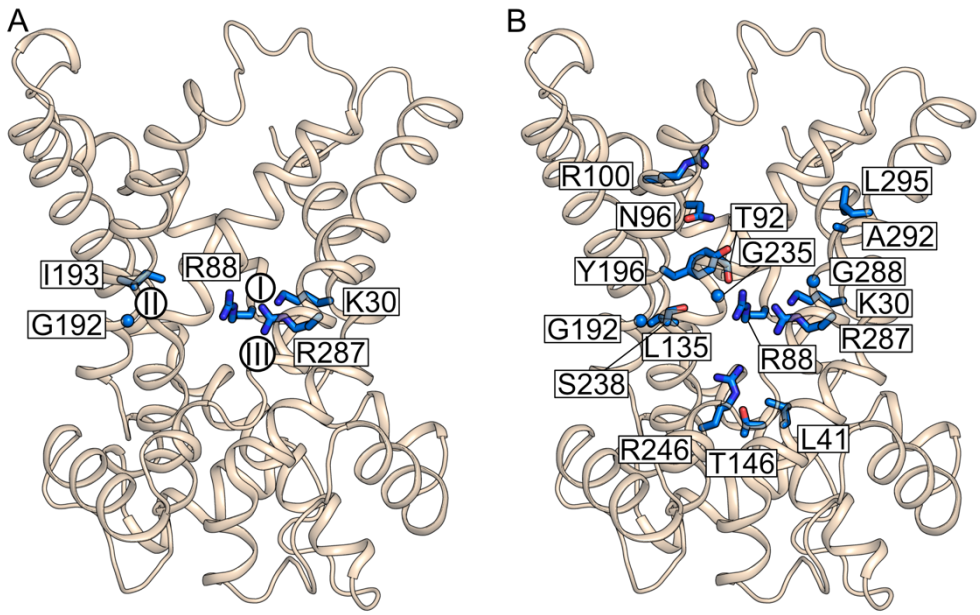

Figure 4.2: Residues proposed to participate in substrate binding based on sequence analysis. Membrane view of homology model of TtAac in the cytoplasmic-open state, generated with Modeller 9.22 based on PDB codes: 1okc, 4c9h, 4c9q and 4c9j showing in marine stick representations the residues proposed to participate in substrate binding based on (A) chemical and distance constraints (Robinson and Kunji, 2006) and (B) analysis of pseudosymmetry (Robinson *et al.*, 2008)

Table 4.1: Residues proposed to participate in interactions (transient or more permanent) with the substrates by molecular dynamics simulation and metadynamics simulations studies

Equivalent TtAac residue	Interaction with P/A/R/AR/N	References	Notes
S29	A	[2, 3]	
K30	P, A	[1, 2, 3, 5]	
E37	N	[5]	matrix network
K40	N	[4, 5]	matrix network
Q44	N	[4]	glutamine brace
R88	P, AR, N	[1, 2, 3, 4, 5]	
T92	N	[4, 5]	
Q93	AR	[1]	
N96	AR, N	[1, 4]	
F97	AR	[1]	hydrophobic plug
R100	P, N	[1, 4, 6]	'tyrosine' brace
K104	P, N	[1, 4, 6]	cytoplasmic network
N123	P, N, A	[1, 4, 6]	
D142	AR, N	[1, 5]	matrix network
R145	P, N	[4, 5]	matrix network
G192	A	[2]	
I193	AR, A, N	[1, 4, 5]	
Y196	R, P, A, N	[1, 2, 3, 4, 5, 6]	
R197	P, A, N	[1, 3, 4, 6]	
Y200	P, AR, N, R	[1, 4, 6]	
F201	N	[4, 6]	hydrophobic plug
Y204	AR, N	[1, 4, 6]	tyrosine brace
K208	N, P	[4, 6]	cytoplasmic network
L216	P	[6]	
W228	N	[2, 4]	
T231	N	[2, 4]	GxxxG motif
T232	N	[2, 4]	
A234	N	[4]	
G235	A, N	[2, 3, 4]	
S238	AR, A	[1, 2, 3]	
D242	N	[5]	matrix network
R245	P, AR, N	[1, 4, 5]	matrix network
R246	P, AR, N	[1, 2, 4, 5]	
N284	AR, N	[1, 4]	
I285	N	[4]	
R287	P, AR, N	[1, 2, 3, 4, 5]	
G288	N	[2]	
A292	A	[2, 3]	

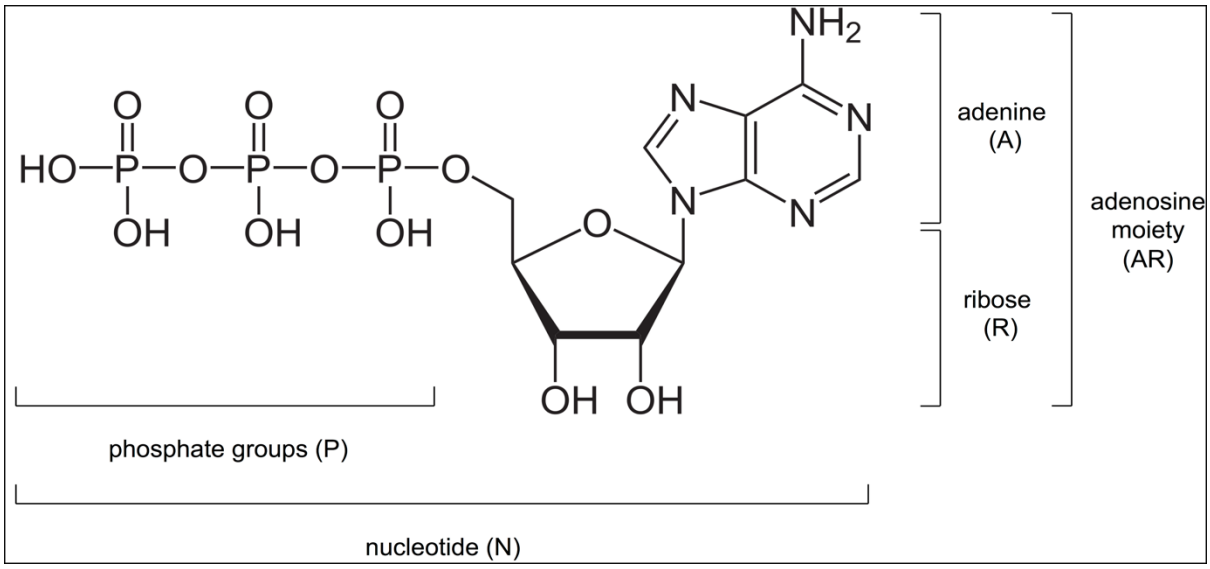

[1] (Dehez *et al.*, 2008), [2] (Wang and Tajkhorshid, 2008), [3] (Mifsud *et al.*, 2013), [4] (Pietropaolo *et al.*, 2016), [5] (Tamura and Hayashi, 2017), [6] (Yao *et al.*, 2021) bioRxiv
P=phosphate groups, A=adenine, R=ribose, AR=adenosine moiety, N=nucleotide

4.1.1. Aims

As shown in **Figures 4.1** and **4.2** and in **Table 4.1**, a large number of residues have been proposed to be involved in substrate binding in AAC, either transiently or more permanently. The majority of these assignments have been made using bioinformatic analyses, but experimental evidence in support is currently limited. The aims of this chapter were to characterise the response of the wild-type protein to substrates ADP and ATP, using the CPM thermostability assay and then to test the response of the variants. A significantly altered response would indicate the involvement of the particular residue in substrate binding.

4.2. The response of the wild-type protein to substrate

It had been previously shown that transport proteins of different families can be stabilised by high concentrations of their substrates (Majd *et al.*, 2018a). This was shown specifically for the ADP/ATP carrier as well, using the CPM thermostability assay. From a screen of different molecules, including all nucleotides, the only compounds that gave a considerable (>3°C) shift were ADP and ATP (Majd *et al.*, 2018a). The closely related AMP molecule, differing only in the number of phosphate groups, did not present a shift, demonstrating the discriminatory nature of the approach.

Here, the effect of the substrate on the thermostability profile of the wild-type protein was analysed, in presence of a temperature ramp and also at a stable temperature as a function of time. The substrate was shown to stabilise the wild-type protein in a concentration-dependent way, as higher substrate concentrations led to higher apparent Tm values (**Figure 4.3**). The substrate effect was titrated in a range between 0.1-50 mM and was shown to follow a sigmoidal trend, reaching saturating levels at around 12 mM (**Figure 4.3**). The shift to higher Tm values was expressed as a ΔTm value, calculated at each concentration by subtracting the apparent Tm at 0 mM substrate from the apparent Tm at each substrate concentration. Starting from 0.2 ± 1.0°C shift at 0.1 mM ADP, the maximal shift, reached at saturating concentrations, was 8.9 ± 1.8°C. This result indicated that the dynamic range to study this process was between 0.1-10 mM. Based on this experiment, five concentrations (0.1, 0.5, 1, 5 and 10 mM) of ADP and ATP were selected to study the substrate binding process with the variants.

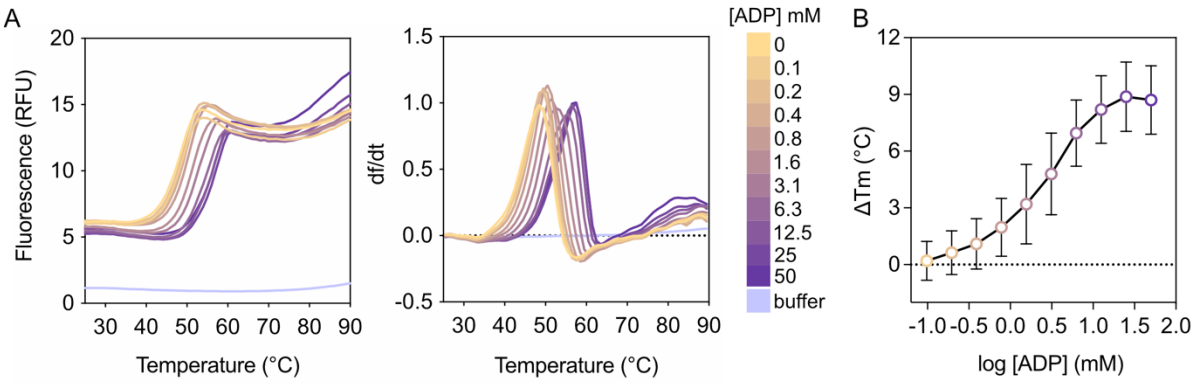

Figure 4.3: Thermostability shifts in the presence of different concentrations of ADP for wild-type TtAac. (A) Thermal denaturation profile (left) and corresponding first derivative (right) of the wild-type protein in presence of 0-50 mM ADP. Each unfolding trace is from one representative experiment. Approximately 3 µg of protein were used for each condition. (B) Titration curve showing the thermostability shift (ΔTm) at each ADP concentration. The circles and error bars represent mean and standard deviation of 4 independent experiments.

A similar result was obtained when the effect of the substrate was titrated over time, at temperatures of 25, 35 and 45°C (**Figure 4.4**). The concentrations tested were 0.01, 0.05, 0.1, 0.5, 1, 5 and 10 mM. The substrate had a protective effect, preventing the protein population from unfolding in a concentration-dependent way. At 25°C, the unfolding traces for all the different substrate concentrations started roughly at the

same level of fluorescence (around 6 RFU), indicating that the protein population is well folded at this temperature. Over time, the population started unfolding, following a linear trend for all concentrations, but with different rates. In presence of 0, 0.01, 0.05 and 0.1 mM substrate, the unfolding was taking place at a very similar rate and the fluorescence reached levels about 15 RFU. At higher concentrations, 0.5 and 1mM, the population was unfolding at a slower rate and reached levels of 11 RFU at the end of the assay, whilst at 5 and 10 mM the population was essentially protected from unfolding during the assay. In these two cases the fluorescence did not exceed 8 RFU (**Figure 4.4**).

At 35°C, the traces started from slightly different levels of fluorescence. The 5 and 10 mM traces still started low (around 6 RFU), but the rest, starting from high to lower concentrations, showed an increase in the initial fluorescence, with the 0 mM trace starting at 9 RFU. The population was unfolding at a rate that decreased as the substrate concentration was increasing, following a linear trend. The lowest substrate concentration and the 0 mM condition reached the highest fluorescence levels, around 21 RFU. Similar to the experiment at 25°C, at 5 and 10 mM substrate the population was unfolding at a very low rate and the fluorescence did not exceed 9 and 8 RFU, respectively (**Figure 4.4**).

At 45°C, the traces for 5 and 10 mM started at 6 RFU, while all other traces started higher, with the lowest concentrations starting at the highest RFU. At this temperature, the population appeared to unfold faster than in the other two, as at the beginning of the experiment, for all concentrations apart from 5 and 10 mM, the trend appeared exponential until about 400s and then continued with a linear trend. The fluorescence reached levels of 20 RFU, similar to the experiment at 35°C. The 5 mM and 10 mM traces followed a more linear trend from the beginning until the end of the assay, showing much slower unfolding rate than all lower concentrations and they reached levels of about 12 RFU (**Figure 4.4**).

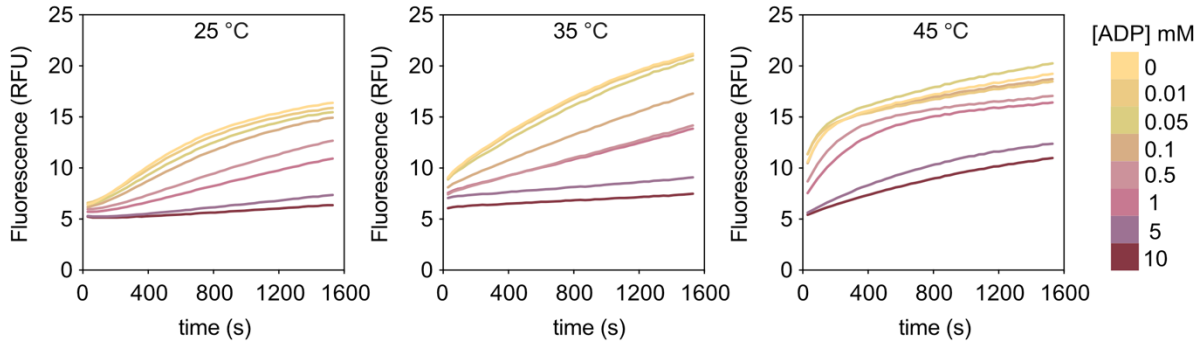

Figure 4.4: The concentration-dependent stabilising effect of the substrate evaluated over time. Unfolding traces at 25°C (left), 35°C (middle) and 45°C (right) of TtAac at increasing concentrations of substrate. Each trace is generated from three technical replicates and approximately 3 µg of protein were used for each condition.

4.3. Residues that are critical for substrate binding

Subsequently, the thermostability shift occurring in presence of ADP and ATP for all 31 folded variants was measured. In contrast to the concentration-dependent response of the wild-type protein, five variants, K30A, R88A, R197A, R246A and R287A, showed no concentration-dependent thermostability shift in presence of either substrate (**Figure 4.5A**). A small destabilisation of the protein population was observed, but it remained constant throughout the concentration range. For variants K30A and R287A the destabilisation was more prominent, whereas for R197A and R88A it did not exceed 2°C. Interestingly, variants K30A (57.3 ± 1.2°C) and R287A (64.4 ± 0.2°C) were significantly more stable (in the 'no effector' condition) than the wild type (50.2 ± 0.6°C) (**Figure 3.13**). It is possible that this is caused by the repulsion of the three positive charges found very close together in the cavity of the wild-type carrier (**Figure 4.5 B**). Removal of one makes the protein more stable, as there is less repulsion. Upon addition of the substrate, however, it is possible that the negative charges (of the substrate) cannot get neutralised, making binding unfavourable and potentially inducing the destabilisation observed.

These five positively charged residues are located in the middle of the water-filled cavity (**Figure 4.5B**). K30, R88 and R287 are found at the same level, roughly 15 Å equidistant from both the intermembrane space and mitochondrial matrix, while R197 and R246 are situated towards the cytoplasmic side and matrix side, respectively. Alanine replacement of these residues results in loss of a positive charge in the central cavity, which changes the electrostatic microenvironment of that area.

The complete abolishment of the substrate-induced shift indicates that each of these residues forms a critical interaction with the substrate.

Consistent with the thermostability shift assay result, these variants showed no growth in the complementation study (**Figures 3.4** and **3.5**). Since they were expressed and targeted to mitochondria, stable (**Figure 3.13**) and well folded (**Figure 3.15**), this result indicated that they have an essential role in the transport cycle. This observation could be further refined (and attributed to substrate binding) by the thermostability shift result in presence of the substrates.

Several computational studies have proposed that residues K30, R88 and R287 form salt bridge interactions with the phosphate groups of the adenine nucleotides (Dehez *et al.*, 2008; Kunji and Robinson, 2006; Mifsud *et al.*, 2013; Robinson and Kunji, 2006; Robinson *et al.*, 2008; Wang and Tajkhorshid, 2008). Residue R246 has also been shown to interact with the β-phosphate of ADP in molecular dynamic simulation studies (Wang and Tajkhorshid, 2008) or in general with the phosphate groups of the nucleotides (Pietropaolo *et al.*, 2016; Tamura and Hayashi, 2017). Residue R197 has also been reported to interact with ADP and ATP in various ways, either with the phosphates or the adenine or the ribose moiety, but no specific role has been proposed (Dehez *et al.*, 2008; Mifsud *et al.*, 2013; Pietropaolo *et al.*, 2016; Yao *et al.*, 2021).

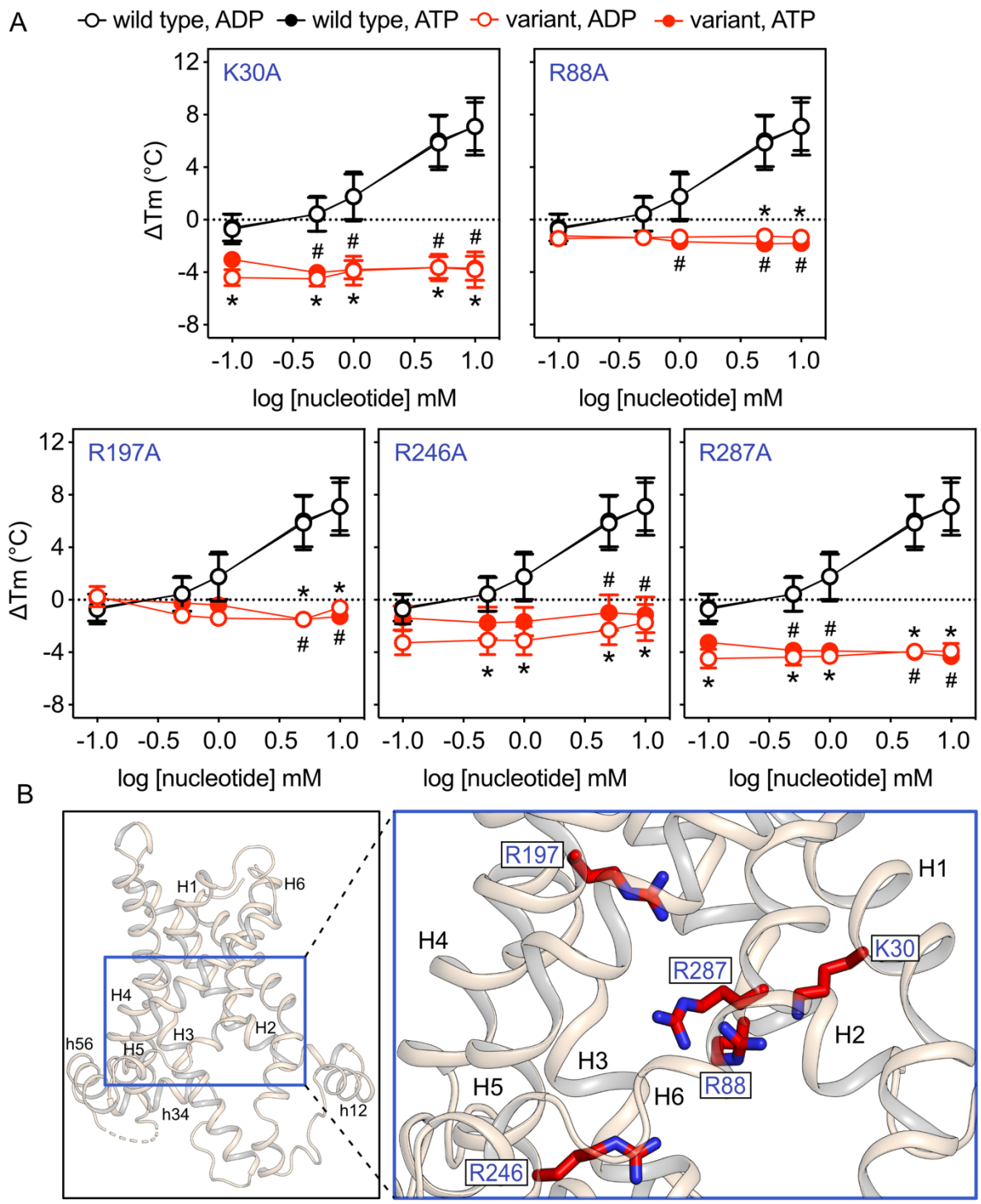

Figure 4.5: Five positively charged residues provide the critical binding interactions (A) Thermostability shift values (ΔTm) determined at 0.1, 0.5, 1, 5, 10 mM substrate concentration for the wild type and single alanine replacement variants. Circles and error bars represent the mean and standard deviation of 8 independent experiments for the wild type and 3-5 for the variants. Empty and filled circles represent ADP and ATP, respectively. Note that in several occasions the mean value and error bars of ADP vs ATP groups are identical and consequently their graphical representation is superimposed, with the ADP marker on top. Error bars are smaller than the symbol whenever not shown. Significant differences for each nucleotide

concentration tested were evaluated by two-way ANOVA with interaction (tests shown in **Appendix 3**). Simple effects between protein variants within the substrate level were analysed and corrected for multiple comparisons using Dunnet post hoc test against the wild-type protein. Significant values ($p \leq 0.01$) are indicated by * or # for ADP and ATP, respectively. (B) TtAac matrix-open BKA-bound structure (PDB code: 6gci chain A) (left) and close-up view (right) showing the analysed residues in red stick representation. Helices are shown in wheat cartoon representation and are labelled.

4.4. Three aliphatic, two polar and one aromatic residue make significant contributions to substrate binding

In the vicinity of the five critical residues, another six residues were found (N85, N96, L135, V138, G192 and Y196), the alanine mutants of which also showed significantly altered thermostability profiles in the presence of substrates, compared to the wild type. Variants N85A, N96A, L135A, V138A, G192A and Y196A did show concentration-dependent shifts in presence of the substrates, but these were significantly smaller than those of the wild-type protein (**Figure 4.6A**). Significant differences were mostly obtained for the two highest concentrations tested for both ADP and ATP (**Figure 4.6A**).

Since the substrate-induced shifts were not completely abolished, each residue possibly makes a contribution to substrate binding. This result can be supported by the complementation assay, as variants L135A, G192A and Y196A did not grow at all (<2.7 %) and N85A (42 ± 23%), N96A (18 ± 10%) and V138A (53 ± 14%) grew significantly less (**Figures 3.4** and **3.5**). For the aliphatic residues of this set, upon alanine replacement, a different sized side-chain is introduced in the central cavity. A smaller side chain for L135A and V138A and bigger for G192A is introduced, while the chemical properties of the original amino acid are maintained. For the substitution of the three polar residues though, both the size and the chemistry change, hence the size and shape of the binding pocket are affected, as well as the chemical microenvironment. Importantly, alanine replacement did not cause protein instability (**Figure 3.13**) or disorder of the binding pocket, for any of these variants, emphasising that the observed effects are specific for substrate binding.

Residue G192 has been proposed by computational analyses, both sequence analysis and dynamic simulations to be in hydrophobic contact with the adenine moiety of the nucleotides (Kunji and Robinson, 2006; Robinson and Kunji, 2006; Robinson *et al.*, 2008; Wang and Tajkhorshid, 2008). Residue Y196 has been identified as

asymmetric (Robinson *et al.*, 2008) and has been shown in molecular dynamic simulations to potentially form a hydrogen bond with the oxygen atom of the hydroxyl group at 3' position of the ribose moiety (Dehez *et al.*, 2008; Wang and Tajkhorshid, 2008) or its phenyl ring to form a π stacking arrangement with the adenine ring (Kunji *et al.*, 2016; Wang and Tajkhorshid, 2008). It is also the third tyrosine of the proposed tyrosine ladder, a 'selectivity filter' proposed to guide the substrate to the binding site (David *et al.*, 2008; Pebay-Peyroula *et al.*, 2003). Residues N96 and L135 have been identified as asymmetric, therefore could potentially have an involvement in substrate binding (Robinson *et al.*, 2008). Residue N96 has been shown to be transiently interacting with the substrate in molecular dynamic simulations (Dehez *et al.*, 2008).

Investigating protein structures that were determined with bound ADP and ATP in Protein Data Bank (Berman et al., 2000), it can be observed that the general consensus is that adenine binding pockets are often constituted by isoleucine, leucine, valine and methionine residues (Kunji and Robinson, 2006). The residues identified here to make contributions to substrate binding match these hydrophobic and aliphatic properties.

It is interesting that many residues of this set are also participating in the binding sites of the inhibitors, confirming their classification as 'competitive inhibitors'. Specifically, residues G192, Y196 and L135 are part of both the CATR and BKA binding sites (**Figure 3.15**) (L135 is listed as non-bonded interaction in the bovine and ScAac3 structure, hence not marked in the figure, which is based on that of ScAac2) (Pebay-Peyroula *et al.*, 2003; Ruprecht *et al.*, 2014; Ruprecht *et al.*, 2019). Residues N96 and V138 are participating in BKA binding (**Figure 3.15**) (Ruprecht *et al.*, 2019).

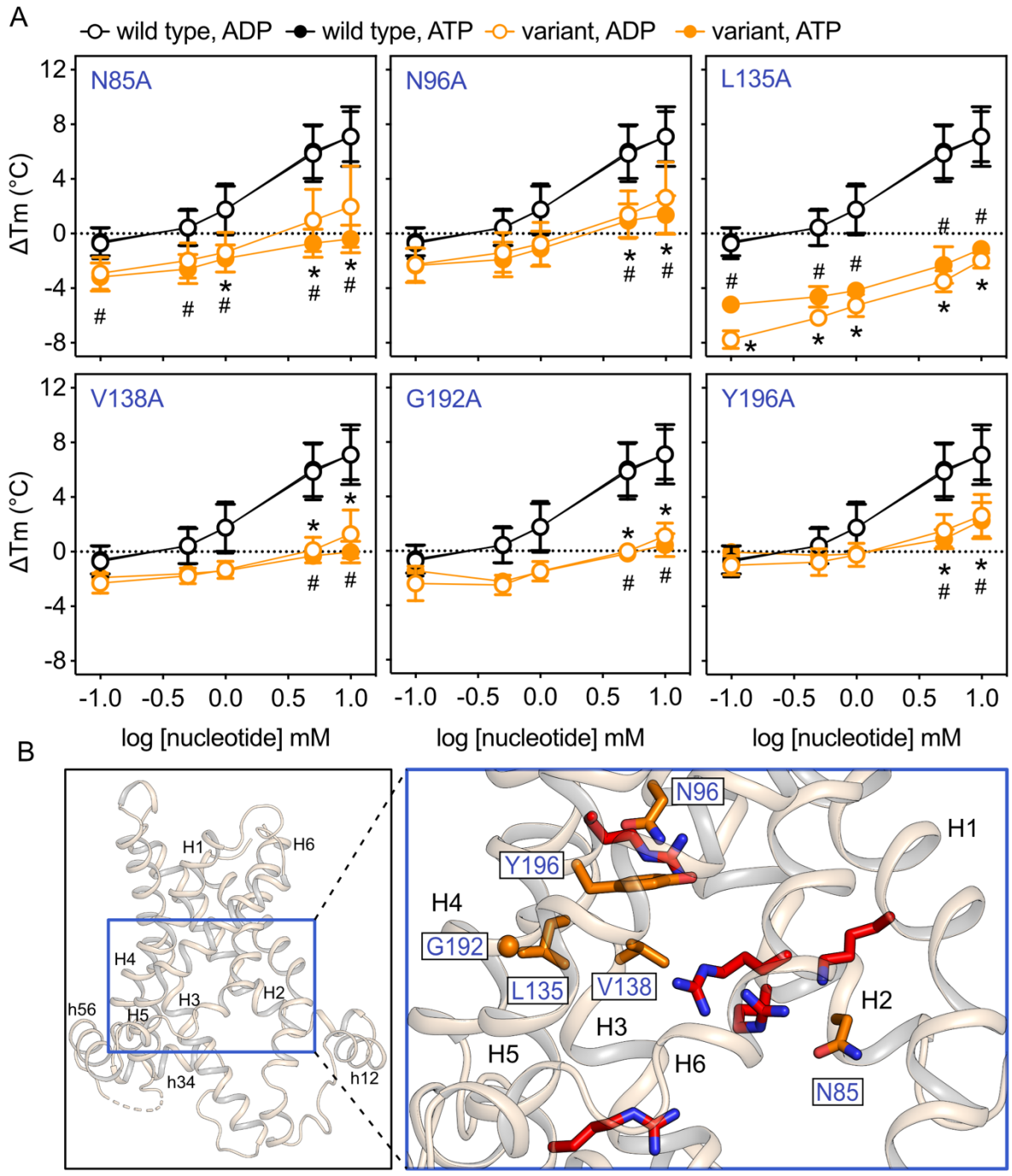

Figure 4.6: Aliphatic, polar and aromatic residues make significant contributions to substrate binding. (A) Thermostability shift values (ΔTm) for the wild type and single alanine replacement variants, determined as in **Figure 4.3A**. Circles and error bars represent the mean and standard deviation of 8 independent experiments for the wild type and 3-7 for the variants. Empty and filled circles represent ADP and ATP, respectively. Notes about superposition of the graphical representations, error bars and calculations of the p values as in **Figure 4.3A**. Significant values ($p \leq 0.01$) are indicated by * or # for ADP and ATP, respectively. (B) TtAac matrix-open BKA-bound structure (PDB code: 6gci chain A) (left) and close-up view (right) showing the analysed residues in orange stick and sphere for Gly

representations. The residues providing critical binding interactions are shown in red stick representation. Helices are shown in wheat cartoon representation and are labelled.

4.5. Substrate binding is confined to a single area in the translocation pathway

Importantly, the majority of the variants analysed, 20 of the 31, presented substrate-induced shifts that were not significantly different from those of the wild-type protein (**Figure 4.7**). The thermostability shifts of mutant proteins S29A, V230A, G288A and G291A were not different from the wild type at any concentration and regardless of the substrate used (**Figure 4.7A**). Additionally, these variants complemented growth of the Aac-deficient strain to wild-type levels (**Figures 3.4** and **3.5**). With the results of both techniques, it could be concluded that these residues do not directly participate in substrate binding. These residues are situated relatively remotely to the residues identified in **sections 4.2** and **4.3** to participate in substrate binding (**Figure 4.7C**).

Although variants F97A, S189A, Y204A, G235A and L295A did not complement growth (<2.6 % of wild-type growth) (**Figures 3.4** and **3.5**), their thermostability shifts in the presence of ADP and ATP were not different from those of the wild type at any concentration (**Figure 4.7A**). Taken together, these results indicated that since these variants did not have expression or folding issues and they responded to substrate like the wild-type protein, they are essential for another step of the transport cycle, but not substrate binding. With the exception of G235, they are also found towards either the cytoplasmic (residues F97, Y204 and L295) or the matrix side (residue S189) of the translocation pathway and not very close to the residues identified to have a role in substrate binding (**Figure 4.7C**).

Variants T92A, Q93A, R100A, S134A, Y200A, T231A and S238A complemented growth of WB-12 strain only partially (**Figures 3.4** and **3.5**), but their response to ADP and ATP were concentration-dependent and not statistically different from the wild type at any concentration (**Figure 4.7A**). Therefore, these residues are probably important for some aspect of the transport mechanism, but not for substrate binding. Interestingly, apart from R100, all these residues are located in the binding pocket area, as designated in **sections 4.3** and **4.4**, so in close proximity to the residues participating in substrate binding. This demonstrated the accuracy of the

method, which allowed the distinction of the interacting residues from those that were in the vicinity.

Finally, there were four variants (Y89A, N123A, I193A and V294A) that presented some differences from the wild type, but not consistently. Mutant carrier Y89A could partially complement growth (36.2 ± 18.9 % of wild-type growth) (**Figures 3.4** and **3.5**) and exhibited greater shifts than the wild type both for ADP and ATP, albeit only for ADP the values were of statistical significance (**Figure 4.7B**). The larger shifts are not likely to indicate involvement in substrate binding, but could be an indirect effect. Variant N123A was functional (50.2 ± 9.2 % of wild-type growth) (**Figures 3.4** and **3.5**) and the substrate-induced shifts were significantly different from the wild type only at 5 mM. Considering, however, the overall response profile and the fact that it reached wild-type levels at the highest concentration, it is unlikely that this residue participates in substrate binding. Variant I193A exhibited variability in stability (**Figures 3.13,** and **4.7B**), precluding an accurate assessment of significance of the substrate-induced shifts. There was a concentration-dependent response, but the ΔTm values were highly variable between the biological repeats. The reason for this observation could be the relative instability of this protein (apparent Tm with no effector 45.2 ± 4.6°C) compared to the wild type (50.2 ± 0.6°C) (**Figure 3.13**). This variant also did not grow in the complementation study (<2.7 % of wild-type growth) (**Figures 3.4** and **3.5**) and in order to be purified, it was necessary to reduce the cleavage time (**section 2.5.3**). Lastly, variant V294A grew on glycerol to wild-type levels (83.6 ± 13.5 % of wild-type growth) (**Figures 3.4** and **3.5**), indicating that the protein is functional and active. However, this protein was more stable (53.7 ± 0.46°C) than the wild type (50.2 ± 0.6°C) (**Figure 3.13**), and this resulted in spurious significance at low substrate concentrations, but it reached wild-type levels at the highest concentration for ATP (**Figure 4.7B**). Comparing the shifts induced by the two nucleotides with each other, they are not different at any concentration (p-value > 0.1 for all concentrations), hence the significance for ADP at high concentrations could most likely be attributed to statistical type I error.

Residues that are not involved in substrate binding were found dispersed throughout the translocation pathway and also in close proximity to the ones identified to have a critical or contributing role with respect to substrate binding (**Figure 4.7C**). These results showed firstly that substrate binding is confined to a single area in the translocation pathway and secondly, that the thermostability shift assays can

accurately discriminate between residues involved in protein-substrate interactions and the ones simply found in the vicinity.

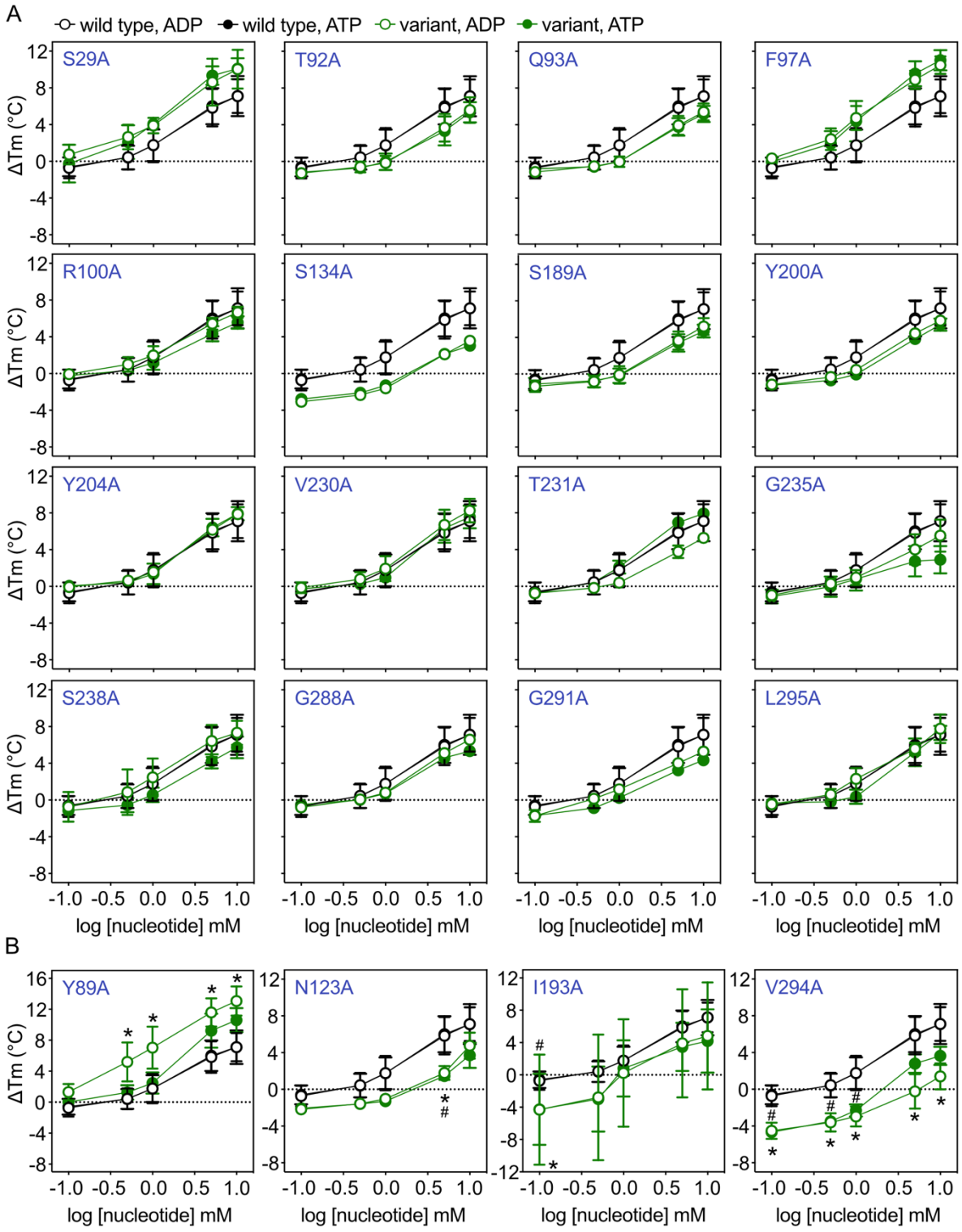

C

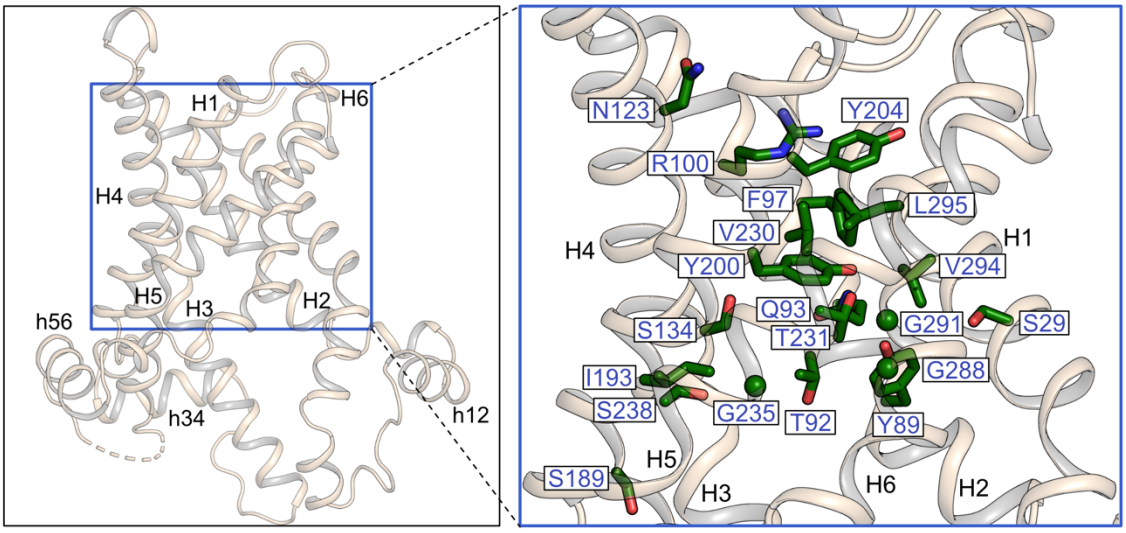

Figure 4.7: Substrate binding is confined to a small area of the translocation pathway. (A), (B) Thermostability shift values (ΔTm) for the wild type and single alanine replacement variants determined as in **Figure 4.3A**. Circles and error bars represent the mean and standard deviation of 8 independent experiments for the wild type and 3-5 for the variants. Empty and filled circles represent ADP and ATP, respectively. Notes about superposition of the graphical representations, error bars and calculations of the p values as in **Figure 4.3A**. Significant values ($p \leq 0.01$) are indicated by * or # for ADP and ATP, respectively. (C) TtAac matrix-open BKA-bound structure (PDB code: 6gci chain A) (left) and close-up view (right) showing the analysed residues in green stick and sphere for Gly representations. Helices are shown in wheat cartoon representation and are labelled.

Several residues of this group have been proposed to participate in substrate binding by other studies, in contrast to the results here. Residues S29 and G235 have been proposed to participate in adenine binding by molecular dynamic simulations (Mifsud *et al.*, 2013; Wang and Tajkhorshid, 2008), while residues T231 and G288 were observed to be part of a transient binding site for the adenine (Wang and Tajkhorshid, 2008). Residue T231 has also been proposed to be part of either ADP or ATP binding sites in different states (Pietropaolo *et al.*, 2016). Residues Q93, F97, Y200 and Y204 were shown to participate in adenine binding, while residues N123 and R100 in binding of the phosphate groups of the nucleotides in molecular dynamic simulations (Dehez *et al.*, 2008). Moreover, residues N123, R100, Y200 and Y204 were shown in metadynamics simulations to be part of ADP and ATP binding sites in different states (Pietropaolo *et al.*, 2016). In all these studies, it can be observed that the adenine moiety binds in several sites (transiently or more permanently) (Dehez *et al.*, 2008; Mifsud *et al.*, 2013; Wang and Tajkhorshid, 2008). In contrast, the phosphate

groups seem to robustly bind to specific positively charged residues, at least in most dynamic simulation studies (Mifsud *et al.*, 2013; Wang and Tajkhorshid, 2008). However, in the study by (Dehez *et al.*, 2008) the results are affected by the initial conditions, hence the way the simulation was set up played a crucial role on the outcome. In the study by (Pietropaolo *et al.*, 2016), a computationally calculated structure of the matrix-open state was used, together with a homology model of HsAAC2 at the cytoplasmic-open state, based on the bovine structure (Pebay-Peyroula *et al.*, 2003). The matrix-open model used does not resemble the determined crystal structure (Ruprecht *et al.*, 2019). Therefore, these results are inconsistent with experimental data.

From the above mentioned residues, F97, R100, Y200 and Y204 are part of the 'cytoplasmic gate', formed in the matrix-open state (Ruprecht *et al.*, 2019). More specifically, residues R100 and Y204 act as braces for the cytoplasmic network, providing additional inter-domain interactions (Ruprecht *et al.*, 2019). Residue Y204 is bracing the K208/D299 salt bridge, as it forms a hydrogen bond with D299. Residue R100 is bracing the K104/D205 salt bridge, forming a hydrogen bond with D205 (Ruprecht *et al.*, 2019). Residue F97 contributes to the hydrophobic plug, due to its bulky and hydrophobic properties (Ruprecht *et al.*, 2019).

Residues Y200 and Y204 have also been proposed to form the 'tyrosine ladder', together with Y196. The tyrosine ladder was considered to act as a 'selectivity filter' that guides the substrate to the binding site (Pebay-Peyroula *et al.*, 2003). However, the results of the current study do not support involvement of these residues in substrate binding, apart from Y196. Furthermore, in a study where the kinetic properties of the equivalent mutants of ScAac2 were examined, it was concluded that only two of the residues forming the 'tyrosine ladder' are crucial for substrate transport. They found that the equivalent variant of Y196A had a 500-fold increased K_m value compared to the wild-type, while the V_{max} value was unaltered (David *et al.*, 2008). The equivalent variant of Y200A had a K_m value similar to that of the wild-type protein but a decreased V_{max}. Finally, the equivalent of Y204A had a decreased V_{max} value (around 2-fold) and an increased K_m value (12.5-fold) compared to the wild type. This result though can be explained by the supportive role of this residue to the cytoplasmic network.

Residues T92, G235, G288 and L295 are asymmetric and therefore, could have a role in substrate binding, either by actively participating, or by needing to

maintain a neutral role to allow substrate binding to occur (Robinson *et al.*, 2008). The second possibility cannot be excluded with the current results, but based on the findings here, they are not likely to actively participate in substrate binding.

Another asymmetric residue that has been reported to interact with the substrate is S238. The backbone oxygen of residue S238 has been proposed to form a hydrogen bond with the N6 of the adenine moiety of the nucleotides (Dehez *et al.*, 2008; Mifsud *et al.*, 2013; Robinson *et al.*, 2008; Wang and Tajkhorshid, 2008). This proposal is not supported by the results in this study. Consistently, it has been shown that mutations of the equivalent residue of ScAac2 to Ala, Cys, Leu, Ile, Val and Thr, still allowed transport of ADP, showing that this residue is not essential for adenine recognition (King *et al.*, 2020).

Finally, sequence analysis studies (Kunji and Robinson, 2006; Robinson and Kunji, 2006;) and molecular dynamic simulation studies (Wang and Tajkhorshid, 2008) proposed residue I193 is in hydrophobic contact with adenine moiety of the nuclotides. Moreover, this residue is part of the 47 amino acid long fragment that was labeled with 2-azido[a^{32}P]-ADP (Dalbon *et al.*, 1988). The label was attached to this residue, together with two other lysine residues (K162 and K165 of the bovine carrier), equivalent of K172 and A175 in TtAac, which are located in matrix helix h34 and are not conserved in AAC orthologues.

4.6. The same residues are involved in binding of both substrates, ADP and ATP

A very interesting finding was that there was no statistical difference between the response induced by ADP and ATP for any of the variants or the wild type at any concentration (detailed results of statistical tests in **Appendix 3**) (**Figure 4.8**). The only exception, variant Y89A showed a difference between the two substrates at 1 mM (p-value = 0.0094) (**Figure 4.8**). Even though this difference could be due to type I error, as it was not reproduced in any of the other concentrations, it could be interesting to investigate that mutant further with regards to its response to the two nucleotides.

This finding demonstrated that the two substrates interact with the translocation pathway residues in the same way, regarding the number of residues, as well as the chemistry and geometry. The same residues were shown to be critical or with

contributing roles for the binding of both substrates and with the same effect. Hence ADP and ATP must bind to the same site in the same way. Since mitochondrial carriers function as monomers (Bamber *et al.*, 2006; Bamber *et al.*, 2007a; Bamber *et al.*, 2007b; Kunji and Crichton, 2010; Kunji and Harding, 2003; Kunji and Ruprecht, 2020; Ruprecht *et al.*, 2019), this indicates that the import and export steps must be consecutive. This further supports the proposals for a ping pong kinetic mechanism (Klingenberg, 2008), as opposed to claims for a simultaneous mechanism (Duyckaerts *et al.*, 1980; Palmieri, 1994). Additionally, the direction of transport, with regards to the properties of the protein, should be fully reversible, as it can be confirmed with transport assays in proteoliposomal systems (**Chapter 5**). What defines directionality of the exchange in mitochondria is the relative concentrations of the two nucleotides on the two sides of the mitochondrial inner membrane and the membrane potential.

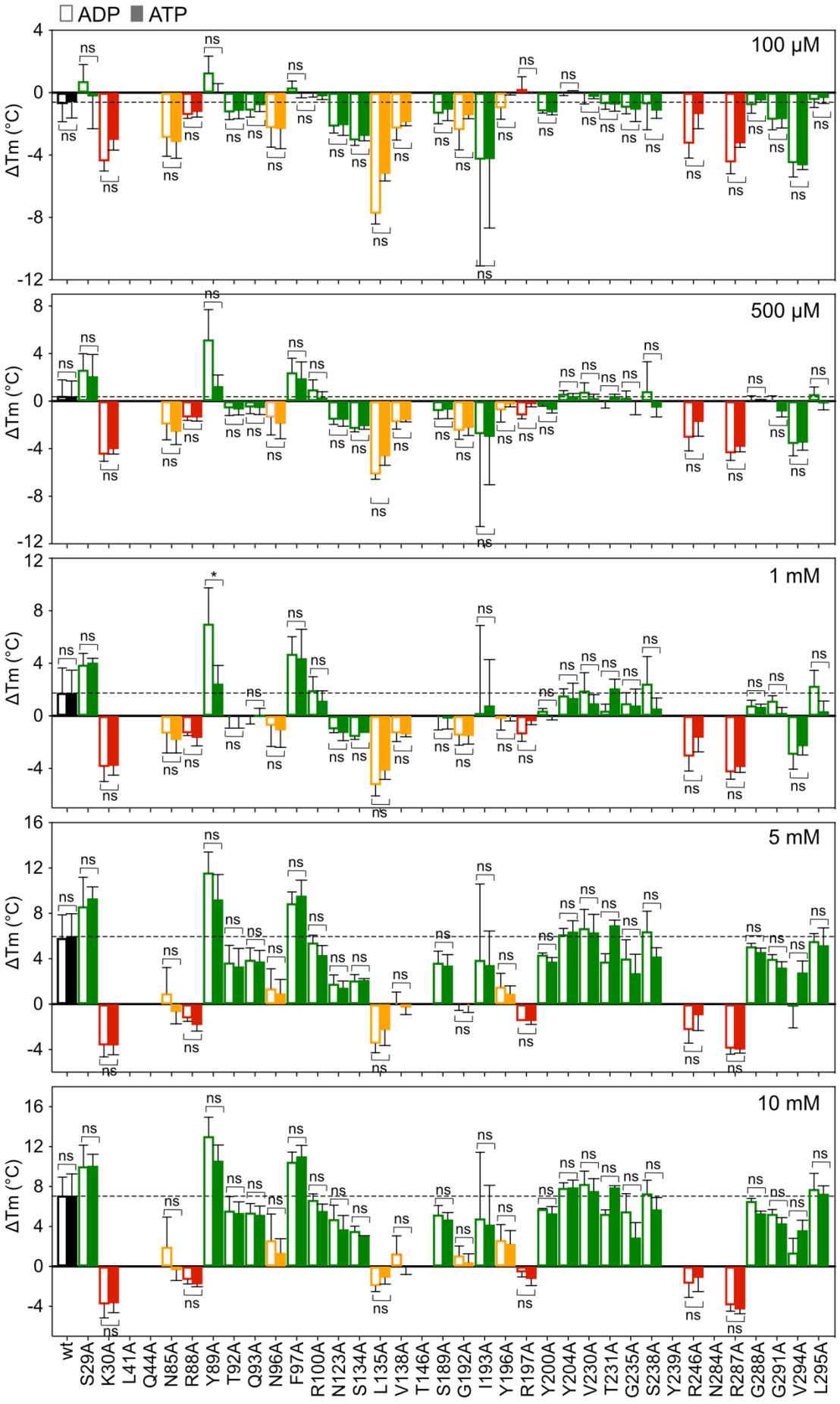
ADP
ATP
100 µM
500 µM
1 mM
5 mM
10 mM
ΔTm (°C)
wt
S29A
K30A
L41A
Q44A
N85A
R88A
Y89A
T92A
Q93A
N96A
F97A
R100A
N123A
S134A
L135A
V138A
T146A
S189A
G192A
I193A
Y196A
R197A
Y200A
Y204A
V230A
T231A
G235A
S238A
Y239A
R246A
N284A
R287A
G288A
G291A
V294A
L295A

Figure 4.8: Thermostability shift values (ΔTm) at 0.1, 0.5, 1, 5 and 10 mM ADP compared with the equivalent shifts induced by ATP for the wild type and all variants. Bars and error bars represent the mean and standard deviation of 3-8 independent experiments. Empty and filled bars represent ADP and ATP, respectively. The colours of the bars are related to the response of the variants to substrate, as defined in **Figures 4.5, 4.6** and **4.7**. Significant differences between the two nucleotides were evaluated by two-way ANOVA with interaction, followed by Šidák post-hoc test to correct for multiple comparisons (tests shown in **Appendix 3**).

4.7. Statistical analysis of the results

Since the differences in the responses of the variants were not always vastly different compared to the wild type, as it was for example for the variants in **section 4.3**, it was essential to have enough independent biological repeats, to accurately represent the variability between experiments. For this purpose, as listed in **Table 4.2**, multiple growths of most constructs were performed, making up to 72 separate fermenter runs/shaker cultures (825 L) for isolation of crude mitochondria. In total, 221 different purifications were performed to be used in biologically independent assays. Furthermore, the choice of statistical analysis was very important, to avoid overinterpretation or misinterpretation of the results.

It was noted that there were factors that could affect the shifts exhibited by the proteins between different purifications. For example, usage of different batches of detergent and lipids (included in the purification buffers) could affect the thermostability shifts. Because of the time scale that the experiments were conducted, it was not possible to keep these conditions exactly the same, using the same batch of lipids or detergent throughout the project. However, it was ensured that the wild-type protein was assayed in the same conditions that were applied to variants, because the variants were always compared against the wild type. As an example, since the detergent-lipid stock that was used in the purifications was a determining factor, the wild type was purified and assayed with all detergent-lipid stocks prepared for the variants and one repeat of each was included in the analysis.

Moreover, it was necessary for some variants to be assayed more times than others (**Table 4.2**). This happened when the result was not entirely clear, hence the reliability on the statistics would be higher. Therefore, a more accurate representation of the variance was required. The statistical analysis though accounts for the slightly different N numbers. Furthermore, attention was paid on the intervals that the means

were presented with before applying any statistics, as recommended by (Habibzadeh and Habibzadeh, 2015).

Different statistical tests were tried in the course of the ongoing experiments. Initially, student t-tests for each substrate at each concentration comparing with the equivalent condition of the wild type were applied. However, in this case, there was the issue of 'multiple testing', meaning that some p-values will be less than the significance level (α) just by chance (Curran-Everett, 2000). Therefore, it was reasoned that ANOVA would be a more suitable analysis, because the means of all groups would be considered and also, there would be the chance to correct for multiple comparisons (Mishra et al., 2019). Since two independent variables were tested (ADP and ATP), a two-way ANOVA test was selected. In this way, the means between the different groups within the substrate level could be compared, but also the means for the two substrates within each protein level. In the first case, the effect of ADP on each variant was compared with the effect of ADP on the wild-type protein and significant differences were identified using Dunnett's post hoc test. The same analysis was conducted for ATP. In the second case, the effect of ADP on each protein (wild type or variant) was compared with the effect of ATP on the same protein. Šídák post-hoc test was used in this case. For the choice of post hoc tests the statistics guide of GraphPad prism was used as the main source (H. J. Motulsky, GraphPad Statistics Guide). One-way ANOVA for each substrate, comparing against the wild type with Dunnett post hoc correction, was tried as well and gave similar outcomes. Two-way ANOVA was chosen as it was thought it could better describe the meaning of the results.

Table 4.2: Number of biological repeats performed in the study.

Protein	No of cultures x volume (L)	No of purifi cations	CPM assay with nucleotides	CPM assay with inhibitors	Reconsti tutions
Wild type	4x50	35	8	8	30
S29A	1x10	4	3	3	
K30A	2x10	8	5	4	5
L41A	1x10 + 1x5	3	protein unfolded		
Q44A	1x10 + 1x5	3	protein unfolded		
N85A	4x10	9	7	5	5
R88A	1x10	6	4	4	3
Y89A	2x10	4	3	2	1
T92A	2x10	5	4	5	
Q93A	1x10	4	4	2	
N96A	3x10	11	6	6	5
F97A	1x10	4	3	3	2
R100A	1x10	3	3	3	
N123A	3x10	12	5	3	5
S134A	2x10	5	3	3	1
L135A	3x10	9	3	2	4
V138A	2x10	8	4	4	5
T146A	1x10 + 1x5	3	protein unfolded		
S189A	1x10	3	3	3	
G192A	3x10	7	3	3	3
I193A	3x10 + 1x5	8	5	2	4
Y196A	2x10	6	4	4	3
R197A	2x10	6	3	3	3
Y200A	1x10	3	3	3	
Y204A	1x10	4	3	2	2
V230A	1x10 + 1x5	3	3	2	
T231A	1x10	4	3	3	
G235A	1x10	3	3	3	
S238A	2x10	3	3	3	1
Y239A	1x10 + 1x5	3	protein unfolded		
R246A	1x10 + 1x5	7	4	4	2
N284A	1x10 + 1x5	3	protein unfolded		
R287A	2x10	7	4	4	5
G288A	1x10	3	3	3	
G291A	1x10	3	3	3	
V294A	1x10 + 1x5	5	5	5	
L295A	2x10	4	3	2	

4.8. Discussion

Various studies made proposals for the location of the substrate binding site in the mitochondrial ADP/ATP carrier (Dalbon *et al.*, 1988; Dehez *et al.*, 2008; Dianoux *et al.*, 2000; Majima *et al.*, 1998; Mayinger *et al.*, 1989; Mifsud *et al.*, 2013; Pietropaolo *et al.*, 2016; Robinson and Kunji, 2006; Robinson *et al.*, 2008; Tamura and Hayashi, 2017; Wang and Tajkhorshid, 2008; Yao *et al.*, 2021). In this chapter, the question of the substrate binding site location, as well as the mechanism with which substrate binding triggers the conformational changes required for translocation have been addressed experimentally with the relevant substrates. The approach made use of a thermostability shift assay which allowed for a complete assessment of the substrate binding process. After investigating all residues of the translocation pathway, residues with critical and contributing binding roles were identified and were shown to cluster in a confined area, roughly in the middle of the translocation pathway. The same residues were shown to be critical and important for binding of both ADP and ATP (**Figures 4.5, 4.6** and **4.8**), implying that the two substrates bind to the carrier in the same way. Since ADP/ATP carriers function as monomers (Bamber *et al.*, 2006; Bamber *et al.*, 2007a; Bamber *et al.*, 2007b; Kunji and Crichton, 2010; Kunji and Harding, 2003; Kunji and Ruprecht, 2020; Ruprecht *et al.*, 2019), this observation indicates that the import and export steps must be consecutive, supporting a ping-pong kinetic mechanism.

In the case of residues K30, R88, R197, R246 and R287, mutation to alanine led to loss of function (**Figure 3.5**) and complete abolishment of the substrate-induced thermostability shifts (**Figure 4.5**). Considering their chemical properties, it is possible that these residues are involved in ionic interactions with the phosphate groups of the nucleotides. Forming such a strong interaction, they can make relatively large contributions to the overall interaction energy of substrate binding (Klingenberg, 2007; Springett *et al.*, 2017). This hypothesis matches with the completely abolished effect upon disruption of the putative interaction. On the other hand, alanine replacement of residues N85, N96, L135, V138, G192 and Y196 resulted in partial or complete loss of function (**Figure 3.5**) and in significantly reduced thermostability shifts in the presence of substrates (**Figure 4.6**). Because the shifts were not completely abolished in these cases and taking the relative positions and chemical properties of these amino acids into account, it is possible that residues L135, V138, G192 and Y196 are jointly involved in binding of the adenosine moiety. They potentially form weaker interactions

than the aforementioned charged residues, e.g. hydrophobic and aromatic stacking interactions and thus they have smaller individual effects on the overall interaction energy of substrate binding. This hypothesis matches with the reduced effect upon disruption of the putative interactions.

Residues R88 and R287, proposed here to form critical interactions with the substrate correspond to 'contact points' I and III, identified with sequence analysis, as analysed in **section 4.1** (Kunji and Robinson, 2006; Robinson and Kunji, 2006). Residue K30 is located between them at the same height in the central cavity. Residues G192 and Y196 identified to have a contributing role to substrate binding correspond to 'contact point II', whereas residues L135 and V138 are nearby at the same level. All these residues are accessible in both conformational states and have similar conformers (**Figure 4.9**). This observation indicates that they can participate in substrate binding with a similar geometry, hence they are likely to form the main binding site. The location of this site is consistent with the proposal that it acts as the fulcrum of all conformational changes occurring during the transport cycle (Ruprecht *et al.*, 2019), since the 'contact points' form hinge points between the core and the gate elements of the protein domains (Ruprecht *et al.*, 2019).

The four other residues shown to participate in substrate binding seem to form two pairs on opposite sides of the main site. One pair N96/R197 is located towards the cytoplasmic side, while the other, made of N85/R246, is located towards the matrix side of the cavity. Comparing the structures of the two conformational states, it can be easily observed that these pairs change conformers in a state-dependent manner. In the cytoplasmic-open state, residues R197 and N96 point towards the opening of the cavity, whereas they are part of the main binding site in the matrix-open state. Conversely, residues R246 and N85 are pointing towards the opening of the cavity in the matrix-open state, whereas they are part of the main binding site in the cytoplasmic-open state (**Figure 4.9**). It is possible that these pairs are responsible for the initial binding of the substrate (when they face the opening of the cavity) and subsequently, they become part of the main site, potentially guiding the substrate to bind with a precise conformation. Finally, they might also participate in the release of the substrate to the other side, becoming also available to bind another substrate on that side, for the cycle to be completed (**Figure 4.9**). These state-dependent interactions could be key for driving the conformational changes in the carrier that are required for substrate translocation. Furthermore, they could potentially contribute to

guiding the adenine moiety to bind with a precise geometry, to ensure the strict specificity of ADP/ATP carriers (De Marcos Lousa et al., 2002; Dolce *et al.*, 2005; King *et al.*, 2020; Mifsud *et al.*, 2013; Pfaff and Klingenberg, 1968). ADP and ATP are large molecules and conformationally diverse, hence they might need these additional interactions in order to be precisely guided, while adapting a series of conformers during the substrate translocation process. The relative position of the central site with the two pairs, as well as the fact that both pairs have the same chemistry may explain why the transport process is fully reversible. The substrates are being involved in similar interactions, independent of the direction they came. These hypotheses are based on the observed conformers in the two available structures, but for their validation structures of the intermediate bound states should be determined, or other techniques should be used. In a first approach, the transport activities of these variants were evaluated in **Chapter 5**.

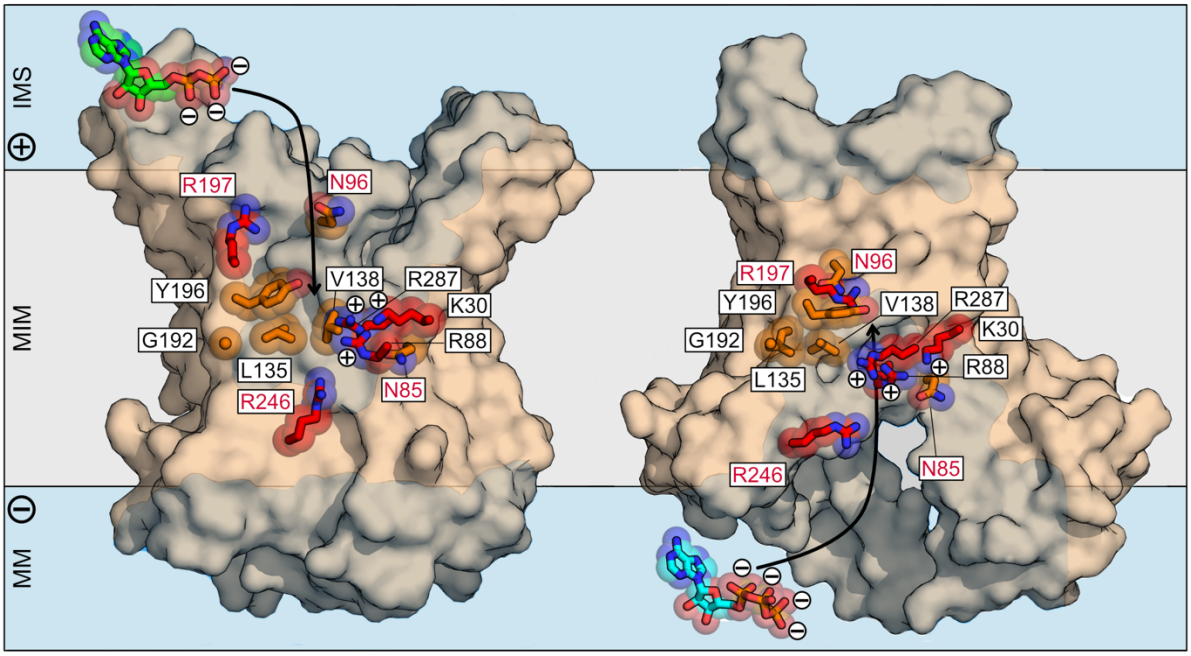

Figure 4.9: **The mitochondrial ADP/ATP carrier has a main substrate binding site accessible in both states and two arginine/asparagine pairs that bind substrates in a state-dependent way.** Lateral views from the membrane of the cytoplasmic-open (left) (PDB code 4c9h chain A) and matrix-open state (PDB code 6gci chain A) (right) of the mitochondrial ADP/ATP carrier (wheat surface). Residues of the water-filled cavity (labeling according to the TtAac orthologue) that have critical and contributing roles in substrate binding are represented in red and orange, respectively, while the substrates ADP and ATP are shown in green and cyan, respectively. The water-accessible surfaces are shown in blue.

Chapter 5: Transport properties of mutants of the residues participating in the substrate binding process

5.1. Introduction

In **Chapter 4** the substrate binding properties of the variants compared to the wild type were evaluated using CPM thermostability shift assays. Based on the response of the variants to the substrates, five residues (K30, R88, R197, R246 and R287) were proposed to participate in critical interactions and another six (N85, N96, L135, V138, G192 and Y196) to have contributing roles in substrate binding. In **Chapter 5** this result was further explored by using substrate uptake assays.

Uptake assays are the key technique for investigating the overall transport activity of a carrier. The transport activity is affected by all of the steps taking place during the transport cycle. Therefore, mutation of a residue participating in any key step of the process is expected to cause either loss of activity, if their role is critical, or differences in the uptake rate compared to the wild-type protein. The analysis usually performed includes the calculation of the half maximal velocity or Michaelis-Menten constant (K_m) and the V_{max} values. The V_{max} is the maximal velocity or maximal rate the reaction (substrate uptake) can take place at. The K_m value represents the concentration at which the reaction takes place with half the maximal velocity. It can be calculated by plotting the initial rates of the reaction at different substrate concentrations (taken from the linear part of the uptake curve) against the concentration range. It is used as an indicative measure for affinity. However, these parameters are affected by factors not limited to the substrate binding step. Hence these results were evaluated in combination with the rest of the assays used in the analysis (functional complementation in **Chapter 3** and thermostability shift assay in **Chapter 4**).

Uptake assays can be performed in various systems, including whole cells, isolated organellar (disrupted) membranes, isolated intact organelles, membranes fused with vesicles or proteoliposomes containing the transporter of interest. In this chapter, uptake assays were performed with purified protein reconstituted into

liposomes. The major advantage of this system is that it is simpler to study, as there is no interference from other proteins (e.g. carriers that transport the same substrate or other proteins that can potentially bind it) and the conditions of the assay can be varied systematically to allow for detailed studies. For example, the internal and external substrate concentrations can be controlled, making it ideal for studying substrate kinetics. With assays conducted in whole cells or isolated mitochondria, it is often difficult to control the internal substrate concentration. Moreover, the amount of protein and the ratio between protein and lipid can be manipulated, to optimise transport rates. Finally, because ADP and especially ATP are common molecules participating in many processes, it is important to study their transport in isolated systems, as they can interact with many proteins, including primary active transporters, such as ABC transporters and different ATPases and other adenine nucleotide carriers in mitochondria, most notably the ATP-Mg/phosphate carriers.

5.1.1. Aims

The aims of this chapter were firstly to establish a suitable reconstitution and uptake assay for the wild-type TtAac and subsequently test the transport properties of selected variants. Primarily, the mutant carriers of the eleven residues proposed in **Chapter 4** to be involved in substrate binding, providing either critical interactions (**Figures 4.5)** or contributing to binding (**Figures 4.6**) were tested. In addition, a selection of variants of residues shown not to be involved in substrate binding was assayed, because they presented some interesting properties or to serve as controls (part of **Figure 4.7**). For example, variant Y89A was stabilised by the substrates to a greater extent than the wild type, hence it was interesting to investigate how this property would influence uptake assays. Residue S134 is in very close proximity to residues identified to be involved in substrate binding, hence it could serve a control.

5.2. Uptake assays of the wild-type protein

In order to assay transport activity, purified proteins were reconstituted into liposomes loaded with substrate, typically 1 mM ATP. Excess substrate was removed from the external environment by gel filtration, after reconstitution had taken place and the uptake was initiated by adding radiolabelled substrate externally. In the experiments described in this Chapter, transport was initiated with 1 μM [^{33}P]-ATP, or 25 μM [^{33}P]-ATP when indicated in the figure, or 0.1, 0.25, 0.5, 1, 5, 25, 50 or 100 μM [^{33}P]-ATP in

the kinetic analysis. The reaction was monitored for 10 min. Proteoliposomes without a counter substrate (no internal control), or with addition of both inhibitors (CATR, BKA) to the external environment were used as controls. Both of these conditions provide a good estimate of the background. Empty liposomes can be used as uniport activity is extremely low for AAC and in the second case, addition of both inhibitors externally fully prevents transport, because the carrier can be trapped in either conformational state. The initial rates of the reaction were calculated from the linear part of the uptake curve, typically between 30 and 60 seconds, dependent on the R squared values.

5.2.1. The effect of different lipids on transport activity

Mitochondrial membranes have a distinct lipid composition compared to other organelles and the plasma membrane. Even from different cell types, mitochondrial membranes share these common features: Low lipid to protein ratios, the dominant phospholipids are phosphatidyl choline (PC) and phosphatidyl ethanolamine (PE) (80%), high cardiolipin (CL) content (10-15%) and low amounts of sterols and sphingolipids (Horvath and Daum, 2013). It has been shown that different lipid composition can greatly affect protein activity and function (Neumann et al., 2017). Consequently, uptake assays in liposomes composed of four different lipid combinations were tested (for the exact lipid composition see **Table 5.1**).

1. *E. coli* polar lipid extract / Egg PC / TOCL at a ratio of 15:5:1 (w/w)
2. Egg PC / TOCL at a ratio of 20:1 (w/w)
3. Bovine heart total extract / Egg PC / TOCL at a ratio of 15:5:1 (w/w)
4. Bovine heart polar extract / Egg PC / TOCL at a ratio of 15:5:1 (w/w)

Egg PC and TOCL were always included in the mixture, because PC is the dominant phospholipid in the mitochondrial inner membrane (Funai et al., 2020), responsible for its structural integrity and fluidity (Mejia and Hatch, 2016) and CL has been proven to be essential for the function of proteins in the mitochondrial inner membrane (Martensson et al., 2017) and specifically for mitochondrial carriers and the ADP/ATP carrier (Klingenberg, 2009; Ruprecht and Kunji, 2020).

Table 5.1: Lipid composition of different mixtures purchased from Avanti polar lipids

	E. coli polar extract	Bovine heart total extract	Bovine heart polar extract	Egg PC	TOCL
Lipid (% w/w)					
PC		5.4	8.6	95.5	
PE	67.0	6.8	13.6		
PG	23.2				
PI		2.5	1.0		
PA		1.1	0.6		
CA	9.8	2.3	1.7		> 99
SM				0.5	
Neutral lipid		49.8	57.7		
Unknown		32.1	16.8		
Order no	100600C	171201C	171204C	840051C	710335C
Notes	Natural lipid. No analytical procedures performed by Avanti	Natural lipid from respective tissue.	Natural lipid, derived from total extract.	Natural lipid, derived from total extract. Mixture of different structures.	Synthetic lipid, 18:1

PC: Phosphatidyl choline, PE: Phosphatidyl ethanolamine, PG: Phosphatidyl glycerol, PI: Phosphatidyl inositol, PA: Phosphatidic acid, CA: cardiolipin, SM: Sphingomyelin

5.2.1.1. Comparison between the combinations: *E. coli* polar lipid extract/ Egg PC/ TOCL and Egg PC/ TOCL

Based on more recent work on mitochondrial carriers, two main lipid combination have been used for uptake assays in proteoliposomes: *E. coli* polar lipid extract/ Egg PC/ TOCL at a ratio of 15:5:1 (w/w) (Jaiquel Baron *et al.*, 2021) and Egg PC/ TOCL at a ratio of 20:1 (w/w) (Harborne *et al.*, 2017; Jabalameli *et al.*, 2021; Lee et al., 2015). Here, comparison between these two combinations for wild-type TtAac showed that even though activity was retained in both mixtures (**Figure 5.1A**), the initial rates for the Egg PC/ TOCL mixture (408 ± 47 nmol [^{33}P]-ATP mg AAC^{-1} min^{-1}) were six-fold higher than in the mixture containing *E. coli* polar lipid extract (67 ± 6 nmol [^{33}P]-ATP mg AAC^{-1} min^{-1}) (**Figure 5.1B**) and it provided better signal to background ratio. Furthermore, the Egg PC/ TOCL combination gave more reproducible results between repeats, while for the mixture including the *E. coli* polar lipid extract there was larger

variation between different lot numbers and sometimes no transport was observed (data not shown). This is reasonable, given that it is the total lipid precipitated with acetone and extracted with diethyl ether from the *E. coli* B (ATCC 11303) strain, hence there could be differences between growths (information obtained from the Avanti polar lipids website). In general, lipid extracts have been reported to be more variable than synthetic lipids (Geertsma et al., 2008), as observed here as well.

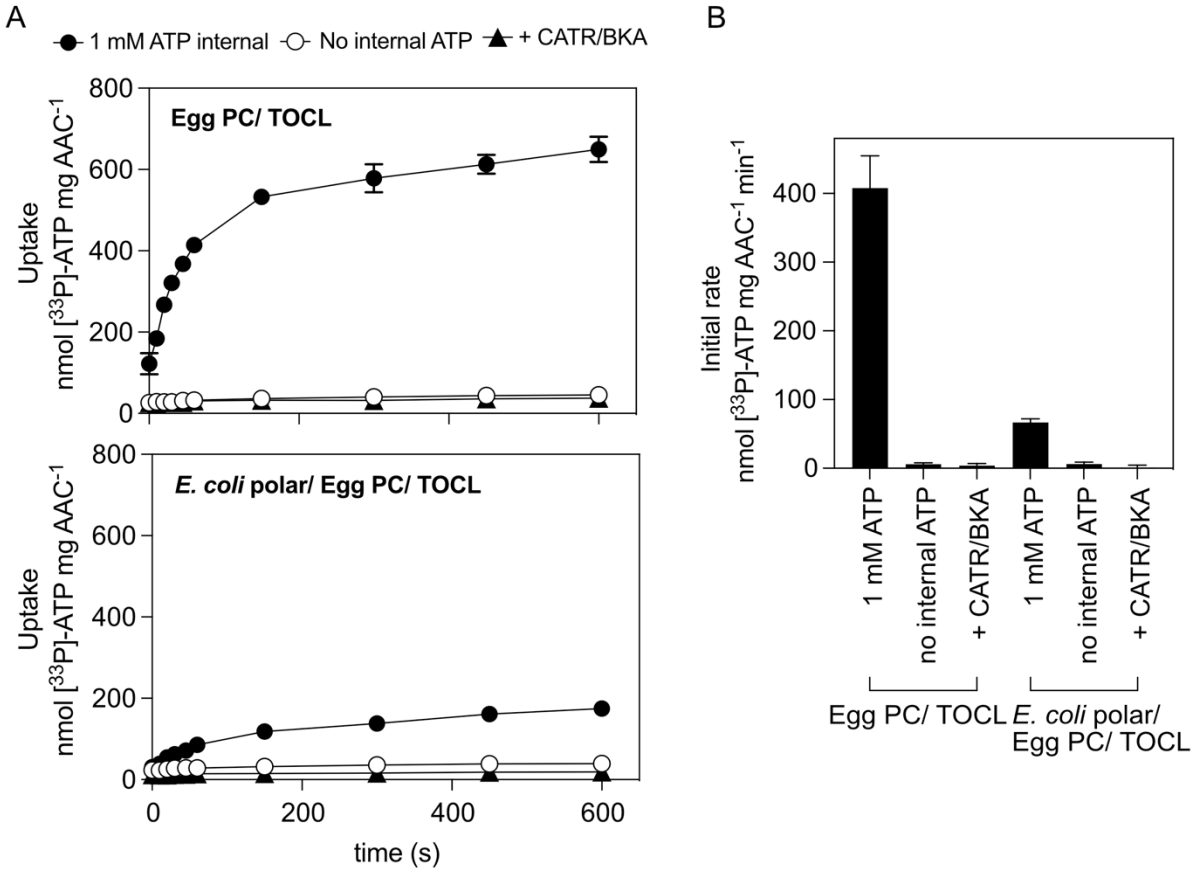

Figure 5.1: Comparison between Egg PC/ TOCL and *E. coli* polar extract/ Egg PC/ TOCL mixtures. (A) Representative uptake assay of [^{33}P]-ATP into proteoliposomes composed of Egg PC/ TOCL (top) and *E. coli* polar extract/ Egg PC/ TOCL (bottom). Filled and empty circles indicate proteoliposomes loaded with 1 mM and 0 mM ATP, respectively and filled triangles proteoliposomes loaded with 1 mM ATP with addition of 10 µM CATR/ BKA externally. The transport was initiated with 1 µM [^{33}P]-ATP. (B) Equivalent initial transport rates determined from the linear part of the uptake curves, typically 30 seconds. The data are represented by the mean and standard deviation of three technical replicates.

5.2.1.2. Comparison between the combinations: Egg PC/ TOCL, Bovine heart polar extract/ Egg PC/ TOCL and Bovine heart total extract/ Egg PC/ TOCL

Subsequently, it was reasoned to also try mixtures that resemble the mitochondrial inner membrane environment better. Hence lipids isolated from bovine heart (total extract and polar extract), which is a tissue rich in mitochondria, were also tried, with the Egg PC/ TOCL combination assayed in parallel. The bovine heart lipids were more difficult to solubilise and they contained some unknown components in their mixtures (**Table 5.1**), that might have affected the reconstitution (**Figure 5.2A**). They required 2.3 times more detergent in order to be solubilised than the Egg PC/ TOCL mixture. However, the same amount of detergent was added to that sample as well, to allow for direct comparison of the uptake. The samples reconstituted in the mixture containing bovine heart total extract were eluted slower from the PD10 column and were not turbid, suggesting that the liposomes were not stable. Protein was detected in all of the samples (**Figure 5.2B**); however, a higher amount of degradation products was present in the samples reconstituted in bovine heart polar extract (**Figure 5.2B**). Furthermore, some protein remained in the stacking gel, indicating that it was precipitated. No uptake was observed in the samples reconstituted in bovine heart lipid extracts, while the Egg PC/ TOCL condition presented uptake with initial rates similar to other experiments, 319 ± 19 nmol [^{33}P]-ATP mg AAC^{-1} min^{-1} (**Figure 5.3**). Therefore, it was concluded that the Egg PC/ TOCL mixture was optimal, as it was providing reproducible results and a high signal to background ratio.

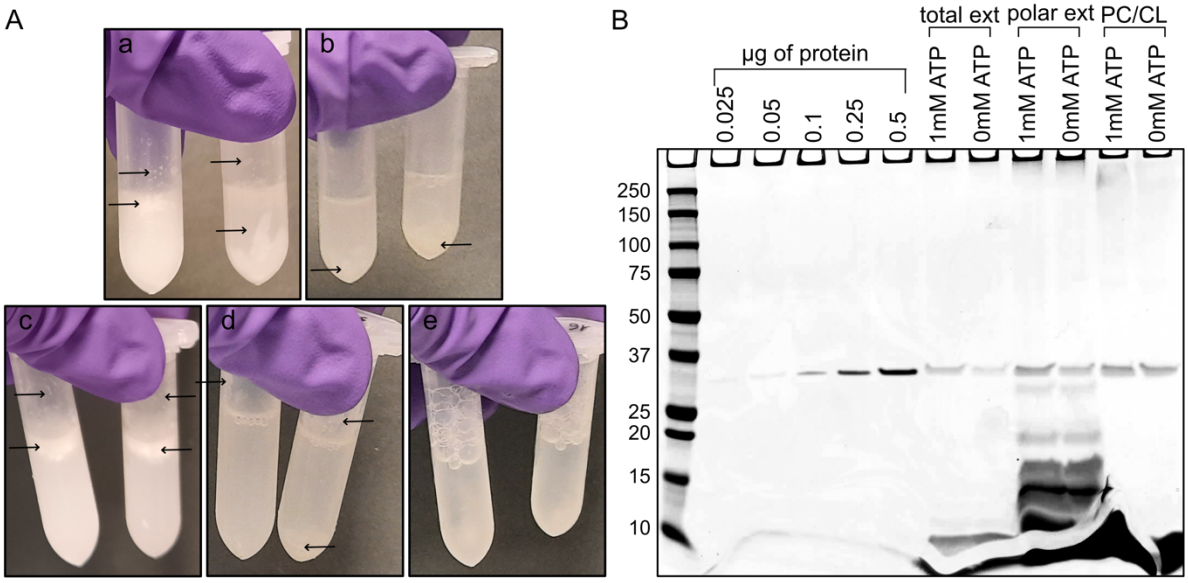

Figure 5.2: Comparison between Egg PC/ TOCL, Bovine heart total extract/ Egg PC/ TOCL and Bovine heart polar extract/ Egg PC/ TOCL mixtures. (A) images taken during the reconstitution process. (a), (b) lipid solubilisation for bovine total extract/ Egg PC/ TOCL and bovine polar extract/ Egg PC/ TOCL mixtures respectively. (c), (d), (e) reconstitution samples before the addition of protein for bovine total extract/ Egg PC/ TOCL, bovine polar extract/ Egg PC/ TOCL and Egg PC/ TOCL respectively. The arrows indicate sediment or suspensions of unknown origin. (B) SDS-PAGE gel of the samples eluted from the PD10 column and used for the uptake assays shown in **Figure 5.3**. Molecular weight marker is shown on the left followed by different amounts of pure protein that were used for protein quantification.

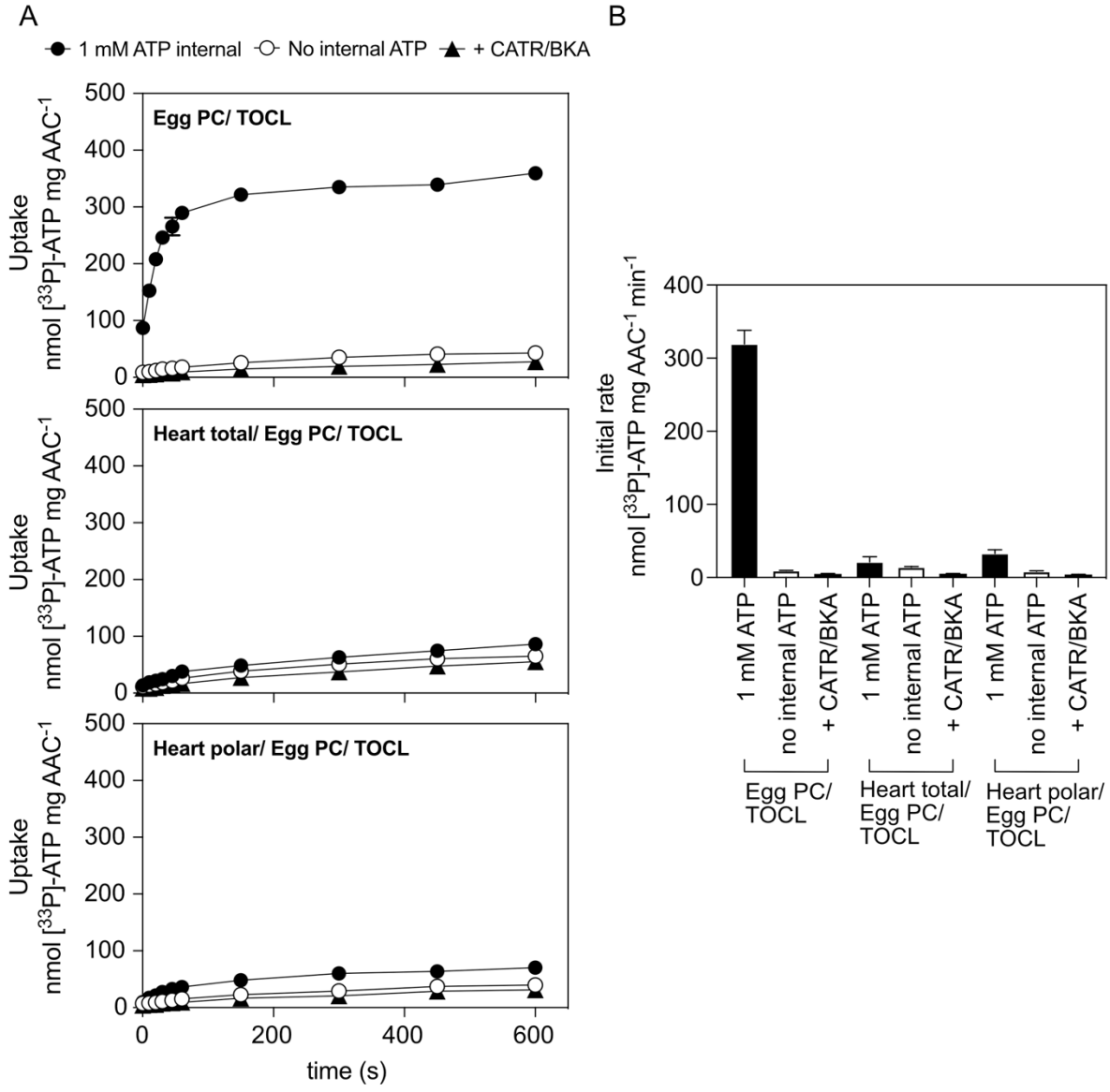

Figure 5.3: Comparison between Egg PC/ TOCL, Bovine heart total extract/ Egg PC/ TOCL and Bovine heart polar extract/ Egg PC/ TOCL mixtures. (A) Representative uptake assay of [^{33}P]-ATP into proteoliposomes composed of the three mixtures. Filled and empty circles indicate proteoliposomes loaded with 1 mM and 0

mM ATP, respectively, whereas filled triangles represent proteoliposomes loaded with 1 mM ATP with addition of 10 µM CATR/ BKA externally. (B) Equivalent initial transport rates determined from the linear part of the uptake curves, typically 30 seconds. The data are represented by the mean and standard deviation of three technical replicates.

5.2.2. The amount of Egg PC is critical for liposome formation

It was noted that uptake rates were affected by the batch of lipids used for reconstitutions, similar to the observations made in **section 4.7** regarding the thermostability shifts. One potential reason could be that the concentration of different batches of lipids provided by Avanti have an up to ±10% error (communication with Avanti). For this reason, in all experiments presented hereafter, the wild type was reconstituted and assayed in parallel with the variants, using the exact same conditions, to allow for comparisons. Furthermore, the minimum amount of Egg PC that is required for formation of intact liposomes was investigated. The wild-type protein was reconstituted in liposomes containing different amounts of Egg PC (6 mg, 12 mg and 18 mg). It was shown that 6 mg of Egg PC are not sufficient to form stable liposomes. After the overnight step of detergent removal, phase separation was observed in those samples (**Figure 5.4A**). Even though roughly the same amount of protein was detected in all samples prior to gel filtration (**Figure 5.4B**), the samples containing 6 mg of Egg PC were eluted from the PD10 column as a transparent solution and no protein could be detected after that step (**Figure 5.4C**), hence no transport activity could be measured. The samples that contained 12 mg and 18 mg Egg PC were successfully reconstituted and the initial rates were similar (12 mg Egg PC: 204 ± 38; 18 mg Egg PC 231 ± 29 nmol [^{33}P]-ATP mg AAC^{-1} min^{-1}) (**Figure 5.4D**). These two conditions gave very similar results and since there were some technical and financial advantages for the smaller lipid amount (lipids drying quicker during reconstitution, faster filtration during the transport assay), the 12 mg Egg PC were used for all the analyses presented in this chapter.

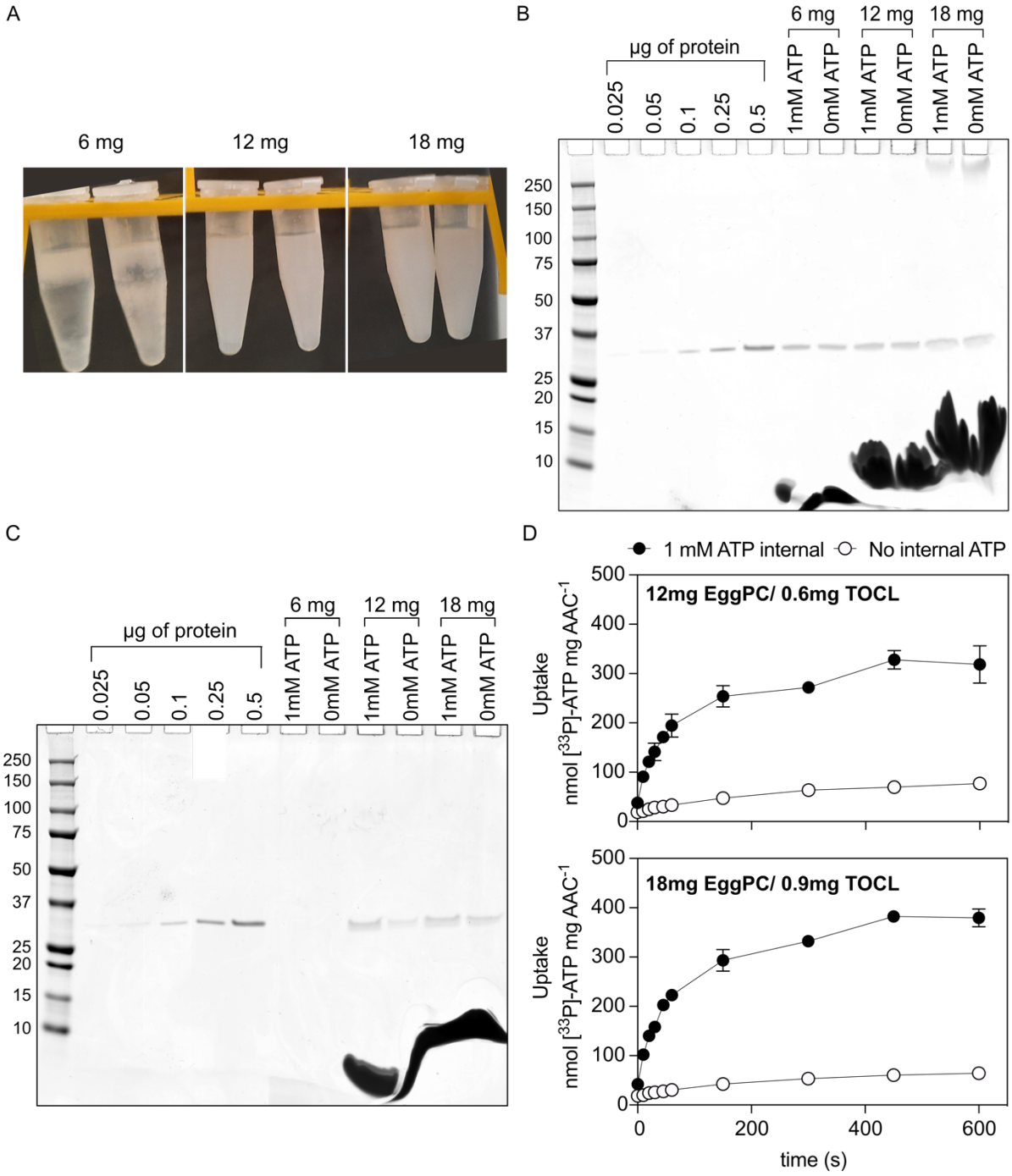

Figure 5.4: Critical amount of Egg PC for the formation of intact liposomes. (A) Image of reconstituted samples after the overnight detergent removal and prior to the gel filtration step. The sample containing 6 mg of Egg PC presents phase separation (B) SDS-PAGE gel of the samples prior to the gel filtration step. Molecular weight marker is shown on the left, followed by different amounts of pure protein that were used for protein quantification. (C) as in (B) after the gel filtration step. (D) Uptake assay of [^{33}P]-ATP into proteoliposomes loaded with 1 mM ATP (filled circles). Proteoliposomes with no internal substrate were used as control (empty circles). Circles and error bars represent the mean and standard deviation of four technical replicates.

5.2.3. The effect of NaCl on reconstitutions

After purification, the protein is stored in a buffer containing 150 mM NaCl. Initially, this NaCl concentration was maintained during reconstitution. However, it was noted that reconstitutions were unsuccessful, as no protein could be detected in those samples (**Figure 5.5A**) and also, no turbid solution was eluted from the PD10 column, suggesting that the liposomes were not stable. Reduction of NaCl concentration to 50 mM resulted in successful reconstitutions and retain of activity (**Figure 5.5B**), hence this condition was used in all experiments shown.

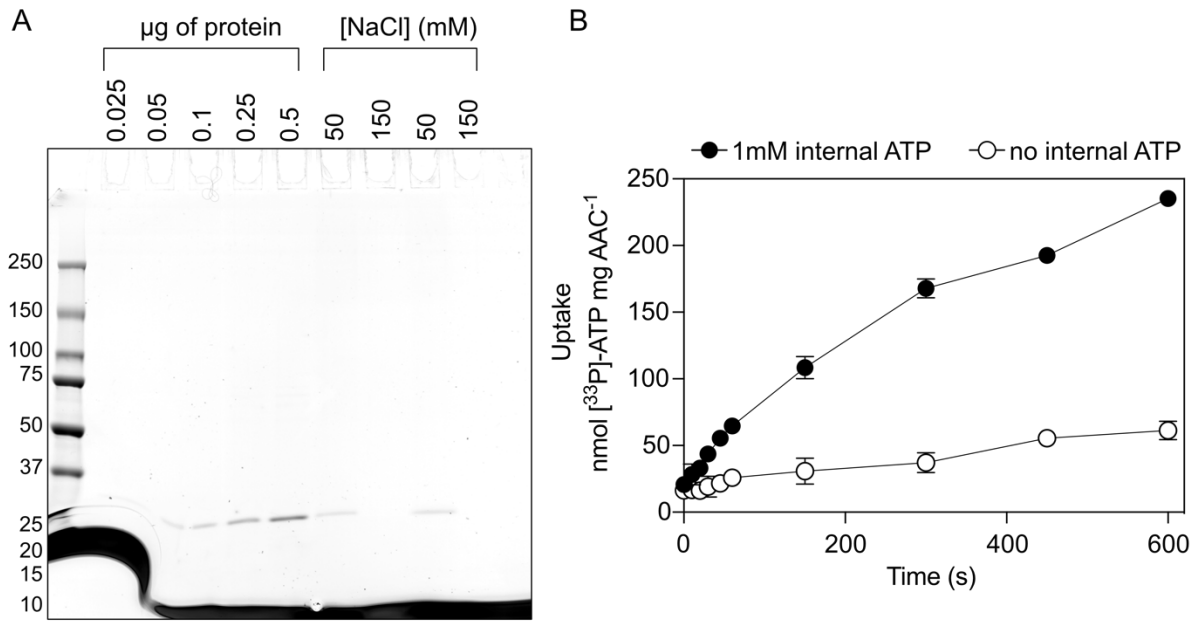

Figure 5.5: The effect of high NaCl concentrations on reconstitutions. (A) SDS-PAGE gel of the samples eluted from the PD10 column after reconstitution in presence of 50 or 150 mM NaCl. Molecular weight marker is shown on the left, followed by different amounts of pure protein that were used for protein quantification. (B) Uptake assay of [^{33}P]-ATP into proteoliposomes loaded with 1 mM ATP (filled circles). Proteoliposomes with no internal substrate were used as control (empty circles). Circles and error bars represent the mean and standard deviation of four technical replicates.

5.2.4. The effect of extrusion on transport rates

It has been shown for the human ADP/ATP carrier that extrusion of the proteoliposomes can improve the transport rates (personal communication with Stephany Jaiquel Baron and Dr Martin King). Hence these two conditions were compared. It was shown that also for TtAac there is a slight increase in transport rates when the proteoliposomes are extruded, the initial rates being 371 ± 42 and 534 ± 21

nmol [^{33}P]-ATP mg AAC^{-1} min^{-1} for non-extruded and extruded samples, respectively (**Figure 5.6**). Reconstitution typically yields multilamellar membranes, which restricts the internal volume of the liposomes, as well as the amount of protein that is exposed to the external solution. Extrusion is thought to enhance the formation of homogeneous proteoliposomes, effectively increasing the internal liposomal volume and the amount of protein that is accessible to interact with the substrate.

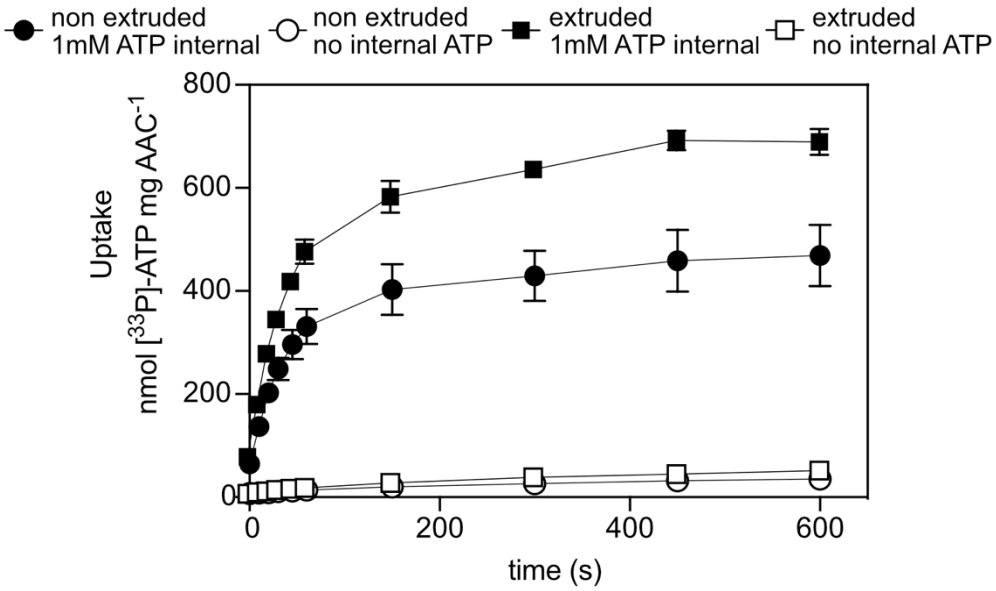

Figure 5.6: Comparison between extruded and non-extruded liposomes. Representative uptake assay of [^{33}P]-ATP into proteoliposomes loaded with 1mM ATP (filled signs). Proteoliposomes with no internal substrate were used as control (empty signs). The data are represented by the mean and standard deviation of four technical replicates for the extruded samples and eight for the non-extruded ones.

5.2.5. Evaluation of background

After deciding on the lipid composition to be used for reconstitution and on the transport assay conditions, the non-related to the protein background of the assay was measured. Optimisation of different buffers and different filters had been performed by other lab members and the use of mixed cellulose ester filters was shown to be compatible with HEPES buffer and [^{33}P]-ATP (personal communication with Dr Martin King and Dr Fiona Fitzpatrick). Here, the DPM increase over time due to interaction of [^{33}P]-ATP with the mixed cellulose ester filters and the liposomes (without protein) was measured. It was shown that the radioactivity remaining bound to the filters was similar when liposomes were present or not (**Figure 5.7A**). Furthermore, these conditions were compared with the 'empty proteoliposomes' condition and showed that the

majority of the background binding in the experimental set-up was due to radioactivity binding to the filters and not to the lipids or the protein (**Figure 5.7A**). However, the background binding was multiple times lower than the uptake observed in proteoliposomes loaded with 1 mM ATP (**Figure 5.7B**), hence these conditions were appropriate to evaluate substrate uptake for the mutant proteins and also, to perform kinetic analyses.

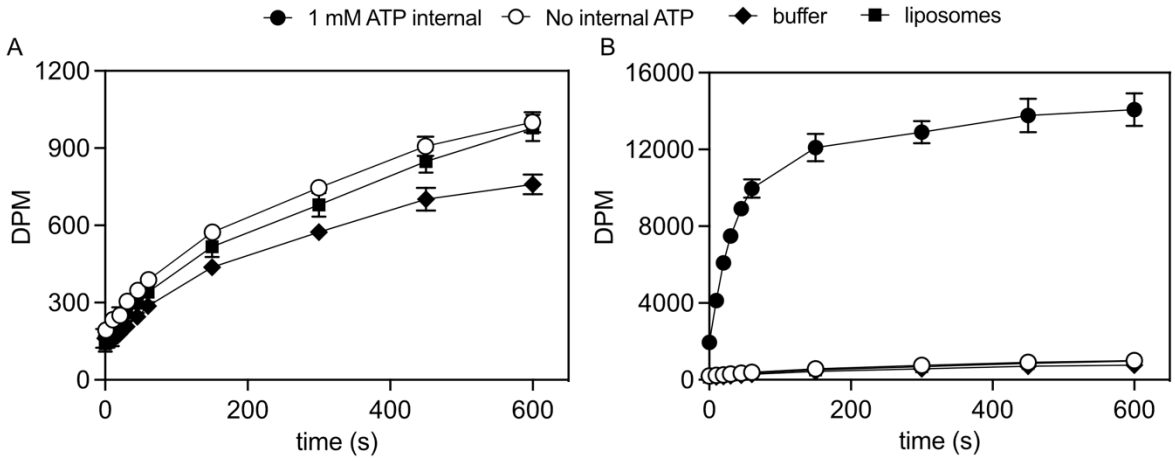

Figure 5.7: Evaluation of background radioactivity binding. (A) DPM values over time obtained in proteoliposomes without internal substrate (empty circles), in liposomes with no protein (filled squares) and by interaction of the filters only with the buffer (filled rhombus). (B) The same conditions were compared with the uptake of substrate in proteoliposomes loaded with 1mM ATP internally (filled circles). The signs and error bars represent the mean and standard deviation of four technical replicates.

5.3. Kinetic characterisation of the wild type

In order to evaluate the transport properties of the wild type, kinetic analysis was performed. The K_m and V_{max} values were obtained by carrying out uptake assays varying the external substrate concentration, while the proteoliposomes were loaded with 1 mM ATP. Proteoliposomes without ATP internally were always assayed in parallel as control. Previous kinetic studies of TtAac performed in lactococcal membranes fused with egg yolk vesicles determined the K_m to be ~ 10 µM (King *et al.*, 2016). Hence a range in low µM concentrations was initially tried and finalised between 0.1-100 µM (**Figure 5.8**). The K_m was determined to be 1.2 µM (95% CI: 0.7-2.3) and the V_{max} 936.1 nmol [^{33}P]-ATP mg^{-1} AAC min^{-1} (95% CI 832.4-1046) from five independent biological repeats. This K_m value is very similar to the one obtained for

the human ADP/ATP carrier (3.2±1.1 μM) assayed in the same system (Jaiquel Baron *et al.*, 2021).

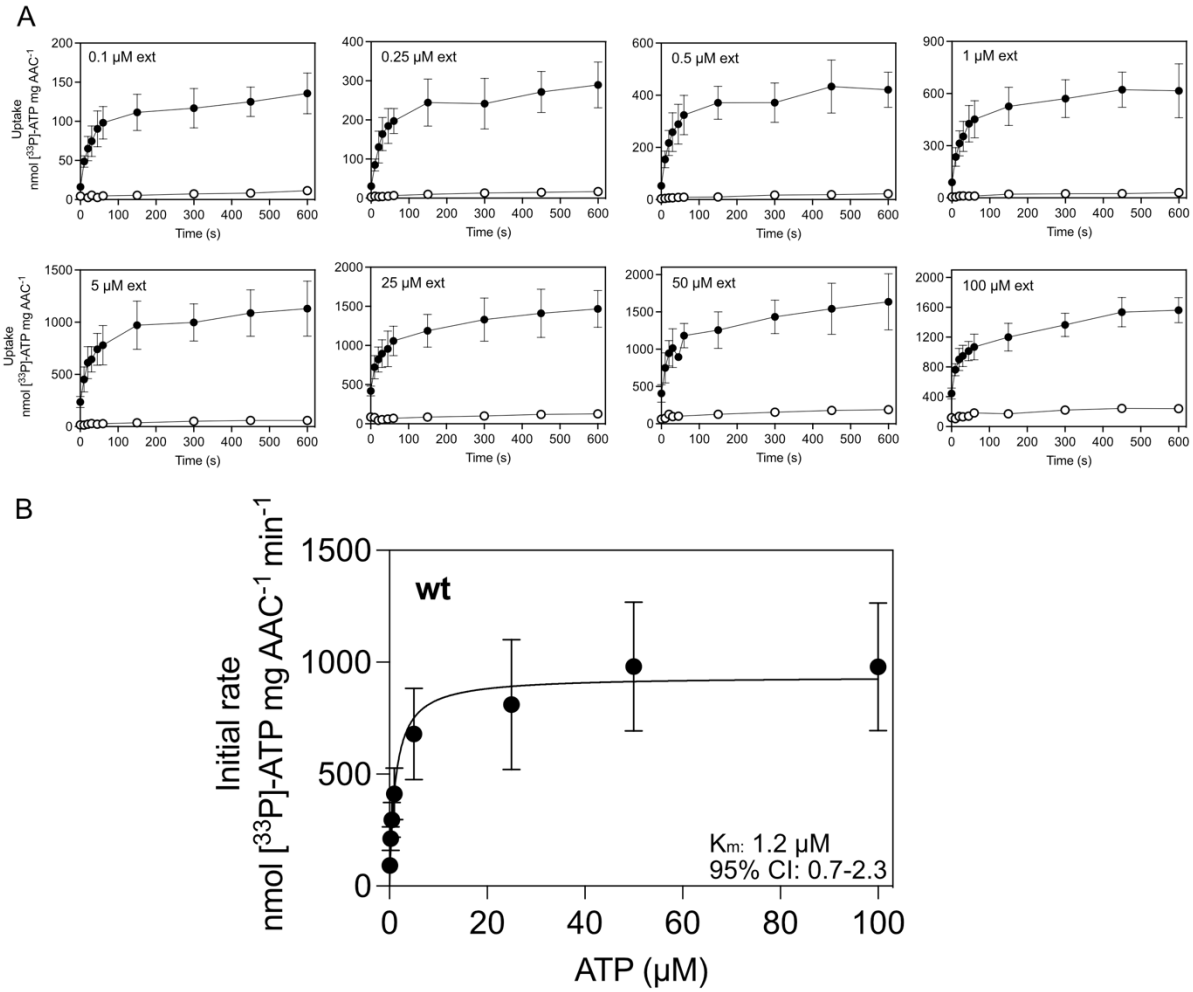

Figure 5.8: Kinetics of ATP uptake for the wild-type protein. (A) Representative uptake curves of [^{33}P]-ATP into proteoliposomes loaded with 1mM ATP (filled circles). Transport was initiated with either 0.1, 0.25, 0.5, 1, 5, 25, 50 or 100 μM [^{33}P]-ATP. Proteoliposomes with no internal substrate were used as control (empty circles). Circles and error bars represent the mean and standard deviation of three technical replicates for loaded proteoliposomes and two for no internal ATP. (B) Initial rates were taken over the linear part of the curves, according to the R-squared values, between 30 and 60 seconds. The circles and error bars represent the mean and standard deviation of five independent biological repeats. The curve was fitted with the Michaelis-Menten function in Prism (GraphPad).

Previous kinetic studies of AAC conducted in mitochondria reported not entirely consistent K_m and maximal rate values. Regarding the K_m, in rat liver mitochondria the values reported were 8.0 ± 1.9 μM (energised mitochondria), 1.9 ± 0.3 (de-energised mitochondria) for ADP and 49.5 ± 11.6 (energised mitochondria), 115.0 ± 10 (de-energised mitochondria) for ATP (Chan and Barbour, 1983). The energised and de-

energised states refer to the presence or absence of membrane potential. In another study using the same system, the K_m values reported were 1.3 μM for ADP and 2.5 μM for ATP (Pfaff et al., 1969). In rat heart mitochondria the values obtained were 1 μM (energised state) and 2 μM (de-energised state) for ADP and 140 (energised state) and 1 μM (de-energised state) for ATP (Duyckaerts *et al.*, 1980). In yeast mitochondria expressing either the human ADP/ATP carriers or ScAac2 the K_m values reported were 3.7 μM (HsAAC1), 2.5 μM (HsAAC2), 8.4 μM (HsAAC3), 1.6 μM (ScAac2) for ADP (De Marcos Lousa *et al.*, 2002). Finally, in a more recent study with TtAac expressed in *L. lactis* membranes which were fused with vesicles composed of *E. coli* polar lipid extract and egg yolk PC the reported value was K_m value 9.3±1.8 μM ADP (King *et al.*, 2016).

Moreover, studies in a liposomal system with carrier purified from beef heart mitochondria and liposomes composed of egg yolk phospholipids gave measurements of K_m (ADP) between 56 and 65 μM, dependent on the type of exchange (homoexchange or heteroexchange) and the direction of transport and K_m (ATP) between 52 and 65 μM in absence of membrane potential and K_m (ADP) between 30 and 75, K_m (ATP) between 68 and 325 μM in presence of membrane potential (Kramer and Klingenberg, 1982). In a more recent study, as mentioned above, where the HsAAC1 was purified and reconstituted in liposomes composed of egg yolk PC and TOCL the value obtained was 3.2 ± 1.1 μM (Jaiquel Baron *et al.*, 2021).

In conclusion, the values reported in the literature for different AAC orthologues and paralogues are in general in the low micromolar range, consistent with this study. The observed differences can be explained taking into consideration the different concentrations applied (or accounted for in intact mitochondria), the presence or absence of membrane potential and the different lipids used, as lipids were shown in **sections 5.2.1.1** and **5.2.1.2** to play a major role for activity.

5.4. Uptake assays of the variants

After the reconstitution and transport conditions were established with the wild-type protein, uptake assays with the variants were carried out. As noted in **section 5.2.2**, the wild-type protein was included in each experiment as a control, to account for differences in lipid preparations and allow for comparisons. For variants that appeared inactive after the initial screening -using liposomes loaded with 1 mM ATP and initiating uptake by adding 1 μM [^{33}P]-ATP externally- a higher external concentration

(25 μM) was also tried. This concentration was selected as it is a concentration at which the wild-type protein approaches V_{max} (**Figure 5.8**). It was reasoned that if activity for the variant could not be observed at the 1 μM external concentration due to a significant increase in the K_m, some activity should be measurable at this concentration. For variants that the initial screening showed transport rates that were measurable, kinetic analysis was also performed (**sections 5.4.1** and **5.1**).

5.4.1. Uptake assays for the mutants of the residues providing critical interactions for substrate binding

Firstly, the variants of the residues proposed in **Chapter 4** to create critical interactions with the substrate were assayed. These variants (K30A, R88A, R197A, R246A and R287A) completely abolished the concentration-dependent thermostability shift occurring in presence of ADP or ATP (**Figure 4.5**) and hence it was proposed that each of these residues forms a critical interaction with the substrate. Consistent with that result, these five variants did not show substrate uptake (**Figures 5.9** and **5.10**). Reconstitution was successful, as protein was detected in SDS-PAGE gels of these variants after the gel filtration step (representative gels for all proteins are shown in **Appendix 4**). However, no activity was observed in 2-5 biological repeats (for the exact number for each variant see **Table 4.2**), even at an external concentration of 25 μM ATP. This result confirmed that these residues play a crucial role in the transport cycle.

In agreement with the results presented here, variants of ScAac2 equivalent to R88A and R88H, R197L, R246I and K30A were shown to be inactive in a system with the carriers reconstituted in phospholipid vesicles (Heidkämper *et al.*, 1996; Klingenberg and Nelson, 1994). Furthermore, similar results were obtained for mutants equivalent to R88H and R246G in *L. lactis* whole cells expressing HsAAC1 (Thompson *et al.*, 2016) and for TtAac mutants K30A, R88A, R197A, R246A in *L. lactis* membranes fused with vesicles (Ruprecht *et al.*, 2019). Additionally, mutants of *Neurospora crassa* AAC equivalent to K30A R88A, R197A, R246A expressed in *E. coli*, refolded from inclusion bodies and reconstituted in liposomes containing PC and TOCL, presented activity between 1-20% (Heimpel *et al.*, 2001). However, in contrast with the present analysis, the equivalent mutant of R287A in ScAac2 was shown to retain full activity (Heidkämper *et al.*, 1996) or 50-72% (Klingenberg and Nelson,

1994). The *N. crassa* orthologue presented 21% activity (Heimpel *et al.*, 2001). In the system where the TtAac orthologue was assayed in *L. lactis* membranes fused with vesicles, the activity of this mutant was less than 10% (Ruprecht *et al.*, 2019).

Additionally, none of these variants complemented growth of the Aac-deficient strain (**Figures 3.4** and **3.5**), a result supported by other studies (**section 3.3** for references). It has also been shown that there is no oxidative phosphorylation in mitochondria of equivalent ScAac2 mutants of R88A, R197L and R246I (Müller *et al.*, 1996).

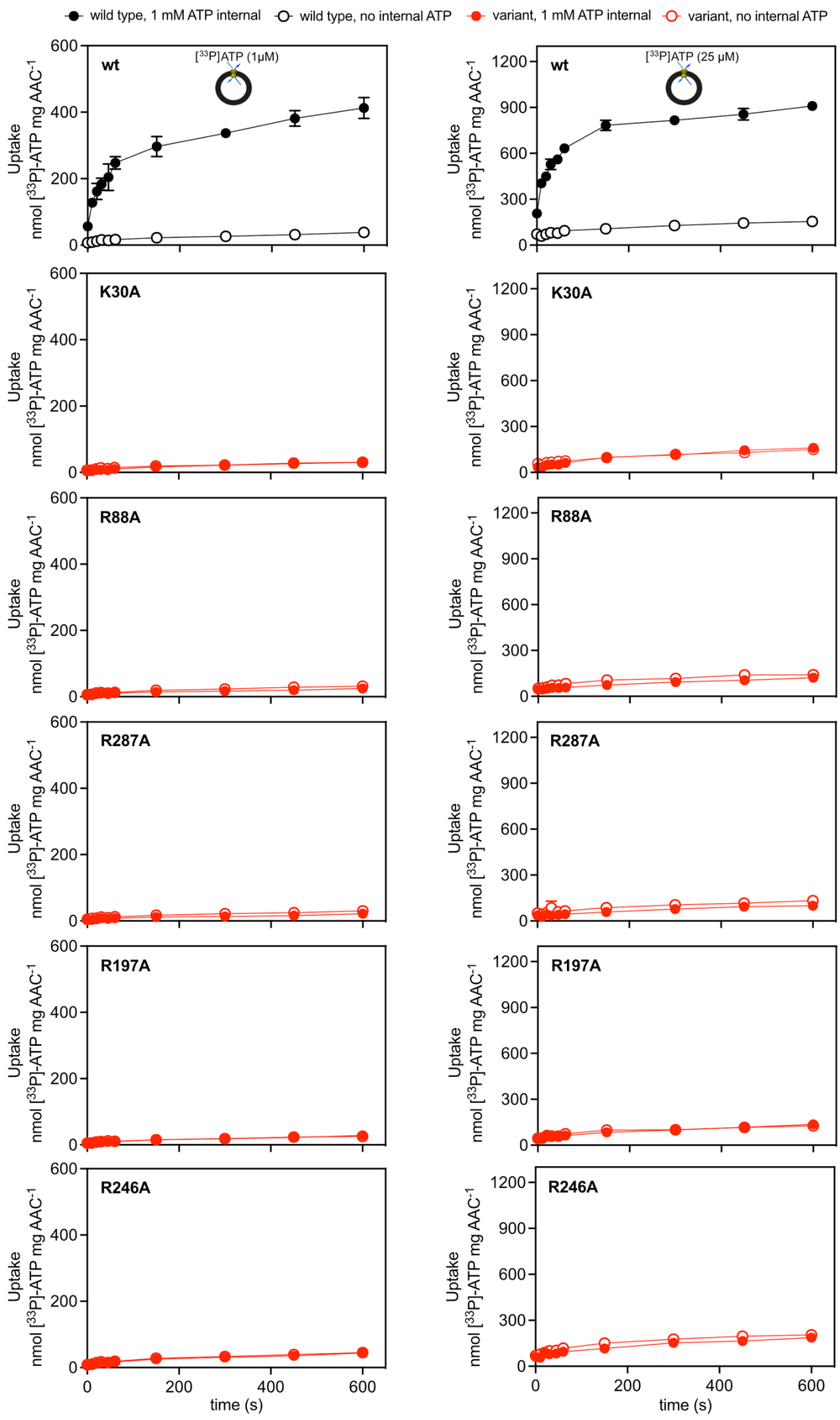
wild type, 1 mM ATP internal
wild type, no internal ATP
variant, 1 mM ATP internal
variant, no internal ATP
wt
[33P]ATP (1µM)
[33P]ATP (25 µM)
K30A
R88A
R287A
R197A
R246A
Uptake
nmol [33P]-ATP mg AAC-1
time (s)

Figure 5.9: Uptake assays for the mutants of the residues providing critical interactions for substrate binding. Representative uptake curve of [^{33}P]-ATP into proteoliposomes loaded with 1mM ATP (filled circles). Proteoliposomes with no internal substrate were used as control (empty circles). Circles and error bars represent the mean and standard deviation of four technical replicates. Error bars are smaller than the symbol whenever not shown.

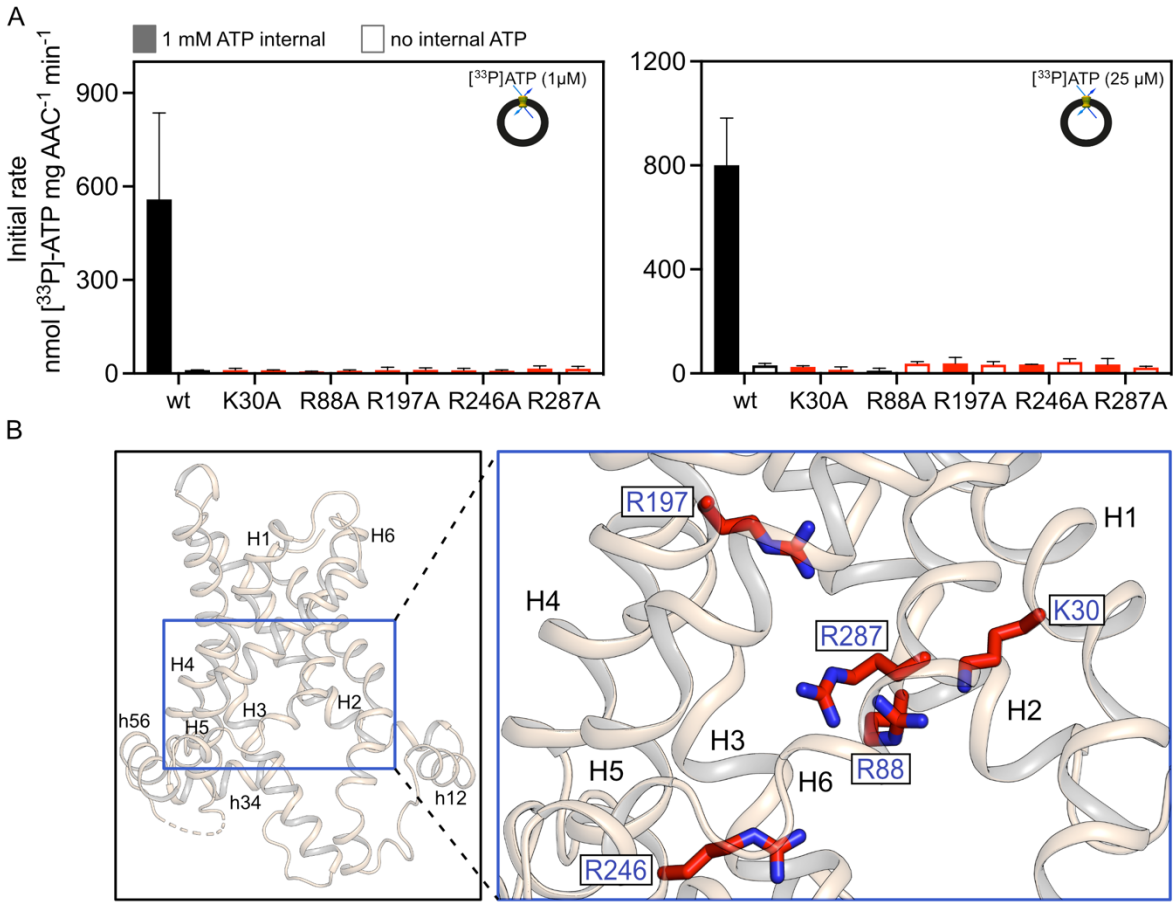

Figure 5.10: The mutants of the residues providing critical interactions for substrate binding are inactive. Initial transport rates determined from the linear part of the uptake curves. Filled (first) and empty (second) bars for each protein represent 1 mM ATP internal and no internal ATP respectively. The bars and error bars represent the mean and standard deviation of three biological repeats for the wild type and two for the variants. (B) TtAac matrix-open structure (PDB code: 6gci chain A) (left) and close-up view (right) showing the analysed residues as in **Figure 4.5**.

5.4.2. Uptake assays for the mutants of the residues with a contributing role to substrate binding

Subsequently, the variants of the residues proposed in **Chapter 4** to contribute to binding were tested. These variants responded to substrate in a concentration-

dependent way, but the thermostability shifts were significantly smaller than that of the wild type (**Figure 4.6**). The initial screening showed that mutants N85A, G192A and Y196A were inactive, while N96A, L135A and V138A presented measurable activity. Therefore, N85A, G192A and Y196A were assayed in presence of two different external [^{33}P]-ATP concentrations (1 and 25 µM) (**Figure 5.11**), while N96A, L135A and V138A were further analysed to determine kinetic parameters (**section 5.4.1**, **Figure 5.13**).

Variants G192A and Y196A presented no activity irrespective of the substrate concentration applied externally (**Figures 5.11** and **5.12**). This confirmed the crucial role of these residues for the transport cycle. Consistently, they did not grow in complementation assays on glycerol (**Figures 3.4** and **3.5**). Transport information is available for these mutants expressed in *L. lactis* and assayed in *L. lactis* membranes fused with vesicles, presenting the same outcome as here (Ruprecht *et al.*, 2019). In another study with the equivalent mutant of Y196A in mitochondria of ScAac2 it was reported that the mutant had 500-fold increased K_m compared to the wild type, but the actual transport data were not presented (David *et al.*, 2008). However, it is evident that the transport activity was severely affected.

Variant N85A presented some activity in one of the biological repeats (7.1% for 1 µM external ATP and 26.8% for 25 µM ATP), but this was not reproduced in the other two biological repeats, where no measurable activity could be obtained (**Figures 5.11** and **5.12**). The wild type assayed in parallel in those experiments though presented results similar to other repeats. This variant could partially complement growth of the Aac-deficient strain (42.4% ± 23.2) (**Figures 3.4** and **3.5**). Therefore, it can be concluded that residue N85 also plays an important role for the transport cycle, but it is not crucial, because the mutation is not detrimental as for residues G192 and Y196. This agrees with the role it may have, proposed in **Chapter 4**, guiding the substrates to bind with a precise geometry and guiding the conformational changes taking place during the transport cycle. This hypothesis, based on its position and state-dependent rotamers, can be supported by these experimental data, since the transport activity is severely affected. There is potentially some residual activity, that could not be accurately determined in the reconstitution system, that allows the Aac-deficient strain expressing this mutant carrier to grow partially.

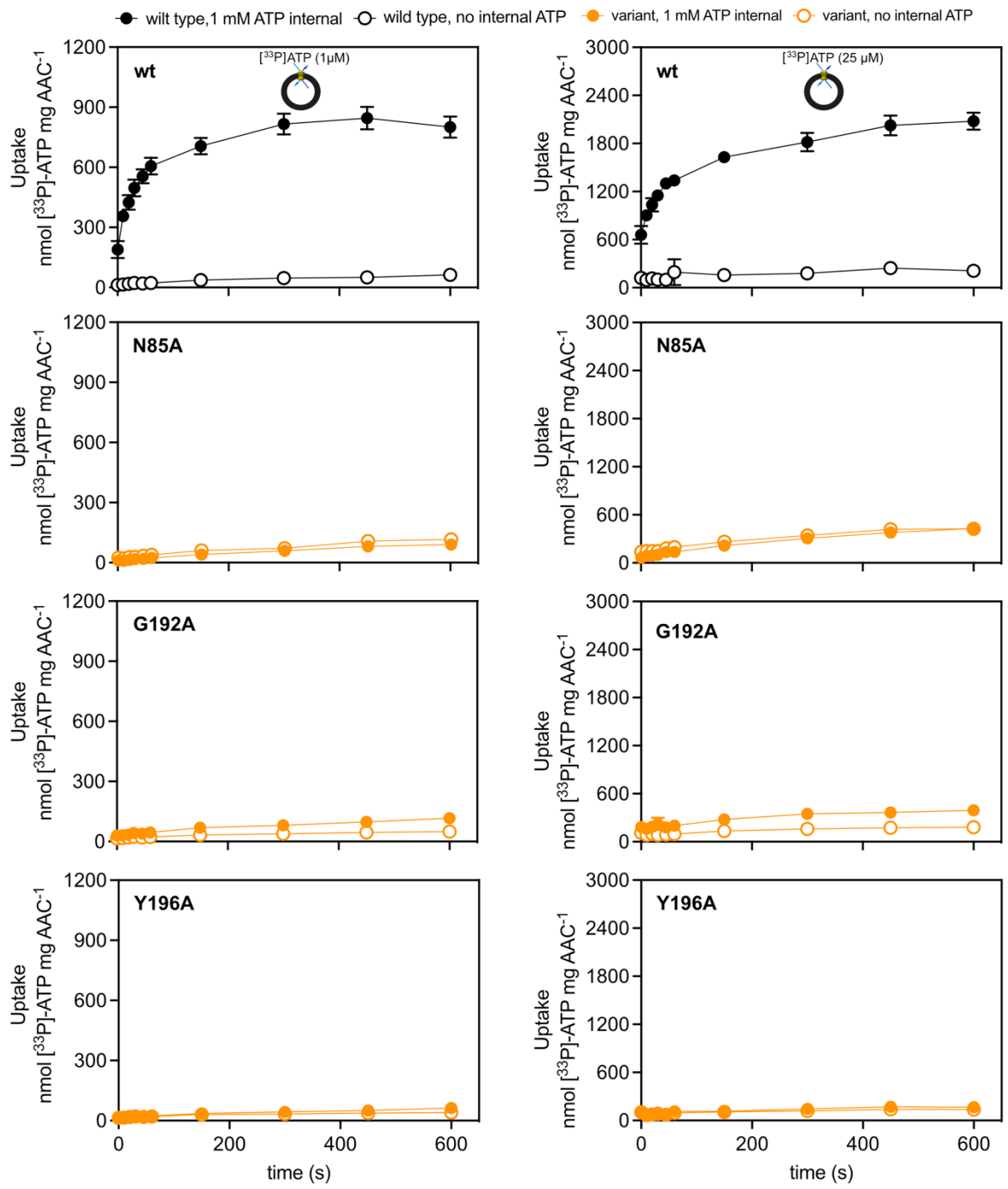

Figure 5.11: Uptake assays for the mutants of three residues that contribute to substrate binding. Representative uptake curve of [^{33}P]-ATP into proteoliposomes loaded with 1mM ATP (filled circles). Proteoliposomes with no internal substrate were used as control (empty circles). Circles and error bars represent the mean and standard deviation of four technical replicates. Error bars are smaller than the symbol whenever not shown.

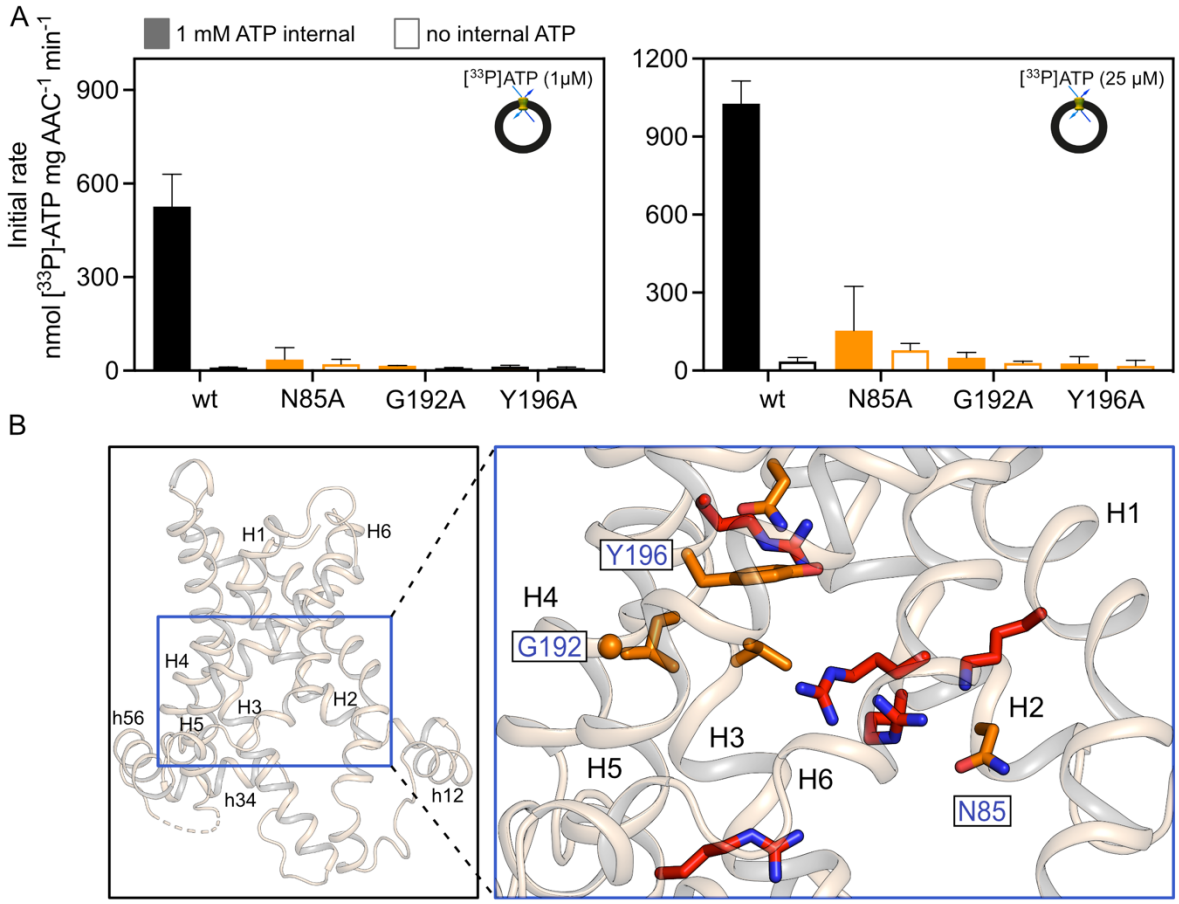

Figure 5.12: The mutants of three residues contributing to substrate binding are inactive. (A) Initial transport rates determined from the linear part of the uptake curve. Filled (first) and empty (second) bars for each protein represent 1 mM ATP internal and no internal ATP respectively. The bars and error bars represent the mean and standard deviation of three biological repeats for the wild type and variant N85A and two for variants G192A and Y196. (B) TtAac matrix-open structure (PDB code: 6gci chain A) (left) and close-up view (right) showing the analysed residues as in **Figure 4.6**.

5.4.2.1. Kinetic characterisation of active mutants of the residues with a contributing role to substrate binding

Variants N96A, L135A and V138A were active to different extents, hence kinetic measurements could be made. Similar to the kinetic characterisation of the wild type (**Figure 5.8**), the initial rates of the substrate uptake at different external substrate concentrations were measured and plotted against the concentration range. Variant N96A had a K_m value (4.1 µM, 95% CI 1.7-11.1) which was about 4-fold higher than that of the wild type (1.2 µM, 95% CI 0.7-2.3), variant V138A had a 1.5-fold higher K_m value (1.8 µM, 95% CI 1.1-2.8), whereas variant L135A had a very similar K_m value

(1.2 µM, 95% CI 0.5-3.2) with the wild type (**Figure 5.13** and **Table 5.2**). In all cases, the values were still in the low micromolar range, indicating that the mutation did not severely alter the affinity of the protein for the substrate. This might not be surprising, considering that probably multiple interactions are formed between the substrate and the protein. Disrupting one might not be enough to affect the substrate uptake severely. A similar observation has been made for inhibitor binding, as mutations of residues shown in the crystal structures to interact with the inhibitors do not abolish inhibition (personal communication with Dr Martin King). Furthermore, it is important to note that especially in the cases of variants L135A and V138A, the mutation to alanine is quite conservative. The aliphatic character of these residues indicates that they probably participate in forming the binding pocket, but they may not be involved in chemical coordination per se. The V_{max} of variant V138A (508.2 nmol [^{33}P]-ATP mg^{-1} AAC min^{-1}, 95% CI 466.1-552.7) was approximately 2-fold reduced compared to the wild type (936.1 nmol [^{33}P]-ATP mg^{-1} AAC min^{-1}, 95% CI 832.4-1046) (**Table 5.2**), indicating importance for the protein activity.

Residue N96 was proposed in **Chapter 4**, based on its position and state-dependent rotamers, to contribute to binding by positioning the substrates and guiding the conformational transitions of the transport cycle, similar to residue N85 discussed in **section 5.4.2**. This might be reflected in the slightly increased K_m and about 2-fold reduced V_{max} value (502.4 nmol [^{33}P]-ATP mg^{-1} AAC min^{-1}, 95% CI 418.8-609.7) compared to the wild type (936.1 nmol [^{33}P]-ATP mg^{-1} AAC min^{-1}, 95% CI 832.4-1046) (**Table 5.2**). Consistent with these results, the WB-12 strain expressing this variant could grow 17.6 ± 9.8%.

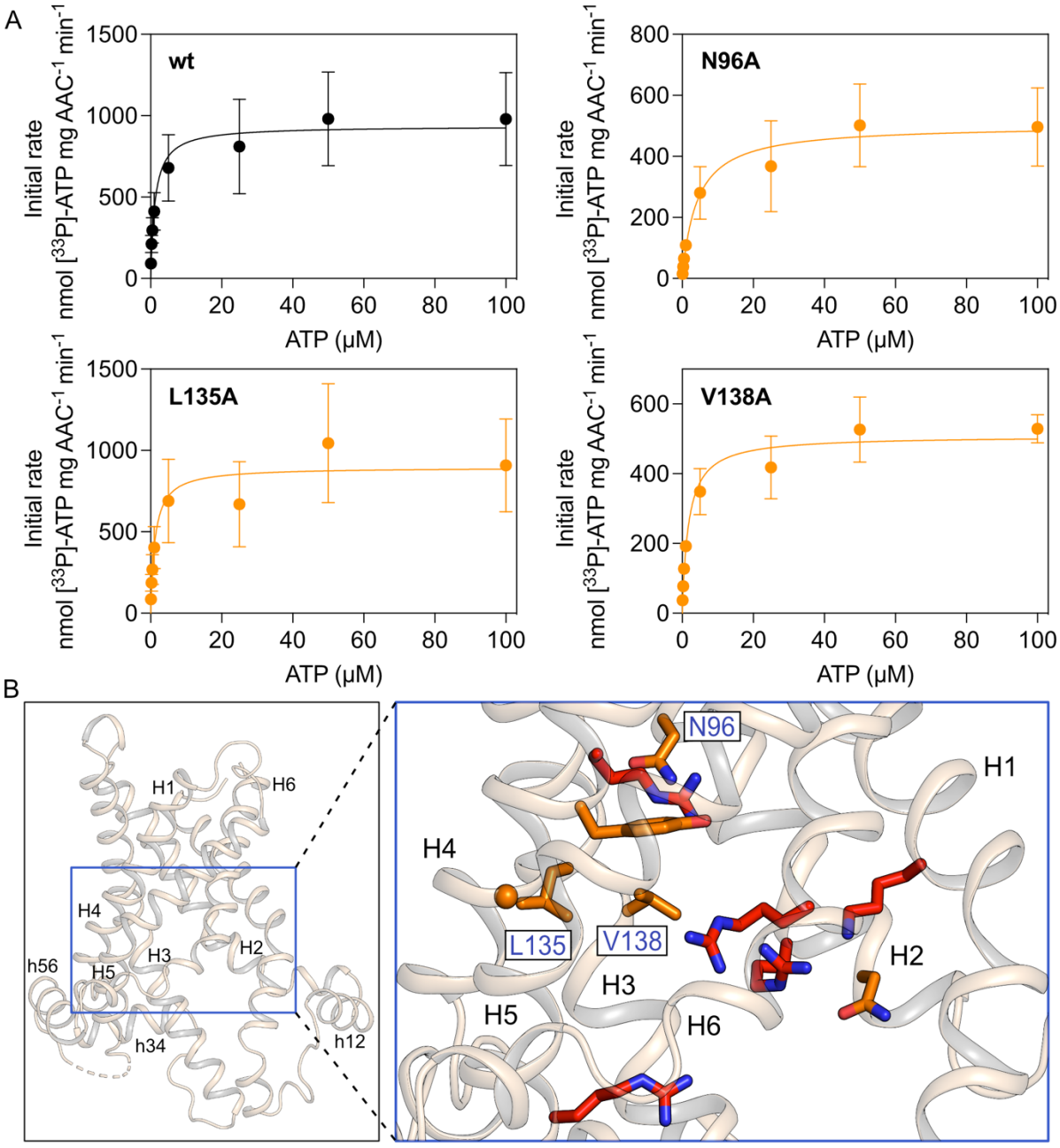

Figure 5.13: Kinetic analysis of the wild type and active variants of residues contributing to binding. (A) Proteoliposomes were loaded with 1 mM ATP and transport was initiated with either 0.1, 0.25, 0.5, 1, 5, 25, 50 or 100 μM [^{33}P]-ATP. Initial rates were taken over the linear part of the curves, according to the R-squared values, between 30 and 60 seconds. The circles and error bars represent the mean and standard deviation of five independent biological repeats for the wild type, three for variants L135A and V138A and two for variant N96A. The curves were fitted with the Michaelis-Menten function in Prism (GraphPad). Note that the y axis is differently labelled for the four proteins. (B) TtAac matrix-open structure (PDB code: 6gci chain A) (left) and close-up view (right) showing the analysed residues as in **Figure 4.6**.

Table 5.2: Kinetic analysis of the wild type and variants N96A, L135A and V138A

Protein	Km (μM)	95% CI	Vmax (nmol [^{33}P]-ATP mg^{-1} AAC min^{-1})	95% CI
Wild type	1.2	0.7-2.3	936.1	832.4-1046
N96A	4.1	1.7-11.1	502.4	418.8-609.7
L135A	1.2	0.5-3.2	895.9	747.8-1056
V138A	1.8	1.1-2.8	508.2	466.1-552.7

5.4.3. Uptake assays for some mutants of residues not involved in substrate binding

Finally, a few mutants of residues shown not to be involved in substrate binding were tested (Y89A, F97A, N123A, S134A, I193A and Y204). For two of them (N123A and I193A) kinetic analysis was performed as well. The variants were selected on the basis of either presenting properties that would be interesting to analyse further, or in order to serve as controls, to validate the assessments presented in previous chapters.

Variants Y89A and F97A were selected because in the thermostability assay, in presence of substrates, they exhibited larger shifts than the wild type; it would be important to investigate how this result would be reflected on uptake assays. Interestingly, despite the large shifts, mutant F97A did not complement growth of the WB-12 strain and variant Y89A complemented 36.2±18.9%, indicating their important function. Variants N123A and S134A were selected to serve as controls. Residue S134 is found in very close proximity to some of the residues proposed to contribute to substrate binding, namely residues L135 and V138 (**Figure 3.2**); therefore, it could serve as a good control to test the accuracy of the thermostability assay. Residue N123 is located at the level of the cytoplasmic network (**Figure 3.2**). Variant N123A presented an inconsistent difference compared to the wild type in the thermostability analysis (**Figure 4.7B**), hence it was reasonable to obtain more information. For this purpose, kinetic analysis was performed for this protein (**section 5.4.3.1**). Variant I193A presented variability in stability (**Figures 3.13** and **4.7B**), impeding an accurate assessment of the significance in its response to substrate. Furthermore, it has been proposed by different studies to be involved in substrate binding (**section 4.5**); therefore, it was important to further analyse this residue. Since the initial screening showed that the variant was active, kinetic analysis was performed (**section 5.4.3.1**). Finally, residue Y204 has an important functional role, being part of the hydrophobic

plug, specifically acting as a tyrosine brace for the salt bridge between residues K208 and D299 of the cytoplasmic network (Ruprecht *et al.*, 2019).

Variants F97A and Y204A did not complement growth of WB-12 strain, while Y89A and S134A complemented to 36.2 ± 18.9% and 64.8 ± 8.8% respectively (**Figures 3.4** and **3.5**). The uptake assays in the reconstitution system showed that except for Y204A, the remaining variants were active to different extents (**Figures 5.14** and **5.15**). For variant Y204A, the lack of activity is consistent with its inability to grow on glycerol and confirms that this residue has an important role (tyrosine brace) for the transport cycle, but not for substrate binding, since the variant presented a shift to wild-type levels in the thermostability assay in the presence of substrate. In agreement, the equivalent mutation of ScAac2 was reported to cause a 12-fold increase in the K_m value (David *et al.*, 2008). Variant F97A presented uptake (the uptake in liposomes loaded with 1 mM ATP was 6-8 times higher than the no internal ATP control), but compared to the wild type the activity was about 6% (initial rates of one experiment 1041 ± 37 (wild type, 1 μM), 60 ± 2 (F97A, 1 μM); 1723 ± 53 (wild type, 25 μM) and 90 ± 8 (F97A, 25 μM) nmol [^{33}P]-ATP mg AAC^{-1} min^{-1}). This estimated rate is probably not enough to support growth of the Aac-deficient strain, explaining the result of the complementation study. The variant shifted to wild-type levels, in presence of substrate, in the thermostability assay, showing that F97 is not involved in substrate binding. All these results can support its proposed role, not related to substrate binding, participating in the hydrophobic plug of the cytoplasmic gate. Variants Y89A and S134A presented similar uptake rates, (577 ± 33 (Y89A, 1 μM), 443 ± 38 (S134A, 1 μM); 985.4 ± 12.5 (Y89A, 25 μM) and 771.2 ± 45 (S134A, 25 μM) nmol [^{33}P]-ATP mg AAC^{-1} min^{-1}) that were about 2-fold decreased compared to the wild type at those concentrations. The measured activity is consistent with their ability to partially complement growth of the WB-12 strain.

These experiments could demonstrate that the transport activity is a sum of all the processes taking place during the transport cycle, including the conformational changes, the substrate binding and release steps, the disruption and formation steps of the two gates. Therefore, it is difficult to evaluate only with uptake experiments why a mutant is inactive. A combination of approaches is usually required in order to reach reliable conclusions.

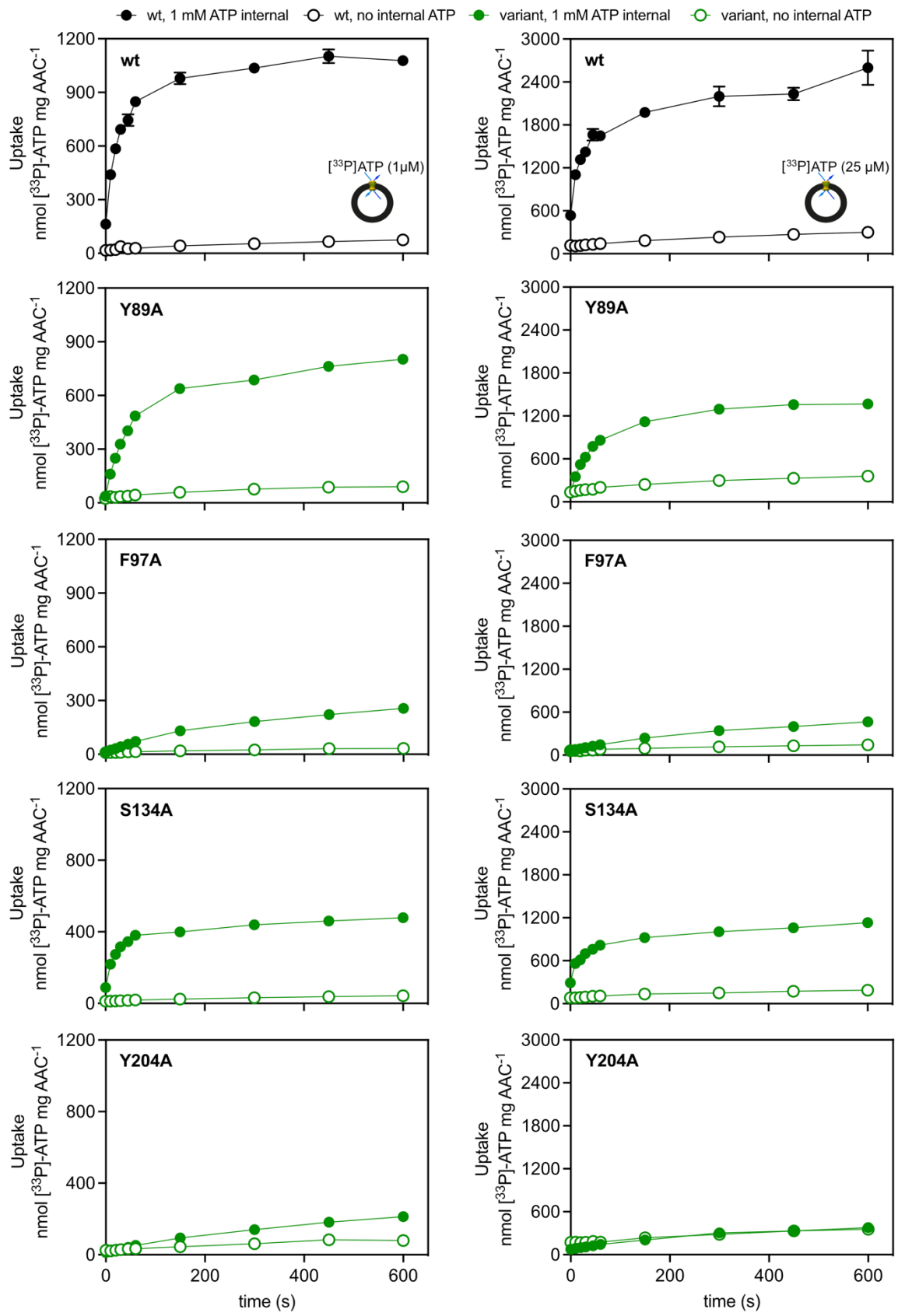

Figure 5.14: Uptake assays for mutants of residues not involved in substrate binding. (A) Uptake curve of [^{33}P]-ATP into proteoliposomes loaded with 1mM ATP (filled circles). Proteoliposomes with no internal substrate were used as control (empty

circles). Circles and error bars represent the mean and standard deviation of four technical replicates. Error bars are smaller than the symbol whenever not shown.

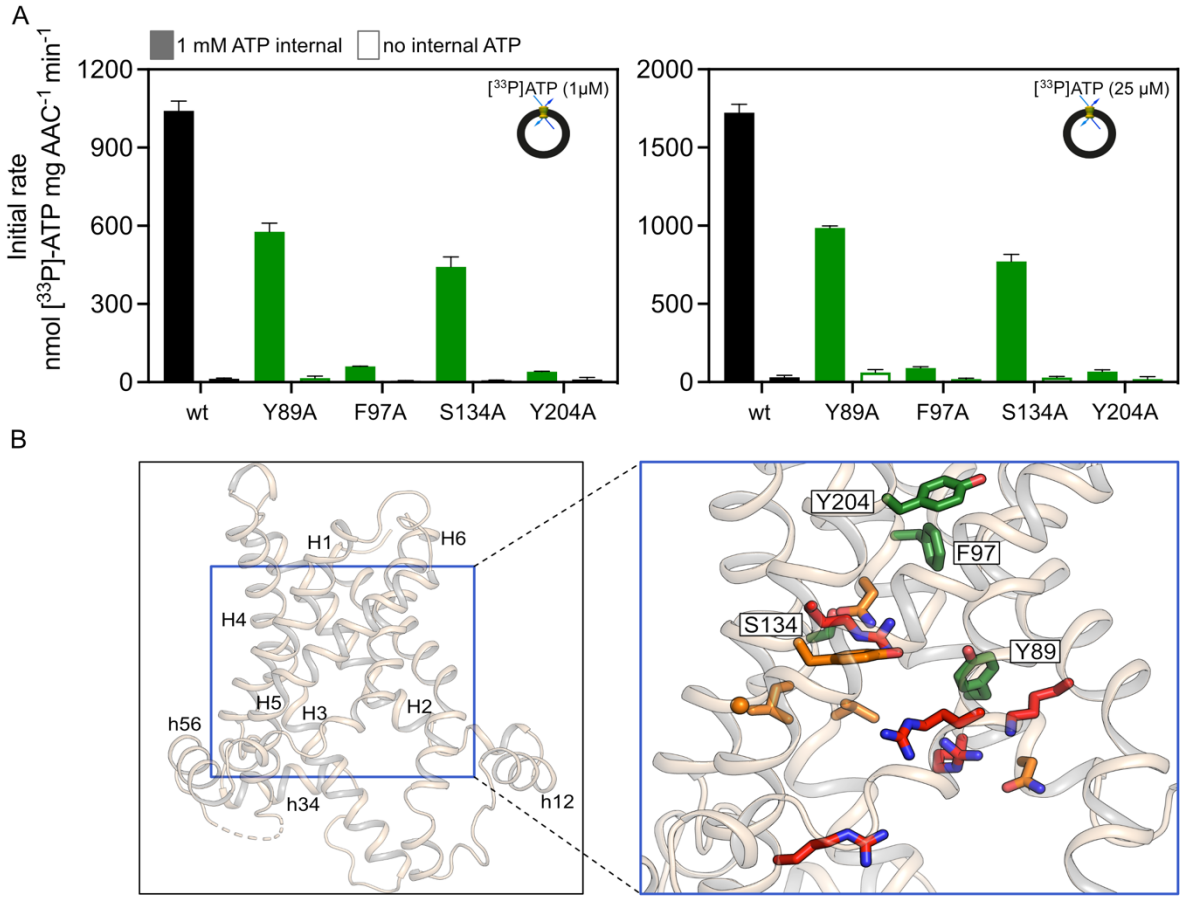

Figure 5.15: The mutants of residues not involved in substrate binding can be active to different extents, as they may participate in other key steps of the transport cycle. (A) Initial transport rates determined from the linear part of the uptake curves. Filled (first) and empty (second) bars for each protein represent 1 mM ATP internal and no internal ATP respectively. The bars and error bars represent the mean and standard deviation of four technical replicates. (B) TtAac matrix-open structure (PDB code: 6gci chain A) (left) and close-up view (right) showing the four analysed residues relatively to the residues identified to be involved in substrate binding.

5.4.3.1. Kinetic characterisation of variants N123A and I193A

Variants N123A and I193A were assayed as described in **sections 5.3** and **5.4.2.1**. The results showed that the K_m value had not been affected in either case (N123A, 1.6 µM, 95% CI 0.5-6.0; I193A 1.1 µM, 95% CI 0.7-1.8; wild type 1.2 µM, 95% CI 0.7-2.3), but the V_{max} was reduced about 3-fold for N123A (368.6 nmol [^{33}P]-ATP mg^{-1} AAC min^{-1}, 95% CI 298.8-454.5; wild type 936.1 nmol [^{33}P]-ATP mg^{-1} AAC min^{-1}, 95% CI 832.4-1046). Variant I193A had a similar V_{max} to the wild type (777.6 nmol [^{33}P]-ATP mg^{-1} AAC min^{-1}, 95% CI 709.8-847.9) (**Figure 5.14** and **Table 5.3**).

Variant N123A could complement growth 50.2 ± 9.2% (**Figures 3.4** and **3.5**) and responded to substrate in a concentration-dependent way, only giving a significantly different value for the response compared to the wild type at 5 mM ADP and ATP. The kinetic analysis indicated that the affinity of the variant for the substrate is similar to wild type, consistent with the thermostability result. The reduced V_{max} can explain the reduced complementation and indicates that this residue might be important for some aspect of the transport mechanism, but not substrate binding.

Surprisingly, variant I193A did not complement growth of WB-12 strain (**Figures 3.4** and **3.5**). Potential reasons for this result could be related to issues in the biogenesis and targeting of this protein, with only a small fraction being translated and correctly targeted to mitochondria. This is consistent with the results of inherent instability of this variant (**Figures 3.13** and **4.7B**) and the necessity to slightly modify the purification protocol (**section 2.5.3**). This fraction could be active like the wild type (**Figure 5.14**) when reconstituted in an isolated system, but potentially not enough to sustain growth in the cellular level. Additionally, it is possible that the conditions applied, for example the substrate concentrations, are more optimal in the reconstituted system than in the WB-12 mitochondria expressing this variant. A similar observation was made for the equivalent variants of R287A and R88H in ScAac2, where no growth on glycerol was observed, but the authors obtained activity in their reconstitution system (Klingenberg and Nelson, 1994). However, in a study where this variant was expressed and assayed in *L. lactis* membranes fused with vesicles, the activity was less than 10% (Ruprecht *et al.*, 2019). The difference could be due to the different expression systems or the different lipid composition. The result obtained here is consistent with the thermostability result, as the variant was responding to substrate in a concentration-dependent way, indicating that the substrate binding step is not impaired.

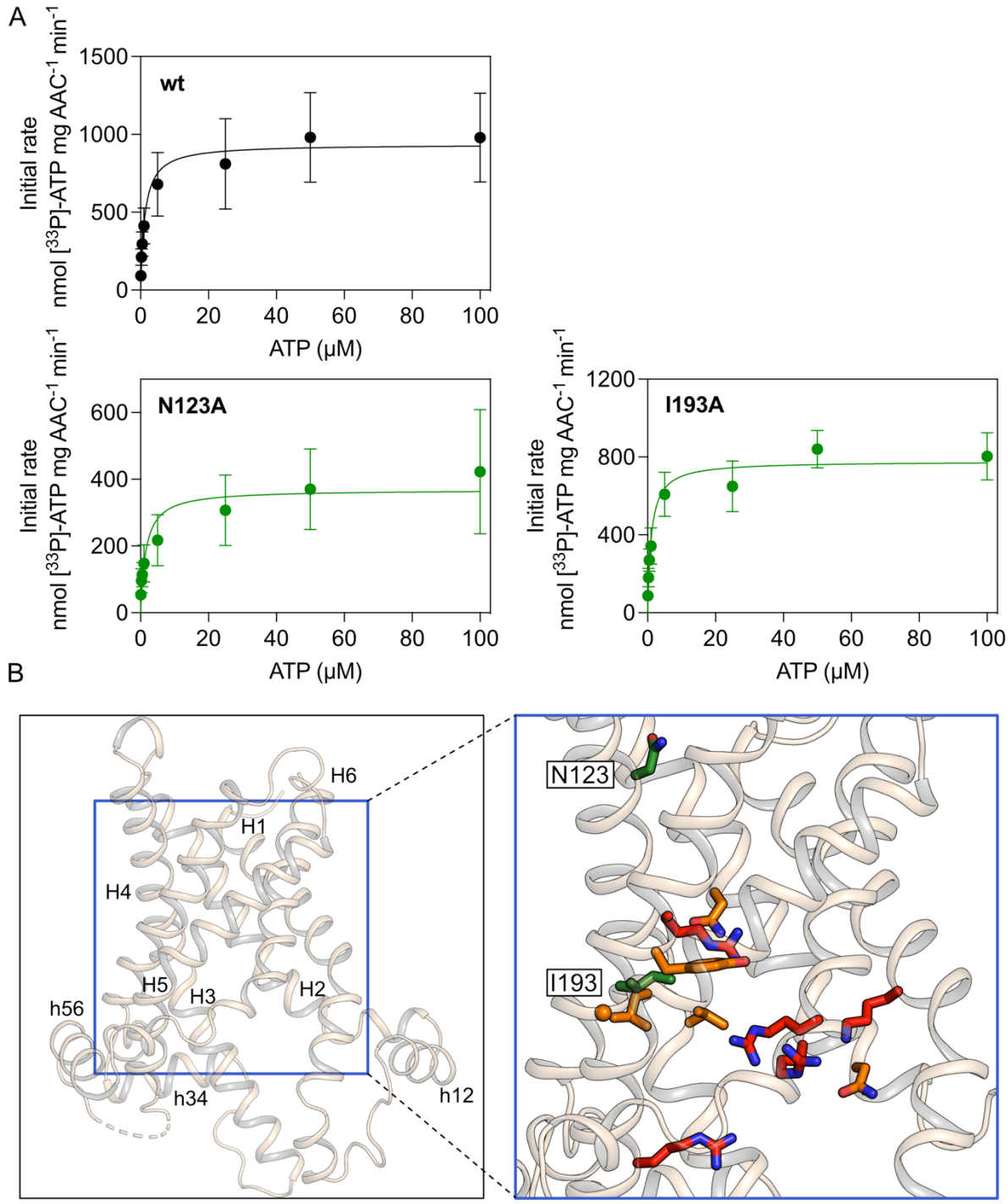

Figure 5.14: Kinetic analysis of the wild type and variants that presented some differences from the wild type in the thermostability assay. (A) Proteoliposomes were loaded with 1 mM ATP internally and transport was initiated with either 0.1, 0.25, 0.5, 1, 5, 25, 50 or 100 μM [^{33}P]-ATP. Initial rates were taken over the linear part of the curves, according to the R-squared values, between 30 and 60 seconds. The circles and error bars the mean and standard deviation of five independent biological repeats for the wild type and three for the variants. The curves were fitted with the Michaelis-Menten function in Prism (GraphPad). Note that the y axis is different for the three proteins. (B) TtAac matrix-open structure (PDB code: 6gci chain A) (left) and

close-up view (right) showing the four analysed residues relatively to the residues identified to be involved in substrate binding.

Table 5.3: Kinetic analysis of the wild type and variants N123A and I193A

Protein	Km (μM)	95% CI	Vmax (nmol [^{33}P]-ATP mg^{-1} AAC min^{-1})	95% CI
Wild type	1.2	0.7-2.3	936.1	832.4-1046
N123A	1.6	0.5-6.0	368.6	298.8-454.5
I193A	1.1	0.7-1.8	777.6	709.8-847.9

5.5. Discussion

In this chapter the transport properties of the wild type and seventeen variants were studied, in order to further investigate the role these residues might have in substrate binding. All mutants of the residues proposed in **Chapter 4** to participate in substrate binding were tested, as well as some selected variants of residues proposed not to be involved in substrate binding. In the latter case, the variants were selected either because they are proposed to have an important role in the transport cycle and it was important to investigate how the mutation would affect the uptake rates, or to validate the thermostability results.

Firstly, the experimental conditions were standardised using the wild-type protein. The obtained kinetic parameters were similar with the results published for other systems or for different AAC orthologues. Subsequently, the same conditions were applied to test the uptake of variants. All variants of the residues proposed to participate in critical for substrate binding interactions (K30, R88, R197, R246 and R287) were shown to be inactive. This result is consistent with their abolished response to substrate in the CPM thermostability assay and their inability to complement growth of the Aac-deficient strain (**Table 5.4**). Therefore, from all of the different approaches it can be concluded that they are critical for substrate binding. Based on their chemical properties, they probably interact with the phosphate groups of the nucleotides.

The mutants of the residues proposed to contribute to substrate binding (N85, N96, L135, V138, G192 and Y196) were shown to be either inactive or presented altered kinetic properties, except for L135A, which had a similar kinetic profile to the wild type. However, it is important to note that some non-ionic interactions might be more difficult to probe, because of their chemical nature. Furthermore, residues L135, V138, G192 and Y196 were proposed, because of their relative positions, to be jointly

involved in binding, each making a contribution. Hence it is possible that altering just one may not affect the overall binding and all subsequent steps of the transport cycle. The transport results are consistent with the functional complementation and thermostability results (**Table 5.4**) and confirm that these six residues are involved in substrate binding, probably interacting with the adenosine moiety of the nucleotides.

Having obtained information from three different techniques, it is interesting to confirm that each can focus on different aspects of the biochemistry of the protein. The complementation study evaluates overall the biogenesis, structure and function of the protein. The CPM thermostability assay focuses on the biophysical properties (stability and folding) and when performed in presence of the substrate or ligands, it can give accurate information on their binding. The uptake assays focus on the transport activity, which, however, reflects the sum of all steps taking place during the transport cycle. Variants F97A and I193A could illustrate these points. Variant F97A did not grow on glycerol and had very limited transport activity (about 6% of the wild type) after reconstitution into liposomes, even when very optimal conditions were applied. However, the protein was stable and responded to the substrates like the wild type, as shown in the thermostability assay (**Table 5.4**). Hence it can be concluded from these data that residue F97 is essential for some aspect of the transport cycle, but not substrate binding. In agreement, it was shown in the crystal structure that it participates in the hydrophobic plug of the cytoplasmic gate (Ruprecht *et al.*, 2019). Variant I193A did not grow on glycerol, but presented uptake rates similar to the wild type. It also responded to substrate in a concentration-dependent way, but displaying large variation and unusual instability. Therefore, it is possible that there are issues in biogenesis and folding, reflected in the complementation assay, but the fraction that can be isolated, purified and reconstituted is active.

To conclude, it is important for mechanistic studies to follow complementary approaches and evaluate all of the results by comparison. Here, the results obtained from the uptake assays were consistent with the results obtained from the complementation study in the majority of cases (**Table 5.4**). They confirmed and strengthened the results of the thermostability shift assays, corroborating which residues are involved in substrate binding.

Table 5.4: Summary results from the three complementary techniques employed for the wild type and 36 variants

Protein	Complementation	Response to substrate (CPM)	Transport activity	Comments (transport assays)
Wild type	**full**	**c dependent**	**(wild-type)**	
S29A	full	ns	nt	
K30A	no	not c dependent	inactive	
L41A	no	protein unfolded	nt	
Q44A	no	protein unfolded	nt	
N85A	sf reduced	sf reduced	inactive	
R88A	no	not c dependent	inactive	
Y89A	sf reduced	ns*, variable	affected?	reduced initial rate
T92A	sf reduced	ns	nt	
Q93A	sf reduced	ns	nt	
N96A	sf reduced	sf reduced	affected	increased K_m, reduced V_{max}
F97A	no	ns	affected?	reduced initial rate
R100A	sf reduced	ns	nt	
N123A	sf reduced	ns*, variable	affected	reduced V_{max}
S134A	sf reduced	ns	affected?	reduced initial rate
L135A	no	sf reduced	wt levels	K_m, V_{max} ns
V138A	sf reduced	sf reduced	affected	reduced V_{max}
T146A	no	protein unfolded	nt	
S189A	no	ns	nt	
G192A	no	sf reduced	inactive	
I193A	no	ns*, variable	wt levels	K_m, V_{max} ns
Y196A	no	sf reduced	inactive	
R197A	no	not c dependent	inactive	
Y200A	sf reduced	ns	nt	
Y204A	no	ns	inactive?	
V230A	full	ns	nt	
T231A	sf reduced	ns	nt	
G235A	no	ns	nt	
S238A	sf reduced	ns	nt	
Y239A	no	protein unfolded	nt	
R246A	no	not c dependent	inactive	
N284A	no	protein unfolded	nt	
R287A	no	not c dependent	inactive	
G288A	full	ns	nt	
G291A	full	ns	nt	
V294A	full	ns*, variable	nt	
L295A	no	ns	nt	

Abbreviations: sf, significantly; c, concentration; ns, not significantly different from the wild type; nt, not tested; wt, wild-type; ?, biological repeats required to gain confidence

Chapter 6: Investigating the molecular basis of substrate specificity

6.1. Introduction

In this chapter, the molecular determinants of the substrate specificity of the mitochondrial ADP/ATP carrier were investigated. This work was carried out as part of studying a mitosomal transporter from *Cryptosporidium parvum* that resembles the mitochondrial ADP/ATP carriers. This work was performed in collaboration with Dr Martin King, Dr Sotiria Tavoulari, Dr John Mifsud and Alannah King and preceded the completion of the work for the experimental identification of the substrate binding site (Chapters 3-5). Hence the experimental design was based on the *in silico* model of the substrate binding site (Kunji *et al.*, 2016). This is composed of residues K30, R88 and R287 for binding of the phosphate groups of the nucleotides and residues G192, I193, Y196 and S238 for binding of the adenosine moiety. Compared to the site experimentally identified in the previous chapters, it does not include residues L135 and V138, which might participate in the binding of the adenosine moiety together with G192 and Y196. Furthermore, the two R-N pairs (residues N96, R197, N85 and R246), potentially involved in substrate binding at different pauses as the substrates traverse the translocation pathway, are not considered. Finally, residues I193 and S238 which are included here were not confirmed experimentally.

Dr Martin King performed the molecular biology described in this chapter and Dr John Mifsud and Alannah King the bioinformatic analysis. My contributions were the growth and preparation of lactococcal membranes and performing transport assays, all in collaboration with Dr Martin King and Dr Sotiria Tavoulari, as well as data analysis together with all the people participating in the project. The majority of the results are published in (King *et al.*, 2020), but here they are discussed in light of the new information obtained from the experimentally determined binding site as well.

C. parvum is a parasitic protist in the lineage of Apicomplexan, responsible for a disease with mostly gastroenteritis symptoms, called cryptosporidiosis. The severity of the symptoms differs dependent on the site of infection, the nutritional state and the immune capacity of the affected individual (Bouzid et al., 2013; Chalmers and Davies, 2010). The parasite usually establishes itself on the apical surface of the epithelial

cells of the host's intestine and severely affects both the absorptive and the secretory functions of the intestine (Bouzid *et al.*, 2013). Even though many aspects of the disease still need to be explored, it has become evident that the pathogenicity of cryptosporidiosis affects humans, domestic animals and wildlife worldwide, with direct social and financial implications. It was hence included in the World Health Organisation Neglected Disease Initiative (Savioli et al., 2006).

As in many anaerobic and microaerophilic parasitic protists, the mitochondria in *C. parvum* have undergone evolutionary reductive alterations of their function and exist in the form of mitosomes (Putignani et al., 2004). The mitosomes of *C. parvum* do not have their own genome (Abrahamsen et al., 2004; Bankier et al., 2003), lack electron transport chain, do not produce ATP nor H_2, do not use electron acceptors and have lost most enzymes of the TCA cycle and of the β-oxidation of fatty acids (Makiuchi and Nozaki, 2014; Muller et al., 2012). However, they retain the machinery of iron-sulphur cluster formation (Seeber et al., 2008).

Sequencing of the genome of *C. parvum* revealed that it contains 69 putative transport proteins, including 9 sugar and 11 amino acid transporters and 17 proteins with mitochondrial targeted signals (Abrahamsen *et al.*, 2004). BLAST searches against yeast mitochondrial carriers (SLC25 family), performed by Dr John Mifsud and Alannah King (MRC, Mitochondrial Biology Unit), identified eight homologues of the mitochondrial carrier family (King *et al.*, 2020). Gene Cgd8_1210 was predicted to be an ADP/ATP carrier (Abrahamsen *et al.*, 2004; King *et al.*, 2020).

6.1.1. Aims

The aims of this chapter were to characterise the mitosomal transporter from *C. parvum* and to determine whether it is an ADP/ATP carrier. It was shown that it resembles ADP/ATP carriers, but has a broader nucleotide specificity. Therefore, the molecular determinants of substrate specificity of the mitochondrial ADP/ATP carriers were investigated.

6.2. Functional characterisation of the mitosomal transporter encoded by the Cgd8_1210 gene

6.2.1. Sequence conservation in relation to the SLC25 family

The sequence of the mitosomal transporter was aligned with the sequences of members of the SLC25 family (**Figure 6.1**). It became clear that the sequence contained the motifs that are typical for mitochondrial carriers. Specifically, the motifs of the matrix ([PS]x[DE]xx[KR]) and cytoplasmic ([FY][DE]xx[RK]) networks were present, as well as the glutamine and tyrosine braces (King *et al.*, 2016; Nelson *et al.*, 1998; Pebay-Peyroula *et al.*, 2003; Robinson *et al.*, 2008; Ruprecht *et al.*, 2014; Ruprecht *et al.*, 2019). Moreover, the GxxxG and πxxxπ motifs, that are important for the structural movements, were also conserved (Ruprecht *et al.*, 2019) (**Figure 6.1**).

Figure 6.1: The mitosomal transporter of *C. parvum* contains the sequence features of the SLC25 family. Alignment of the parasitic transporter (last sequence) with different mitochondrial carriers from yeast (top to bottom: acetyl-CoA transporter, putative NAD^+ carrier, putative pyridoxal phosphate transporter, oxaloacetate transporter, phosphate carrier isoform 2, phosphate carrier isoform 1, putative glycine transporter, ADP/ATP carrier 2). Amino acids are coloured based on their properties (Zappo colour scheme): Lys, Arg, His (basic) are blue; Asp, Glu (acidic) red; Asn, Gln, Ser and Thr (polar) green; Ala, Ile, Leu, Met, Val (aliphatic) pink; Phe, Tyr and Trp (aromatic) orange; Gly and Pro (structurally important) magenta and Cys yellow. Important structural and mechanistic motifs are indicated: GxxxG motif, Black arrow for proline kink (P), matrix network (M.N), glutamine brace (**Q**), πxxxπ motif, tyrosine brace (**Y**), cytoplasmic network (C.N).

6.2.2. Conservation of the inhibitor and proposed substrate binding site residues in relation to mitochondrial ADP/ATP carriers

The product of the Cgd8_1210 gene was subsequently also compared with sequences of ADP/ATP carriers, to establish whether the residues involved in inhibitor binding, as shown in the crystal structures, were conserved (Pebay-Peyroula *et al.*, 2003; Ruprecht *et al.*, 2014; Ruprecht *et al.*, 2019). Furthermore, the residues forming the 'consensus substrate binding site', as proposed by computational analyses, were also investigated (Kunji *et al.*, 2016) (**Figure 6.2**) (the accession codes for a larger alignment of 128 AAC sequences is presented in **Appendix 2**). This site includes the residues that are consistently proposed by sequence analysis (Robinson and Kunji, 2006; Robinson *et al.*, 2008) (**Figure 4.2**) and some molecular dynamics simulations studies (Dehez *et al.*, 2008; Mifsud *et al.*, 2013; Wang and Tajkhorshid, 2008) (**Table 4.1**) to constitute the substrate binding site.

Regarding the CATR binding site, it was shown that the majority of the residues involved in salt bridges and hydrogen bonds in bovine and yeast orthologues were conserved in the mitosomal transporter. Residue $N104_{ScAac2}/N96_{TtAac}$ that potentially forms a hydrogen bond with the sulphate moiety of CATR (observed in PDB entries 4c9h chain B, 4c9q, 4c9j and 1okc, but not in 4c9g, 4c9h chain A and 2c3e) is replaced by a glycine (G99) in the mitosomal sequence. Additionally, residues $L248_{ScAca2}/L241_{TtAac}$ and $S245_{ScAac2}/S238_{TtAac}$ which are participating in van der Waals interactions (**Figure 3.15**) are replaced by cysteine (C238) and phenylalanine (F241) respectively. Regarding BKA binding, all residues participating in polar interactions are conserved apart from $N96_{TtAac}$, which is glycine (G99), as noted above. Furthermore,

residues L135$_{TtAac}$ and S238$_{TtAac}$ that are involved in van der Waals interactions (**Figure 3.15**) are S138 and C238 in the mitosomal protein. Overall, the binding sites of the two inhibitors are well conserved, with the majority of polar interactions retained.

Regarding substrate binding, all residues of the 'consensus substrate binding site' (K30$_{TtAac}$, R88$_{TtAac}$, G192$_{TtAac}$, I193$_{TtAac}$, Y196$_{TtAac}$, S238$_{TtAac}$ and R287$_{TtAac}$) are conserved, apart from S238 which is a cysteine (C238) in the mitosomal protein. This suggests that ADP and ATP can bind to that site. Furthermore, it contains the RRRMMM motif, that is characteristic of mitochondrial ADP/ATP carriers (Klingenberg, 1989). Overall, the mitosomal transporter retains the functional features of ADP/ATP carriers, with regards to inhibitor and substrate binding, in addition to the structural and mechanistic features of the SLC25 family. Therefore, hereafter in this chapter the product of the Cgd8_1210 gene will be referred to as CpAAC.

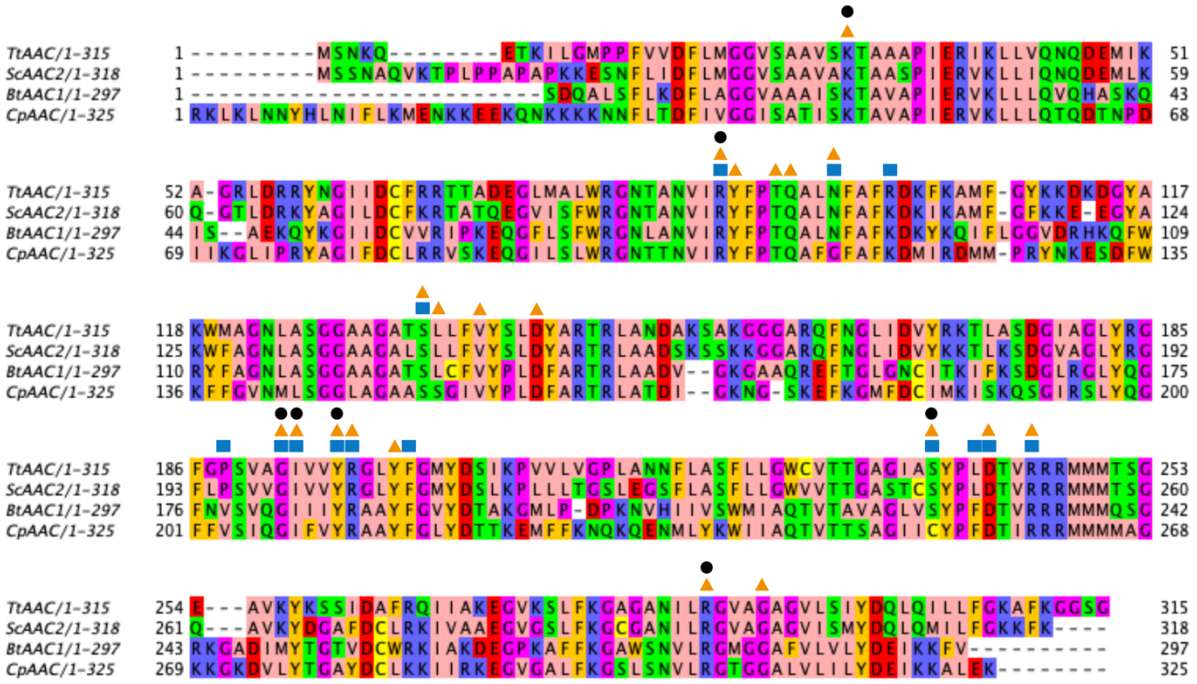

Figure 6.2: The mitosomal transporter resembles the mitochondrial ADP/ATP carriers. Sequence alignment of the parasitic transporter (last sequence) with different ADP/ATP carrier orthologues. Amino acids are coloured based on their properties (Zappo colour scheme), as in **Figure 6.1**. Residues participating in CATR and BKA binding sites (**Figure 3.15**) are indicated with a blue square and orange triangle respectively. The van der Waals interactions in the CATR binding site differ slightly between the solved structures. Here the ones observed in PDB entry 4c9h chain B are indicated. Residues of the *in silico* substrate binding site are indicated with black spheres.

6.2.3. Experimental validation of ADP/ATP carrier activity with uptake assays

To test experimentally whether CpAAC functions as an ADP/ATP carrier, transport assays with [^{14}C]-ADP were performed, in presence and absence of inhibitors CATR and BKA. For this purpose, the protein was expressed in the cytoplasmic membrane of *L. lactis* and the experiments were performed in disrupted lactococcal membranes fused with liposomes. This expression system and experimental set-up have been proven to be very successful for studying mitochondrial carriers (Booty et al., 2015; Chan *et al.*, 2005; King et al., 2015; Kunji et al., 2005; Kunji et al., 2003; Majd et al., 2018b; Mifsud *et al.*, 2013; Monné et al., 2005). The major advantages are that the introduced protein is expressed and targeted to the cytoplasmic membrane of this bacterium and not into inclusion bodies as in *E. coli*, thus no refolding procedures are necessary. Furthermore, expression is tightly regulated through the nisin controlled gene expression (NICE) system (de Ruyter *et al.*, 1996; Kunji *et al.*, 2003). Lactococcal membranes expressing an empty pNZ vector (**Figure 2.1**) were assayed in parallel as a control. It was shown that CpAAC can catalyse ADP/ADP homoexchange with high rates, which could be inhibited by addition of CATR and BKA (**Figure 6.3**).

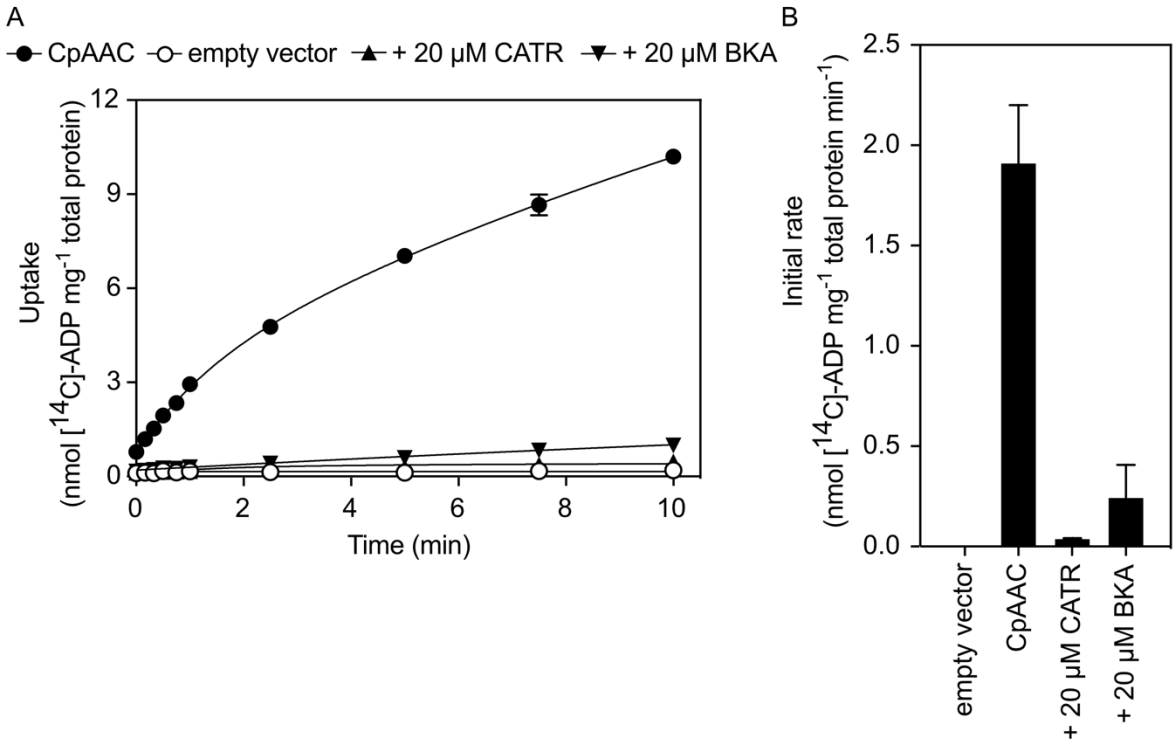

Figure 6.3: CpAac can facilitate ADP transport with rates that are inhibited by the AAC canonical inhibitors CATR and BKA. (A) Fused lactococcal membranes expressing CpAAC were loaded with 5mM ADP in the absence (solid circles) or

presence of 20 μM CATR (triangles) or BKA (inverted triangles). Uptake was initiated by addition of 1.5 μM [^{14}C]-ADP. Membranes expressing an empty pNZ vector (empty circles) were assayed in parallel as a control. Signs and error bars represent the mean and standard deviation of four technical replicates. (B) Initial transport rates determined from the linear part of the uptake curves (60 seconds). Bars and error bars represent the mean and standard deviation of two biological repeats. Figure adapted from (King *et al.*, 2020).

6.2.4. Substrate specificity of CpAAC in comparison with ScAac2 and TtAac

Subsequently, the specificity of this transporter was investigated. Initially, competition experiments were performed, in which [^{14}C]-ADP uptake into vesicles was monitored in the presence of a 1667-fold excess of external non-labelled nucleotides (**Figure 6.4**). The nucleotides that were found to compete with ADP for binding were then tested in transport assays (**Figure 6.6**).

All nucleoside di- and tri- phosphates (**Figure 6.5**) were shown to compete with ADP successfully, when they were present in large excess, as they could inhibit transport of ADP, similar to the inhibitor BKA. Nucleoside mono- phosphates did not seem to compete for binding, apart from AMP, which had a similar profile as the nucleoside di- and tri- phosphates, inhibiting ADP transport by 93% (**Figure 6.4**). This profile presents some differences compared to that of the human AAC1 (Mifsud *et al.*, 2013). In a similar competition experiment, where the carrier was assayed in lactococcal membranes, the only nucleoside di-phosphates that could inhibit uptake of [^{14}C]-ADP were ADP, d-ADP (complete inhibition) and GDP (approximately 25% inhibition). From the nucleoside tri-phosphates, UTP (approximately 30% inhibition), TTP (approximately 45% inhibition), CTP (approximately 40% inhibition), GTP (approximately 30% inhibition) in addition to ATP and dATP (complete inhibition inhibition) could compete, whereas ITP did not compete (Mifsud *et al.*, 2013). These results indicated that CpAAC has a broader substrate specificity than the human AAC1.

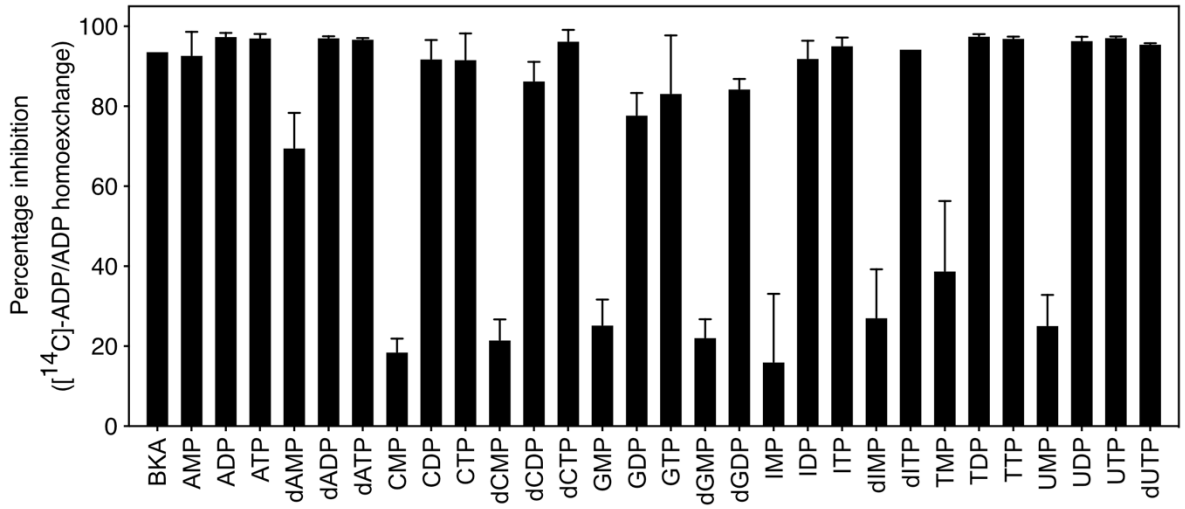

Figure 6.4: Nucleotide competition experiments for candidate binding molecules. Percentage inhibition of ADP homoexchange reaction in 1667-fold excess of non-radiolabelled nucleotides (2.5 mM). Fused lactococcal membranes expressing CpAAC were loaded with 5 mM ADP and uptake was initiated by addition of 1.5 µM of [^{14}C]-ADP. Bars and error bars represent the mean and standard deviation of two biological repeats. Figure adapted from (King *et al.*, 2020).

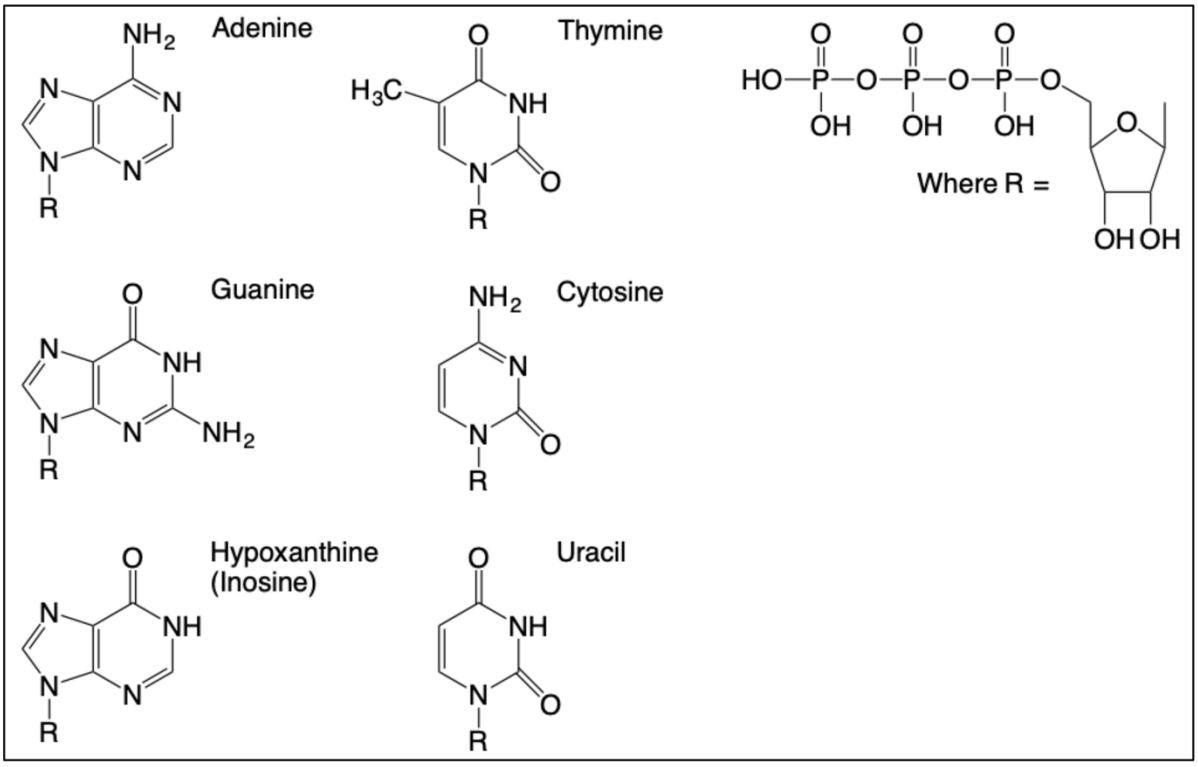

Figure 6.5: Chemical structures of the bases included in the nucleotides used in the study.

This experiment showed that the nucleoside di- and tri- phosphates of all bases can compete with ADP for binding to the CpAAC binding site, when they are present in

excess. However, it was necessary to validate which ones are actually transported. Therefore, transport assays were performed (**Figure 6.6**), where fused vesicles were loaded with the relevant nucleotide and transport was initiated in a heteroexchange reaction with [^{14}C]-ADP. Only when the internal compound is a transportable substrate uptake of [^{14}C]-ADP would occur. Fused lactococcal membranes expressing an empty pNZ vector were assayed in parallel as control. The specificity profile was compared with those of ScAac2 and TtAac (**Figure 6.6**). In contrast with these orthologues and the human and bovine orthologues that transport only ADP, ATP and the deoxy-forms (De Marcos Lousa *et al.*, 2002; Dolce *et al.*, 2005; Mifsud *et al.*, 2013; Pfaff and Klingenberg, 1968), CpAAC had a broad nucleotide specificity. In addition to these adenine nucleotides, it could also transport TDP, TTP, UDP, UTP and to a lesser extent CDP, CTP, IDP and ITP (**Figure 6.6**). The initial rates from two biological repeats were ADP, 1.66 ± 0.59 nmol [^{14}C]-ADP mg^{-1} total protein min^{-1}; ATP, 2.72 ± 1.97 nmol [^{14}C]-ADP mg^{-1} total protein min^{-1}; TDP, 3.41 ± 2.49 nmol [^{14}C]-ADP mg^{-1} total protein min^{-1}; TTP, 4.13 ± 2.12 nmol [^{14}C]-ADP mg^{-1} total protein min^{-1}; UDP, 2.56 ± 0.32 nmol [^{14}C]-ADP mg^{-1} total protein min^{-1}; UTP, 4.36 ± 2.31 nmol [^{14}C]-ADP mg^{-1} total protein min^{-1}; CDP, 1.00 ± 0.40 nmol [^{14}C]-ADP mg^{-1} total protein min^{-1}; CTP, 1.11 ± 0.18 nmol [^{14}C]-ADP mg^{-1} total protein min^{-1}; IDP, 0.77 ± 0.10 nmol [^{14}C]-ADP mg^{-1} total protein min^{-1}; ITP, 1.27 ± 0.47 nmol [^{14}C]-ADP mg^{-1} total protein min^{-1}. The rates for the uracil and thymine nucleotides were 1.5 times higher than those of their equivalent adenine nucleoside di- and tri- phosphates. The rate of transport for guanosine nucleotides was low (initial rate of GDP, 0.26 ± 0.02 nmol [^{14}C]-ADP mg^{-1} total protein min^{-1} and GTP, 0.37 ± 0.08 nmol [^{14}C]-ADP mg^{-1} total protein min^{-1}), despite near complete inhibition in the competition assays, suggesting these nucleotides can compete for substrate binding, but are not transported.

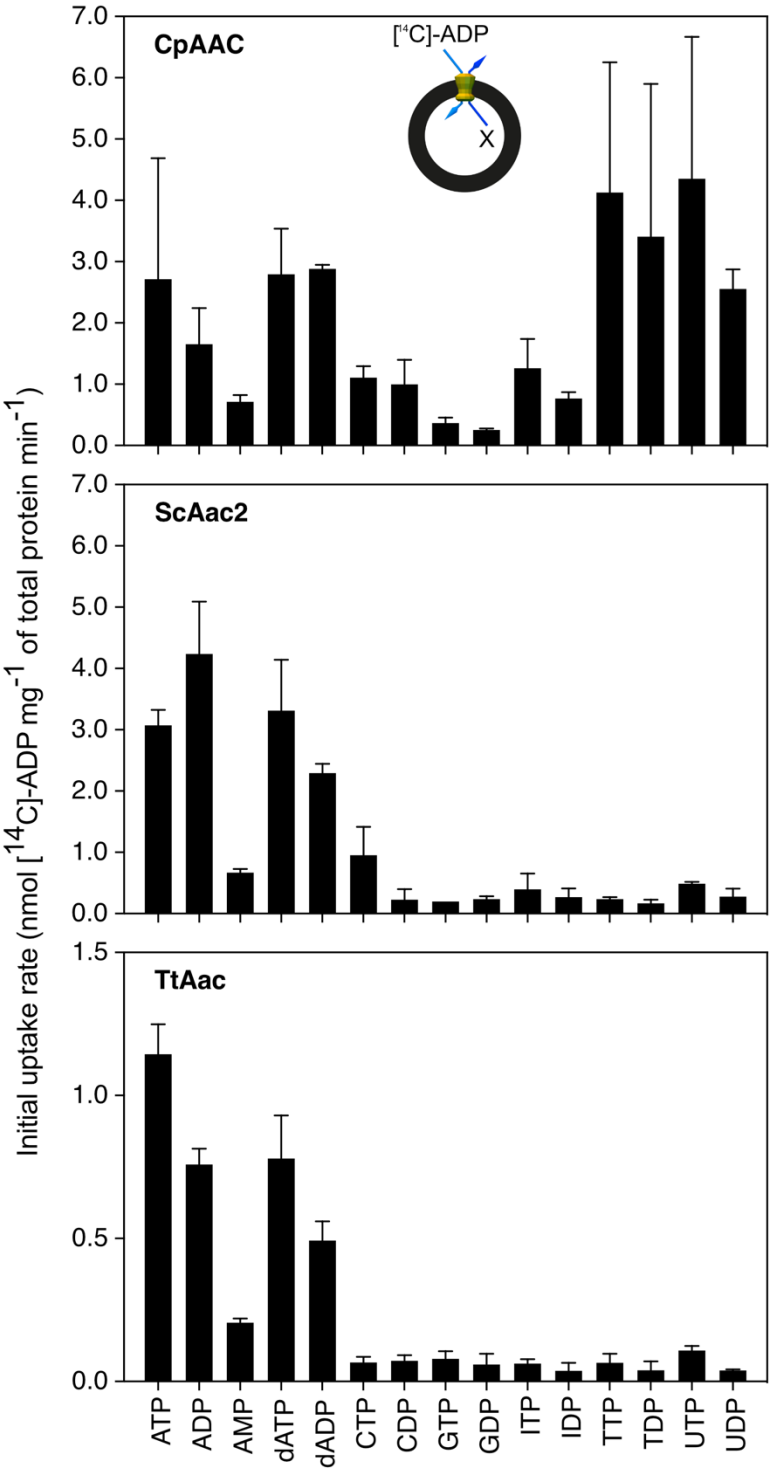

Figure 6.6: CpAAC has a broader nucleotide specificity than eukaryotic ADP/ATP carriers. Fused lactococcal membranes expressing either CpAAC (top), ScAac2 (middle) or TtAac (bottom) were loaded with 2.5 mM of the indicated substrate and exchange uptake was initiated by addition of 1.5 µM [^{14}C]-ADP externally. The initial rates were determined over the linear part of the uptake curves, here 60 seconds. Bars and error bars represent the mean and standard deviation of two biological repeats for CpAAC and ScAac2 and four technical repeats for TtAac. Note

that the y axis range is different for the bottom panel. Figure adapted from (King *et al.*, 2020).

6.1. A cysteine residue in the translocation pathway of CpAAC confers a broad nucleotide specificity

Interestingly, despite presenting extensive conservation of most residues with a key role in inhibitor and substrate binding, CpAAC displayed a broader nucleotide specificity than the characterised mitochondrial AAC. Inspecting the sequences, the only residue of the *in silico* identified substrate binding site that is different is $S238_{TtAac}$, ($S245_{ScAac2}$, $S227_{BtAac1}$), the equivalent of $C238_{CpAAC}$ (**Figure 6.2**). A cysteine residue in that position is observed only in certain mitosomal carriers, while in the known mitochondrial orthologues a serine is found. Therefore, point mutations on that position were designed, in order to investigate if this residue plays a role in determining the substrate specificity. For this work, the ScAac2 orthologue was used, because at the time of the experimental design, structural information was available for the yeast orthologues, but not for TtAac. Furthermore, TtAac is not well expressed in *L. lactis*. The two proteins presented the same specificity profile (**Figure 6.6**), they share 74 % sequence identity and all residues participating in inhibitor binding or are proposed to be involved in substrate binding are conserved, allowing for interchangeable use of information. For the specificity experiments heteroexchange reactions were performed with nucleoside tri-phosphates and ADP.

Initially, the serine to cysteine mutation was made ($S245C_{ScAac2}$). Interestingly, this mutant protein presented a very similar specificity profile to that of CpAAC, catalysing the exchange of UTP and TTP, in addition to ADP and ATP. The rates for UTP and TTP were 3.2 and 2.6 times higher than those of wild type ScAac2, while the rate for adenine nucleotide was very similar (**Figure 6.7**). This result indicated that this residue is indeed important for the specificity determination. Subsequently, other mutations to hydrophobic aliphatic (Ala, Leu, Ile, Val) or polar (Thr) amino acid residues were introduced to study the molecular basis of specificity further.

The alanine, valine and threonine mutants had a similar specificity profile to the wild type. They could all transport only adenine nucleotides. The rates were similar to wild type for S245A and S245V, while for S245T were 1.8 times lower (**Figure 6.7**). However, the leucine and isoleucine mutants replicated the profile of the cysteine mutant and CpAAC, as they could transport uracil and thymine nucleotides, in addition

to adenine nucleotides. The rates for adenine nucleotides were 1.2 and 1.3 times higher than those of the wild type (and S245C) for S245L and S245I, respectively. Mutant S245L exhibited 6.5 times higher rates than the wild type for TTP and 2.5 times higher than S245C. Regarding UTP, it presented 4.7 times higher rates than the wild type and 1.5 times higher than mutant 245C. Mutant S245I presented 5.3 times higher rates than the wild type for TTP and 2 times higher than S245C, while for UTP the rates were 2 times higher than wild-type rates and similar to mutant S245C. Surprisingly, despite transporting thymine and uracil nucleotides, these mutants did not transport cytosine nucleotides, even though all pyrimidine bases are structurally similar (**Figure 6.5**).

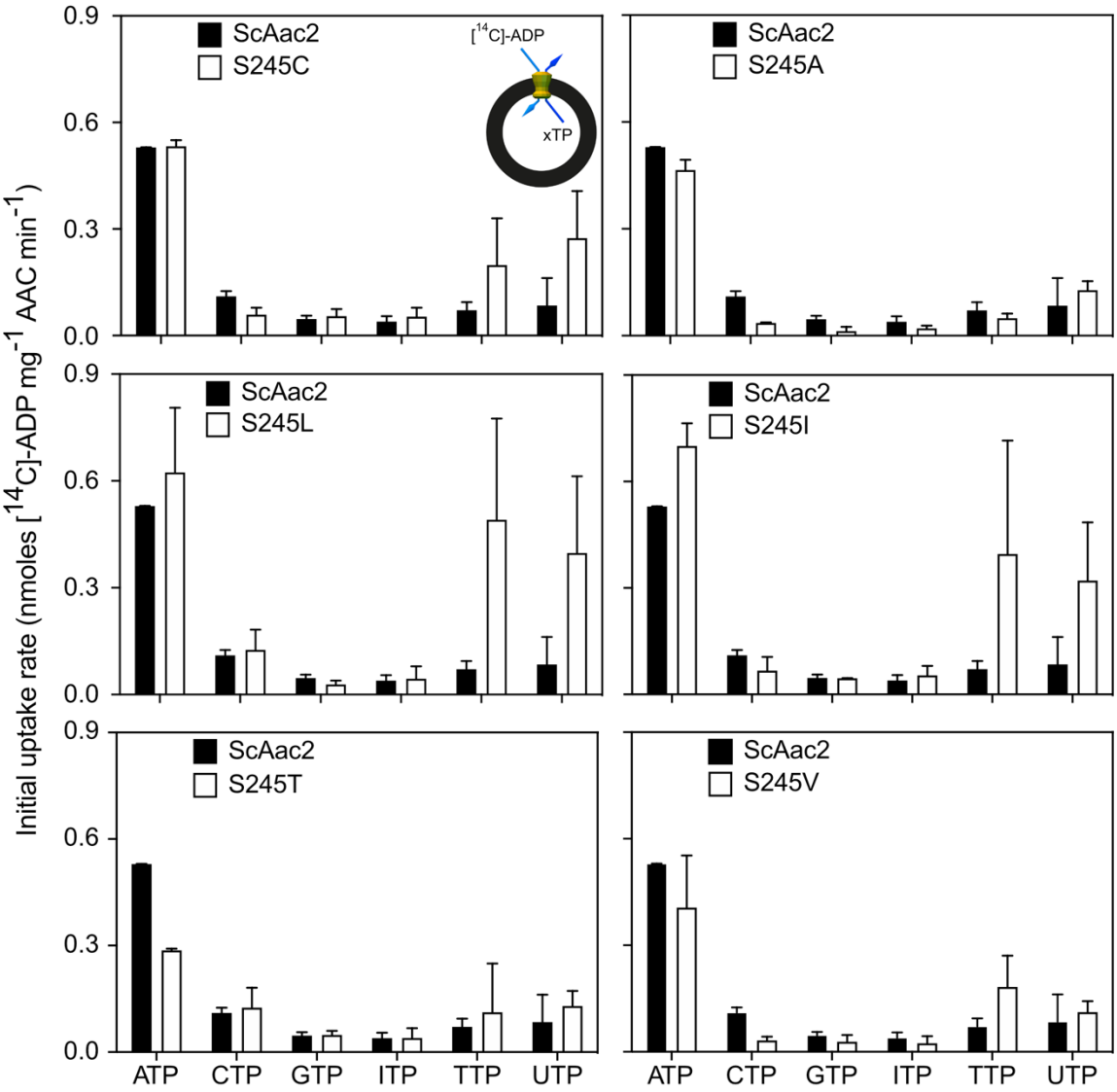

Figure 6.7: Investigation of the molecular basis for the broader nucleotide specificity of CpAAC. Fused lactococcal membranes expressing the wild type ScAac2 (filled bars) or mutant variants of position 245 (empty bars) were loaded with

2.5 mM of the indicated nucleotide and exchange uptake was initiated by addition of 1.5 μM [^{14}C]-ADP externally. The initial rates were determined over the linear part of the uptake curves, here 60 seconds. Bars and error bars represent the mean and standard deviation of two biological repeats. Figure adapted from (King *et al.*, 2020).

6.2. Discussion

In this chapter a mitosomal transporter from the anaerobic parasitic protist *Cryptosporidium parvum* was characterised. *C. parvum* is of great medical and veterinary importance and its study has been encouraged the last decades, with the aim to promote socioeconomical improvements and developmental progress, especially in developing countries (Henriquez et al., 2005). It was shown here that the transporter-product of gene Cgd8_1210 is phylogenetically related to mitochondrial ADP/ATP carriers, but exhibits a broader nucleotide specificity. In addition to adenine nucleoside di- and tri- phosohates, which are the transported substrates of all so far characterised mitochondrial ADP/ATP carriers (De Marcos Lousa *et al.*, 2002; Dolce *et al.*, 2005; Mifsud *et al.*, 2013; Pfaff and Klingenberg, 1968), it can also transport uracil and thymine nucleoside di- and tri- phosphates. The transport rates can be still inhibited by the AAC classic inhibitors, CATR and BKA.

Investigating the molecular basis for the broader specificity, the residues proposed by *in silico* analysis to be involved in substrate binding were considered (Kunji *et al.*, 2016). The only one of these residues that was different between the CpAAC and the mitochondrial orthologues was a serine residue ($S245_{ScAac2}$, $S238_{TtAac}$), which is cysteine in CpAAC. This residue has been proposed to participate in adenine binding, by forming a hydrogen bond with the N6 of the adenine moiety of the nucleotides (Dehez *et al.*, 2008; Mifsud *et al.*, 2013; Robinson *et al.*, 2008; Wang and Tajkhorshid, 2008). Here, it was shown that this residue indeed plays a role in determining the substrate specificity, as mutating the serine at that position to cysteine in the yeast ScAac2, altered the specificity of this carrier and made it match the specificity of the mitosomal transporter.

However, it can be concluded from the experiments with other substitutions that this residue is not directly involved in base recognition, but its selective role is conferred in an indirect way. Substitutions to other amino acids, either hydrophobic (Ala, Val, Leu, Ile) or polar (Thr), generated mutants that could still transport adenine nucleotides, showing that the adenine can still be accommodated in this binding pocket. However, the Leu and Ile mutants had a similar specificity profile to that of the

Cys mutant and of CpAAC, but they showed even higher rates for uracil and thymine nucleotides than the Cys mutant.

These results can be explained considering the hydrophobicity and the size of the binding pocket in each case and the difference in specificity it caused. Electrostatic surface calculations of the nucleotide bases demonstrated that cytosine and guanine are actually polar, because of strong negative partial charge around the ketone group at N6 and N2 respectively (Lucas et al., 2016) (**Figure 6.5**). Adenine, uracil and thymine have more equally distributed electrons (Lucas *et al.*, 2016). The Cys, Leu and Ile substitutions that introduced a larger and more hydrophobic amino acid than serine, making the binding pocket smaller, enabled the transport of uracil and thymine nucleotides, that are smaller than adenine nucleotides. It is possible that in the binding pocket of the wild type the pyrimidine bases fit very loosely and thus do not get transported, but this changes upon introduction of the larger amino acids. Cytosine nucleotides are not transported, despite the smaller pyrimidine base, probably because of the polar nature of this base. Adenine nucleotides are still transported by these mutants, as mentioned above, possibly because despite the decrease in size, the binding pocket still remains hydrophobic. When the polar amino acid Thr was introduced, that is bigger than serine and also polar, adenine nucleotides were transported less effectively, in agreement with the assessment that the decrease in size, in combination with the polar character are not as favourable for adenine binding. Introduction of the smaller substitutions of Ala and Val did not alter the specificity of the protein, since they increased the size of the binding pocket, making it hard for pyrimidine bases to bind, while still allowing adenine binding. Guanine and inosine nucleotides did not seem to fit in any binding pocket, because of their size or polar nature.

Therefore, the hydrophobicity and size of the adenine binding pocket are probably the main factors that influence the substrate specificity, rather than direct interactions with this serine residue. This assessment is in agreement with the result that it is not directly involved in substrate binding, as demonstrated in **Chapters 3** and **4** for TtAac. The thermostability profile of the alanine variant was not different from the wild type at any concentration (**Figure 4.7A**) and this variant could complement growth of the Aac-deficient strain (**Figures 3.4** and **3.5**). Hence all results show that this residue is important for the specificity, but not through a direct interaction with the nucleotide base.

It would be interesting to investigate if other residues in the vicinity of the base binding site can have a similar effect on the specificity, or if there are residues that have a more direct involvement. For example, residues $N96_{TtAac}$ and $L135_{TtAac}$, that have been shown to contribute to substrate binding (**Figures 4.6** and **5.13**) are also different between CpAAC and the mitochondrial orthologues (**Figure 6.2**). CpAAC has a glycine residue (G99) in place of the asparagine and a serine (S138) in place of the leucine. Furthermore, the rest of the residues shown to be important for substrate binding, proposed to interact with the adenosine (V138, G192, Y196) (**Figures 4.6, 5.11** and **5.13**) could be essential for adenine recognition. The investigation of the potential role that these residues might have is an interesting point for further investigation, as it will shed more light on how base selectivity occurs, ensuring the strict substrate specificity that the mitochondrial ADP/ATP carriers present.

Chapter 7: Conclusions and future perspectives

7.1. Brief recapitulation of the results of this study

The mitochondrial ADP/ATP carriers have unique features that enable them to achieve a very high flux of ADP and ATP across the mitochondrial inner membrane, to fuel eukaryotic oxidative phosphorylation. They are proposed to operate via an alternating access mechanism and structural studies have shown that this mechanism includes motions of six mobile structural elements (Ruprecht and Kunji, 2019; Ruprecht and Kunji, 2020). Despite extensive studies, aspects of the mechanism remain unresolved, in particular regarding substrate binding and its effect on the interconversion between the matrix- and cytoplasmic-open states. In this work, alanine mutagenesis studies were employed to identify experimentally the residues involved in the substrate binding process. Thirty-six residues were targeted as candidates, based on their position (facing the solvent-filled carrier cavity and being between the matrix and the cytoplasmic salt bridge networks) and on their conservation among ADP/ATP carrier orthologues.

Initially, functional complementation assays (**Chapter 3**), performed with a yeast strain that in aerobic conditions lacks endogenous ADP/ATP carriers, demonstrated that the majority of the targeted residues are functionally important at the cellular level. However, no information on the biophysical properties of the variants could be obtained, nor could it be deduced which aspect of function or structure was affected by the mutation. To investigate that, the variants were purified and the CPM thermostability assay was used to evaluate their folding state and the integrity of their binding pockets. The latter was assessed by performing assays with the competitive and state-specific inhibitors CATR and BKA. Inhibitor binding, reflected as a positive shift in the thermostability of the protein population is indicative of well folded protein. Even though all thirty-six variants were successfully purified, five of them were unfolded, hence they were not included in further analyses. These five residues are situated in the matrix gate (**Figure 7.1**).

The thirty-one folded proteins were subsequently tested for substrate binding using the CPM thermostability assay (**Chapter 4**). The substrates, when present in

concentrations higher than the apparent K_d, were known to enhance the protein population stability, due to specific protein-substrate interactions (Majd *et al.*, 2018a). It was confirmed that this effect is concentration-dependent for the wild-type protein and it was postulated that by systematically disrupting the interactions (through mutations) that are responsible for the increase in thermostability, the substrate binding site could be mapped. As proof of principle, it was shown that this approach could map relatively well the binding sites of the inhibitors CATR and BKA, which are known from crystal structures. The substrate binding analysis showed that five positively charged residues (K30, R88, R197, R246 and R287) are critical for substrate binding, because the variants completely abolished the concentration-dependent response to substrate. Additionally, another six residues (N85, N96, L135, V138, G192 and Y196), located in the vicinity, were proposed to make contributions to binding, because their response to substrate was significantly different than that of the wild type. Importantly, all other tested residues were shown not to be involved in substrate binding (**Figure 7.1**).

The transport properties of these eleven variants (**Chapter 5**) in general supported the thermostability results. The variants of residues K30, R88, R197, R246 and R287, proposed to be involved in critical interactions, presented no activity. Three variants of the residues proposed to contribute to binding (N85, G192 and Y196) were also inactive. From the other three, N96A and V138A presented uptake with slightly altered kinetic properties compared to the wild type. N96A had a four-fold increased K_m value and a two-fold decreased V_{max} and V138A a two-fold increased K_m and two-fold decreased V_{max} value. Variant L135A showed very similar transport properties with the wild type. This could be due to the conservative mutation, as both residues are aliphatic. It is also possible that residues L135, V138, G192 and Y196 are jointly involved in the binding process and hence, modifying just one with a mild mutation, might not have a dramatic effect on the overall transport activity of the protein.

In **Chapter 6**, the study of a mitosomal transporter that resembles the ADP/ATP carrier provided the opportunity to gain molecular information about the determinants of substrate specificity. The mitosomal transporter had all the sequence features that are characteristic for ADP/ATP carriers, but exhibited a wider substrate specificity, transporting thymine and uracil nucleoside di- and tri- phosphates, in addition to ADP and ATP. Investigating the molecular basis for this difference, a residue in the vicinity of the binding pocket, but not directly involved in substrate binding, was identified. This

residue is a cysteine in the mitosomal transporter and serine in the ADP/ATP carriers. By creating point mutations, altering the size and hydrophobicity of the side chain, and testing the specificity change of the mutants, it could be concluded that the nucleotide base recognition is probably governed by the size and hydrophobicity of the whole binding pocket, rather than by interaction with this specific residue. This observation may also explain why the mutation of some of the residues proposed to form the adenine binding pocket was not detrimental for transport.

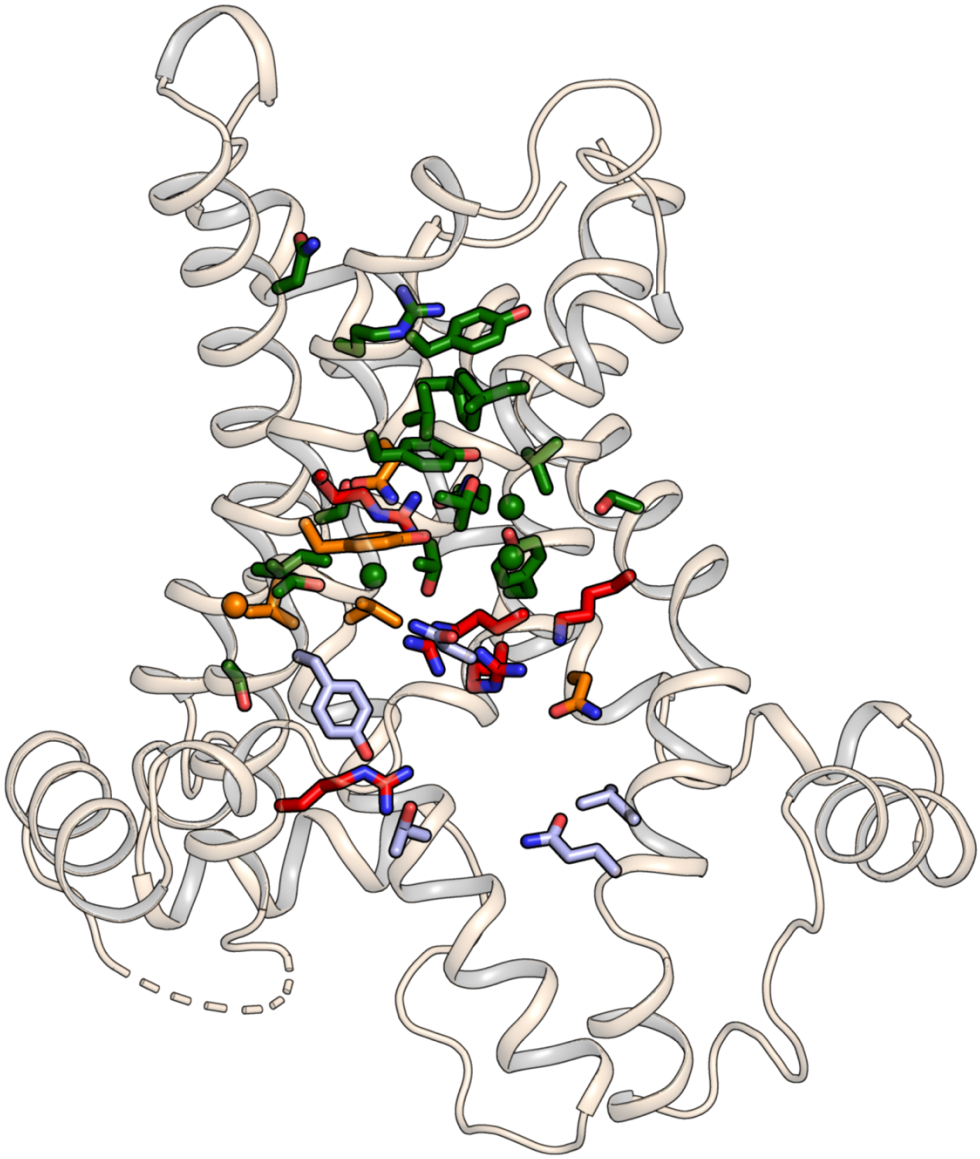

Figure 7.1: Residues participating in the substrate binding process. TtAac matrix-open structure (PDB code: 6gci chain A) showing all the residues analysed in this study. Red and orange sticks and sphere for Gly indicate the residues identified to be critical and to make significant contributions to substrate binding, respectively. Green sticks and spheres for Gly indicate the residues shown not to be involved in the

process and light purple sticks the residues alanine mutation of which yielded unfolded proteins.

7.2. The substrate binding mechanism of the mitochondrial ADP/ATP carrier

Considering the results from all three techniques together (functional complementation, thermostability shift and transport assays) and combining them with the valuable information that can be obtained from having structures of the protein in two conformational states, a model for the substrate binding process is proposed (**Figure 7.2**). Given that there was no difference in the interaction of ADP and ATP with any of the residues, as both substrates induced shifts of similar magnitudes to the wild type and all variants, this model can describe the complete transport cycle. It is possible that the terminal phosphate in each case, the β phosphate in the case of ADP and the γ phosphate in the case of ATP (that in both cases carries two negative charges), serves the same role.

Inspecting the position of the eleven residues found to participate in substrate binding in the structures of the two conformational states, it can be observed that K30, R88, L135, V138, G192, Y196 and R287 are at the same plane in the carrier cavity and are found with similar conformers in both structures. Contrarily, residues N96 and R197 are situated in the cytoplasmic side of this central area and residues N85 and R246 are on the matrix side. Furthermore, they appear to change conformers in a state-dependent way. Therefore, it was proposed that these two pairs of residues are responsible for the initial binding and guiding of the substrate to the 'main site', composed of the rest seven residues, that are accessible in the same way in both conformational states. Subsequently, they might also be involved in the release of the substrate on the other side of the membrane, becoming available to bind the counter substrate.

More specifically, in the cytoplasmic-open state, the carrier cavity is accessible to receive ADP from the intermembrane space. ADP probably initially binds to residues N96 and R197, interacting with its phosphate groups, while the adenine finds its place in the main site. Given their relative positions, chemistry and the results of the mutants in thermostability and transport assays, residues L135, V138, G192 and Y196 are probably cooperatively involved in binding of the adenine or adenosine moiety. Subsequently, the phosphate groups bind to the three positively charged residues of

the main site (K30, R88, R287). The conformational changes then continue to the “occluded state”, in which the substrate binding site is occupied and inaccessible from both sides of the membrane. The phosphate groups of ADP are attracted to bind to residues N85 and R246, simultaneously driving the carrier to change conformation and start opening the cavity towards the mitochondrial matrix. This leads to the narrowing of the centre of the cavity and the substrate is displaced from the binding pocket. Now the carrier is in the matrix-open state and the substrate binding site is accessible to bind ATP. The ATP molecule will follow the same journey, interacting with the same residues as ADP and driving the same structural movements, but in reverse. The phosphate groups will be initially attracted and will bind to residues N85/ R246, while the adenosine will find its pocket, formed by residues L135, V138, G192 and Y196. The phosphate groups will then bind to K30, R88 and R287. These steps are interconnected with conformational changes that lead to formation of the occluded state. The phosphates will bind to N96/ R197, driving the transition to the cytoplasmic-open state and release of ATP to the intermembrane space. This model is logical, taking into account the results of biophysical and biochemical functional assays and putting them in the context of the two available structures, which though represent conformations that are abortive. For the validation of the model, regarding the exact binding steps, structures of the intermediate states are required.

The identified binding site is consistent with the structural movements proposed based on structural analysis and modelling and supports a ping pong kinetic mechanism. The identified residues can act as fulcrums for the proposed movements (Ruprecht and Kunji, 2019) and the existence of one binding site for ADP and ATP, in combination with the fact that ADP/ATP carriers exist and function as monomers (Kunji and Crichton, 2010; Kunji and Ruprecht, 2020), explain the reversibility of transport.

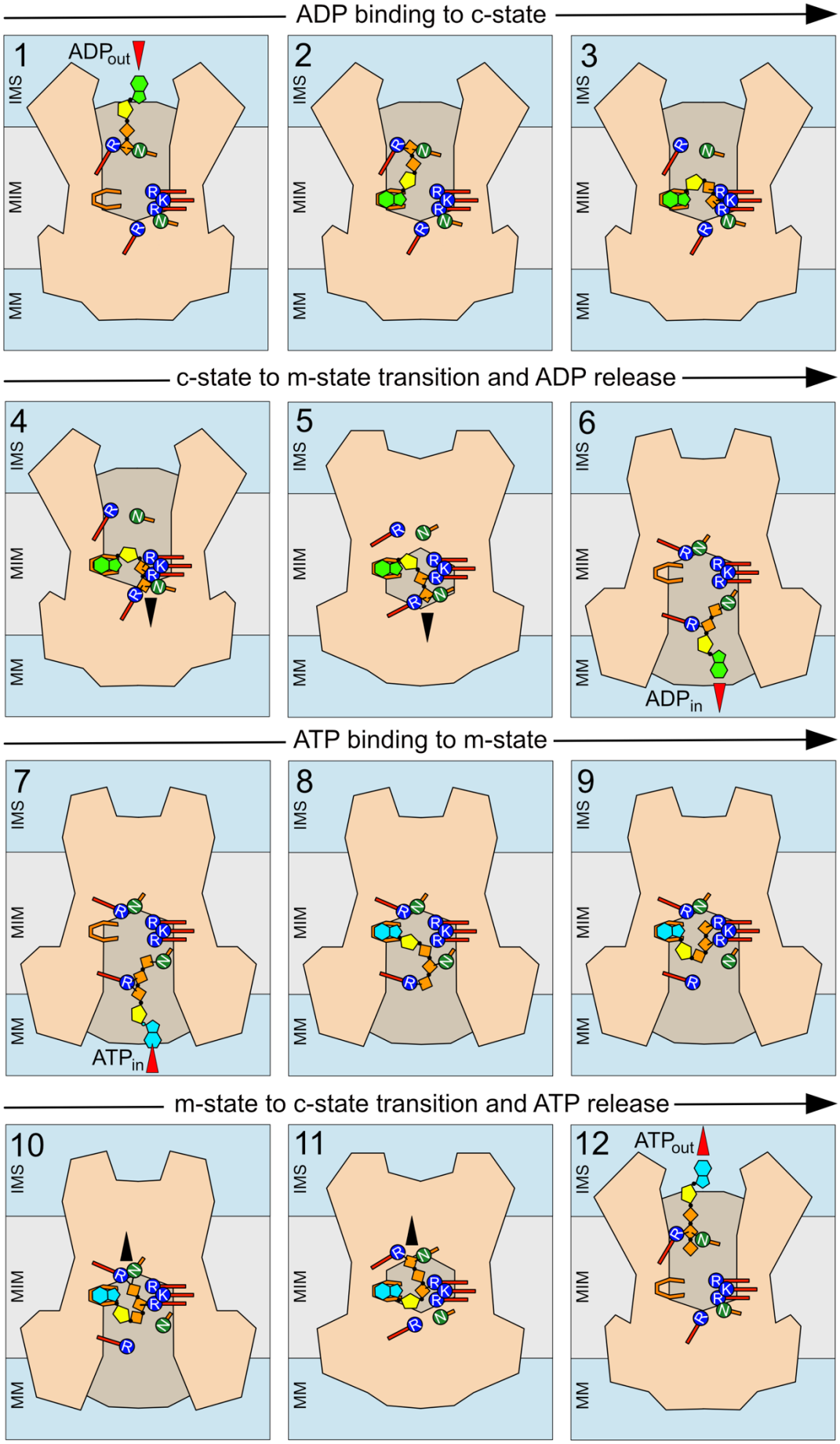
ADP binding to c-state
1
ADPout
2
3
IMS
MIM
MM
c-state to m-state transition and ADP release
4
5
6
ADPin
ATP binding to m-state
7
ATPin
8
9
m-state to c-state transition and ATP release
10
11
12
ATPout

Figure 7.2: Schematic representation of the proposed substrate binding events. The adenine moiety is represented by green and cyan (for ADP and ATP respectively) hexagon/pentagon shape, the ribose by a yellow pentagon and the phosphates by orange rhombus. The adenosine binding site is represented by a petal shape, whereas positively charged and polar residues of the binding site are shown in blue and green, respectively. The black arrows indicate the substrate movements that induce the conversion between states, whereas the red ones indicate entry and exit of the substrates. Figure prepared by Prof Edmund Kunji.

Moreover, the electrostatic properties of the identified binding residues can explain an important aspect of bioenergetics, regarding the transport of ADP against the membrane potential, which has been held as an argument against a ping-pong mechanism. The properties of the binding site are key to understanding this process. During export of ATP four negative charges are moved towards the positive side of the membrane potential, but during import of ADP three negative charges are moved against it. The charge movements have been measured directly using caged nucleotides, giving values of +0.3 or +0.5 for the ADP import step and -0.7 or -0.5 for the ATP export step (Brustovetsky et al., 1996; Gropp et al., 1999). Based on these observations, it was proposed that the substrate binding site should contain 3.3 or 3.5 positive counter charges (Brustovetsky *et al.*, 1996; Gropp *et al.*, 1999). These measurements agree reasonably well with the three positive charges of K30, R88 and R287 in the main binding site, which reorient with the substrate to the other compartment, as the carrier changes conformation. The partial formal charges could be due to the state-dependent interactions with either residue R197 or R246. The partial charges minimise the electrophoretic force of the membrane potential on both the bound substrates in the occluded state and stimulate both the import of ADP and export of ATP.

Finally, the geometry of the site might explain why the carrier does not spontaneously interconverts between states in absence of substrate. Variants K30A, R88A and R287A, as noted in **Chapter 3**, are more thermostable than the wild type (K30A 57.3 ± 1.2°C, R88A 53.1 ± 1°C, R287A 64.4 ± 0.2°C and wild type 50.2 ± 0.6°C), indicating that probably in the wild-type cavity the positive charges are repelled, placing the carrier in a ‘high energy’ state. In the presence of substrate, the positive charges are neutralised and the energy barrier is lowered, allowing for the conformational changes to occur.

7.3. Future perspectives

In the course of this study different aspects of the substrate binding mechanism were tried to be addressed with other techniques and some promising preliminary results were obtained, which are worth further investigation. Furthermore, some of the obtained information can be useful for future functional and structural studies.

7.3.1. Library of mutations to assist structural and functional studies

The created set of single alanine replacement variants can be helpful for other future studies. Some of the created mutations are in positions that have been reported to contain pathogenic mutations, either in the ADP/ATP carrier, or in other members of the SLC25 family (**Figure 7.3**). All residues identified to be involved in substrate binding have at least one reported mutation in some member of the family, even though for most of them there is currently no experimental investigation of the induced effect. The results of this study can be useful to provide information on the stability of the mutant protein, its response to substrate, its transport activity or even on its function at the cellular level. This information may broaden the understanding of the pathogenicity to assist studies for potential treatment.

Additionally, variants with different properties have been created. For example, some of them were shown to be more stable than the wild-type protein (e.g. K30A, R88A, R100A, R287A and V294A) and some were shown to be stabilised by the substrates to a greater extent than the wild type (e.g. Y89A and F97A). These properties might be exploited for structural studies. In the first case, potentially the uninhibited substrate-free states could be probed, while in the latter, the substrate-bound states. Furthermore, the participation of the two arginine-asparagine pairs indicated that the substrate binding process includes a continuum of substrate-bound states. Some of these states may be selectively enhanced when these residues are mutated, halting the binding process at different stages. These ideas have already been explored to some extent in collaboration with other members of the laboratory, who work on these structural issues (Dr Deepak Chand and Dr Jonathan Ruprecht). Towards this plan, the arginine residues of the arginine/ asparagine pairs have also been mutated to glutamine (mutagenesis performed by Dr Martin King and Dr Deepak Chand), which is a less radical mutation, compared to the alanine and might maintain some properties of the wild-type protein.

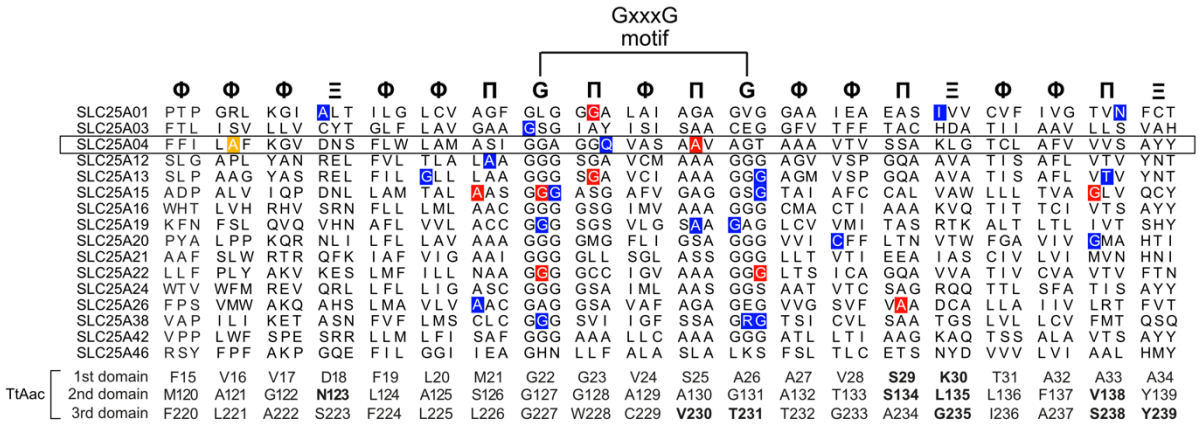
GxxxG motif
Φ Φ Φ Ξ Φ Φ Π G Π Φ Π G Φ Φ Π Ξ Φ Φ Π Ξ
SLC25A01 PTP GRL KGI ALT ILG LCV AGF GLG GGA LAI AGA GVG GAA IEA EAS IVV CVF IVG TVN FCT
SLC25A03 FTL ISV LLV CYT GLF LAV GAA GSG IAY ISI SAA CEG GFV TFF TAC HDA TII AAV LLS VAH
SLC25A04 FFI LAF KGV DNS FLW LAM ASI GGA GGQ VAS AAV AGT AAA VTV SSA KLG TCL AFV VVS AYY
SLC25A12 SLG APL YAN REL FVL TLA LAA GGG SGA VCM AAA GGG AGV VSP GQA AVA TIS AFL VTV YNT
SLC25A13 SLP AAG YAS REL FIL GLL LAA GGG SGA VCI AAA GGC AGM VSP GQA AVA TIS AFL VTV YNT
SLC25A15 ADP ALV IQP DNL LAM TAL AAS GGG ASG AFV GAG GSG TAI AFC CAL VAW LLL TVA GLV QCY
SLC25A16 WHT LVH RHV SRN FLL LML AAC GGG GSG IMV AAA GGG CMA CTI AAA KVQ TIT TCI VTS AYY
SLC25A19 KFN FSL QVQ VHN AFL VVL ACC GCG SGS VLG SAA GAG LCV VMI TAS RTK ALT LTL IVT SHY
SLC25A20 PYA LPP KQR NLI LFL LAV AAA GGG GMG FLI GSA GGG VVI CFF LTN VTW FGA VIV CMA HTI
SLC25A21 AAF SLW RTR QFK IAF VIG AAI GGG GLL SGL ASS GGG LLT VTI EEA IAS CIV LVI MVN HNI
SLC25A22 LLF PLY AKV KES LMF ILL NAA GCG GCC IGV AAA GGG LTS ICA GQA VVA TIV CVA VTV FTN
SLC25A24 WTV WFM REV QRL LFL LIG ASC GGG GSA IML AAS GGS AAT VTC SAG RQQ TTL SFA TIS AYY
SLC25A26 FPS VMW AKQ AHS LMA VLV AAC GAG GSA VAF AGA GEG VVG SVF VAA DCA LLA IIV LRT FVT
SLC25A38 VAP ILI KET ASN FVF LMS CLC GCG SVI IGF SSA GRG TSI CVL SAA TGS LVL LCV FMT QSQ
SLC25A42 VPP LWF SPE SRR LLM LFI SAF GGG AAA LLC AAA GGG ATL LTI AAG KAQ TSS ALA VTS AYY
SLC25A46 RSY FPF AKP GQE FIL GGI IEA GHN LLF ALA SLA LKS FSL TLC ETS NYD VVV LVI AAL HMY
1st domain F15 V16 V17 D18 F19 L20 M21 G22 G23 V24 S25 A26 A27 V28 S29 K30 T31 A32 A33 A34
TtAac 2nd domain M120 A121 G122 N123 L124 A125 S126 G127 G128 A129 A130 G131 A132 T133 S134 L135 L136 F137 V138 Y139
3rd domain F220 L221 A222 S223 F224 L225 L226 G227 W228 C229 V230 T231 T232 G233 A234 G235 I236 A237 S238 Y239

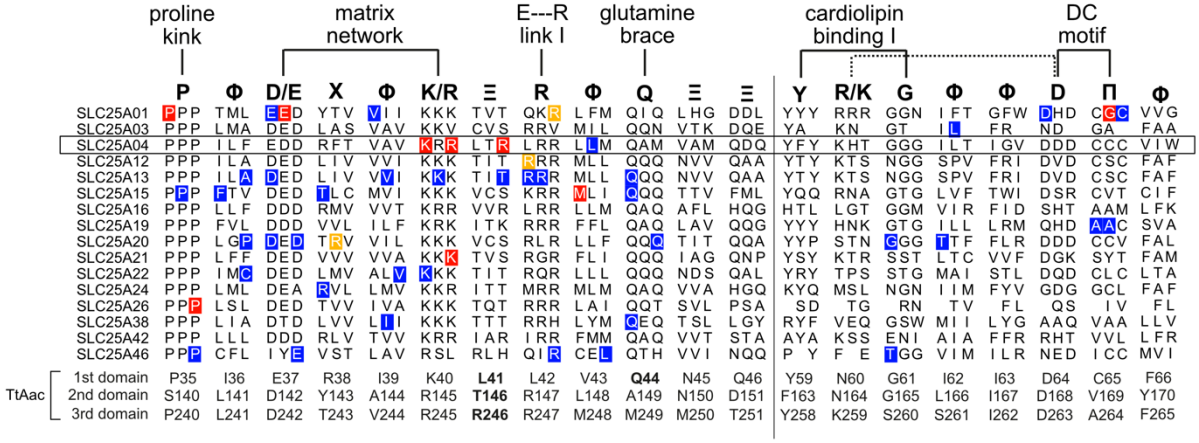
proline kink
matrix network
E---R link I
glutamine brace
cardiolipin binding I
DC motif
P Φ D/E X Φ K/R Ξ R Φ Q Ξ Ξ Y R/K G Φ Φ D Π Φ
SLC25A01 FPP TML EED YTV VII KKK TVT QKR LFM QIQ LHG DDL YYY RRR GGN IFT GFW DHD CGC VVG
SLC25A03 PPP LMA DED LAS VAV KKV CVS RRV MIL QQN VTK DQE YA KN GT IL FR ND GA FAA
SLC25A04 PPP ILF EDD RFT VAV KRR LTR LRR LLM QAM VAM QDQ YFY KHT GGG ILT IGV DDD CCC VIW
SLC25A12 PPP ILA DED LIV VVI KKK TIT RRR MLL QQQ NVV QAA YTY KTS NGG SPV FRI DVD CSC FAF
SLC25A13 PPP ILA DED LIV VVI KKK TIT RRR MLL QQQ NVV QAA YTY KTS NGG SPV FRI DVD CSC FAF
SLC25A15 PPP FTV DED TLC MVI KKK VCS KRR MLI QQQ TTV FML YQQ RNA GTG LVF TWI DSR CVT CIF
SLC25A16 PPP LLF DDD RMV VVT KRR VVR LRR LLM QAQ AFL HQG HTL LGT GGM VIR FID SHT AAM LFK
SLC25A19 PPP FVL DDD VVL ILF KRK ITK RRR FFL QAQ LAV QQG YYY HNK GTG ILL LRM QHD AAC SVA
SLC25A20 PPP LGP DED TRV VIL KKK VCS RLR LLF QQQ TIT QQA YYP STN GGG TTF FLR DDD CCV FAL
SLC25A21 PPP LFF DED VVV VVA KKK TVS RGR FLI QQQ IAG QNP YSY KTR SST LTC VVF DGK SYT FAM
SLC25A22 PPP IMC DED LMV ALV KKK TIT RQR LLL QQQ NDS QAL YRY TPS STG MAI STL DQD CLC LTA
SLC25A24 PPP LML DEA RVL LMV KKR ITT MRR MLM QAQ VVA HGQ KYQ MSL NGN IIM FYV GDG GCL FAF
SLC25A26 PPP LSL DED TVV IVA KKK TQT RRR LAI QQT SVL PSA SD TG RN TV FL QS IV FL
SLC25A38 PPP LIA DTD LVV LII KKK TTT RRH LYM QEQ TSL LGY RYF VEQ GSW MII LYG AAQ VAA LLV
SLC25A42 PPP LLL DDD RLV TVV KRR IAR IRR FMM QAQ VVT STA AYA KSS ENI AIA FFR RHT VVL LFR
SLC25A46 PPP CFL IYE VST LAV RSL RLH QIR CEL QTH VVI NQQ P Y F E TGG VIM ILR NED ICC MVI
1st domain P35 I36 E37 R38 I39 K40 L41 L42 V43 Q44 N45 Q46 Y59 N60 G61 I62 I63 D64 C65 F66
TtAac 2nd domain S140 L141 D142 Y143 A144 R145 T146 R147 L148 A149 N150 D151 F163 N164 G165 L166 I167 D168 V169 Y170
3rd domain P240 L241 D242 T243 V244 R245 R246 R247 M248 M249 M250 T251 Y258 K259 S260 S261 I262 D263 A264 F265

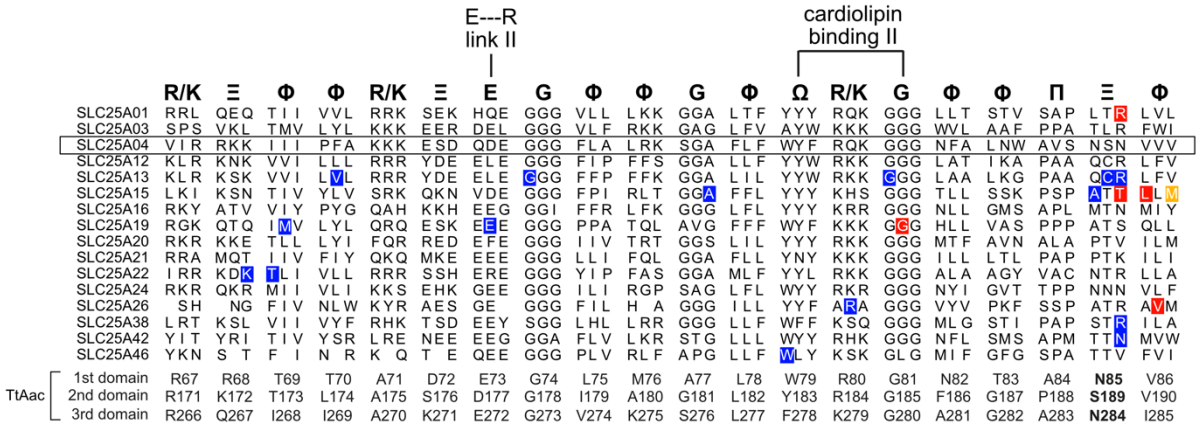
E---R link II
cardiolipin binding II
R/K Ξ Φ Φ R/K Ξ E G Φ Φ G Φ Ω R/K G Φ Φ Π Ξ Φ
SLC25A01 RRL QEQ TII VVL RRK SEK HQE GGG VLL LKK GGA LTF YYY RQK GGG LLT STV SAP LTR LVL
SLC25A03 SPS VKL TMV LYL KKK EER DEL GGG VLF RKK GAG LFV AYW KKK GGG WVL AAF PPA TLR FWI
SLC25A04 VIR RKK III PFA KKK ESD QDE GGG FLA LRK SGA FLF WYF RQK GGG NFA LNW AVS NSN VVV
SLC25A12 KLR KNK VVI LLL RRR YDE ELE GGG FIP FFS GGA LLF YYW RKK GGG LAT IKA PAA QCR LFV
SLC25A13 KLR KSK VVI LVL RRR YDE ELE GGG FFP FFK GGA LIL YYW RKK GGG LAA LKG PAA QCR LFV
SLC25A15 LKI KSN TIV YLV SRK QKN VDE GGG FPI RLT GGA FFL YYY KHS GGG TLL SSK PSP ATT LLM
SLC25A16 RKY ATV VIY PYG QAH KKH EEG GGI FFR LFK GGG LFL YYY KRR GGG NLL GMS APL MTN MIY
SLC25A19 RGK QTQ IMV LYL QRQ ESK EEE GGG PPA TQL AVG FFF WYF KKK GGG HLL VAS PPP ATS QLL
SLC25A20 RKR KKE TLL LYI FQR RED EFE GGG IIV TRT GGS LIL YYY RKK GGG MTF AVN ALA PTV ILM
SLC25A21 RRA MQT IIV FIY QKQ MKE EEE GGG LLI FQL GGA FLL YNY KKK GGG ILL LTL PAP PTK ILI
SLC25A22 IRR KDK TLI VLL RRR SSH ERE GGG YIP FAS GGA MLF YYL RKK GGG ALA AGY VAC NTR LLA
SLC25A24 RKR QKR MII VLI KKS EHK GEE GGG ILI RGP SAG LFL WYY RKR GGG NYI GVT TPP NNN VLF
SLC25A26 SH NG FIV NLW KYR AES GE GGG FIL H A GGG ILL YYF ARA GGG VYV PKF SSP ATR AVM
SLC25A38 LRT KSL VII VYF RHK TSD EEY SGG LHL LRR GGG LLF WFF KSQ GGG MLG STI PAP STR ILA
SLC25A42 YIT YRI TIV YSR LRE NEE EEG GGA FLV LKR STG LLL WYY RHK GGG NFL SMS APM TTN MVW
SLC25A46 YKN S T F I N R K Q T E QEE GGG PLV RLF APG LLF WLY KSK GLG MIF GFG SPA TTV FVI
1st domain R67 R68 T69 T70 A71 D72 E73 G74 L75 M76 A77 L78 W79 R80 G81 N82 T83 A84 N85 V86
TtAac 2nd domain R171 K172 T173 L174 A175 S176 D177 G178 I179 A180 G181 L182 Y183 R184 G185 F186 G187 P188 S189 V190
3rd domain R266 Q267 I268 I269 A270 K271 E272 G273 V274 K275 S276 L277 F278 K279 G280 A281 G282 A283 N284 I285

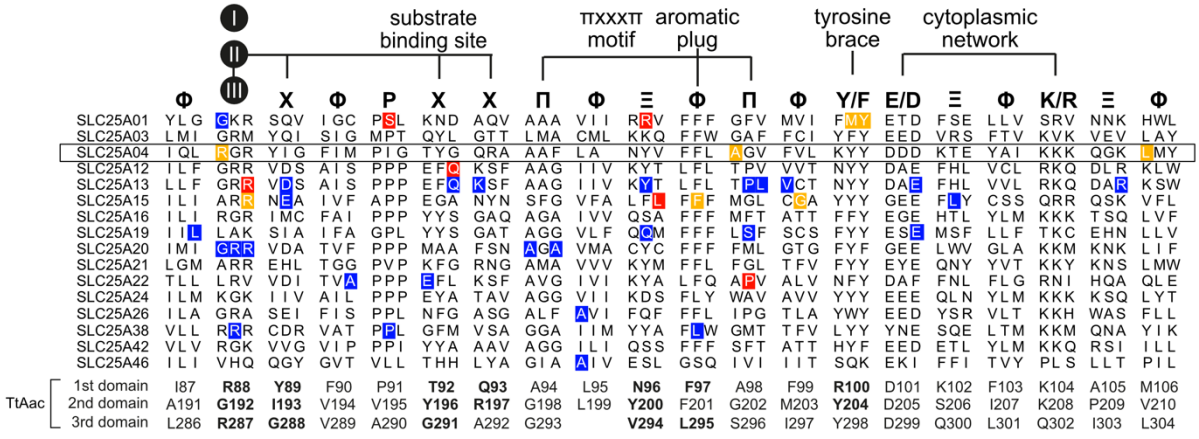
I
II
III
substrate binding site
πxxxxπ motif
aromatic plug
tyrosine brace
cytoplasmic network
Φ X Φ P X X Π Φ Ξ Φ Π Φ Y/F E/D Ξ Φ K/R Ξ Φ
SLC25A01 YLG GKR SQV IGC PSL KND AQV AAA VII RRV FFF GFV MVI FMY ETD FSE LLV SRV NNK HWL
SLC25A03 LMI GRM YQI SIG MPT QYL GTT LMA CML KKQ FFW GAF FCI YFY EED VRS FTV KVK VEV LAY
SLC25A04 IQL RGR YIG FIM PIG TYG QRA AAF LA NYV FFL AGV FVL KYY DDD KTE YAI KKK QGK LMY
SLC25A12 ILF GRR VDS AIS PPP EFQ KSF AAG IIV KYT LFL TPV VVT NYY DAE FHL VCL RKQ DLR KLW
SLC25A13 LLF GRR VDS AIS PPP EFQ KSF AAG IIV KYT LFL TPL VCT NYY DAE FHL VVL RKQ DAR KSW
SLC25A15 ILI ARR NEA IVF APP EGA NYN SFG VFA LFL FFF MGL CGA YYY GEE FLY CSS QRR QSK VFL
SLC25A16 ILI RGR IMC FAI PPP YYS GAQ AGA IVV QSA FFF MFT ATT FFY EGE HTL YLM KKK TSQ LVF
SLC25A19 IIL LAK SIA IFA GPL YYS GAT AGG VLF QQM FFF LSF SCS FYY ESE MSF LLF TKC EHN LLV
SLC25A20 IMI GRR VDA TVF PPP MAA FSN AGA VMA CYC FFF FML GTG FYF GEE LWV GLA KKM KNK LIF
SLC25A21 LGM ARR EHL TGG PVP KFG RNG AMA VVV KYM FFL FGL TFV FYY EYE QNY YVT KKY KNS LMW
SLC25A22 TLL LRV VDI TVA PPP EFL KSF AVG IVI KYA LFQ APV ALV NFY DAF FNL FLG RNI HQA QLE
SLC25A24 ILM KGK IIV AIL PPP EYA TAV AGG VII KDS FLY WAV AVV YYY EEE QLN YLM KKK KSQ LYT
SLC25A26 ILA GRA SEI FIS PPL NFG ASG ALF AVI FQF FFL IPG TLA YWY EED YSR VLT KKH WAS FLL
SLC25A38 VLL RRR CDR VAT PPL GFM VSA GGA IIM YYA FLW GMT TFV LYY YNE SQE LTM KKM QNA YIK
SLC25A42 VLV RGK VVG VIP PPI YYA AAV AGG ILI QSS FFF SFT ATT HYF EED ETL YLM KKQ RSI ILL
SLC25A46 ILI VHQ QGY GVT VLL THH LYA GIA AIV ESL GSQ IVI IIT SQK EKI FFI TVY PLS LLT PIL
1st domain I87 R88 Y89 F90 P91 T92 Q93 A94 L95 N96 F97 A98 F99 R100 D101 K102 F103 K104 A105 M106
TtAac 2nd domain A191 G192 I193 V194 V195 Y196 R197 G198 L199 Y200 F201 G202 M203 Y204 D205 S206 I207 K208 P209 V210
3rd domain L286 R287 G288 V289 A290 G291 A292 G293 V294 L295 S296 I297 Y298 D299 Q300 L301 Q302 I303 L304

Figure 7.3: Pathogenic mutations of mitochondrial carriers. Aligned triplets of the 16 mitochondrial carriers associated with developmental, metabolic and neuromuscular diseases. Red boxes indicate mutations that have a severe effect on function and yellow those that have milder effects. Blue boxes indicate mutations identified by genetic analysis, but their effect has not been studied experimentally. At the bottom are the residue triplets of TtAac for reference. The residues analysed in this study are indicated with bold letters. Empty black boxes indicate the human AAC for easier comparison. The triplet is labeled by the one-letter code of the most conserved residue or by the most common property: π, small amino acids; Φ, hydrophobic amino acids; ξ, hydrophilic amino acids; Ω, aromatic amino acids; or by X for any amino acid. The black spheres with roman numerals are the 'contact points' of the substrate binding site. H6 in the ADP/ATP carrier is one residue shorter than other carriers and lacks a residue in triplet 90. The matrix loops, as well as the cytoplasmic loops and amino- and carboxy-termini have been omitted. Figure adapted from (Kunji *et al.*, 2020).

7.3.2. Studying the electrostatics of substrate binding and translocation: Preliminary results with Solid Supported Membrane (SSM)- based electrophysiology

Transport of ADP and ATP by the ADP/ATP carrier is electrogenic (Klingenberg, 2008). Some preliminary work on studying the electrostatics of this process has been carried out, by using SSM based electrophysiology. This work was performed in collaboration with Dr Andre Bazzone (Nanion Technologies, Munich, Germany). My role in the project was to purify the protein (**section 2.5.3**) and reconstitute it into liposomes (**section 2.5.5**), while Dr Bazzone was performing the electrophysiology experiments, analysed the data and prepared the presented figures (**Figure 7.4**). Prof Edmund Kunji has now received a research grant for a 7-month usage of a SURFE^{2}R N1 instrument, so the work can continue at the MRC Mitochondrial Biology Unit.

In this technique, charge movements (e.g. transport of charged substrates) generate membrane potential in the set-up, which consists of a gold electrode coated with an alkane thiol and a phospholipid layer, where membranes (or liposomes) containing the protein of study are absorbed, creating small compartments. The built-up of a membrane potential can be measured as transient electrical currents (Bazzone and Barthmes, 2020). The polarity of the translocated charges and the direction of their transport determine the sign of the detected currents, while the kinetics of the currents depend on the protein activity. Peak amplitudes may be used for the analysis

of transport activity, whereas integration can be used to measure the total charge movement, if calibrated to a standard.

Initial experiments with the wild-type TtAac reproduced results of previous work obtained with the bovine and porcine AAC (Gropp *et al.*, 1999; Watzke et al., 2010). In proteoliposomes without internal substrate pre-steady state currents of ADP and ATP could be measured, which reflect the electrogenicity of the re-orientation of the substrate binding site plus the translocation of a single molecule of substrate by the population of the carriers (Bazzone et al., 2017). ADP generates a positive current, while ATP a negative current. When the proteoliposomes were loaded with substrate, currents of greater amplitude and longer duration could be detected (steady-state currents), with the sign determined by the nucleotide supplied externally (**Figure 7.4A**).

Experiments with some of the mutants gave some preliminary results, the interpretation of which requires further investigation. An interesting observation was made about mutant R287A, in which the ADP-generated current was reversed in direction, resembling the ATP-generated current (**Figure 7.4B**). Although tentative, this result may indicate that this residue is one of the three that reorient with the substrate to the other compartment. Further experiments need to follow, as well as experiments with other mutants to confirm this result. The aim of this project is to study the electrostatic properties of the substrate binding site, using the wild type and the generated variants. In principle, information about the movement of charged residues inside the protein or the shielding of charged residues upon substrate binding can be acquired from the pre-steady state currents (Bazzone *et al.*, 2017). Therefore, it should be possible to unravel the contributions each positively charged residue makes to the charge transfer in the transport cycle.

A

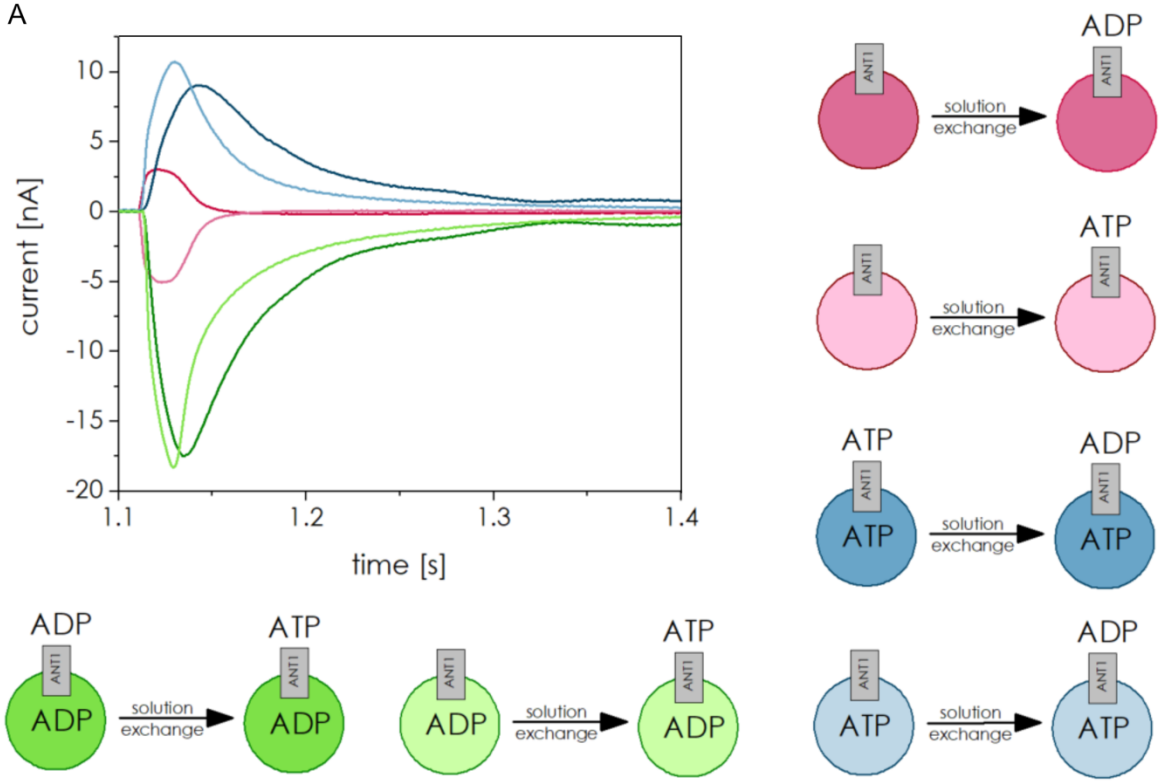

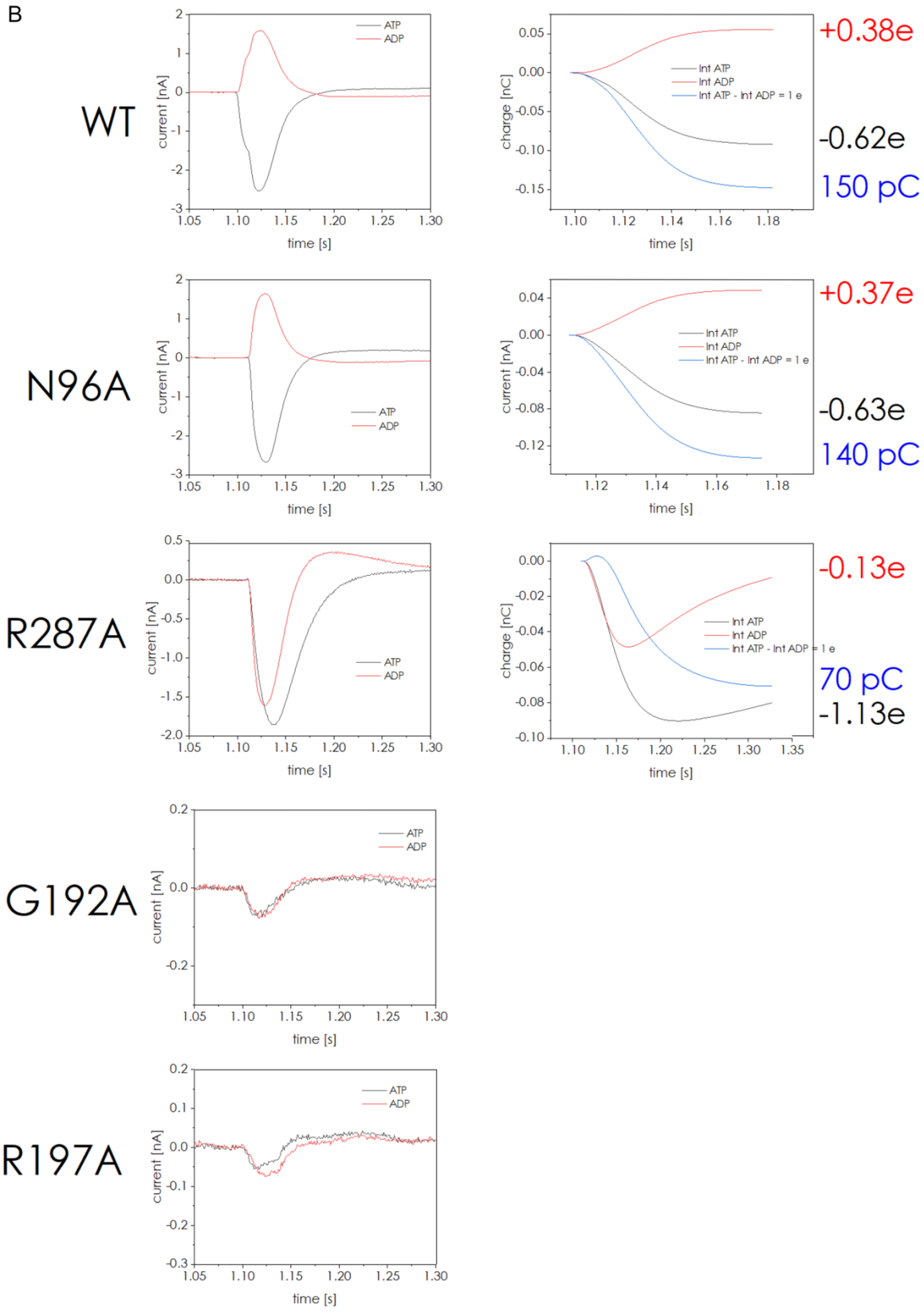

Figure 7.4: Studying the electrostatic properties of the substrate binding site with SSM- based electrophysiology. (A) AAC-dependent currents in proteoliposomes without internal substrate (pre-steady state currents), activating the transporter with nucleotides applied externally (dark and light pink for ADP and ATP

respectively, 500 μM concentration). In proteoliposomes loaded with substrates, two experiments were performed. In the first, a concentration jump simultaneously removed nucleotide 1 from the sensor and applied nucleotide 2, triggering heteroexchange reaction (dark blue and dark green for propteoliposomes loaded with ATP and ADP respectively). In the second, nucleotide 1 was first removed from the sensor and heteroexchange was triggered by subsequently adding nucleotide 2 to the sensor (light blue and light green for propteoliposomes loaded with ATP and ADP respectively). The data represent the average of six sensor read-outs for each condition. (B) Pre-steady state currents (left) detected in proteoliposomes not loaded with substrate, triggering transport with ADP (red trace) or ATP (black trace) and integration of their signal (right) until 1.3 seconds. Variants G192A and R197A were not functional. The data represents the average of five different sensor read-outs for each protein. Figures prepared by Dr Andre Bazzone.

7.3.3. Preliminary results with native mass spectrometry

Native mass spectrometry was tried in order to investigate whether nucleotides bound to the carrier could be detected in the mass spectra. This work was done in collaboration with Dr Shahid Mehmood (Francis Crick Institute, London, UK), but ended after limited number of experiments, as he left from the institute. My role in the collaboration was to purify the protein using the described protocol (**section 2.5.3**) and Dr Mehmood and Prof Kunji performed the mass spectrometry experiments and the former analysed the data and prepared the figure shown (**Figure 7.5**).

In this technique, a membrane protein, either reconstituted in membrane mimetics (e.g. bicelles, nanodiscs, liposomes or amphipols) or in detergent micelles can be introduced into the mass spectrometer via nano-electrospray ionisation. This ionisation process can preserve noncovalent interactions, because it requires less harsh conditions to evaporate the solvent and can be applied directly to aqueous solutions (no need for volatile organic solvents) (Mehmood et al., 2015). Briefly, a high electrical potential is applied on a capillary containing the solution to be studied, causing an accumulation of positive ions at the tip of the capillary, which subsequently promotes the evolution of charged droplets carrying the precursors of the charged gas-phase ions. The limited space the ions can occupy inside the droplets causes electrostatic repulsion, leading to droplet fission and ultimately yields the gas-phase ions. Evaporation of the solvent is hence critical, as it promotes the Coulombic repulsion between ions. The small droplet size should prevent non-specific interactions (Mehmood *et al.*, 2015). For membrane proteins, bound lipids or ligands appear as adduct peaks on protein peaks. The characteristic mass differences

between the protein and adduct peaks can identify the associated molecule (Bolla et al., 2019).

In the experiments presented here, bound cardiolipins were detected in the carrier, as well as ADP and ATP molecules (when added in 1 mM concentration). They were identified in the spectra as peaks shifted from the protein peak by the molecular mass of the molecule species. As a control, AMP, which is not transported by AAC, was tried in parallel, showing no association. This result showed that actual substrates can stay bound to part of the protein population under these experimental conditions. Therefore, in principle, the technique can be used to confirm potential substrates or to test the ability of mutant proteins to bind substrate. Successful application of the technique will depend on the affinity of the protein for the substrate. The preliminary results for wild-type TtAac were positive, hence it would be interesting to continue the work with the alanine replacement variants.

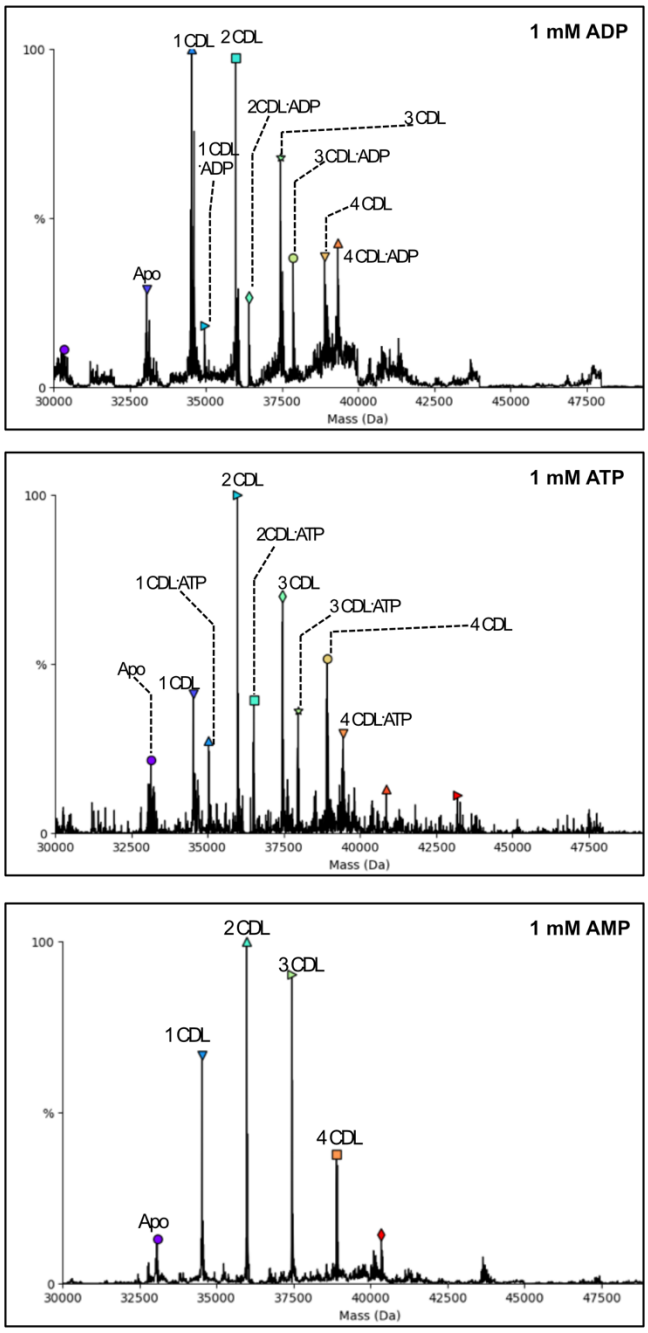

Figure 7.5: Substrates ADP and ATP are detected bound to the ADP/ATP carrier in native mass spectrometry. Mass spectra of purified TtAac in detergent solution supplemented with TOCL (**section 2.5.3**). AMP in the same conditions does not yield association peaks, confirming the results are substrate-specific. Cardiolipin molecules are also detected bound to the carrier. Figure prepared by Dr Shahid Mehmood.

7.3.4. Efforts towards obtaining affinity parameters

It was thought that being able to measure affinity parameters (e.g K_d values) for the wild-type TtAac and the relevant variants would provide more information about the involvement of specific residues in the binding process. From the CPM thermostability

measurements, it is difficult to extract this type of information, because the on and off rates of the reaction change as the temperature increases. Additionally, the unfolding of the protein population and the reaction with the CPM molecule are irreversible. Therefore, other techniques were considered, including microscale thermophoresis. In this technique, the thermophoresis pattern (directed movement of molecules induced by temperature gradients) of the studied protein at different concentrations of a ligand can provide information on the affinity (Wienken *et al.*, 2010). For these experiments, the protein needs to be labelled. There is a Monolith NT.115 instrument situated at the MRC Laboratory of Molecular Biology and Dr Chris Johnson kindly provided us with access shortly before the start of the Covid-19 pandemic. There was no time to obtain results with this approach, but some work was done on the preparation of the sample to make it suitable for histidine labelling. This work could continue in the future, or the obtained protocol can be used for other approaches that require histidine-labelled protein.

The construct of TtAac is ideal for histidine labelling, as the protein sequence contains no histidine residues (**Figure 2.2**). Lysine labelling, which is another way to introduce fluorescent labels, would make the interpretation of results more difficult, as many lysine residues are key for the mechanism and one is found in the proposed substrate binding site (K30). In order for the His tag to be preserved and used for labelling, the purification protocol needed to be modified, so that the protein could be eluted from the column without cleavage of the tag.

Some rounds of optimisation resulted in reasonably pure protein, that was folded and could respond to inhibitors CATR and BKA, as assessed by the CPM thermostability assay (**Figure 7.6A** and **7.6B**). The obtained protein was also tested for activity and shown to be fully active with initial rates (318 ± 13 nmol [^{33}P]-ATP mg AAC^{-1} min^{-1}) which could be fully inhibited by the two inhibitors (**Figure 7.6C**). The protocol required minor modifications compared to **section 2.5.3**, including addition of 40 mM imidazole during the binding step (batch binding), while it was removed from the solubilisation step. Additionally, purification Buffer A was supplemented with 50 mM imidazole. Finally, the protein was eluted from the column by addition of 400 mM imidazole and immediately exchanged (2 times) in a buffer containing no imidazole, using Zeba Spin Desalting Columns, 7K MWCO. In order to improve purity, the protein was passed through a Q ion exchange column, where most of contaminants bind (**Figure 7.6A**). Thus, this type of analysis can continue using this purification protocol.

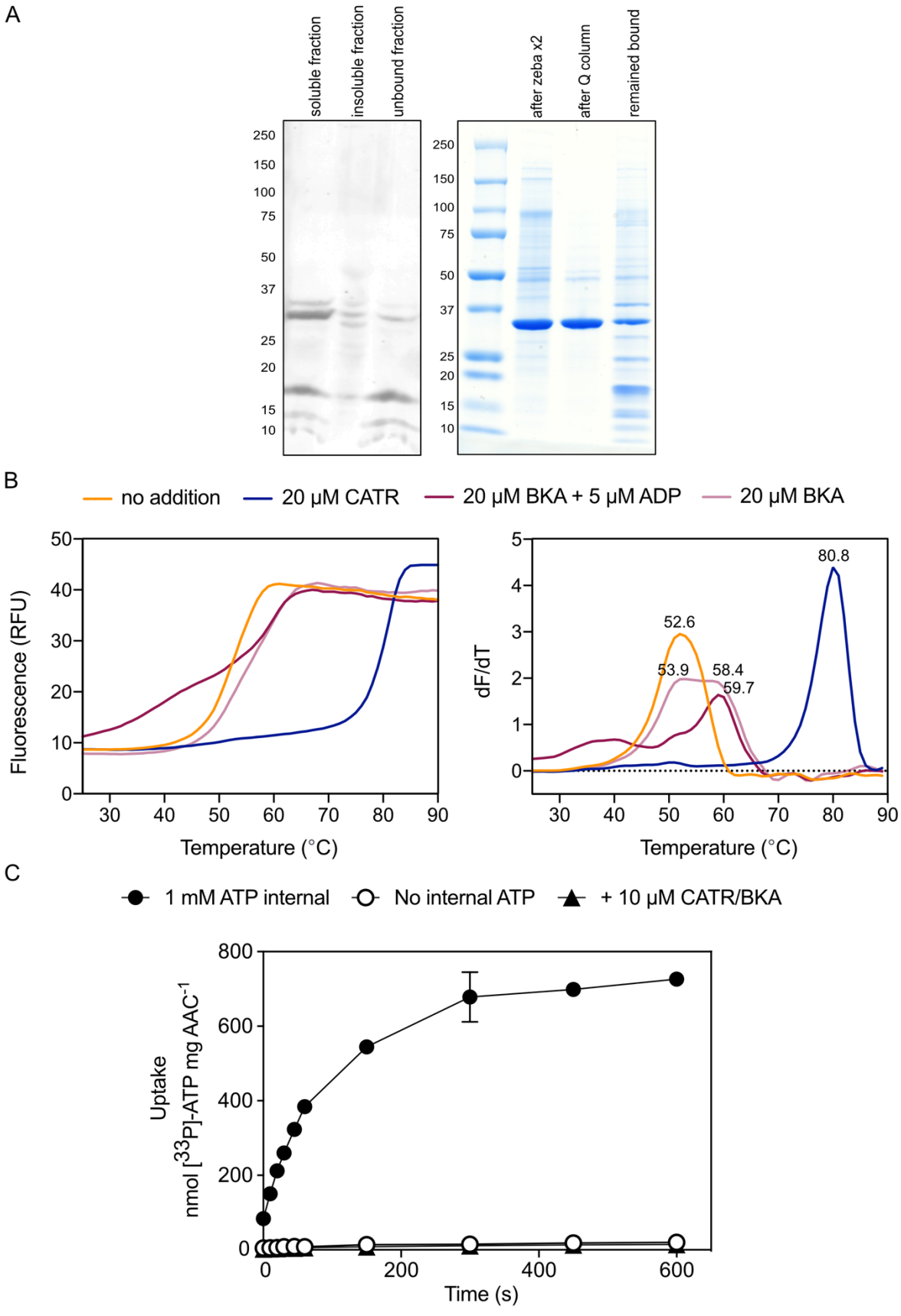
A
soluble fraction
insoluble fraction
unbound fraction
after zeba x2
after Q column
remained bound
250
150
100
75
50
37
25
20
15
10
B
no addition
20 µM CATR
20 µM BKA + 5 µM ADP
20 µM BKA
Fluorescence (RFU)
Temperature (°C)
dF/dT
80.8
52.6
53.9
58.4
59.7
C
1 mM ATP internal
No internal ATP
+ 10 µM CATR/BKA
Uptake
nmol [33P]-ATP mg AAC-1
Time (s)

Figure 7.6: Purification of wild-type TtAac by elution from the column with imidazole. (A) Western blot analysis was performed to detect His-tagged protein in the different steps of the purification procedure. 15 µL of each sample (volume of the original samples was made equal) were separated on a 4-20 % SDS-PAGE gel and transferred onto a PVDF membrane. TtAac was detected with an anti-His antibody (Abcam, rabbit, 1:5,000) and a fluorescent anti-rabbit secondary antibody (Li-COR, 1:20,000). The steps after elution were analysed by SDS-PAGE. 5 µL of each sample (volume of the original samples was made equal) were separated on a 4-20 % SDS-PAGE gel and the bands were visualized by Coomassie Blue stain. Molecular weight markers are indicated. (B) Typical thermal denaturation curves (left) and corresponding first derivatives (right) without addition of any effector and in the presence of the state-specific inhibitors CATR and BKA. Approximately 3 µg of protein were used in each condition and the assay was performed with three technical replicates. (C) Typical uptake curve of [^{33}P]-ATP into proteoliposomes loaded with 1 mM ATP (filled circles). Addition of 10 µM CATR/ BKA externally (filled triangles) or proteoliposomes with no internal substrate (empty circles) and were used as control. The data are represented by the mean and standard deviation of three technical replicates.

Elucidating the substrate binding mechanism of the ADP/ATP carrier has been a problem studied for many decades (Dalbon *et al.*, 1988; Dehez *et al.*, 2008; Dianoux *et al.*, 2000; Majima *et al.*, 1998; Mayinger *et al.*, 1989; Mifsud *et al.*, 2013; Robinson and Kunji, 2006; Robinson *et al.*, 2008; Tamura and Hayashi, 2017; Wang and Tajkhorshid, 2008; Yao *et al.*, 2021). The obtained information about substrate binding in this work, together with the rest of the knowledge about the transport mechanism, is an important advance in understanding the operation of this metabolically central and vital membrane protein. Moreover, the results may assist the studies of the other members of the SLC25 family, many of which are implicated in severe human diseases (Kunji *et al.*, 2020; Palmieri *et al.*, 2020) and about 15 still remain uncharacterised in humans (Kunji *et al.*, 2020). Finally, some preliminary results set the basis for measuring affinity parameters for the substrate and for investigating the electrostatics of the substrate binding process.

Appendices

Appendix 1

Appendix 1.1: Sequence of the ADP/ATP carrier gene from *Thermothelomyces thermophila*

> TtAac (ADP/ATP carrier from *Thermothelomyces thermophila*)

ATGGCTCATCATCACCATCACCATCATCATTCCGATAGAGCAATTGAAGGTAGGACAGCAAC
CTCAGAGAAAATTTTAGGAATGCCACCCTTCGTGGTGGATTTTCTTATGGGTGGTGTTTCTG
CAGCAGTTAGTAAAACAGCTGCTGCTCCAATTGAAAGAATTAAGTTGTTGGTACAAAACCAA
GATGAAATGATTAAGGCTGGTAGACTTGATAGGAGATACAATGGTATTATTGATTGTTTCAG
AAGAACTACAGCTGATGAGGGACTAATGGCCTTATGGAGAGGTAATACTGCCAACGTTATAA
GATATTTTCCAACCCAGGCATTGAACTTTGCTTTTAGAGATAAGTTTAAGGCCATGTTTGGC
TATAAGAAGGATAAAGATGGCTATGCCAAATGGATGGCAGGTAATCTAGCCAGCGGTGGTGC
AGCTGGTGCCACCTCGTTGTTGTTTGTATACAGCTTGGACTATGCAAGAACCAGATTGGCTA
ATGATGCAAAGAGTGCCAAAGGTGGAGGTGCAAGACAGTTTAATGGACTTATCGACGTTTAC
AGAAAGACATTGGCATCAGATGGCATAGCTGGTTTGTACAGAGGTTTCGGTCCATCCGTGGC
CGGTATTGTTGTTTACAGAGGTTTATATTTCGGTATGTATGACTCAATTAAGCCAGTCGTCC
TGGTTGGTCCCTTAGCAAATAACTTCTTGGCATCCTTTCTTTTAGGTTGGTGTGTTACTACC
GGTGCCGGTATTGCCTCCTATCCATTAGACACCGTGAGAAGAAGAATGATGATGACATCAGG
CGAGGCTGTAAAGTACAAGTCCTCGATCGATGCATTCAGACAAATTATTGCTAAAGAAGGCG
TTAAATCTTTGTTTAAGGGAGCTGGTGCTAATATCTTGAGAGGCGTTGCTGGTGCAGGTGTG
TTGTCCATATACGATCAATTGCAAATTCTACTATTCGGCAAATGA

Appendix 1.2: Oligonucleotides used in this thesis for cloning, mutagenesis and sequencing

Oligonucleotide	**Sequence 5′-3′**
Cloning primers	
TtAac no tag forward	CATGACATGTCTAAACAAGAAACTAAAATTTTAGGAATGCCACCC TTCGTG
TtAac no tag reverse	CTAGCTCGAGCTATCATTAACCAGATCCACCTTTAAAAGCTTTGC CGAATAGTAGAATTTGC
TtAac His tag factor Xa forward	GACTCATTGACAGTTGTAAAGCCATGGCTCATCATCACCATCACC AT
TtAac His tag factor Xa reverse	TCTAGACTCGAGTCTAGATCATTTGCCGAATAGTAGAATTTGCAA TTGATCG
Primers for site-directed mutagenesis	

S29A forward	GTGGTGTTTCTGCAGCAGTTGCTAAAACAGCTGCTGCTCCAAT
S29A reverse	ATTGGAGCAGCAGCTGTTTTAGCAACTGCTGCAGAAACACCAC
K30A forward	CTGCAGCAGTTAGTGCTACAGCTGC
K30A reverse	GCAGCTGTAGCACTAACTGCTGCAG
L41A forward	GCTGCTCCAATTGAAAGAATTAAGGCTTTGGTACAAAACCAAGATGAAATG
L41A reverse	CATTTCATCTTGGTTTTGTACCAAAGCCTTAATTCTTTCAATTGGAGCAGC
Q44A forward	AATTGAAAGAATTAAGTTGTTGGTAGCTAACCAAGATGAAATGATTAAGGCTG
Q44A reverse	CAGCCTTAATCATTTCATCTTGGTTAGCTACCAACAACTTAATTCTTTCAATT
N85A forward	TTATGGAGAGGTAATACTGCCGCTGTTATAAGATATTTTCCAACC
N85A reverse	GGTTGGAAAATATCTTATAACAGCGGCAGTATTACCTCTCCATAA
R88A forward	GCCAACGTTATAGCTTATTTTCCAACCCAG
R88A reverse	CTGGGTTGGAAAATAAGCTATAACGTTGGC
Y89A forward	ATACTGCCAACGTTATAAGAGCTTTTCCAACCCAGGCATTGAA
Y89A reverse	TTCAATGCCTGGGTTGGAAAAGCTCTTATAACGTTGGCAGTAT
T92A forward	CCAACGTTATAAGATATTTTCCAGCTCAGGCATTGAACTTTGCTTTTAG
T92A reverse	CTAAAAGCAAAGTTCAATGCCTGAGCTGGAAAATATCTTATAACGTTGG
Q93A forward	CGTTATAAGATATTTTCCAACCGCTGCATTGAACTTTGCTTTTAGAG
Q93A reverse	CTCTAAAAGCAAAGTTCAATGCAGCGGTTGGAAAATATCTTATAACG
N96A forward	GATATTTTCCAACCCAGGCATTGGCTTTTGCTTTTAGAGATAAGTTTAA
N96A reverse	TTAAACTTATCTCTAAAAGCAAAAGCCAATGCCTGGGTTGGAAAATATC
F97A forward	TTCCAACCCAGGCATTGAACGCTGCTTTTAGAGATAAGTTTAA
F97A reverse	TTAAACTTATCTCTAAAAGCAGCGTTCAATGCCTGGGTTGGAA
R100A forward	GAACTTTGCTTTTGCTGATAAGTTTAAGGC
R100A reverse	GCCTTAAACTTATCAGCAAAAGCAAAGTTC
N123A forward	ATGCCAAATGGATGGCAGGTGCTCTAGCCAGCGGTGGTGCAGC
N123A reverse	GCTGCACCACCGCTGGCTAGAGCACCTGCCATCCATTTGGCAT

S134A forward	GTGGTGCAGCTGGTGCCACCGCTTTGTTGTTTGTATACAGCTT
S134A reverse	AAGCTGTATACAAACAACAAAGCGGTGGCACCAGCTGCACCAC
L135A forward	GTGCAGCTGGTGCCACCTCGGCTTTGTTTGTATACAGCTTGGA
L135A reverse	TCCAAGCTGTATACAAACAAAGCCGAGGTGGCACCAGCTGCAC
V138A forward	GTGCCACCTCGTTGTTGTTTGCTTACAGCTTGGACTATGCAAG
V138A reverse	CTTGCATAGTCCAAGCTGTAAGCAAACAACAACGAGGTGGCAC
T146A forward	ACAGCTTGGACTATGCAAGAGCTAGATTGGCTAATGATGCAAA
T146A reverse	TTTGCATCATTAGCCAATCTAGCTCTTGCATAGTCCAAGCTGT
S189A forward	TGTACAGAGGTTTCGGTCCAGCTGTGGCCGGTATTGTTGTTTA
S189A reverse	TAAACAACAATACCGGCCACAGCTGGACCGAAACCTCTGTACA
G192A forward	GGTCCATCCGTGGCCGCTATTGTTGTTTACAGA
G192A reverse	TCTGTAAACAACAATAGCGGCCACGGATGGACC
I193A forward	CCATCCGTGGCCGGTGCTGTTGTTTACAGAGGT
I193A reverse	ACCTCTGTAAACAACAGCACCGGCCACGGATGG
Y196A forward	GCCGGTATTGTTGTTGCTAGAGGTTTATATTTC
Y196A reverse	GAAATATAAACCTCTAGCAACAACAATACCGGC
R197A forward	GGTATTGTTGTTTACGCTGGTTTATATTTCGGT
R197A reverse	ACCGAAATATAAACCAGCGTAAACAACAATACC
Y200A forward	GGTATTGTTGTTTACAGAGGTTTAGCTTTCGGTATGTATGACTCA ATTAAG
Y200A reverse	CTTAATTGAGTCATACATACCGAAAGCTAAACCTCTGTAAACAAC AATACC
Y204A forward	GAGGTTTATATTTCGGTATGGCTGACTCAATTAAGCCAGTCGT
Y204A reverse	ACGACTGGCTTAATTGAGTCAGCCATACCGAAATATAAACCTC
V230A forward	CCTTTCTTTTAGGTTGGTGTGCTACTACCGGTGCCGGTATTGC
V230A reverse	GCAATACCGGCACCGGTAGTAGCACACCAACCTAAAAGAAAGG
T231A forward	TTCTTTTAGGTTGGTGTGTTGCTACCGGTGCCGGTATTGCCTC
T231A reverse	GAGGCAATACCGGCACCGGTAGCAACACACCAACCTAAAAGAA

G235A forward	GGTGTGTTACTACCGGTGCCGCTATTGCCTCCTATCCATTAGA
G235A reverse	TCTAATGGATAGGAGGCAATAGCGGCACCGGTAGTAACACACC
S238A forward	GGTGCCGGTATTGCCGCTTATCCATTAGACACC
S238A reverse	GGTGTCTAATGGATAAGCGGCAATACCGGCACC
Y239A forward	CCGGTGCCGGTATTGCCTCCGCTCCATTAGACACCGTGAGAAG
Y239A reverse	CTTCTCACGGTGTCTAATGGAGCGGAGGCAATACCGGCACCGG
R246A forward	TTAGACACCGTGAGAGCTAGAATGATGATGACA
R246A reverse	TGTCATCATCATTCTAGCTCTCACGGTGTCTAA
N284A reverse	TCCCGGCTCGAGTCTAGATCATTTGCCGAATAGTAGAATTTGCAA TTGATCGTATATGGACAACACACCTGCACCAGCAACGCCTCTCAA GATAGCAGCACCAGCTCCCTTAA
R287A forward	GCTAATATCTTGGCTGGCGTTGCTGGTGCA
R287A reverse	TGCACCAGCAACGCCAGCCAAGATATTAGC
G288A reverse	TCCCGGCTCGAGTCTAGATCATTTGCCGAATAGTAGAATTTGCAA TTGATCGTATATGGACAACACACCTGCACCAGCAACAGCTCTCAA GATATTAGCAC
G291A reverse	TCCCGGCTCGAGTCTAGATCATTTGCCGAATAGTAGAATTTGCAA TTGATCGTATATGGACAACACACCTGCAGCAGCAACGCCTCTCAA GA
V294A reverse	TCCCGGCTCGAGTCTAGATCATTTGCCGAATAGTAGAATTTGCAA TTGATCGTATATGGACAAAGCACCTGCACCAGCAACGC
L295A reverse	TCCCGGCTCGAGTCTAGATCATTTGCCGAATAGTAGAATTTGCAA TTGATCGTATATGGAAGCCACACCTGCACCAGCAA
Primers for sequencing	
pPIC2 forward	GTTCTGTTATTGTTTTAATTCTA
pPIC2 reverse	ACGCGTAGAATCGAGACCGAGGA

Appendix 2: List of UniProt accession codes used for the ADP/ATP carrier multiple sequence alignment

#	Accession number	Entry name	Organism	Length
1	G2QNH0	ADT_MYCTT	*Thermothelomyces thermophila* (strain ATCC 42464 / BCRC 31852 / DSM 1799) (Sporotrichum thermophile)	315
2	P12235	ADT1_HUMAN	*Homo sapiens* (Human)	298
3	P05141	ADT2_HUMAN	*Homo sapiens* (Human)	298
4	P12236	ADT3_HUMAN	*Homo sapiens* (Human)	298
5	Q9H0C2	ADT4_HUMAN	*Homo sapiens* (Human)	315
6	P02722	ADT1_BOVIN	*Bos taurus* (Bovine)	298
7	Q8SQH5	ADT2_BOVIN	*Bos taurus* (Bovine)	298
8	P32007	ADT3_BOVIN	*Bos taurus* (Bovine)	298
9	Q2YDD9	ADT4_BOVIN	*Bos taurus* (Bovine)	323
10	P04710	ADT1_YEAST	*Saccharomyces cerevisiae* (strain ATCC 204508 / S288c) (Baker's yeast)	309
11	P18239	ADT2_YEAST	*Saccharomyces cerevisiae* (strain ATCC 204508 / S288c) (Baker's yeast)	318
12	P18238	ADT3_YEAST	*Saccharomyces cerevisiae* (strain ATCC 204508 / S288c) (Baker's yeast)	307
13	P48962	ADT1_MOUSE	*Mus musculus* (Mouse)	298
14	P51881	ADT2_MOUSE	*Mus musculus* (Mouse)	298
15	Q3V132	ADT4_MOUSE	*Mus musculus* (Mouse)	320
16	Q05962	ADT1_RAT	*Rattus norvegicus* (Rat)	298
17	Q09073	ADT2_RAT	*Rattus norvegicus* (Rat)	298
18	Q6P9Y4	Q6P9Y4_RAT	*Rattus norvegicus* (Rat)	298
19	Q6QRN9	ADT3_PIG	*Sus scrofa* (Pig)	298
20	O46373	ADT1_RABIT	*Oryctolagus cuniculus* (Rabbit)	298
21	Q4R8M0	ADT4_MACFA	*Macaca fascicularis* (Crab-eating macaque) (Cynomolgus monkey)	315
22	Q000K2	ADT2_TACAC	*Tachyglossus aculeatus aculeatus* (Southeast Australian short-beaked echidna)	298
23	P31167	ADT1_ARATH	*Arabidopsis thaliana* (Mouse-ear cress)	381
24	P40941	ADT2_ARATH	*Arabidopsis thaliana* (Mouse-ear cress)	385
25	O49447	ADT3_ARATH	*Arabidopsis thaliana* (Mouse-ear cress)	379
26	P04709	ADT1_MAIZE	*Zea mays* (Maize)	387
27	P12857	ADT2_MAIZE	*Zea mays* (Maize)	387
28	P02723	ADT_NEUCR	*Neurospora crassa* (strain ATCC 24698 / 74-OR23-1A / CBS 708.71 / DSM 1257 / FGSC 987)	313

29	Q09188	ADT_SCHPO	*Schizosaccharomyces pombe* (strain 972 / ATCC 24843) (Fission yeast)	322
30	Q27238	ADT1_ANOGA	*Anopheles gambiae* (African malaria mosquito)	301
31	P49382	ADT_KLULA	*Kluyveromyces lactis* (strain ATCC 8585 / CBS 2359 / DSM 70799 / NBRC 1267 / NRRL Y-1140 / WM37) (Yeast) (Candida sphaerica)	305
32	Q7PQV7	ADT2_ANOGA	*Anopheles gambiae* (African malaria mosquito)	300
33	P25083	ADT1_SOLTU	*Solanum tuberosum* (Potato)	386
34	Q41629	ADT1_WHEAT	*Triticum aestivum* (Wheat)	331
35	P27081	ADT2_SOLTU	*Solanum tuberosum* (Potato)	386
36	Q41630	ADT2_WHEAT	*Triticum aestivum* (Wheat)	331
37	O22342	ADT1_GOSHI	*Gossypium hirsutum* (Upland cotton) (*Gossypium mexicanum*)	386
38	P27080	ADT_CHLRE	*Chlamydomonas reinhardtii* (*Chlamydomonas smithii*)	308
39	Q5B5W6	Q5B5W6_EMENI	*Emericella nidulans* (strain FGSC A4 / ATCC 38163 / CBS 112.46 / NRRL 194 / M139) (*Aspergillus nidulans*)	311
40	J9VV25	J9VV25_CRYNH	*Cryptococcus neoformans* var. grubii serotype A (strain H99 / ATCC 208821 / CBS 10515 / FGSC 9487) (*Filobasidiella neoformans* var. grubii)	319
41	A4HY43	A4HY43_LEIIN	*Leishmania infantum*	317
42	O62526	O62526_DROME	*Drosophila melanogaster* (Fruit fly)	307
43	E6RF63	E6RF63_CRYGW	*Cryptococcus gattii* serotype B (strain WM276 / ATCC MYA-4071) (*Filobasidiella gattii*) (*Cryptococcus bacillisporus*)	319
44	E6RF62	E6RF62_CRYGW	*Cryptococcus gattii* serotype B (strain WM276 / ATCC MYA-4071) (*Filobasidiella gattii*) (*Cryptococcus bacillisporus*)	313
45	B6HCW6	B6HCW6_PENRW	*Penicillium rubens* (strain ATCC 28089 / DSM 1075 / NRRL 1951 / Wisconsin 54-1255) (*Penicillium chrysogenum*)	315
46	Q2UU95	Q2UU95_ASPOR	*Aspergillus oryzae* (strain ATCC 42149 / RIB 40) (Yellow koji mold)	312
47	Q5A516	Q5A516_CANAL	*Candida albicans* (strain SC5314 / ATCC MYA-2876) (Yeast)	301
48	Q4WJN2	Q4WJN2_ASPFU	*Neosartorya fumigata* (strain ATCC MYA-4609 / Af293 / CBS 101355 / FGSC A1100) (*Aspergillus fumigatus*)	308

49	H6BUP8	H6BUP8_EXODN	*Exophiala dermatitidis* (strain ATCC 34100 / CBS 525.76 / NIH/UT8656) (Black yeast) (*Wangiella dermatitidis*)	318
50	D3TNQ0	D3TNQ0_GLOMM	*Glossina morsitans morsitans* (Savannah tsetse fly)	300
51	Q5CW91	Q5CW91_CRYPI	*Cryptosporidium parvum* (strain Iowa II)	325
52	K9G2S1	K9G2S1_PEND1	*Penicillium digitatum* (strain Pd1 / CECT 20795) (Green mold)	314
53	K9FID0	K9FID0_PEND2	*Penicillium digitatum* (strain PHI26 / CECT 20796) (Green mold)	314
54	M9LUG4	M9LUG4_PSEA3	*Pseudozyma antarctica* (strain T-34) (Yeast) (*Candida antarctica*)	317
55	A1CRC7	A1CRC7_ASPCL	*Aspergillus clavatus* (strain ATCC 1007 / CBS 513.65 / DSM 816 / NCTC 3887 / NRRL 1 / QM 1276 / 107)	315
56	A1D489	A1D489_NEOFI	*Neosartorya fischeri* (strain ATCC 1020 / DSM 3700 / CBS 544.65 / FGSC A1164 / JCM 1740 / NRRL 181 / WB 181) (*Aspergillus fischerianus*)	319
57	A3LZD4	A3LZD4_PICST	*Scheffersomyces stipitis* (strain ATCC 58785 / CBS 6054 / NBRC 10063 / NRRL Y-11545) (Yeast) (*Pichia stipitis*)	300
58	J3KCU0	J3KCU0_COCIM	*Coccidioides immitis* (strain RS) (Valley fever fungus)	390
59	K7WP02	K7WP02_SOLTU	*Solanum tuberosum* (Potato)	387
60	A0A061IWT3	A0A061IWT3_TRYRA	*Trypanosoma rangeli* SC58	310
61	B0XP31	B0XP31_ASPFC	*Neosartorya fumigata* (strain CEA10 / CBS 144.89 / FGSC A1163) (*Aspergillus fumigatus*)	308
62	B8NRS8	B8NRS8_ASPFN	*Aspergillus flavus* (strain ATCC 200026 / FGSC A1120 / IAM 13836 / NRRL 3357 / JCM 12722 / SRRC 167)	312
63	V5F3N6	V5F3N6_KALBG	*Kalmanozyma brasiliensis* (strain GHG001) (Yeast) (*Pseudozyma brasiliensis*)	317
64	Q4DYK2	Q4DYK2_TRYCC	*Trypanosoma cruzi* (strain CL Brener)	314
65	Q4DD13	Q4DD13_TRYCC	*Trypanosoma cruzi* (strain CL Brener)	314
66	A5DQZ9	A5DQZ9_PICGU	*Meyerozyma guilliermondii* (strain ATCC 6260 / CBS 566 / DSM 6381 / JCM 1539 / NBRC 10279 / NRRL Y-324) (Yeast) (*Candida guilliermondii*)	299
67	A5E290	A5E290_LODEL	*Lodderomyces elongisporus* (strain ATCC 11503 / CBS 2605 / JCM 1781 / NBRC 1676 /	305

			NRRL YB-4239) (Yeast) (*Saccharomyces elongisporus*)	
68	G7IUC4	G7IUC4_MEDTR	*Medicago truncatula* (Barrel medic) (*Medicago tribuloides*)	362
69	G7J7N8	G7J7N8_MEDTR	*Medicago truncatula* (Barrel medic) (*Medicago tribuloides*)	326
70	G4MKR0	G4MKR0_MAGO7	*Magnaporthe oryzae* (strain 70-15 / ATCC MYA-4617 / FGSC 8958) (Rice blast fungus) (*Pyricularia oryzae*)	315
71	E3KWD3	E3KWD3_PUCGT	*Puccinia graminis* f. sp. *tritici* (strain CRL 75-36-700-3 / race SCCL) (Black stem rust fungus)	246
72	B4FSA7	B4FSA7_MAIZE	*Zea mays* (Maize)	380
73	Q4QDK0	Q4QDK0_LEIMA	*Leishmania major*	317
74	K2NR29	K2NR29_TRYCR	*Trypanosoma cruzi marinkellei*	314
75	Q8J0M1	Q8J0M1_YARLL	*Yarrowia lipolytica* (*Candida lipolytica*)	312
76	E9BE16	E9BE16_LEIDB	*Leishmania donovani* (strain BPK282A1)	317
77	B6Q6K3	B6Q6K3_TALMQ	*Talaromyces marneffei* (strain ATCC 18224 / CBS 334.59 / QM 7333) (*Penicillium marneffei*)	267
78	B6Q6K2	B6Q6K2_TALMQ	*Talaromyces marneffei* (strain ATCC 18224 / CBS 334.59 / QM 7333) (*Penicillium marneffei*)	315
79	B8M5Y9	B8M5Y9_TALSN	*Talaromyces stipitatus* (strain ATCC 10500 / CBS 375.48 / QM 6759 / NRRL 1006) (*Penicillium stipitatum*)	315
80	C6ZQT4	C6ZQT4_OCHTR	*Ochlerotatus triseriatus* (Eastern treehole mosquito) (*Aedes triseriatus*)	274
81	B5M0S7	B5M0S7_SIMVI	*Simulium vittatum* (Striped black fly)	249
82	D1FQF0	D1FQF0_9DIPT	*Simulium nigrimanum*	249
83	L8GVJ4	L8GVJ4_ACACA	*Acanthamoeba castellanii* str. Neff	331
84	E9CZR7	E9CZR7_COCPS	*Coccidioides posadasii* (strain RMSCC 757 / Silveira) (Valley fever fungus)	319
85	M7YQE1	M7YQE1_TRIUA	*Triticum urartu* (Red wild einkorn) (*Crithodium urartu*)	378
86	R7W2R7	R7W2R7_AEGTA	*Aegilops tauschii* (Tausch's goatgrass) (*Aegilops squarrosa*)	378
87	F1L6K2	F1L6K2_ASCSU	*Ascaris suum* (Pig roundworm) (*Ascaris lumbricoides*)	320
88	D7FW17	D7FW17_ECTSI	*Ectocarpus siliculosus* (Brown alga) (*Conferva siliculosa*)	313
89	O74260	O74260_CANPA	*Candida parapsilosis* (Yeast)	303
90	B2W2V5	B2W2V5_PYRTR	*Pyrenophora tritici-repentis* (strain Pt-1C-BFP) (Wheat tan spot fungus) (*Drechslera tritici-repentis*)	313

91	G2XBK3	G2XBK3_VERDV	*Verticillium dahliae* (strain VdLs.17 / ATCC MYA-4575 / FGSC 10137) (*Verticillium wilt*)	310
92	C5FDW0	C5FDW0_ARTOC	*Arthroderma otae* (strain ATCC MYA-4605 / CBS 113480) (*Microsporum canis*)	311
93	F2SFR9	F2SFR9_TRIRC	*Trichophyton rubrum* (strain ATCC MYA-4607 / CBS 118892) (Athlete's foot fungus)	312
94	H8X895	H8X895_CANO9	*Candida orthopsilosis* (strain 90-125) (Yeast)	303
95	F8MR87	F8MR87_NEUT8	*Neurospora tetrasperma* (strain FGSC 2508 / ATCC MYA-4615 / P0657)	313
96	T5A9S2	T5A9S2_OPHSC	*Ophiocordyceps sinensis* (strain Co18 / CGMCC 3.14243) (*Yarsagumba caterpillar* fungus) (*Hirsutella sinensis*)	313
97	G7X943	G7X943_ASPKW	*Aspergillus kawachii* (strain NBRC 4308) (White koji mold) (*Aspergillus awamori* var. *kawachi*)	319
98	G0S1Y8	G0S1Y8_CHATD	*Chaetomium thermophilum* (strain DSM 1495 / CBS 144.50 / IMI 039719)	315
99	U1GH21	U1GH21_ENDPU	*Endocarpon pusillum* (strain Z07020 / HMAS-L-300199) (Lichen-forming fungus)	316
100	J5JFV8	J5JFV8_BEAB2	*Beauveria bassiana* (strain ARSEF 2860) (White muscardine disease fungus) (*Tritirachium shiotae*)	314
101	G4UV77	G4UV77_NEUT9	*Neurospora tetrasperma* (strain FGSC 2509 / P0656)	313
102	E9E196	E9E196_METAQ	*Metarhizium acridum* (strain CQMa 102)	315
103	C9SLB6	C9SLB6_VERA1	*Verticillium alfalfae* (strain VaMs.102 / ATCC MYA-4576 / FGSC 10136) (*Verticillium wilt* of alfalfa) (*Verticillium albo-atrum*)	310
104	G3ANG4	G3ANG4_SPAPN	*Spathaspora passalidarum* (strain NRRL Y-27907 / 11-Y1)	300
105	G3J303	G3J303_CORMM	*Cordyceps militaris* (strain CM01) (*Caterpillar fungus*)	317
106	R9ARV1	R9ARV1_WALI9	*Wallemia ichthyophaga* (strain EXF-994 / CBS 113033)	312
107	E1ZZX0	E1ZZX0_CAMFO	*Camponotus floridanus* (Florida carpenter ant)	300
108	E2AAQ2	E2AAQ2_CAMFO	*Camponotus floridanus* (Florida carpenter ant)	305
109	E2BR21	E2BR21_HARSA	*Harpegnathos saltator* (Jerdon's jumping ant)	300
110	C4JK52	C4JK52_UNCRE	*Uncinocarpus reesii* (strain UAMH 1704)	269

111	E5QYH3	E5QYH3_ARTGP	*Arthroderma gypseum* (strain ATCC MYA-4604 / CBS 118893) (*Microsporum gypseum*)	312
112	C1HCX9	C1HCX9_PARBA	*Paracoccidioides lutzii* (strain ATCC MYA-826 / Pb01) (*Paracoccidioides brasiliensis*)	309
113	I1BRC7	I1BRC7_RHIO9	*Rhizopus delemar* (strain RA 99-880 / ATCC MYA-4621 / FGSC 9543 / NRRL 43880) (Mucormycosis agent) (*Rhizopus arrhizus* var. *delemar*)	304
114	K0K8A9	K0K8A9_WICCF	*Wickerhamomyces ciferrii* (strain ATCC 14091 / BCRC 22168 / CBS 111 / JCM 3599 / NBRC 0793 / NRRL Y-1031 F-60-10) (Yeast) (*Pichia ciferrii*)	318
115	K0KJF6	K0KJF6_WICCF	*Wickerhamomyces ciferrii* (strain ATCC 14091 / BCRC 22168 / CBS 111 / JCM 3599 / NBRC 0793 / NRRL Y-1031 F-60-10) (Yeast) (*Pichia ciferrii*)	305
116	C5MGR4	C5MGR4_CANTT	*Candida tropicalis* (strain ATCC MYA-3404 / T1) (Yeast)	308
117	C1G3C4	C1G3C4_PARBD	*Paracoccidioides brasiliensis* (strain Pb18)	309
118	C0S685	C0S685_PARBP	*Paracoccidioides brasiliensis* (strain Pb03)	309
119	W1Q6U7	W1Q6U7_OGAPD	*Ogataea parapolymorpha* (strain ATCC 26012 / BCRC 20466 / JCM 22074 / NRRL Y-7560 / DL-1) (Yeast) (*Hansenula polymorpha*)	301
120	F2PKM3	F2PKM3_TRIEC	*Trichophyton equinum* (strain ATCC MYA-4606 / CBS 127.97) (Horse ringworm fungus)	312
121	L8WTQ0	L8WTQ0_THACA	*Thanatephorus cucumeris* (strain AG1-IA) (Rice sheath blight fungus) (*Rhizoctonia solani*)	303
122	C4YQV6	C4YQV6_CANAW	*Candida albicans* (strain WO-1) (Yeast)	301
123	A0A067QTT0	A0A067QTT0_ZOONE	*Zootermopsis nevadensis* (*Dampwood termite*)	300
124	F4WTW2	F4WTW2_ACREC	*Acromyrmex echinatior* (Panamanian leafcutter ant) (*Acromyrmex octospinosus echinatior*)	300
125	X8IVT8	X8IVT8_9AGAM	*Rhizoctonia solani* AG-3 Rhs1AP	314
126	H1UY15	H1UY15_COLHI	*Colletotrichum higginsianum* (strain IMI 349063) (Crucifer anthracnose fungus)	315
127	Q0CT97	Q0CT97_ASPTN	*Aspergillus terreus* (strain NIH 2624 / FGSC A1156)	315
128	W7ME05	W7ME05_GIBM7	*Gibberella moniliformis* (strain M3125 / FGSC 7600) (Maize ear	311

			and stalk rot fungus) (*Fusarium verticillioides*)	

Appendix 3: Statistical tests performed in the analysis

One sample t-test

	S29A	K30A	L41A	Q44A	N85A	R88A	Y89A	T92A	Q93A	N96A	F97A	R100A
Theoretical mean	100	100	100	100	100	100	100	100	100	100	100	100
Actual mean	84.73	-1.925	-0.825	-0.125	42.4	-0.05	36.2	26.48	67.93	17.55	2.55	68.65
Number of values	4	4	4	4	4	4	4	4	4	4	4	4
One sample t test												
t, df	t=1.459, df=3	t=486.1, df=3	t=106.7, df=3	t=87.07, df=3	t=4.959, df=3	t=234.2, df=3	t=6.747, df=3	t=10.31, df=3	t=3.697, df=3	t=16.87, df=3	t=88.81, df=3	t=4.578, df=3
P value (two tailed)	0.2408	<0.0001	<0.0001	<0.0001	0.0157	<0.0001	0.0067	0.0019	0.0344	0.0005	<0.0001	0.0196
P value summary	ns	****	****	****	*	****	**	**	*	***	****	*
Significant (alpha=0.05)?	No	Yes	Yes	Yes	Yes	Yes	Yes	Yes	Yes	Yes	Yes	Yes
How big is the discrepancy?												
Discrepancy	-15.28	-101.9	-100.8	-100.1	-57.6	-100.1	-63.8	-73.53	-32.08	-82.45	-97.45	-31.35
SD of discrepancy	20.95	0.4193	1.889	2.3	23.23	0.8544	18.91	14.26	17.35	9.773	2.195	13.7
SEM of discrepancy	10.47	0.2097	0.9446	1.15	11.62	0.4272	9.457	7.128	8.677	4.886	1.097	6.848
95% confidence interval	-48.60 to 18.05	-102.6 to -101.3	-103.8 to -97.82	-103.8 to -96.47	-94.57 to -20.63	-101.4 to -98.69	-93.90 to -33.70	-96.21 to -50.84	-59.69 to -4.461	-98.00 to -66.90	-100.9 to -93.96	-53.14 to -9.557
R squared (partial eta squared)	0.4149	1	0.9997	0.9996	0.8913	0.9999	0.9382	0.9726	0.82	0.9896	0.9996	0.8748

	N123A	S134A	L135A	V138A	T146A	S189A	G192A	I193A	Y196A	R197A	Y200A	Y204A
Theoretical mean	100	100	100	100	100	100	100	100	100	100	100	100
Actual mean	50.15	64.78	1.2	52.45	-1	0.25	-0.65	0.5	0	0.25	75.78	0.275
Number of values	4	4	4	4	2	4	4	4	4	4	4	4
One sample t test												
t, df	t=10.85, df=3	t=7.979, df=3	t=83.65, df=3	t=7.015, df=3	t=91.82, df=1	t=291.0, df=3	t=148.8, df=3	t=148.1, df=3	t=414.0, df=3	t=147.7, df=3	t=7.016, df=3	t=96.53, df=3
P value (two tailed)	0.0017	0.0041	<0.0001	0.006	0.0069	<0.0001	<0.0001	<0.0001	<0.0001	<0.0001	0.0059	<0.0001
P value summary	**	**	****	**	**	****	****	****	****	****	**	****
Significant (alpha=0.05)?	Yes	Yes	Yes	Yes	Yes	Yes	Yes	Yes	Yes	Yes	Yes	Yes
How big is the discrepancy?												
Discrepancy												
SD of discrepancy	-49.85	-35.23	-98.8	-47.55	-101	-99.75	-100.7	-99.5	-100	-99.75	-24.23	-99.73
SEM of discrepancy	9.19	8.829	2.362	13.56	1.556	0.6856	1.353	1.344	0.483	1.35	6.906	2.066
95% confidence interval	4.595	4.415	1.181	6.779	1.1	0.3428	0.6764	0.6721	0.2415	0.6752	3.453	1.033
R squared (partial eta squared)	-64.47 to -35.23	-49.27 to -21.18	-102.6 to -95.04	-69.12 to -25.98	-115.0 to -87.02	-100.8 to -98.66	-102.8 to -98.50	-101.6 to -97.36	-100.8 to -99.23	-101.9 to -97.60	-35.21 to -13.24	-103.0 to -96.44
	0.9751	0.955	0.9996	0.9425	0.9999	1	0.9999	0.9999	1	0.9999	0.9426	0.9997

	V230A	T231A	G235A	S238A	Y239A	R246A	N284A	R287A	G288A	G291A	V294A	L295A
Theoretical mean	100	100	100	100	100	100	100	100	100	100	100	100
Actual mean	82.1	24.45	1.275	46.53	-0.225	-0.925	-0.9	-0.375	58.6	102.5	83.58	0.4
Number of values	4	4	4	4	4	4	4	4	4	4	4	4
One sample t test												
t, df	t=1.927, df=3	t=12.35, df=3	t=205.6, df=3	t=5.045, df=3	t=98.41, df=3	t=98.23, df=3	t=137.7, df=3	t=152.7, df=3	t=3.150, df=3	t=0.4698, df=3	t=2.431, df=3	t=120.8, df=3
P value (two tailed)	0.1496	0.0011	<0.0001	0.015	<0.0001	<0.0001	<0.0001	<0.0001	0.0513	0.6705	0.0932	<0.0001
P value summary	ns	**	****	*	****	****	****	****	ns	ns	ns	****
Significant (alpha=0.05)?	No	Yes	Yes	Yes	Yes	Yes	Yes	Yes	No	No	No	Yes
How big is the discrepancy?												
Discrepancy												
SD of discrepancy	-17.9	-75.55	-98.73	-53.48	-100.2	-100.9	-100.9	-100.4	-41.4	2.475	-16.43	-99.6
SEM of discrepancy	18.58	12.23	0.9605	21.2	2.037	2.055	1.465	1.315	26.29	10.54	13.51	1.649
95% confidence interval	9.289 to 11.66	6.116 to -56.09	0.4802 to -97.20	10.6 to -19.74	1.018 to -96.98	1.027 to -97.66	0.7326 to -98.57	0.6575 to -98.28	13.14 to 0.4277	5.268 to 19.24	6.756 to 5.075	0.8246 to -96.98
R squared (partial eta squared)	-47.46 to 0.5531	-95.01 to -0.9807	-100.3 to -0.9999	-87.21 to -0.8945	-103.5 to -0.9997	-104.2 to -0.9997	-103.2 to -0.9998	-102.5 to -0.9999	-83.23 to -0.7678	-14.29 to -0.06854	-37.92 to -0.6633	-102.2 to -0.9998

Two-way ANOVA tests

Table Analyzed	**ADP_ATP_10mM_2wayANOVA**				
Two-way ANOVA	Ordinary				
Alpha	0.01				
Source of Variation	% of total variation	P value	Significant?		
Interaction	1.72	0.7752	No		
substrate	0.2893	0.0436	No		
mutation	85.49	<0.0001	Yes		
ANOVA table	SS (Type III)	DF	MS	F (DFn, DFd)	P value
Interaction	75.44	31	2.433	F (31, 178) = 0.7922	P=0.7752
substrate	12.68	1	12.68	F (1, 178) = 4.129	P=0.0436
mutation	3748	31	120.9	F (31, 178) = 39.36	P<0.0001
Residual	546.8	178	3.072		
Difference between row means					
Predicted (LS) mean of ŒîTm 10 mM ADP	4.19				
Predicted (LS) mean of ŒîTm 10 mM ATP	3.715				
Difference between predicted means	0.4748				
SE of difference	0.2337				
Data summary					
Number of columns (mutation)	32				
Number of rows (substrate)	2				
Number of values	242				

Within each row, compare columns (simple effects within rows)

Number of families: 2

Number of comparisons per family: 31

Alpha 0.01

Dunnett's multiple comparisons test	ΔTm 10 mM ADP				ΔTm 10 mM ATP			
	Prd (LS) mean diff.	99.00% CI of diff.	Below threshold?	Adjusted P Value	Prd (LS) mean diff.	99.00% CI of diff.	Below threshold?	Adjusted P Value
wt vs. S29A	-2.921	-7.244 to 1.402	No	0.2842	-3	-7.323 to 1.323	No	0.2461
wt vs. K30A	10.91	7.272 to 14.55	Yes	<0.0001	10.8	7.160 to 14.44	Yes	<0.0001
wt vs. N85A	5.141	1.836 to 8.446	Yes	<0.0001	7.486	4.181 to 10.79	Yes	<0.0001
wt vs. R88A	8.463	4.552 to 12.37	Yes	<0.0001	8.9	4.990 to 12.81	Yes	<0.0001
wt vs. Y89A	-5.954	-10.28 to -1.631	Yes	<0.0001	-3.5	-7.823 to 0.8229	No	0.0868
wt vs. T92A	1.513	-2.810 to 5.835	No	0.9922	1.733	-2.590 to 6.056	No	0.964
wt vs. Q93A	1.713	-2.198 to 5.623	No	0.9154	1.925	-1.985 to 5.835	No	0.7978
wt vs. N96A	4.473	0.8323 to 8.113	Yes	0.0004	5.74	2.100 to 9.380	Yes	<0.0001
wt vs. F97A	-3.387	-7.710 to 0.9354	No	0.1119	-3.933	-8.256 to 0.3895	No	0.0296
wt vs. R100A	0.4458	-3.877 to 4.769	No	0.9996	1.533	-2.790 to 5.856	No	0.9859
wt vs. N123A	2.363	-1.278 to 6.003	No	0.3462	3.39	-0.2502 to 7.030	No	0.0231
wt vs. S134A	3.546	-0.7770 to 7.869	No	0.078	4.067	-0.2562 to 8.390	No	0.0207
wt vs. L135A	9.079	4.756 to 13.40	Yes	<0.0001	8.233	3.910 to 12.56	Yes	<0.0001
wt vs. V138A	5.813	1.902 to 9.723	Yes	<0.0001	7.125	3.215 to 11.04	Yes	<0.0001
wt vs. S189A	1.913	-2.410 to 6.235	No	0.9079	2.4	-1.923 to 6.723	No	0.614
wt vs. G192A	6.013	1.690 to 10.34	Yes	<0.0001	6.667	2.344 to 10.99	Yes	<0.0001
wt vs. I193A	2.293	-1.348 to 5.933	No	0.3953	2.9	-0.7402 to 6.540	No	0.0986
wt vs. Y196A	4.463	0.5523 to 8.373	Yes	0.0015	4.825	0.9148 to 8.735	Yes	0.0004
wt vs. R197A	7.713	3.390 to 12.04	Yes	<0.0001	8.367	4.044 to 12.69	Yes	<0.0001
wt vs. Y200A	1.346	-2.977 to 5.669	No	0.9939	1.767	-2.556 to 6.090	No	0.9556
wt vs. Y204A	-0.7542	-5.077 to 3.569	No	0.9993	-0.8333	-5.156 to 3.490	No	0.9992

wt vs. V230A	-1.154	-5.477 to 3.169	No	0.9987	-0.4667	-4.790 to 3.856	No	0.9996
wt vs. T231A	1.846	-2.477 to 6.169	No	0.9325	-0.8333	-5.156 to 3.490	No	0.9992
wt vs. G235A	1.579	-2.744 to 5.902	No	0.9845	4.2	-0.1229 to 8.523	No	0.0143
wt vs. S238A	-0.2208	-4.544 to 4.102	No	0.9998	1.367	-2.956 to 5.690	No	0.9937
wt vs. R246A	8.838	4.927 to 12.75	Yes	<0.0001	8.25	4.340 to 12.16	Yes	<0.0001
wt vs. R287A	11.01	7.102 to 14.92	Yes	<0.0001	11.43	7.515 to 15.34	Yes	<0.0001
wt vs. G288A	0.5458	-3.777 to 4.869	No	0.9995	1.767	-2.556 to 6.090	No	0.9556
wt vs. G291A	1.846	-2.477 to 6.169	No	0.9325	2.767	-1.556 to 7.090	No	0.3687
wt vs. V294A	5.713	2.072 to 9.353	Yes	<0.0001	3.46	-0.1802 to 7.100	No	0.0184
wt vs. L295A	-0.6542	-4.977 to 3.669	No	0.9994	-0.2	-4.523 to 4.123	No	0.9999

	ΔTm 10 mM ADP								ΔTm 10 mM ATP							
Test details	Prd (LS) mean 1	Prd (LS) mean 2	Prd (LS) mean diff.	SE of diff.	N1	N2	q	DF	Prd (LS) mean 1	Prd (LS) mean 2	Prd (LS) mean diff.	SE of diff.	N1	N2	q	DF
wt vs. S29A	7.113	10.03	-2.921	1.187	8	3	2.462	178	7.1	10.1	-3	1.187	8	3	2.528	178
wt vs. K30A	7.113	-3.8	10.91	0.9992	8	5	10.92	178	7.1	-3.7	10.8	0.9992	8	5	10.81	178
wt vs. N85A	7.113	1.971	5.141	0.9071	8	7	5.668	178	7.1	-0.3857	7.486	0.9071	8	7	8.252	178
wt vs. R88A	7.113	-1.35	8.463	1.073	8	4	7.885	178	7.1	-1.8	8.9	1.073	8	4	8.292	178
wt vs. Y89A	7.113	13.07	-5.954	1.187	8	3	5.018	178	7.1	10.6	-3.5	1.187	8	3	2.95	178
wt vs. T92A	7.113	5.6	1.513	1.187	8	3	1.275	178	7.1	5.367	1.733	1.187	8	3	1.461	178
wt vs. Q93A	7.113	5.4	1.713	1.073	8	4	1.596	178	7.1	5.175	1.925	1.073	8	4	1.794	178
wt vs. N96A	7.113	2.64	4.473	0.9992	8	5	4.476	178	7.1	1.36	5.74	0.9992	8	5	5.745	178
wt vs. F97A	7.113	10.5	-3.387	1.187	8	3	2.855	178	7.1	11.03	-3.933	1.187	8	3	3.315	178
wt vs. R100A	7.113	6.667	0.4458	1.187	8	3	0.3757	178	7.1	5.567	1.533	1.187	8	3	1.292	178
wt vs. N123A	7.113	4.75	2.363	0.9992	8	5	2.364	178	7.1	3.71	3.39	0.9992	8	5	3.393	178
wt vs. S134A	7.113	3.567	3.546	1.187	8	3	2.988	178	7.1	3.033	4.067	1.187	8	3	3.427	178
wt vs. L135A	7.113	-1.967	9.079	1.187	8	3	7.652	178	7.1	-1.133	8.233	1.187	8	3	6.939	178
wt vs. V138A	7.113	1.3	5.813	1.073	8	4	5.416	178	7.1	-0.025	7.125	1.073	8	4	6.638	178

wt vs. S189A	7.113	5.2	1.913	1.187	8	3	1.612	178	7.1	4.7	2.4	1.187	8	3	2.023	178
wt vs. G192A	7.113	1.1	6.013	1.187	8	3	5.067	178	7.1	0.4333	6.667	1.187	8	3	5.618	178
wt vs. I193A	7.113	4.82	2.293	0.9992	8	5	2.294	178	7.1	4.2	2.9	0.9992	8	5	2.902	178
wt vs. Y196A	7.113	2.65	4.463	1.073	8	4	4.158	178	7.1	2.275	4.825	1.073	8	4	4.495	178
wt vs. R197A	7.113	-0.6	7.713	1.187	8	3	6.5	178	7.1	-1.267	8.367	1.187	8	3	7.051	178
wt vs. Y200A	7.113	5.767	1.346	1.187	8	3	1.134	178	7.1	5.333	1.767	1.187	8	3	1.489	178
wt vs. Y204A	7.113	7.867	-0.7542	1.187	8	3	0.6356	178	7.1	7.933	-0.8333	1.187	8	3	0.7023	178
wt vs. V230A	7.113	8.267	-1.154	1.187	8	3	0.9727	178	7.1	7.567	-0.4667	1.187	8	3	0.3933	178
wt vs. T231A	7.113	5.267	1.846	1.187	8	3	1.556	178	7.1	7.933	-0.8333	1.187	8	3	0.7023	178
wt vs. G235A	7.113	5.533	1.579	1.187	8	3	1.331	178	7.1	2.9	4.2	1.187	8	3	3.54	178
wt vs. S238A	7.113	7.333	-0.2208	1.187	8	3	0.1861	178	7.1	5.733	1.367	1.187	8	3	1.152	178
wt vs. R246A	7.113	-1.725	8.838	1.073	8	4	8.234	178	7.1	-1.15	8.25	1.073	8	4	7.687	178
wt vs. R287A	7.113	-3.9	11.01	1.073	8	4	10.26	178	7.1	-4.325	11.43	1.073	8	4	10.64	178
wt vs. G288A	7.113	6.567	0.5458	1.187	8	3	0.46	178	7.1	5.333	1.767	1.187	8	3	1.489	178
wt vs. G291A	7.113	5.267	1.846	1.187	8	3	1.556	178	7.1	4.333	2.767	1.187	8	3	2.332	178
wt vs. V294A	7.113	1.4	5.713	0.9992	8	5	5.717	178	7.1	3.64	3.46	0.9992	8	5	3.463	178
wt vs. L295A	7.113	7.767	-0.6542	1.187	8	3	0.5513	178	7.1	7.3	-0.2	1.187	8	3	0.1686	178

Compare each cell mean with the other cell mean in that column

Number of families: 1

Number of comparisons per family: 32

Alpha 0.01

ΔTm 10 mM ADP - ΔTm 10 mM ATP

Sidak's multiple comparisons test	Prd (LS) mean diff.	99.00% CI of diff.	Below threshold?	Adjusted P Value	Prd (LS) mean 1	Prd (LS) mean 2	Prd (LS) mean diff.	SE of diff.	N1	N2	t	DF
wild type	0.0125	-3.208 to 3.233	No	>0.9999	7.113	7.1	0.0125	0.8763	8	8	0.01426	178
S29A	-0.06667	-5.327 to 5.193	No	>0.9999	10.03	10.1	-0.06667	1.431	3	3	0.04659	178
K30A	-0.1	-4.174 to 3.974	No	>0.9999	-3.8	-3.7	-0.1	1.108	5	5	0.09021	178
N85A	2.357	-1.086 to 5.801	No	0.3368	1.971	-0.3857	2.357	0.9369	7	7	2.516	178
R88A	0.45	-4.105 to 5.005	No	>0.9999	-1.35	-1.8	0.45	1.239	4	4	0.3631	178
Y89A	2.467	-2.793 to 7.727	No	0.9447	13.07	10.6	2.467	1.431	3	3	1.724	178
T92A	0.2333	-5.027 to 5.493	No	>0.9999	5.6	5.367	0.2333	1.431	3	3	0.163	178
Q93A	0.225	-4.330 to 4.780	No	>0.9999	5.4	5.175	0.225	1.239	4	4	0.1815	178
N96A	1.28	-2.794 to 5.354	No	0.9999	2.64	1.36	1.28	1.108	5	5	1.155	178
F97A	-0.5333	-5.793 to 4.727	No	>0.9999	10.5	11.03	-0.5333	1.431	3	3	0.3727	178
R100A	1.1	-4.160 to 6.360	No	>0.9999	6.667	5.567	1.1	1.431	3	3	0.7687	178
N123A	1.04	-3.034 to 5.114	No	>0.9999	4.75	3.71	1.04	1.108	5	5	0.9382	178
S134A	0.5333	-4.727 to 5.793	No	>0.9999	3.567	3.033	0.5333	1.431	3	3	0.3727	178
L135A	-0.8333	-6.093 to 4.427	No	>0.9999	-1.967	-1.133	-0.8333	1.431	3	3	0.5823	178
V138A	1.325	-3.230 to 5.880	No	>0.9999	1.3	-0.025	1.325	1.239	4	4	1.069	178
S189A	0.5	-4.760 to 5.760	No	>0.9999	5.2	4.7	0.5	1.431	3	3	0.3494	178
G192A	0.6667	-4.593 to 5.927	No	>0.9999	1.1	0.4333	0.6667	1.431	3	3	0.4659	178
I193A	0.62	-3.454 to 4.694	No	>0.9999	4.82	4.2	0.62	1.108	5	5	0.5593	178
Y196A	0.375	-4.180 to 4.930	No	>0.9999	2.65	2.275	0.375	1.239	4	4	0.3026	178
R197A	0.6667	-4.593 to 5.927	No	>0.9999	-0.6	-1.267	0.6667	1.431	3	3	0.4659	178

Y200A	0.4333	-4.827 to 5.693	No	>0.9999	5.767	5.333	0.4333	1.431	3	3	0.3028	178
Y204A	-0.06667	-5.327 to 5.193	No	>0.9999	7.867	7.933	-0.06667	1.431	3	3	0.04659	178
V230A	0.7	-4.560 to 5.960	No	>0.9999	8.267	7.567	0.7	1.431	3	3	0.4891	178
T231A	-2.667	-7.927 to 2.593	No	0.8798	5.267	7.933	-2.667	1.431	3	3	1.863	178
G235A	2.633	-2.627 to 7.893	No	0.8928	5.533	2.9	2.633	1.431	3	3	1.84	178
S238A	1.6	-3.660 to 6.860	No	>0.9999	7.333	5.733	1.6	1.431	3	3	1.118	178
R246A	-0.575	-5.130 to 3.980	No	>0.9999	-1.725	-1.15	-0.575	1.239	4	4	0.464	178
R287A	0.425	-4.130 to 4.980	No	>0.9999	-3.9	-4.325	0.425	1.239	4	4	0.3429	178
G288A	1.233	-4.027 to 6.493	No	>0.9999	6.567	5.333	1.233	1.431	3	3	0.8618	178
G291A	0.9333	-4.327 to 6.193	No	>0.9999	5.267	4.333	0.9333	1.431	3	3	0.6522	178
V294A	-2.24	-6.314 to 1.834	No	0.7693	1.4	3.64	-2.24	1.108	5	5	2.021	178
L295A	0.4667	-4.793 to 5.727	No	>0.9999	7.767	7.3	0.4667	1.431	3	3	0.3261	178

Table Analyzed	**ADP_ATP_5mM_2wayANOVA**				
Two-way ANOVA	Ordinary				
Alpha	0.01				
Source of Variation	% of total variation	P value	Significant?		
Interaction	2.238	0.5656	No		
substrate	0.03201	0.5198	No		
mutation	84.03	<0.0001	Yes		
ANOVA table	SS (Type III)	DF	MS	F (DFn, DFd)	P value
Interaction	79.87	31	2.576	F (31, 178) = 0.9381	P=0.5656
substrate	1.143	1	1.143	F (1, 178) = 0.4160	P=0.5198
mutation	2999	31	96.75	F (31, 178) = 35.23	P<0.0001
Residual	488.9	178	2.746		
Difference between row means					
Predicted (LS) mean of ŒîTm 5 mM ADP	2.914				
Predicted (LS) mean of ŒîTm 5 mM ATP	2.77				
Difference between predicted means	0.1433				
SE of difference	0.2222				
Data summary					
Number of columns (mutation)	32				
Number of rows (substrate)	2				
Number of values	242				

Within each row, compare columns (simple effects within rows)

Number of families: 2

Number of comparisons per family: 31

Alpha 0.01

Dunnett's multiple comparisons test	ΔTm 5 mM ADP				ΔTm 5 mM ATP			
	Prd (LS) mean diff.	99.00% CI of diff.	Below threshold?	Adjusted P Value	Prd (LS) mean diff.	99.00% CI of diff.	Below threshold?	Adjusted P Value
wt vs. S29A	-2.796	-6.883 to 1.292	No	0.2666	-3.333	-7.421 to 0.7542	No	0.0819
wt vs. K30A	9.477	6.035 to 12.92	Yes	<0.0001	9.64	6.198 to 13.08	Yes	<0.0001
wt vs. N85A	4.88	1.756 to 8.005	Yes	<0.0001	6.7	3.575 to 9.825	Yes	<0.0001
wt vs. R88A	7.088	3.390 to 10.78	Yes	<0.0001	7.85	4.153 to 11.55	Yes	<0.0001
wt vs. Y89A	-5.763	-9.850 to -1.675	Yes	<0.0001	-3.233	-7.321 to 0.8542	No	0.1043
wt vs. T92A	2.163	-1.535 to 5.860	No	0.5239	2.675	-1.022 to 6.372	No	0.1929
wt vs. Q93A	1.913	-1.785 to 5.610	No	0.729	2.225	-1.472 to 5.922	No	0.4741
wt vs. N96A	4.454	1.193 to 7.715	Yes	<0.0001	5.05	1.789 to 8.311	Yes	<0.0001
wt vs. F97A	-3.063	-7.150 to 1.025	No	0.1541	-3.567	-7.654 to 0.5209	No	0.045
wt vs. R100A	0.4042	-3.683 to 4.492	No	0.9996	1.667	-2.421 to 5.754	No	0.9568
wt vs. N123A	4.05	0.3527 to 7.747	Yes	0.0028	4.55	0.8527 to 8.247	Yes	0.0004
wt vs. S134A	3.738	-0.3500 to 7.825	No	0.0281	3.867	-0.2209 to 7.954	No	0.0194
wt vs. L135A	9.338	5.250 to 13.43	Yes	<0.0001	8.3	4.212 to 12.39	Yes	<0.0001
wt vs. V138A	5.713	2.015 to 9.410	Yes	<0.0001	6.3	2.603 to 9.997	Yes	<0.0001
wt vs. S189A	2.171	-1.917 to 6.258	No	0.688	2.6	-1.488 to 6.688	No	0.3792
wt vs. G192A	5.871	1.783 to 9.958	Yes	<0.0001	6.2	2.112 to 10.29	Yes	<0.0001
wt vs. I193A	1.938	-1.505 to 5.380	No	0.5908	2.54	-0.9020 to 5.982	No	0.1702
wt vs. Y196A	4.288	0.5902 to 7.985	Yes	0.0012	5.075	1.378 to 8.772	Yes	<0.0001
wt vs. R197A	7.338	2.564 to 12.11	Yes	<0.0001	7.5	2.727 to 12.27	Yes	<0.0001
wt vs. Y200A	1.471	-2.617 to 5.558	No	0.9853	2.233	-1.854 to 6.321	No	0.6416
wt vs. Y204A	-0.3292	-4.417 to 3.758	No	0.9997	-0.4	-4.488 to 3.688	No	0.9996

wt vs. V230A	-0.8625	-4.950 to 3.225	No	0.9991	-0.3333	-4.421 to 3.754	No	0.9997
wt vs. T231A	2.071	-2.017 to 6.158	No	0.7595	-0.9667	-5.054 to 3.121	No	0.999
wt vs. G235A	1.804	-2.283 to 5.892	No	0.91	3.267	-0.8209 to 7.354	No	0.0963
wt vs. S238A	-0.5958	-4.683 to 3.492	No	0.9994	1.8	-2.288 to 5.888	No	0.9119
wt vs. R246A	8.138	4.440 to 11.83	Yes	<0.0001	6.975	3.278 to 10.67	Yes	<0.0001
wt vs. R287A	9.763	6.065 to 13.46	Yes	<0.0001	10	6.303 to 13.70	Yes	<0.0001
wt vs. G288A	0.7375	-3.350 to 4.825	No	0.9993	1.4	-2.688 to 5.488	No	0.9926
wt vs. G291A	1.838	-2.250 to 5.925	No	0.8952	2.767	-1.321 to 6.854	No	0.2818
wt vs. V294A	6.058	2.615 to 9.500	Yes	<0.0001	3.2	-0.2420 to 6.642	No	0.0235
wt vs. L295A	0.2708	-3.817 to 4.358	No	0.9997	0.8	-3.288 to 4.888	No	0.9992

	ΔTm 5 mM ADP								ΔTm 5 mM ATP							
Test details	Prd (LS) mean 1	Prd (LS) mean 2	Prd (LS) mean diff.	SE of diff.	N1	N2	q	DF	Prd (LS) mean 1	Prd (LS) mean 2	Prd (LS) mean diff.	SE of diff.	N1	N2	q	DF
wt vs. S29A	5.838	8.633	-2.796	1.122	8	3	2.492	178	6	9.333	-3.333	1.122	8	3	2.971	178
wt vs. K30A	5.838	-3.64	9.477	0.9448	8	5	10.03	178	6	-3.64	9.64	0.9448	8	5	10.2	178
wt vs. N85A	5.838	0.9571	4.88	0.8577	8	7	5.69	178	6	-0.7	6.7	0.8577	8	7	7.812	178
wt vs. R88A	5.838	-1.25	7.088	1.015	8	4	6.984	178	6	-1.85	7.85	1.015	8	4	7.735	178
wt vs. Y89A	5.838	11.6	-5.763	1.122	8	3	5.136	178	6	9.233	-3.233	1.122	8	3	2.882	178
wt vs. T92A	5.838	3.675	2.163	1.015	8	4	2.131	178	6	3.325	2.675	1.015	8	4	2.636	178
wt vs. Q93A	5.838	3.925	1.913	1.015	8	4	1.885	178	6	3.775	2.225	1.015	8	4	2.192	178
wt vs. N96A	5.838	1.383	4.454	0.895	8	6	4.977	178	6	0.95	5.05	0.895	8	6	5.642	178
wt vs. F97A	5.838	8.9	-3.063	1.122	8	3	2.73	178	6	9.567	-3.567	1.122	8	3	3.179	178
wt vs. R100A	5.838	5.433	0.4042	1.122	8	3	0.3602	178	6	4.333	1.667	1.122	8	3	1.485	178
wt vs. N123A	5.838	1.788	4.05	1.015	8	4	3.991	178	6	1.45	4.55	1.015	8	4	4.483	178
wt vs. S134A	5.838	2.1	3.738	1.122	8	3	3.331	178	6	2.133	3.867	1.122	8	3	3.446	178
wt vs. L135A	5.838	-3.5	9.338	1.122	8	3	8.323	178	6	-2.3	8.3	1.122	8	3	7.398	178
wt vs. V138A	5.838	0.125	5.713	1.015	8	4	5.629	178	6	-0.3	6.3	1.015	8	4	6.208	178
wt vs. S189A	5.838	3.667	2.171	1.122	8	3	1.935	178	6	3.4	2.6	1.122	8	3	2.317	178

wt vs. G192A	5.838	-0.03333	5.871	1.122	8	3	5.233	178	6	-0.2	6.2	1.122	8	3	5.526	178
wt vs. I193A	5.838	3.9	1.938	0.9448	8	5	2.051	178	6	3.46	2.54	0.9448	8	5	2.688	178
wt vs. Y196A	5.838	1.55	4.288	1.015	8	4	4.225	178	6	0.925	5.075	1.015	8	4	5.001	178
wt vs. R197A	5.838	-1.5	7.338	1.31	8	2	5.6	178	6	-1.5	7.5	1.31	8	2	5.724	178
wt vs. Y200A	5.838	4.367	1.471	1.122	8	3	1.311	178	6	3.767	2.233	1.122	8	3	1.991	178
wt vs. Y204A	5.838	6.167	-0.3292	1.122	8	3	0.2934	178	6	6.4	-0.4	1.122	8	3	0.3565	178
wt vs. V230A	5.838	6.7	-0.8625	1.122	8	3	0.7687	178	6	6.333	-0.3333	1.122	8	3	0.2971	178
wt vs. T231A	5.838	3.767	2.071	1.122	8	3	1.846	178	6	6.967	-0.9667	1.122	8	3	0.8616	178
wt vs. G235A	5.838	4.033	1.804	1.122	8	3	1.608	178	6	2.733	3.267	1.122	8	3	2.912	178
wt vs. S238A	5.838	6.433	-0.5958	1.122	8	3	0.5311	178	6	4.2	1.8	1.122	8	3	1.604	178
wt vs. R246A	5.838	-2.3	8.138	1.015	8	4	8.018	178	6	-0.975	6.975	1.015	8	4	6.873	178
wt vs. R287A	5.838	-3.925	9.763	1.015	8	4	9.62	178	6	-4	10	1.015	8	4	9.854	178
wt vs. G288A	5.838	5.1	0.7375	1.122	8	3	0.6573	178	6	4.6	1.4	1.122	8	3	1.248	178
wt vs. G291A	5.838	4	1.838	1.122	8	3	1.638	178	6	3.233	2.767	1.122	8	3	2.466	178
wt vs. V294A	5.838	-0.22	6.058	0.9448	8	5	6.412	178	6	2.8	3.2	0.9448	8	5	3.387	178
wt vs. L295A	5.838	5.567	0.2708	1.122	8	3	0.2414	178	6	5.2	0.8	1.122	8	3	0.713	178

Compare each cell mean with the other cell mean in that column

Number of families: 1

Number of comparisons per family: 32

Alpha 0.01

ΔTm 5 mM ADP - ΔTm 5 mM ATP

Sidak's multiple comparisons test	Prd (LS) mean diff.	99.00% CI of diff.	Below threshold?	Adjusted P Value	Prd (LS) mean 1	Prd (LS) mean 2	Prd (LS) mean diff.	SE of diff.	N1	N2	t	DF
wild type	-0.1625	-3.208 to 2.883	No	>0.9999	5.838	6	-0.1625	0.8286	8	8	0.1961	178
S29A	-0.7	-5.673 to 4.273	No	>0.9999	8.633	9.333	-0.7	1.353	3	3	0.5173	178
K30A	0	-3.852 to 3.852	No	>0.9999	-3.64	-3.64	0	1.048	5	5	0	178
N85A	1.657	-1.599 to 4.913	No	0.8755	0.9571	-0.7	1.657	0.8858	7	7	1.871	178
R88A	0.6	-3.707 to 4.907	No	>0.9999	-1.25	-1.85	0.6	1.172	4	4	0.512	178
Y89A	2.367	-2.607 to 7.340	No	0.9353	11.6	9.233	2.367	1.353	3	3	1.749	178
T92A	0.35	-3.957 to 4.657	No	>0.9999	3.675	3.325	0.35	1.172	4	4	0.2987	178
Q93A	0.15	-4.157 to 4.457	No	>0.9999	3.925	3.775	0.15	1.172	4	4	0.128	178
N96A	0.4333	-3.083 to 3.950	No	>0.9999	1.383	0.95	0.4333	0.9568	6	6	0.4529	178
F97A	-0.6667	-5.640 to 4.307	No	>0.9999	8.9	9.567	-0.6667	1.353	3	3	0.4927	178
R100A	1.1	-3.873 to 6.073	No	>0.9999	5.433	4.333	1.1	1.353	3	3	0.8129	178
N123A	0.3375	-3.970 to 4.645	No	>0.9999	1.788	1.45	0.3375	1.172	4	4	0.288	178
S134A	-0.03333	-5.007 to 4.940	No	>0.9999	2.1	2.133	-0.03333	1.353	3	3	0.02463	178
L135A	-1.2	-6.173 to 3.773	No	>0.9999	-3.5	-2.3	-1.2	1.353	3	3	0.8868	178
V138A	0.425	-3.882 to 4.732	No	>0.9999	0.125	-0.3	0.425	1.172	4	4	0.3627	178
S189A	0.2667	-4.707 to 5.240	No	>0.9999	3.667	3.4	0.2667	1.353	3	3	0.1971	178
G192A	0.1667	-4.807 to 5.140	No	>0.9999	-0.0333	-0.2	0.1667	1.353	3	3	0.1232	178
I193A	0.44	-3.412 to 4.292	No	>0.9999	3.9	3.46	0.44	1.048	5	5	0.4198	178
Y196A	0.625	-3.682 to 4.932	No	>0.9999	1.55	0.925	0.625	1.172	4	4	0.5333	178
R197A	-1.33E-15	-6.091 to 6.091	No	>0.9999	-1.5	-1.5	-1.33E-15	1.657	2	2	8.04E-16	178

Y200A	0.6	-4.373 to 5.573	No	>0.9999	4.367	3.767	0.6	1.353	3	3	0.4434	178
Y204A	-0.2333	-5.207 to 4.740	No	>0.9999	6.167	6.4	-0.2333	1.353	3	3	0.1724	178
V230A	0.3667	-4.607 to 5.340	No	>0.9999	6.7	6.333	0.3667	1.353	3	3	0.271	178
T231A	-3.2	-8.173 to 1.773	No	0.4607	3.767	6.967	-3.2	1.353	3	3	2.365	178
G235A	1.3	-3.673 to 6.273	No	>0.9999	4.033	2.733	1.3	1.353	3	3	0.9607	178
S238A	2.233	-2.740 to 7.207	No	0.9664	6.433	4.2	2.233	1.353	3	3	1.65	178
R246A	-1.325	-5.632 to 2.982	No	>0.9999	-2.3	-0.975	-1.325	1.172	4	4	1.131	178
R287A	0.075	-4.232 to 4.382	No	>0.9999	-3.925	-4	0.075	1.172	4	4	0.064	178
G288A	0.5	-4.473 to 5.473	No	>0.9999	5.1	4.6	0.5	1.353	3	3	0.3695	178
G291A	0.7667	-4.207 to 5.740	No	>0.9999	4	3.233	0.7667	1.353	3	3	0.5666	178
V294A	-3.02	-6.872 to 0.8324	No	0.1329	-0.22	2.8	-3.02	1.048	5	5	2.881	178
L295A	0.3667	-4.607 to 5.340	No	>0.9999	5.567	5.2	0.3667	1.353	3	3	0.271	178

Table Analyzed	**ADP_ATP_1mM_2wayANOVA**				
Two-way ANOVA	Ordinary				
Alpha	0.01				
Source of Variation	% of total variation	P value	Significant?		
Interaction	3.79	0.684	No		
substrate	0.1418	0.3196	No		
mutation	70.2	<0.0001	Yes		
ANOVA table	SS (Type III)	DF	MS	F (DFn, DFd)	P value
Interaction	61.11	31	1.971	F (31, 182) = 0.8584	P=0.6840
substrate	2.287	1	2.287	F (1, 182) = 0.9958	P=0.3196
mutation	1132	31	36.52	F (31, 182) = 15.90	P<0.0001
Residual	418	182	2.297		
Difference between row means					
Predicted (LS) mean of ŒîTm 1 mM ADP	0.04194				
Predicted (LS) mean of ŒîTm 1 mM ATP	-0.1584				
Difference between predicted means	0.2003				
SE of difference	0.2007				
Data summary					
Number of columns (mutation)	32				
Number of rows (substrate)	2				
Number of values	246				

Within each row, compare columns (simple effects within rows)

Number of families: 2

Number of comparisons per family: 31

Alpha 0.01

	ΔTm 1 mM ADP				ΔTm 1 mM ATP			
Dunnett's multiple comparisons test	Prd (LS) mean diff.	99.00% CI of diff.	Below threshold?	Adjusted P Value	Prd (LS) mean diff.	99.00% CI of diff.	Below threshold?	Adjusted P Value
wt vs. S29A	-2.138	-5.873 to 1.598	No	0.5608	-2.317	-6.052 to 1.419	No	0.4209
wt vs. K30A	5.643	2.497 to 8.788	Yes	<0.0001	5.55	2.404 to 8.696	Yes	<0.0001
wt vs. N85A	3.12	0.2639 to 5.975	Yes	0.003	3.579	0.7228 to 6.434	Yes	0.0003
wt vs. R88A	3.088	-0.2914 to 6.466	No	0.0284	3.425	0.04606 to 6.804	Yes	0.0084
wt vs. Y89A	-5.271	-9.006 to -1.535	Yes	<0.0001	-0.7167	-4.452 to 3.019	No	0.9992
wt vs. T92A	1.913	-1.466 to 5.291	No	0.5796	1.775	-1.604 to 5.154	No	0.7036
wt vs. Q93A	1.788	-1.591 to 5.166	No	0.6923	1.75	-1.629 to 5.129	No	0.7253
wt vs. N96A	2.513	-0.4674 to 5.492	No	0.0616	2.85	-0.1299 to 5.830	No	0.0171
wt vs. F97A	-2.971	-6.706 to 0.7647	No	0.0998	-2.65	-6.386 to 1.086	No	0.2169
wt vs. R100A	-0.2042	-3.940 to 3.531	No	0.9998	0.5833	-3.152 to 4.319	No	0.9994
wt vs. N123A	2.793	-0.3531 to 5.938	No	0.038	3.04	-0.1056 to 6.186	No	0.0152
wt vs. S134A	3.363	-0.3731 to 7.098	No	0.0331	3.05	-0.6856 to 6.786	No	0.0809
wt vs. L135A	7.029	3.294 to 10.76	Yes	<0.0001	5.917	2.181 to 9.652	Yes	<0.0001
wt vs. V138A	3.088	-0.2914 to 6.466	No	0.0284	3.15	-0.2289 to 6.529	No	0.0229
wt vs. S189A	1.863	-1.873 to 5.598	No	0.7795	1.95	-1.786 to 5.686	No	0.7133
wt vs. G192A	3.263	-0.4731 to 6.998	No	0.0445	3.283	-0.4522 to 7.019	No	0.0419
wt vs. I193A	1.523	-1.623 to 4.668	No	0.8176	0.95	-2.196 to 4.096	No	0.9943
wt vs. Y196A	1.988	-1.391 to 5.366	No	0.5122	1.9	-1.479 to 5.279	No	0.591
wt vs. R197A	3.163	-0.5731 to 6.898	No	0.0594	2.15	-1.586 to 5.886	No	0.5508
wt vs. Y200A	1.363	-2.373 to 5.098	No	0.9845	1.85	-1.886 to 5.586	No	0.789

wt vs. Y204A	0.1958	-3.540 to 3.931	No	0.9998	0.3833	-3.352 to 4.119	No	0.9996
wt vs. V230A	-0.1708	-3.906 to 3.565	No	0.9999	0.7833	-2.952 to 4.519	No	0.9991
wt vs. T231A	1.363	-2.373 to 5.098	No	0.9845	-0.35	-4.086 to 3.386	No	0.9996
wt vs. G235A	0.7958	-2.940 to 4.531	No	0.9991	0.95	-2.786 to 4.686	No	0.9988
wt vs. S238A	-0.7042	-4.440 to 3.031	No	0.9992	1.183	-2.552 to 4.919	No	0.9937
wt vs. R246A	4.863	1.484 to 8.241	Yes	<0.0001	3.4	0.02106 to 6.779	Yes	0.0092
wt vs. R287A	6.063	2.684 to 9.441	Yes	<0.0001	5.65	2.271 to 9.029	Yes	<0.0001
wt vs. G288A	0.9625	-2.773 to 4.698	No	0.9988	1.05	-2.686 to 4.786	No	0.9986
wt vs. G291A	0.5958	-3.140 to 4.331	No	0.9994	1.517	-2.219 to 5.252	No	0.958
wt vs. V294A	4.723	1.577 to 7.868	Yes	<0.0001	4.05	0.9044 to 7.196	Yes	0.0002
wt vs. L295A	-0.5375	-4.273 to 3.198	No	0.9994	1.383	-2.352 to 5.119	No	0.9836

	ΔTm 1 mM ADP								ΔTm 1 mM ATP							
Test details	Prd (LS) mean 1	Prd (LS) mean 2	Prd (LS) mean diff.	SE of diff.	N1	N2	q	DF	Prd (LS) mean 1	Prd (LS) mean 2	Prd (LS) mean diff.	SE of diff.	N1	N2	q	DF
wt vs. S29A	1.763	3.9	-2.138	1.026	8	3	2.083	182	1.75	4.067	-2.317	1.026	8	3	2.258	182
wt vs. K30A	1.763	-3.88	5.643	0.8639	8	5	6.531	182	1.75	-3.8	5.55	0.8639	8	5	6.424	182
wt vs. N85A	1.763	-1.357	3.12	0.7843	8	7	3.978	182	1.75	-1.829	3.579	0.7843	8	7	4.563	182
wt vs. R88A	1.763	-1.325	3.088	0.928	8	4	3.327	182	1.75	-1.675	3.425	0.928	8	4	3.691	182
wt vs. Y89A	1.763	7.033	-5.271	1.026	8	3	5.137	182	1.75	2.467	-0.7167	1.026	8	3	0.6985	182
wt vs. T92A	1.763	-0.15	1.913	0.928	8	4	2.061	182	1.75	-0.025	1.775	0.928	8	4	1.913	182
wt vs. Q93A	1.763	-0.025	1.788	0.928	8	4	1.926	182	1.75	1.67E-16	1.75	0.928	8	4	1.886	182
wt vs. N96A	1.763	-0.75	2.513	0.8184	8	6	3.07	182	1.75	-1.1	2.85	0.8184	8	6	3.482	182
wt vs. F97A	1.763	4.733	-2.971	1.026	8	3	2.896	182	1.75	4.4	-2.65	1.026	8	3	2.583	182
wt vs. R100A	1.763	1.967	-0.2042	1.026	8	3	0.199	182	1.75	1.167	0.5833	1.026	8	3	0.5686	182
wt vs. N123A	1.763	-1.03	2.793	0.8639	8	5	3.232	182	1.75	-1.29	3.04	0.8639	8	5	3.519	182
wt vs. S134A	1.763	-1.6	3.363	1.026	8	3	3.277	182	1.75	-1.3	3.05	1.026	8	3	2.973	182
wt vs. L135A	1.763	-5.267	7.029	1.026	8	3	6.851	182	1.75	-4.167	5.917	1.026	8	3	5.767	182
wt vs. V138A	1.763	-1.325	3.088	0.928	8	4	3.327	182	1.75	-1.4	3.15	0.928	8	4	3.394	182
wt vs. S189A	1.763	-0.1	1.863	1.026	8	3	1.815	182	1.75	-0.2	1.95	1.026	8	3	1.901	182

wt vs. G192A	1.763	-1.5	3.263	1.026	8	3	3.18	182	1.75	-1.533	3.283	1.026	8	3	3.2	182
wt vs. I193A	1.763	0.24	1.523	0.8639	8	5	1.762	182	1.75	0.8	0.95	0.8639	8	5	1.1	182
wt vs. Y196A	1.763	-0.225	1.988	0.928	8	4	2.142	182	1.75	-0.15	1.9	0.928	8	4	2.047	182
wt vs. R197A	1.763	-1.4	3.163	1.026	8	3	3.082	182	1.75	-0.4	2.15	1.026	8	3	2.096	182
wt vs. Y200A	1.763	0.4	1.363	1.026	8	3	1.328	182	1.75	-0.1	1.85	1.026	8	3	1.803	182
wt vs. Y204A	1.763	1.567	0.1958	1.026	8	3	0.1909	182	1.75	1.367	0.3833	1.026	8	3	0.3736	182
wt vs. V230A	1.763	1.933	-0.1708	1.026	8	3	0.1665	182	1.75	0.9667	0.7833	1.026	8	3	0.7635	182
wt vs. T231A	1.763	0.4	1.363	1.026	8	3	1.328	182	1.75	2.1	-0.35	1.026	8	3	0.3411	182
wt vs. G235A	1.763	0.9667	0.7958	1.026	8	3	0.7757	182	1.75	0.8	0.95	1.026	8	3	0.926	182
wt vs. S238A	1.763	2.467	-0.7042	1.026	8	3	0.6863	182	1.75	0.5667	1.183	1.026	8	3	1.153	182
wt vs. R246A	1.763	-3.1	4.863	0.928	8	4	5.24	182	1.75	-1.65	3.4	0.928	8	4	3.664	182
wt vs. R287A	1.763	-4.3	6.063	0.928	8	4	6.533	182	1.75	-3.9	5.65	0.928	8	4	6.088	182
wt vs. G288A	1.763	0.8	0.9625	1.026	8	3	0.9381	182	1.75	0.7	1.05	1.026	8	3	1.023	182
wt vs. G291A	1.763	1.167	0.5958	1.026	8	3	0.5808	182	1.75	0.2333	1.517	1.026	8	3	1.478	182
wt vs. V294A	1.763	-2.96	4.723	0.8639	8	5	5.466	182	1.75	-2.3	4.05	0.8639	8	5	4.688	182
wt vs. L295A	1.763	2.3	-0.5375	1.026	8	3	0.5239	182	1.75	0.3667	1.383	1.026	8	3	1.348	182

Compare each cell mean with the other cell mean in that column

Number of families: 1

Number of comparisons per family: 32

Alpha 0.01

ΔTm 1 mM ADP - ΔTm 1 mM ATP

Sidak's multiple comparisons test	Prd (LS) mean diff.	99.00% CI of diff.	Below threshold?	Adjusted P Value	Prd (LS) mean 1	Prd (LS) mean 2	Prd (LS) mean diff.	SE of diff.	N1	N2	t	DF
wild type	0.0125	-2.771 to 2.796	No	>0.9999	1.763	1.75	0.0125	0.7577	8	8	0.0165	182
S29A	-0.1667	-4.713 to 4.379	No	>0.9999	3.9	4.067	-0.1667	1.237	3	3	0.1347	182
K30A	-0.08	-3.601 to 3.441	No	>0.9999	-3.88	-3.8	-0.08	0.9585	5	5	0.08347	182
N85A	0.4714	-2.505 to 3.447	No	>0.9999	-1.357	-1.829	0.4714	0.81	7	7	0.582	182
R88A	0.35	-3.587 to 4.287	No	>0.9999	-1.325	-1.675	0.35	1.072	4	4	0.3266	182
Y89A	4.567	0.02076 to 9.113	Yes	0.0094	7.033	2.467	4.567	1.237	3	3	3.691	182
T92A	-0.125	-4.062 to 3.812	No	>0.9999	-0.15	-0.025	-0.125	1.072	4	4	0.1166	182
Q93A	-0.025	-3.962 to 3.912	No	>0.9999	-0.025	1.67E-16	-0.025	1.072	4	4	0.02333	182
N96A	0.35	-2.864 to 3.564	No	>0.9999	-0.75	-1.1	0.35	0.8749	6	6	0.4	182
F97A	0.3333	-4.213 to 4.879	No	>0.9999	4.733	4.4	0.3333	1.237	3	3	0.2694	182
R100A	0.8	-3.746 to 5.346	No	>0.9999	1.967	1.167	0.8	1.237	3	3	0.6465	182
N123A	0.26	-3.261 to 3.781	No	>0.9999	-1.03	-1.29	0.26	0.9585	5	5	0.2713	182
S134A	-0.3	-4.846 to 4.246	No	>0.9999	-1.6	-1.3	-0.3	1.237	3	3	0.2425	182
L135A	-1.1	-5.646 to 3.446	No	>0.9999	-5.267	-4.167	-1.1	1.237	3	3	0.889	182
V138A	0.075	-3.862 to 4.012	No	>0.9999	-1.325	-1.4	0.075	1.072	4	4	0.06999	182
S189A	0.1	-4.446 to 4.646	No	>0.9999	-0.1	-0.2	0.1	1.237	3	3	0.08082	182
G192A	0.03333	-4.513 to 4.579	No	>0.9999	-1.5	-1.533	0.03333	1.237	3	3	0.02694	182
I193A	-0.56	-4.081 to 2.961	No	>0.9999	0.24	0.8	-0.56	0.9585	5	5	0.5843	182
Y196A	-0.075	-4.012 to 3.862	No	>0.9999	-0.225	-0.15	-0.075	1.072	4	4	0.06999	182
R197A	-1	-5.546 to 3.546	No	>0.9999	-1.4	-0.4	-1	1.237	3	3	0.8082	182
Y200A	0.5	-4.046 to 5.046	No	>0.9999	0.4	-0.1	0.5	1.237	3	3	0.4041	182

Y204A	0.2	-4.346 to 4.746	No	>0.9999	1.567	1.367	0.2	1.237	3	3	0.1616	182
V230A	0.9667	-3.579 to 5.513	No	>0.9999	1.933	0.9667	0.9667	1.237	3	3	0.7812	182
T231A	-1.7	-6.246 to 2.846	No	0.9975	0.4	2.1	-1.7	1.237	3	3	1.374	182
G235A	0.1667	-4.379 to 4.713	No	>0.9999	0.9667	0.8	0.1667	1.237	3	3	0.1347	182
S238A	1.9	-2.646 to 6.446	No	0.9868	2.467	0.5667	1.9	1.237	3	3	1.536	182
R246A	-1.45	-5.387 to 2.487	No	0.9981	-3.1	-1.65	-1.45	1.072	4	4	1.353	182
R287A	-0.4	-4.337 to 3.537	No	>0.9999	-4.3	-3.9	-0.4	1.072	4	4	0.3733	182
G288A	0.1	-4.446 to 4.646	No	>0.9999	0.8	0.7	0.1	1.237	3	3	0.08082	182
G291A	0.9333	-3.613 to 5.479	No	>0.9999	1.167	0.2333	0.9333	1.237	3	3	0.7543	182
V294A	-0.66	-4.181 to 2.861	No	>0.9999	-2.96	-2.3	-0.66	0.9585	5	5	0.6886	182
L295A	1.933	-2.613 to 6.479	No	0.9832	2.3	0.3667	1.933	1.237	3	3	1.562	182

Table Analyzed	**ADP_ATP_500uM_2wayANOVA**				
Two-way ANOVA	Ordinary				
Alpha	0.01				
Source of Variation	% of total variation	P value	Significant?		
Interaction	3.578	0.9437	No		
substrate	0.1121	0.4408	No		
mutation	66.73	<0.0001	Yes		
ANOVA table	SS (Type III)	DF	MS	F (DFn, DFd)	P value
Interaction	40.93	31	1.32	F (31, 158) = 0.6151	P=0.9437
substrate	1.282	1	1.282	F (1, 158) = 0.5973	P=0.4408
mutation	763.3	31	24.62	F (31, 158) = 11.47	P<0.0001
Residual	339.1	158	2.146		
Difference between row means					
Predicted (LS) mean of ŒîTm 500 uM ADP	-0.8358				
Predicted (LS) mean of ŒîTm 500 uM ATP	-0.995				
Difference between predicted means	0.1592				
SE of difference	0.206				
Data summary					
Number of columns (mutation)	32				
Number of rows (substrate)	2				
Number of values	222				

Within each row, compare columns (simple effects within rows)

Number of families: 2

Number of comparisons per family: 31

Alpha 0.01

	ΔTm 500 µM ADP				ΔTm 500 µM ATP			
Dunnett's multiple comparisons test	Prd (LS) mean diff	99.00% CI of diff.	Below threshold?	Adjusted P Value	Prd (LS) mean diff.	99.00% CI of diff.	Below threshold?	Adjusted P Value
wt vs. S29A	-2.207	-6.494 to 2.080	No	0.7255	-1.686	-5.973 to 2.602	No	0.9686
wt vs. K30A	4.943	1.592 to 8.294	Yes	<0.0001	4.439	1.088 to 7.791	Yes	<0.0001
wt vs. N85A	2.414	-0.4435 to 5.272	No	0.0598	2.998	0.02254 to 5.973	Yes	0.0091
wt vs. R88A	1.81	-1.880 to 5.499	No	0.7936	1.781	-1.909 to 5.471	No	0.8151
wt vs. Y89A	-4.757	-8.447 to -1.068	Yes	0.0002	-0.8524	-4.543 to 2.838	No	0.999
wt vs. T92A	1.043	-2.647 to 4.732	No	0.9986	1.114	-2.576 to 4.804	No	0.9942
wt vs. Q93A	0.9679	-2.383 to 4.319	No	0.996	0.9893	-2.362 to 4.341	No	0.9945
wt vs. N96A	1.826	-1.148 to 4.801	No	0.4312	2.314	-0.6608 to 5.289	No	0.1165
wt vs. F97A	-1.99	-5.680 to 1.699	No	0.6523	-1.519	-5.209 to 2.171	No	0.9488
wt vs. R100A	-0.5571	-4.247 to 3.132	No	0.9994	0.08095	-3.609 to 3.771	No	>0.9999
wt vs. N123A	2.018	-1.333 to 5.369	No	0.4644	2.002	-1.350 to 5.354	No	0.48
wt vs. S134A	2.776	-0.9132 to 6.466	No	0.1469	2.514	-1.176 to 6.204	No	0.2679
wt vs. L135A	6.61	2.920 to 10.30	Yes	<0.0001	5.048	1.357 to 8.738	Yes	<0.0001
wt vs. V138A	2.218	-1.133 to 5.569	No	0.3096	2.014	-1.337 to 5.366	No	0.4692
wt vs. S189A	1.276	-2.413 to 4.966	No	0.9923	1.148	-2.543 to 4.838	No	0.9938
wt vs. G192A	2.943	-1.344 to 7.230	No	0.2564	2.664	-1.623 to 6.952	No	0.4121
wt vs. I193A	3.218	-0.1332 to 6.569	No	0.0163	3.414	-0.2759 to 7.104	No	0.0246
wt vs. Y196A	1.21	-2.480 to 4.899	No	0.9931	0.681	-3.009 to 4.371	No	0.9992
wt vs. R197A	1.643	-2.644 to 5.930	No	0.9757	0.6643	-3.623 to 4.952	No	0.9994
wt vs. Y200A	0.8095	-2.880 to 4.499	No	0.999	1.148	-2.543 to 4.838	No	0.9938

wt vs. Y204A	-0.1905	-3.880 to 3.499	No	0.9998	-0.01905	-3.709 to 3.671	No	>0.9999
wt vs. V230A	-0.3571	-4.047 to 3.332	No	0.9996	0.1476	-3.543 to 3.838	No	0.9999
wt vs. T231A	0.6095	-3.080 to 4.299	No	0.9993	-0.01905	-3.709 to 3.671	No	>0.9999
wt vs. G235A	0.1429	-3.547 to 3.832	No	0.9999	0.4476	-3.243 to 4.138	No	0.9995
wt vs. S238A	-0.4071	-4.694 to 3.880	No	0.9996	0.9643	-3.323 to 5.252	No	0.999
wt vs. R246A	3.518	0.1668 to 6.869	Yes	0.0053	2.164	-1.187 to 5.516	No	0.3489
wt vs. R287A	4.818	1.467 to 8.169	Yes	<0.0001	4.264	0.9126 to 7.616	Yes	0.0002
wt vs. G288A	0.3762	-3.313 to 4.066	No	0.9996	0.381	-3.309 to 4.071	No	0.9996
wt vs. G291A	0.3095	-3.380 to 3.999	No	0.9997	1.281	-2.409 to 4.971	No	0.9922
wt vs. V294A	4.043	0.9123 to 7.173	Yes	0.0002	3.914	0.7831 to 7.045	Yes	0.0003
wt vs. L295A	-0.1571	-3.847 to 3.532	No	0.9999	0.6143	-3.076 to 4.304	No	0.9993

	ΔTm 500 µM ADP								ΔTm 500 µM ATP							
Test details	Prd (LS) mean 1	Prd (LS) mean 2	Prd (LS) mean diff.	SE of diff.	N1	N2	q	DF	Prd (LS) mean 1	Prd (LS) mean 2	Prd (LS) mean diff.	SE of diff.	N1	N2	q	DF
wt vs. S29A	0.4429	2.65	-2.207	1.175	7	2	1.879	158	0.4143	2.1	-1.686	1.175	7	2	1.435	158
wt vs. K30A	0.4429	-4.5	4.943	0.9183	7	4	5.383	158	0.4143	-4.025	4.439	0.9183	7	4	4.834	158
wt vs. N85A	0.4429	-1.971	2.414	0.7831	7	7	3.083	158	0.4143	-2.583	2.998	0.8151	7	6	3.678	158
wt vs. R88A	0.4429	-1.367	1.81	1.011	7	3	1.79	158	0.4143	-1.367	1.781	1.011	7	3	1.762	158
wt vs. Y89A	0.4429	5.2	-4.757	1.011	7	3	4.706	158	0.4143	1.267	-0.8524	1.011	7	3	0.8431	158
wt vs. T92A	0.4429	-0.6	1.043	1.011	7	3	1.032	158	0.4143	-0.7	1.114	1.011	7	3	1.102	158
wt vs. Q93A	0.4429	-0.525	0.9679	0.9183	7	4	1.054	158	0.4143	-0.575	0.9893	0.9183	7	4	1.077	158
wt vs. N96A	0.4429	-1.383	1.826	0.8151	7	6	2.241	158	0.4143	-1.9	2.314	0.8151	7	6	2.839	158
wt vs. F97A	0.4429	2.433	-1.99	1.011	7	3	1.969	158	0.4143	1.933	-1.519	1.011	7	3	1.503	158
wt vs. R100A	0.4429	1	-0.5571	1.011	7	3	0.5511	158	0.4143	0.3333	0.08095	1.011	7	3	0.08007	158
wt vs. N123A	0.4429	-1.575	2.018	0.9183	7	4	2.197	158	0.4143	-1.588	2.002	0.9183	7	4	2.18	158
wt vs. S134A	0.4429	-2.333	2.776	1.011	7	3	2.746	158	0.4143	-2.1	2.514	1.011	7	3	2.487	158
wt vs. L135A	0.4429	-6.167	6.61	1.011	7	3	6.538	158	0.4143	-4.633	5.048	1.011	7	3	4.993	158
wt vs. V138A	0.4429	-1.775	2.218	0.9183	7	4	2.415	158	0.4143	-1.6	2.014	0.9183	7	4	2.194	158
wt vs. S189A	0.4429	-0.8333	1.276	1.011	7	3	1.262	158	0.4143	-0.7333	1.148	1.011	7	3	1.135	158

wt vs. G192A	0.4429	-2.5	2.943	1.175	7	2	2.505	158	0.4143	-2.25	2.664	1.175	7	2	2.268	158
wt vs. I193A	0.4429	-2.775	3.218	0.9183	7	4	3.504	158	0.4143	-3	3.414	1.011	7	3	3.377	158
wt vs. Y196A	0.4429	-0.7667	1.21	1.011	7	3	1.196	158	0.4143	-0.2667	0.681	1.011	7	3	0.6736	158
wt vs. R197A	0.4429	-1.2	1.643	1.175	7	2	1.399	158	0.4143	-0.25	0.6643	1.175	7	2	0.5655	158
wt vs. Y200A	0.4429	-0.3667	0.8095	1.011	7	3	0.8007	158	0.4143	-0.7333	1.148	1.011	7	3	1.135	158
wt vs. Y204A	0.4429	0.6333	-0.1905	1.011	7	3	0.1884	158	0.4143	0.4333	-0.01905	1.011	7	3	0.01884	158
wt vs. V230A	0.4429	0.8	-0.3571	1.011	7	3	0.3533	158	0.4143	0.2667	0.1476	1.011	7	3	0.146	158
wt vs. T231A	0.4429	-0.1667	0.6095	1.011	7	3	0.6029	158	0.4143	0.4333	-0.01905	1.011	7	3	0.01884	158
wt vs. G235A	0.4429	0.3	0.1429	1.011	7	3	0.1413	158	0.4143	-0.03333	0.4476	1.011	7	3	0.4428	158
wt vs. S238A	0.4429	0.85	-0.4071	1.175	7	2	0.3466	158	0.4143	-0.55	0.9643	1.175	7	2	0.8209	158
wt vs. R246A	0.4429	-3.075	3.518	0.9183	7	4	3.831	158	0.4143	-1.75	2.164	0.9183	7	4	2.357	158
wt vs. R287A	0.4429	-4.375	4.818	0.9183	7	4	5.247	158	0.4143	-3.85	4.264	0.9183	7	4	4.644	158
wt vs. G288A	0.4429	0.06667	0.3762	1.011	7	3	0.3721	158	0.4143	0.03333	0.381	1.011	7	3	0.3768	158
wt vs. G291A	0.4429	0.1333	0.3095	1.011	7	3	0.3062	158	0.4143	-0.8667	1.281	1.011	7	3	1.267	158
wt vs. V294A	0.4429	-3.6	4.043	0.8578	7	5	4.713	158	0.4143	-3.5	3.914	0.8578	7	5	4.563	158
wt vs. L295A	0.4429	0.6	-0.1571	1.011	7	3	0.1554	158	0.4143	-0.2	0.6143	1.011	7	3	0.6076	158

Compare each cell mean with the other cell mean in that column

Number of families: 1

Number of comparisons per family: 32

Alpha 0.01

ΔTm 500 µM ADP - ΔTm 500 µM ATP

Sidak's multiple comparisons test	Prd (LS) mean diff.	99.00% CI of diff.	Below threshold ?	Adjusted P Value	Prd (LS) mean 1	Prd (LS) mean 2	Prd (LS) mean diff.	SE of diff.	N1	N2	t	DF
wild type	0.02857	-2.857 to 2.914	No	>0.9999	0.4429	0.4143	0.02857	0.7831	7	7	0.03649	158
S29A	0.55	-4.848 to 5.948	No	>0.9999	2.65	2.1	0.55	1.465	2	2	0.3754	158
K30A	-0.475	-4.292 to 3.342	No	>0.9999	-4.5	-4.025	-0.475	1.036	4	4	0.4585	158
N85A	0.6119	-2.391 to 3.615	No	>0.9999	-1.971	-2.583	0.6119	0.8151	7	6	0.7507	158
R88A	0	-4.408 to 4.408	No	>0.9999	-1.367	-1.367	0	1.196	3	3	0	158
Y89A	3.933	-0.4744 to 8.341	No	0.039	5.2	1.267	3.933	1.196	3	3	3.288	158
T92A	0.1	-4.308 to 4.508	No	>0.9999	-0.6	-0.7	0.1	1.196	3	3	0.0836	158
Q93A	0.05	-3.767 to 3.867	No	>0.9999	-0.525	-0.575	0.05	1.036	4	4	0.04827	158
N96A	0.5167	-2.600 to 3.633	No	>0.9999	-1.383	-1.9	0.5167	0.8458	6	6	0.6108	158
F97A	0.5	-3.908 to 4.908	No	>0.9999	2.433	1.933	0.5	1.196	3	3	0.418	158
R100A	0.6667	-3.741 to 5.074	No	>0.9999	1	0.3333	0.6667	1.196	3	3	0.5573	158
N123A	0.0125	-3.805 to 3.830	No	>0.9999	-1.575	-1.588	0.0125	1.036	4	4	0.01207	158
S134A	-0.2333	-4.641 to 4.174	No	>0.9999	-2.333	-2.1	-0.2333	1.196	3	3	0.1951	158
L135A	-1.533	-5.941 to 2.874	No	0.9993	-6.167	-4.633	-1.533	1.196	3	3	1.282	158
V138A	-0.175	-3.992 to 3.642	No	>0.9999	-1.775	-1.6	-0.175	1.036	4	4	0.1689	158
S189A	-0.1	-4.508 to 4.308	No	>0.9999	-0.8333	-0.7333	-0.1	1.196	3	3	0.0836	158
G192A	-0.25	-5.648 to 5.148	No	>0.9999	-2.5	-2.25	-0.25	1.465	2	2	0.1706	158
I193A	0.225	-3.898 to 4.348	No	>0.9999	-2.775	-3	0.225	1.119	4	3	0.2011	158
Y196A	-0.5	-4.908 to 3.908	No	>0.9999	-0.7667	-0.2667	-0.5	1.196	3	3	0.418	158
R197A	-0.95	-6.348 to 4.448	No	>0.9999	-1.2	-0.25	-0.95	1.465	2	2	0.6484	158

Y200A	0.3667	-4.041 to 4.774	No	>0.9999	-0.3667	-0.7333	0.3667	1.196	3	3	0.3065	158
Y204A	0.2	-4.208 to 4.608	No	>0.9999	0.6333	0.4333	0.2	1.196	3	3	0.1672	158
V230A	0.5333	-3.874 to 4.941	No	>0.9999	0.8	0.2667	0.5333	1.196	3	3	0.4459	158
T231A	-0.6	-5.008 to 3.808	No	>0.9999	-0.1667	0.4333	-0.6	1.196	3	3	0.5016	158
G235A	0.3333	-4.074 to 4.741	No	>0.9999	0.3	-0.03333	0.3333	1.196	3	3	0.2787	158
S238A	1.4	-3.998 to 6.798	No	>0.9999	0.85	-0.55	1.4	1.465	2	2	0.9556	158
R246A	-1.325	-5.142 to 2.492	No	0.9993	-3.075	-1.75	-1.325	1.036	4	4	1.279	158
R287A	-0.525	-4.342 to 3.292	No	>0.9999	-4.375	-3.85	-0.525	1.036	4	4	0.5068	158
G288A	0.03333	-4.374 to 4.441	No	>0.9999	0.06667	0.03333	0.03333	1.196	3	3	0.02787	158
G291A	1	-3.408 to 5.408	No	>0.9999	0.1333	-0.8667	1	1.196	3	3	0.836	158
V294A	-0.1	-3.514 to 3.314	No	>0.9999	-3.6	-3.5	-0.1	0.9266	5	5	0.1079	158
L295A	0.8	-3.608 to 5.208	No	>0.9999	0.6	-0.2	0.8	1.196	3	3	0.6688	158

Table Analyzed	**ADP_ATP_100uM_2wayANOVA**				
Two-way ANOVA	Ordinary				
Alpha	0.01				
Source of Variation	% of total variation	P value	Significant?		
Interaction	3.28	0.9728	No		
substrate	0.2981	0.2136	No		
mutation	65.62	<0.0001	Yes		
ANOVA table	SS (Type III)	DF	MS	F (DFn, DFd)	P value
Interaction	28.36	31	0.9149	F (31, 160) = 0.5534	P=0.9728
substrate	2.578	1	2.578	F (1, 160) = 1.559	P=0.2136
mutation	567.4	31	18.3	F (31, 160) = 11.07	P<0.0001
Residual	264.5	160	1.653		
Difference between row means					
Predicted (LS) mean of ŒîTm 100 uM ADP	-1.719				
Predicted (LS) mean of ŒîTm 100 uM ATP	-1.493				
Difference between predicted means	-0.226				
SE of difference	0.181				
Data summary					
Number of columns (mutation)	32				
Number of rows (substrate)	2				
Number of values	224				

Within each row, compare columns (simple effects within rows)

Number of families: 2

Number of comparisons per family: 31

Alpha 0.01

Dunnett's multiple comparisons test	ΔTm 100 µM ADP				ΔTm 100 µM ATP			
	Prd (LS) mean diff.	99.00% CI of diff.	Below threshold?	Adjusted P Value	Prd (LS) mean diff.	99.00% CI of diff.	Below threshold?	Adjusted P Value
wt vs. S29A	-1.479	-5.240 to 2.283	No	0.9684	-0.3357	-4.097 to 3.426	No	0.9997
wt vs. K30A	3.671	0.7310 to 6.612	Yes	0.0003	2.439	-0.5011 to 5.380	No	0.07
wt vs. N85A	2.171	-0.3362 to 4.679	No	0.0478	2.586	0.07816 to 5.093	Yes	0.0067
wt vs. R88A	0.7048	-2.533 to 3.942	No	0.999	0.6476	-2.590 to 3.885	No	0.9991
wt vs. Y89A	-2.029	-5.266 to 1.209	No	0.3975	-0.619	-3.856 to 2.618	No	0.9992
wt vs. T92A	0.5381	-2.699 to 3.775	No	0.9993	0.581	-2.656 to 3.818	No	0.9993
wt vs. Q93A	0.4214	-2.519 to 3.362	No	0.9994	0.2143	-2.726 to 3.155	No	0.9997
wt vs. N96A	1.538	-1.072 to 4.148	No	0.5022	1.748	-0.8623 to 4.358	No	0.2925
wt vs. F97A	-1.062	-4.299 to 2.175	No	0.9932	-0.5524	-3.790 to 2.685	No	0.9993
wt vs. R100A	-0.6619	-3.899 to 2.575	No	0.9991	-0.3524	-3.590 to 2.885	No	0.9996
wt vs. N123A	1.441	-1.305 to 4.188	No	0.6977	1.484	-1.263 to 4.231	No	0.6504
wt vs. S134A	2.338	-0.8992 to 5.575	No	0.1917	2.181	-1.056 to 5.418	No	0.2832
wt vs. L135A	7.038	3.801 to 10.28	Yes	<0.0001	4.614	1.377 to 7.852	Yes	<0.0001
wt vs. V138A	1.571	-1.369 to 4.512	No	0.6687	1.314	-1.626 to 4.255	No	0.8936
wt vs. S189A	0.6214	-3.140 to 4.383	No	0.9993	0.5143	-2.723 to 3.752	No	0.9994
wt vs. G192A	1.671	-2.090 to 5.433	No	0.8987	0.8643	-2.897 to 4.626	No	0.999
wt vs. I193A	3.571	0.6310 to 6.512	Yes	0.0005	3.681	0.4437 to 6.918	Yes	0.0016
wt vs. Y196A	0.2714	-2.966 to 3.509	No	0.9997	-0.5524	-3.790 to 2.685	No	0.9993
wt vs. R197A	-0.9786	-4.740 to 2.783	No	0.9988	-0.6857	-4.447 to 3.076	No	0.9993
wt vs. Y200A	0.4714	-2.766 to 3.709	No	0.9994	0.681	-2.556 to 3.918	No	0.9991

wt vs. Y204A	-0.6952	-3.933 to 2.542	No	0.999	-0.6524	-3.890 to 2.585	No	0.9991
wt vs. V230A	-0.5952	-3.833 to 2.642	No	0.9992	-0.319	-3.556 to 2.918	No	0.9996
wt vs. T231A	0.004762	-3.233 to 3.242	No	>0.9999	0.181	-3.056 to 3.418	No	0.9998
wt vs. G235A	0.2381	-2.999 to 3.475	No	0.9997	0.5143	-2.723 to 3.752	No	0.9994
wt vs. S238A	0.02143	-3.740 to 3.783	No	>0.9999	0.5643	-3.197 to 4.326	No	0.9994
wt vs. R246A	2.546	-0.3940 to 5.487	No	0.0478	0.7893	-2.151 to 3.730	No	0.9987
wt vs. R287A	3.746	0.8060 to 6.687	Yes	0.0002	2.664	-0.2761 to 5.605	No	0.0307
wt vs. G288A	0.07143	-3.166 to 3.309	No	>0.9999	-0.08571	-3.323 to 3.152	No	>0.9999
wt vs. G291A	1.005	-2.233 to 4.242	No	0.9938	1.114	-2.123 to 4.352	No	0.9924
wt vs. V294A	3.791	1.045 to 6.538	Yes	<0.0001	4.074	1.327 to 6.821	Yes	<0.0001
wt vs. L295A	-0.2619	-3.499 to 2.975	No	0.9997	-0.2524	-3.490 to 2.985	No	0.9997

	ΔTm 100 µM ADP								ΔTm 100 µM ATP							
Test details	Prd (LS) mean 1	Prd (LS) mean 2	Prd (LS) mean diff.	SE of diff.	N1	N2	q	DF	Prd (LS) mean 1	Prd (LS) mean 2	Prd (LS) mean diff.	SE of diff.	N1	N2	q	DF
wt vs. S29A	-0.7286	0.75	-1.479	1.031	7	2	1.434	160	-0.5857	-0.25	-0.3357	1.031	7	2	0.3256	160
wt vs. K30A	-0.7286	-4.4	3.671	0.8059	7	4	4.556	160	-0.5857	-3.025	2.439	0.8059	7	4	3.027	160
wt vs. N85A	-0.7286	-2.9	2.171	0.6873	7	7	3.159	160	-0.5857	-3.171	2.586	0.6873	7	7	3.762	160
wt vs. R88A	-0.7286	-1.433	0.7048	0.8873	7	3	0.7943	160	-0.5857	-1.233	0.6476	0.8873	7	3	0.7299	160
wt vs. Y89A	-0.7286	1.3	-2.029	0.8873	7	3	2.286	160	-0.5857	0.03333	-0.619	0.8873	7	3	0.6977	160
wt vs. T92A	-0.7286	-1.267	0.5381	0.8873	7	3	0.6065	160	-0.5857	-1.167	0.581	0.8873	7	3	0.6548	160
wt vs. Q93A	-0.7286	-1.15	0.4214	0.8059	7	4	0.5229	160	-0.5857	-0.8	0.2143	0.8059	7	4	0.2659	160
wt vs. N96A	-0.7286	-2.267	1.538	0.7153	7	6	2.15	160	-0.5857	-2.333	1.748	0.7153	7	6	2.443	160
wt vs. F97A	-0.7286	0.3333	-1.062	0.8873	7	3	1.197	160	-0.5857	-0.03333	-0.5524	0.8873	7	3	0.6226	160
wt vs. R100A	-0.7286	-0.06667	-0.6619	0.8873	7	3	0.746	160	-0.5857	-0.2333	-0.3524	0.8873	7	3	0.3971	160
wt vs. N123A	-0.7286	-2.17	1.441	0.7529	7	5	1.915	160	-0.5857	-2.07	1.484	0.7529	7	5	1.971	160
wt vs. S134A	-0.7286	-3.067	2.338	0.8873	7	3	2.635	160	-0.5857	-2.767	2.181	0.8873	7	3	2.458	160
wt vs. L135A	-0.7286	-7.767	7.038	0.8873	7	3	7.932	160	-0.5857	-5.2	4.614	0.8873	7	3	5.2	160
wt vs. V138A	-0.7286	-2.3	1.571	0.8059	7	4	1.95	160	-0.5857	-1.9	1.314	0.8059	7	4	1.631	160
wt vs. S189A	-0.7286	-1.35	0.6214	1.031	7	2	0.6028	160	-0.5857	-1.1	0.5143	0.8873	7	3	0.5796	160

wt vs. G192A	-0.7286	-2.4	1.671	1.031	7	2	1.621	160	-0.5857	-1.45	0.8643	1.031	7	2	0.8384	160
wt vs. I193A	-0.7286	-4.3	3.571	0.8059	7	4	4.432	160	-0.5857	-4.267	3.681	0.8873	7	3	4.149	160
wt vs. Y196A	-0.7286	-1	0.2714	0.8873	7	3	0.3059	160	-0.5857	-0.03333	-0.5524	0.8873	7	3	0.6226	160
wt vs. R197A	-0.7286	0.25	-0.9786	1.031	7	2	0.9492	160	-0.5857	0.1	-0.6857	1.031	7	2	0.6651	160
wt vs. Y200A	-0.7286	-1.2	0.4714	0.8873	7	3	0.5313	160	-0.5857	-1.267	0.681	0.8873	7	3	0.7675	160
wt vs. Y204A	-0.7286	-0.03333	-0.6952	0.8873	7	3	0.7836	160	-0.5857	0.06667	-0.6524	0.8873	7	3	0.7353	160
wt vs. V230A	-0.7286	-0.1333	-0.5952	0.8873	7	3	0.6709	160	-0.5857	-0.2667	-0.319	0.8873	7	3	0.3596	160
wt vs. T231A	-0.7286	-0.7333	0.00476	0.8873	7	3	0.00537	160	-0.5857	-0.7667	0.181	0.8873	7	3	0.2039	160
wt vs. G235A	-0.7286	-0.9667	0.2381	0.8873	7	3	0.2683	160	-0.5857	-1.1	0.5143	0.8873	7	3	0.5796	160
wt vs. S238A	-0.7286	-0.75	0.02143	1.031	7	2	0.02079	160	-0.5857	-1.15	0.5643	1.031	7	2	0.5474	160
wt vs. R246A	-0.7286	-3.275	2.546	0.8059	7	4	3.16	160	-0.5857	-1.375	0.7893	0.8059	7	4	0.9794	160
wt vs. R287A	-0.7286	-4.475	3.746	0.8059	7	4	4.649	160	-0.5857	-3.25	2.664	0.8059	7	4	3.306	160
wt vs. G288A	-0.7286	-0.8	0.07143	0.8873	7	3	0.0805	160	-0.5857	-0.5	-0.08571	0.8873	7	3	0.0966	160
wt vs. G291A	-0.7286	-1.733	1.005	0.8873	7	3	1.132	160	-0.5857	-1.7	1.114	0.8873	7	3	1.256	160
wt vs. V294A	-0.7286	-4.52	3.791	0.7529	7	5	5.036	160	-0.5857	-4.66	4.074	0.7529	7	5	5.412	160
wt vs. L295A	-0.7286	-0.4667	-0.2619	0.8873	7	3	0.2952	160	-0.5857	-0.3333	-0.2524	0.8873	7	3	0.2844	160

Compare each cell mean with the other cell mean in that column

Number of families: 1

Number of comparisons per family: 32

Alpha 0.01

ΔTm 100 µM ADP - ΔTm 100 µM ATP

Sidak's multiple comparisons test	Prd (LS) mean diff.	99.00% CI of diff.	Below threshold ?	Adjusted P Value	Prd (LS) mean 1	Prd (LS) mean 2	Prd (LS) mean diff.	SE of diff.	N1	N2	t	DF
wild type	-0.1429	-2.675 to 2.389	No	>0.9999	-0.7286	-0.5857	-0.1429	0.6873	7	7	0.2079	160
S29A	1	-3.737 to 5.737	No	>0.9999	0.75	-0.25	1	1.286	2	2	0.7777	160
K30A	-1.375	-4.724 to 1.974	No	0.9894	-4.4	-3.025	-1.375	0.9092	4	4	1.512	160
N85A	0.2714	-2.260 to 2.803	No	>0.9999	-2.9	-3.171	0.2714	0.6873	7	7	0.3949	160
R88A	-0.2	-4.067 to 3.667	No	>0.9999	-1.433	-1.233	-0.2	1.05	3	3	0.1905	160
Y89A	1.267	-2.601 to 5.134	No	0.9998	1.3	0.03333	1.267	1.05	3	3	1.207	160
T92A	-0.1	-3.967 to 3.767	No	>0.9999	-1.267	-1.167	-0.1	1.05	3	3	0.09525	160
Q93A	-0.35	-3.699 to 2.999	No	>0.9999	-1.15	-0.8	-0.35	0.9092	4	4	0.385	160
N96A	0.06667	-2.668 to 2.801	No	>0.9999	-2.267	-2.333	0.06667	0.7424	6	6	0.0898	160
F97A	0.3667	-3.501 to 4.234	No	>0.9999	0.3333	-0.03333	0.3667	1.05	3	3	0.3493	160
R100A	0.1667	-3.701 to 4.034	No	>0.9999	-0.0667	-0.2333	0.1667	1.05	3	3	0.1588	160
N123A	-0.1	-3.096 to 2.896	No	>0.9999	-2.17	-2.07	-0.1	0.8132	5	5	0.123	160
S134A	-0.3	-4.167 to 3.567	No	>0.9999	-3.067	-2.767	-0.3	1.05	3	3	0.2858	160
L135A	-2.567	-6.434 to 1.301	No	0.3949	-7.767	-5.2	-2.567	1.05	3	3	2.445	160
V138A	-0.4	-3.749 to 2.949	No	>0.9999	-2.3	-1.9	-0.4	0.9092	4	4	0.44	160
S189A	-0.25	-4.574 to 4.074	No	>0.9999	-1.35	-1.1	-0.25	1.174	2	3	0.213	160
G192A	-0.95	-5.687 to 3.787	No	>0.9999	-2.4	-1.45	-0.95	1.286	2	2	0.7388	160
I193A	-0.03333	-3.651 to 3.584	No	>0.9999	-4.3	-4.267	-0.03333	0.982	4	3	0.03394	160
Y196A	-0.9667	-4.834 to 2.901	No	>0.9999	-1	-0.03333	-0.9667	1.05	3	3	0.9208	160
R197A	0.15	-4.587 to 4.887	No	>0.9999	0.25	0.1	0.15	1.286	2	2	0.1167	160

Y200A	0.06667	-3.801 to 3.934	No	>0.9999	-1.2	-1.267	0.06667	1.05	3	3	0.0635	160
Y204A	-0.1	-3.967 to 3.767	No	>0.9999	-0.0333	0.06667	-0.1	1.05	3	3	0.09525	160
V230A	0.1333	-3.734 to 4.001	No	>0.9999	-0.1333	-0.2667	0.1333	1.05	3	3	0.127	160
T231A	0.03333	-3.834 to 3.901	No	>0.9999	-0.7333	-0.7667	0.03333	1.05	3	3	0.03175	160
G235A	0.1333	-3.734 to 4.001	No	>0.9999	-0.9667	-1.1	0.1333	1.05	3	3	0.127	160
S238A	0.4	-4.337 to 5.137	No	>0.9999	-0.75	-1.15	0.4	1.286	2	2	0.3111	160
R246A	-1.9	-5.249 to 1.449	No	0.7126	-3.275	-1.375	-1.9	0.9092	4	4	2.09	160
R287A	-1.225	-4.574 to 2.124	No	0.9982	-4.475	-3.25	-1.225	0.9092	4	4	1.347	160
G288A	-0.3	-4.167 to 3.567	No	>0.9999	-0.8	-0.5	-0.3	1.05	3	3	0.2858	160
G291A	-0.03333	-3.901 to 3.834	No	>0.9999	-1.733	-1.7	-0.03333	1.05	3	3	0.03175	160
V294A	0.14	-2.856 to 3.136	No	>0.9999	-4.52	-4.66	0.14	0.8132	5	5	0.1722	160
L295A	-0.1333	-4.001 to 3.734	No	>0.9999	-0.4667	-0.3333	-0.1333	1.05	3	3	0.127	160

Appendix 4: Representative gels (at least one experiment for each protein shown) for the quantification of transport assays

Liposome samples eluted from the PD10 column (and used for uptake assays) were separated on 4-12% SDS-PAGE gels. The gels were stained with InstantBlue coomassie stain. The last gel shown was stained with Flamingo fluorescent gel stain (Bio-Rad, Watford, Hertfordshire, UK).

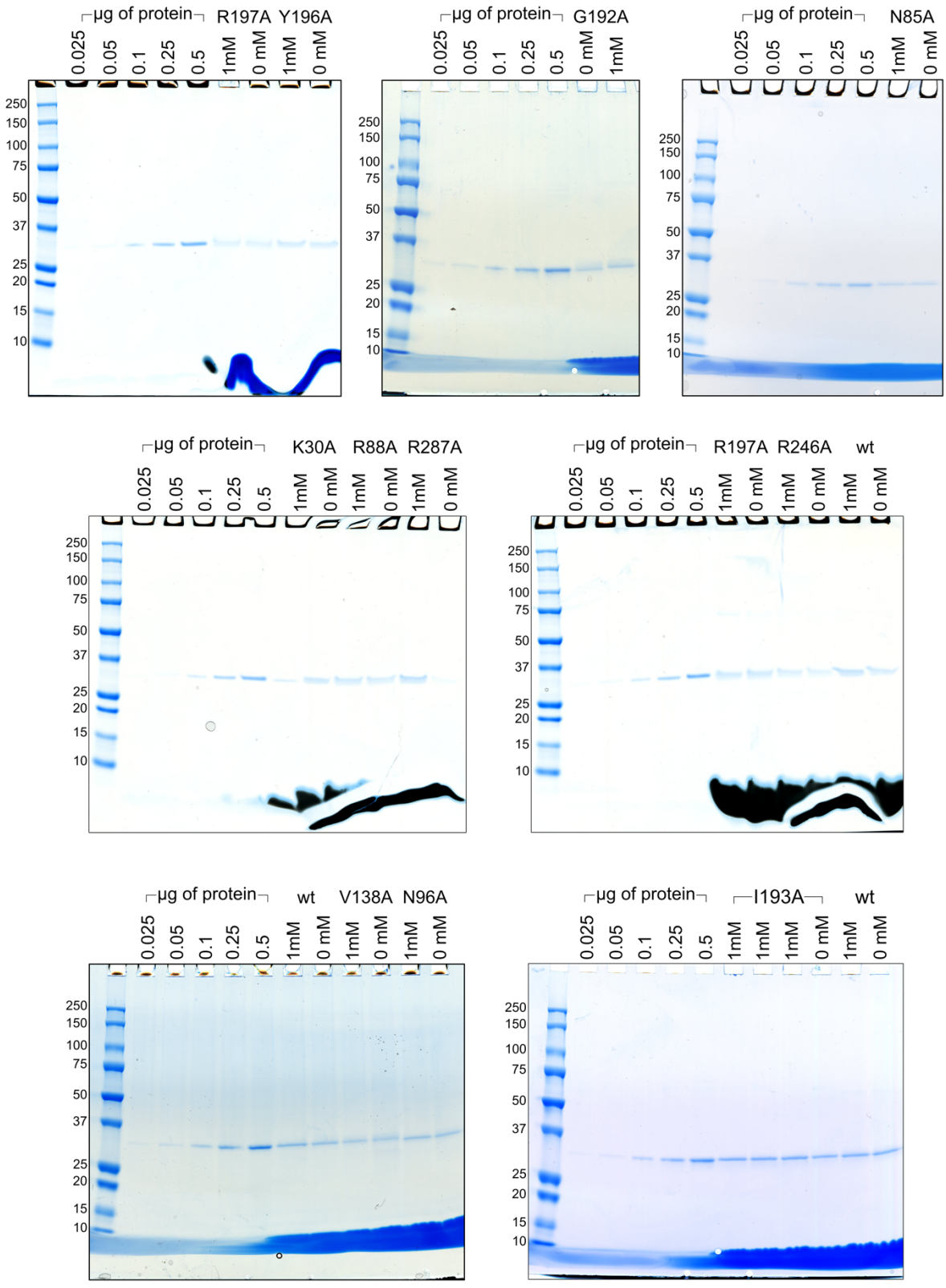
µg of protein
R197A Y196A
G192A
N85A
K30A R88A R287A
R197A R246A wt
wt V138A N96A
I193A wt
0.025 0.05 0.1 0.25 0.5 1mM 0 mM
250 150 100 75 50 37 25 20 15 10

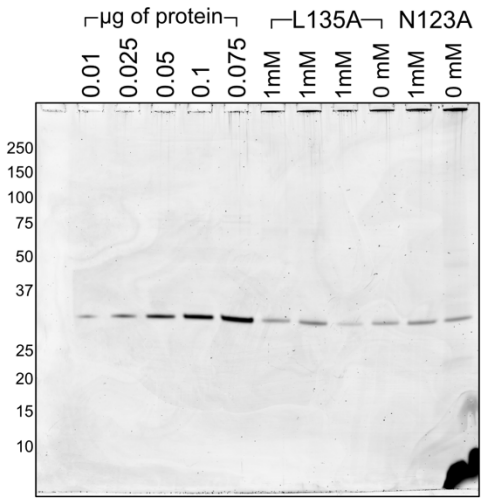
µg of protein
L135A
N123A
0.01
0.025
0.05
0.1
0.075
1mM
1mM
1mM
0 mM
1mM
0 mM
250
150
100
75
50
37
25
20
15
10

References

Abrahams, J.P., Leslie, A.G., Lutter, R., and Walker, J.E. (1994). Structure at 2.8 A resolution of F1-ATPase from bovine heart mitochondria. Nature *370*, 621-628.

Abrahamsen, M.S., Templeton, T.J., Enomoto, S., Abrahante, J.E., Zhu, G., Lancto, C.A., Deng, M., Liu, C., Widmer, G., Tzipori, S., et al. (2004). Complete genome sequence of the apicomplexan, *Cryptosporidium parvum*. Science *304*, 441-445.

Abrams, A.J., Hufnagel, R.B., Rebelo, A., Zanna, C., Patel, N., Gonzalez, M.A., Campeanu, I.J., Griffin, L.B., Groenewald, S., Strickland, A.V., et al. (2015). Mutations in SLC25A46, encoding a UGO1-like protein, cause an optic atrophy spectrum disorder. Nat Genet *47*, 926-932.

Agip, A.A., Blaza, J.N., Fedor, J.G., and Hirst, J. (2019). Mammalian Respiratory Complex I Through the Lens of Cryo-EM. Annu Rev Biophys *48*, 165-184.

Agrimi, G., Di Noia, M.A., Marobbio, C.M., Fiermonte, G., Lasorsa, F.M., and Palmieri, F. (2004). Identification of the human mitochondrial S-adenosylmethionine transporter: bacterial expression, reconstitution, functional characterization and tissue distribution. Biochem J *379*, 183-190.

Alevriadou, B.R., Patel, A., Noble, M., Ghosh, S., Gohil, V.M., Stathopulos, P.B., and Madesh, M. (2021). Molecular nature and physiological role of the mitochondrial calcium uniporter channel. Am J Physiol Cell Physiol *320*, C465-C482.

Alexandrov, A.I., Mileni, M., Chien, E.Y., Hanson, M.A., and Stevens, R.C. (2008). Microscale fluorescent thermal stability assay for membrane proteins. Structure *16*, 351-359.

Anderson, S., Bankier, A.T., Barrell, B.G., de Bruijn, M.H., Coulson, A.R., Drouin, J., Eperon, I.C., Nierlich, D.P., Roe, B.A., Sanger, F., et al. (1981). Sequence and organization of the human mitochondrial genome. Nature *290*, 457-465.

Aquila, H., Misra, D., Eulitz, M., and Klingenberg, M. (1982). Complete amino acid sequence of the ADP/ATP carrier from beef heart mitochondria. Hoppe Seylers Z Physiol Chem *363*, 345-349.

Austin, J., and Aprille, J.R. (1984). Carboxyatractyloside-insensitive influx and efflux of adenine nucleotides in rat liver mitochondria. J Biol Chem *259*, 154-160.

Axelrod, H.L., Feher, G., Allen, J.P., Chirino, A.J., Day, M.W., Hsu, B.T., and Rees, D.C. (1994). Crystallization and X-ray structure determination of cytochrome c2 from Rhodobacter sphaeroides in three crystal forms. Acta Crystallogr D Biol Crystallogr *50*, 596-602.

Babot, M., Blancard, C., Pelosi, L., Lauquin, G.J., and Trézéguet, V. (2012). The transmembrane prolines of the mitochondrial ADP/ATP carrier are involved in nucleotide binding and transport and its biogenesis. J Biol Chem *287*, 10368-10378.

Baines, C.P., and Gutierrez-Aguilar, M. (2018). The still uncertain identity of the channel-forming unit(s) of the mitochondrial permeability transition pore. Cell Calcium *73*, 121-130.

Bamber, L., Harding, M., Butler, P.J., and Kunji, E.R. (2006). Yeast mitochondrial ADP/ATP carriers are monomeric in detergents. Proc Natl Acad Sci U S A *103*, 16224-16229.

Bamber, L., Harding, M., Monné, M., Slotboom, D.J., and Kunji, E.R. (2007a). The yeast mitochondrial ADP/ATP carrier functions as a monomer in mitochondrial membranes. Proc Natl Acad Sci U S A *104*, 10830-10834.

Bamber, L., Slotboom, D.J., and Kunji, E.R. (2007b). Yeast mitochondrial ADP/ATP carriers are monomeric in detergents as demonstrated by differential affinity purification. J Mol Biol *371*, 388-395.

Bankier, A.T., Spriggs, H.F., Fartmann, B., Konfortov, B.A., Madera, M., Vogel, C., Teichmann, S.A., Ivens, A., and Dear, P.H. (2003). Integrated mapping, chromosomal sequencing and sequence analysis of *Cryptosporidium parvum*. Genome Res *13*, 1787-1799.

Baradaran, R., Berrisford, J.M., Minhas, G.S., and Sazanov, L.A. (2013). Crystal structure of the entire respiratory complex I. Nature *494*, 443-448.

Baughman, J.M., Perocchi, F., Girgis, H.S., Plovanich, M., Belcher-Timme, C.A., Sancak, Y., Bao, X.R., Strittmatter, L., Goldberger, O., Bogorad, R.L., et al. (2011). Integrative genomics identifies MCU as an essential component of the mitochondrial calcium uniporter. Nature *476*, 341-345.

Bazzone, A., and Barthmes, M. (2020). Functional Characterization of SLC Transporters Using Solid Supported Membranes. Methods Mol Biol *2168*, 73-103.

Bazzone, A., Barthmes, M., and Fendler, K. (2017). SSM-Based Electrophysiology for Transporter Research. Methods Enzymol *594*, 31-83.

Benz R, P.B., Wiesner P, Schmid A (1995). The mitochondrial porins. Progress in Cell Research *Volume 5*, 107-112.

Berman, H.M., Westbrook, J., Feng, Z., Gilliland, G., Bhat, T.N., Weissig, H., Shindyalov, I.N., and Bourne, P.E. (2000). The Protein Data Bank. Nucleic Acids Res *28*, 235-242.

Bertholet, A.M., Chouchani, E.T., Kazak, L., Angelin, A., Fedorenko, A., Long, J.Z., Vidoni, S., Garrity, R., Cho, J., Terada, N., et al. (2019). H(+) transport is an integral function of the mitochondrial ADP/ATP carrier. Nature *571*, 515-520.

Bertholet, A.M., and Kirichok, Y. (2021). Mitochondrial H(+) Leak and Thermogenesis. Annu Rev Physiol.

Bolla, J.R., Agasid, M.T., Mehmood, S., and Robinson, C.V. (2019). Membrane Protein-Lipid Interactions Probed Using Mass Spectrometry. Annu Rev Biochem *88*, 85-111.

Boore, J.L. (1999). Animal mitochondrial genomes. Nucleic Acids Res *27*, 1767-1780.

Booty, L.M., King, M.S., Thangaratnarajah, C., Majd, H., James, A.M., Kunji, E.R., and Murphy, M.P. (2015). The mitochondrial dicarboxylate and 2-oxoglutarate carriers do not transport glutathione. FEBS Lett *589*, 621-628.

Bouzid, M., Hunter, P.R., Chalmers, R.M., and Tyler, K.M. (2013). Cryptosporidium pathogenicity and virulence. Clin Microbiol Rev *26*, 115-134.

Brand, M.D., Pakay, J.L., Ocloo, A., Kokoszka, J., Wallace, D.C., Brookes, P.S., and Cornwall, E.J. (2005). The basal proton conductance of mitochondria depends on adenine nucleotide translocase content. Biochem J *392*, 353-362.

Bravo-Sagua, R., Parra, V., Lopez-Crisosto, C., Diaz, P., Quest, A.F., and Lavandero, S. (2017). Calcium Transport and Signaling in Mitochondria. Compr Physiol *7*, 623-634.

Bricker, D.K., Taylor, E.B., Schell, J.C., Orsak, T., Boutron, A., Chen, Y.C., Cox, J.E., Cardon, C.M., Van Vranken, J.G., Dephoure, N., et al. (2012). A mitochondrial pyruvate carrier required for pyruvate uptake in yeast, Drosophila, and humans. Science *337*, 96-100.

Bruni, A., and Luciani, S. (1962). Effects of atractyloside and oligomycin on magnesium-stimulated adenosine triphosphatase and on adenosine triphosphate-induced contraction of swollen mitochondria. Nature *196*, 578-580.

Bruni, A., Luciani, S., and Contessa, A.R. (1964). Inhibition by Atractyloside of the Binding of Adenine-Nucleotides to Rat-Liver Mitochondria. Nature *201*, 1219-1220.

Brustovetsky, N. (2020). The Role of Adenine Nucleotide Translocase in the Mitochondrial Permeability Transition. Cells *9*.

Brustovetsky, N., Becker, A., Klingenberg, M., and Bamberg, E. (1996). Electrical currents associated with nucleotide transport by the reconstituted mitochondrial ADP/ATP carrier. Proc Natl Acad Sci U S A *93*, 664-668.

Brustovetsky, N., and Klingenberg, M. (1994). The reconstituted ADP/ATP carrier can mediate H+ transport by free fatty acids, which is further stimulated by mersalyl. J Biol Chem *269*, 27329-27336.

Carrer, A., Laquatra, C., Tommasin, L., and Carraro, M. (2021). Modulation and Pharmacology of the Mitochondrial Permeability Transition: A Journey from F-ATP Synthase to ANT. Molecules *26*.

Cavero, S., Vozza, A., del Arco, A., Palmieri, L., Villa, A., Blanco, E., Runswick, M.J., Walker, J.E., Cerdan, S., Palmieri, F., and Satrustegui, J. (2003). Identification and metabolic role of the mitochondrial aspartate-glutamate transporter in *Saccharomyces cerevisiae*. Mol Microbiol *50*, 1257-1269.

Chalmers, R.M., and Davies, A.P. (2010). Minireview: clinical cryptosporidiosis. Exp Parasitol *124*, 138-146.

Chan, K.W., Slotboom, D.J., Cox, S., Embley, T.M., Fabre, O., van der Giezen, M., Harding, M., Horner, D.S., Kunji, E.R., Leon-Avila, G., and Tovar, J. (2005). A novel ADP/ATP transporter in the mitosome of the microaerophilic human parasite Entamoeba histolytica. Curr Biol *15*, 737-742.

Chan, S.H., and Barbour, R.L. (1983). Adenine nucleotide transport in hepatoma mitochondria. Characterization of factors influencing the kinetics of ADP and ATP uptake. Biochim Biophys Acta *723*, 104-113.

Chen, X.J. (2004). Sal1p, a calcium-dependent carrier protein that suppresses an essential cellular function associated With the Aac2 isoform of ADP/ATP translocase in *Saccharomyces cerevisiae*. Genetics *167*, 607-617.

Chorev, D.S., Baker, L.A., Wu, D., Beilsten-Edmands, V., Rouse, S.L., Zeev-Ben-Mordehai, T., Jiko, C., Samsudin, F., Gerle, C., Khalid, S., et al. (2018). Protein assemblies ejected directly from native membranes yield complexes for mass spectrometry. Science *362*, 829-834.

Chorev, D.S., and Robinson, C.V. (2019). Response to Comment on "Protein assemblies ejected directly from native membranes yield complexes for mass spectrometry". Science *366*.

Claypool, S.M. (2009). Cardiolipin, a critical determinant of mitochondrial carrier protein assembly and function. Biochim Biophys Acta *1788*, 2059-2068.

Clemencon, B. (2012). Yeast mitochondrial interactosome model: metabolon membrane proteins complex involved in the channeling of ADP/ATP. Int J Mol Sci *13*, 1858-1885.

Cozens, A.L., Runswick, M.J., and Walker, J.E. (1989). DNA sequences of two expressed nuclear genes for human mitochondrial ADP/ATP translocase. J Mol Biol *206*, 261-280.

Crichton, P.G., Harding, M., Ruprecht, J.J., Lee, Y., and Kunji, E.R. (2013). Lipid, detergent, and Coomassie Blue G-250 affect the migration of small membrane proteins in blue native gels: mitochondrial carriers migrate as monomers not dimers. J Biol Chem *288*, 22163-22173.

Crichton, P.G., Lee, Y., Ruprecht, J.J., Cerson, E., Thangaratnarajah, C., King, M.S., and Kunji, E.R. (2015). Trends in thermostability provide information on the nature of substrate, inhibitor, and lipid interactions with mitochondrial carriers. J Biol Chem *290*, 8206-8217.

Cunningham, B.C., and Wells, J.A. (1989). High-resolution epitope mapping of hGH-receptor interactions by alanine-scanning mutagenesis. Science *244*, 1081-1085.

Curran-Everett, D. (2000). Multiple comparisons: philosophies and illustrations. Am J Physiol Regul Integr Comp Physiol *279*, R1-8.

Dalbon, P., Brandolin, G., Boulay, F., Hoppe, J., and Vignais, P.V. (1988). Mapping of the nucleotide-binding sites in the ADP/ATP carrier of beef heart mitochondria by photolabeling with 2-azido[alpha-32P]adenosine diphosphate. Biochemistry *27*, 5141-5149.

David, C., Arnou, B., Sanchez, J.F., Pelosi, L., Brandolin, G., Lauquin, G.J., and Trézéguet, V. (2008). Two residues of a conserved aromatic ladder of the mitochondrial ADP/ATP carrier are crucial to nucleotide transport. Biochemistry *47*, 13223-13231.

Davies, K.M., Anselmi, C., Wittig, I., Faraldo-Gomez, J.D., and Kuhlbrandt, W. (2012). Structure of the yeast F1Fo-ATP synthase dimer and its role in shaping the mitochondrial cristae. Proc Natl Acad Sci U S A *109*, 13602-13607.

De Marcos Lousa, C., Trezeguet, V., Dianoux, A.C., Brandolin, G., and Lauquin, G.J. (2002). The human mitochondrial ADP/ATP carriers: kinetic properties and biogenesis of wild-type and mutant proteins in the yeast S. *cerevisiae*. Biochemistry *41*, 14412-14420.

de Ruyter, P.G., Kuipers, O.P., and de Vos, W.M. (1996). Controlled gene expression systems for Lactococcus lactis with the food-grade inducer nisin. Appl Environ Microbiol *62*, 3662-3667.

De Stefani, D., Raffaello, A., Teardo, E., Szabo, I., and Rizzuto, R. (2011). A forty-kilodalton protein of the inner membrane is the mitochondrial calcium uniporter. Nature *476*, 336-340.

Dehez, F., Pebay-Peyroula, E., and Chipot, C. (2008). Binding of ADP in the mitochondrial ADP/ATP carrier is driven by an electrostatic funnel. J Am Chem Soc *130*, 12725-12733.

del Arco, A., and Satrustegui, J. (2004). Identification of a novel human subfamily of mitochondrial carriers with calcium-binding domains. J Biol Chem *279*, 24701-24713.

DeSantis, K., Reed, A., Rahhal, R., and Reinking, J. (2012). Use of differential scanning fluorimetry as a high-throughput assay to identify nuclear receptor ligands. Nucl Recept Signal *10*, e002.

Di Noia, M.A., Todisco, S., Cirigliano, A., Rinaldi, T., Agrimi, G., Iacobazzi, V., and Palmieri, F. (2014). The human SLC25A33 and SLC25A36 genes of solute carrier family 25 encode two mitochondrial pyrimidine nucleotide transporters. J Biol Chem *289*, 33137-33148.

Dianoux, A.C., Noël, F., Fiore, C., Trézéguet, V., Kieffer, S., Jaquinod, M., Lauquin, G.J., and Brandolin, G. (2000). Two distinct regions of the yeast mitochondrial ADP/ATP carrier are photolabeled by a new ADP analogue: 2-azido-3'-O-naphthoyl-[beta-32P]ADP. Identification of the binding segments by mass spectrometry. Biochemistry *39*, 11477-11487.

Dienhart, M.K., and Stuart, R.A. (2008). The yeast Aac2 protein exists in physical association with the cytochrome bc1-COX supercomplex and the TIM23 machinery. Mol Biol Cell *19*, 3934-3943.

Dolce, V., Scarcia, P., Iacopetta, D., and Palmieri, F. (2005). A fourth ADP/ATP carrier isoform in man: identification, bacterial expression, functional characterization and tissue distribution. FEBS Lett *579*, 633-637.

Duee, E.D., and Vignais, P.V. (1969). Kinetics and specificity of the adenine nucleotide translocation in rat liver mitochondria. J Biol Chem *244*, 3920-3931.

Duyckaerts, C., Sluse-Goffart, C.M., Fux, J.P., Sluse, F.E., and Liebecq, C. (1980). Kinetic mechanism of the exchanges catalysed by the adenine-nucleotide carrier. Eur J Biochem *106*, 1-6.

Edman, P. (1949). A method for the determination of amino acid sequence in peptides. Arch Biochem *22*, 475.

Erdelt, H., Weidemann, M.J., Buchholz, M., and Klingenberg, M. (1972). Some principle effects of bongkrekic acid on the binding of adenine nucleotides to mitochondrial membranes. Eur J Biochem *30*, 107-122.

Errey, J.C., Doré, A.S., Zhukov, A., Marshall, F.H., and Cooke, R.M. (2015). Purification of Stabilized GPCRs for Structural and Biophysical Analyses. Methods Mol Biol *1335*, 1-15.

Estaquier, J., Vallette, F., Vayssiere, J.L., and Mignotte, B. (2012). The mitochondrial pathways of apoptosis. Adv Exp Med Biol *942*, 157-183.

Fiermonte, G., De Leonardis, F., Todisco, S., Palmieri, L., Lasorsa, F.M., and Palmieri, F. (2004). Identification of the mitochondrial ATP-Mg/Pi transporter. Bacterial expression, reconstitution, functional characterization, and tissue distribution. J Biol Chem *279*, 30722-30730.

Fiermonte, G., Dolce, V., David, L., Santorelli, F.M., Dionisi-Vici, C., Palmieri, F., and Walker, J.E. (2003). The mitochondrial ornithine transporter. Bacterial expression, reconstitution, functional characterization, and tissue distribution of two human isoforms. J Biol Chem *278*, 32778-32783.

Fiermonte, G., Dolce, V., Palmieri, L., Ventura, M., Runswick, M.J., Palmieri, F., and Walker, J.E. (2001). Identification of the human mitochondrial oxodicarboxylate carrier. Bacterial expression, reconstitution, functional characterization, tissue distribution, and chromosomal location. J Biol Chem *276*, 8225-8230.

Fiermonte, G., Palmieri, L., Todisco, S., Agrimi, G., Palmieri, F., and Walker, J.E. (2002). Identification of the mitochondrial glutamate transporter. Bacterial expression, reconstitution, functional characterization, and tissue distribution of two human isoforms. J Biol Chem *277*, 19289-19294.

Fiermonte, G., Paradies, E., Todisco, S., Marobbio, C.M., and Palmieri, F. (2009). A novel member of solute carrier family 25 (SLC25A42) is a transporter of coenzyme A and adenosine 3',5'-diphosphate in human mitochondria. J Biol Chem *284*, 18152-18159.

Fontanesi, F., Palmieri, L., Scarcia, P., Lodi, T., Donnini, C., Limongelli, A., Tiranti, V., Zeviani, M., Ferrero, I., and Viola, A.M. (2004). Mutations in AAC2, equivalent to human adPEO-associated ANT1 mutations, lead to defective oxidative phosphorylation in *Saccharomyces cerevisiae* and affect mitochondrial DNA stability. Hum Mol Genet *13*, 923-934.

Foury, F., Roganti, T., Lecrenier, N., and Purnelle, B. (1998). The complete sequence of the mitochondrial genome of S*accharomyces cerevisiae*. FEBS Lett *440*, 325-331.

Freel, K.C., Friedrich, A., and Schacherer, J. (2015). Mitochondrial genome evolution in yeasts: an all-encompassing view. FEMS Yeast Res *15*, fov023.

Frey, T.G., Renken, C.W., and Perkins, G.A. (2002). Insight into mitochondrial structure and function from electron tomography. Biochim Biophys Acta *1555*, 196-203.

Funai, K., Summers, S.A., and Rutter, J. (2020). Reign in the membrane: How common lipids govern mitochondrial function. Curr Opin Cell Biol *63*, 162-173.

Gawaz, M., Douglas, M.G., and Klingenberg, M. (1990). Structure-function studies of adenine nucleotide transport in mitochondria. II. Biochemical analysis of distinct AAC1 and AAC2 proteins in yeast. J Biol Chem *265*, 14202-14208.

Geertsma, E.R., Nik Mahmood, N.A., Schuurman-Wolters, G.K., and Poolman, B. (2008). Membrane reconstitution of ABC transporters and assays of translocator function. Nat Protoc *3*, 256-266.

Giacomello, M., Pyakurel, A., Glytsou, C., and Scorrano, L. (2020). The cell biology of mitochondrial membrane dynamics. Nat Rev Mol Cell Biol *21*, 204-224.

Gietz, R.D., and Schiestl, R.H. (2007). High-efficiency yeast transformation using the LiAc/SS carrier DNA/PEG method. Nat Protoc *2*, 31-34.

Girardi, E., Agrimi, G., Goldmann, U., Fiume, G., Lindinger, S., Sedlyarov, V., Srndic, I., Gurtl, B., Agerer, B., Kartnig, F., et al. (2020). Epistasis-driven identification of SLC25A51 as a regulator of human mitochondrial NAD import. Nat Commun *11*, 6145.

Gropp, T., Brustovetsky, N., Klingenberg, M., Müller, V., Fendler, K., and Bamberg, E. (1999). Kinetics of electrogenic transport by the ADP/ATP carrier. Biophys J *77*, 714-726.

Habibzadeh, F., and Habibzadeh, P. (2015). How much precision in reporting statistics is enough? Croat Med J *56*, 490-492.

Halestrap, A.P. (2009). What is the mitochondrial permeability transition pore? J Mol Cell Cardiol *46*, 821-831.

Harborne, S.P., King, M.S., Crichton, P.G., and Kunji, E.R. (2017). Calcium regulation of the human mitochondrial ATP-Mg/Pi carrier SLC25A24 uses a locking pin mechanism. Sci Rep *7*, 45383.

Harborne, S.P., Ruprecht, J.J., and Kunji, E.R. (2015). Calcium-induced conformational changes in the regulatory domain of the human mitochondrial ATP-Mg/Pi carrier. Biochim Biophys Acta *1847*, 1245-1253.

Hashimoto, M., Shinohara, Y., Majima, E., Hatanaka, T., Yamazaki, N., and Terada, H. (1999). Expression of the bovine heart mitochondrial ADP/ATP carrier in yeast mitochondria: significantly enhanced expression by replacement of the N-terminal region of the bovine carrier by the corresponding regions of the yeast carriers. Biochim Biophys Acta *1409*, 113-124.

Hattori, M., Hibbs, R.E., and Gouaux, E. (2012). A fluorescence-detection size-exclusion chromatography-based thermostability assay for membrane protein precrystallization screening. Structure *20*, 1293-1299.

Heidkämper, D., Müller, V., Nelson, D.R., and Klingenberg, M. (1996). Probing the role of positive residues in the ADP/ATP carrier from yeast. The effect of six arginine mutations on transport and the four ATP versus ADP exchange modes. Biochemistry *35*, 16144-16152.

Heimpel, S., Basset, G., Odoy, S., and Klingenberg, M. (2001). Expression of the mitochondrial ADP/ATP carrier in *Escherichia coli*. Renaturation, reconstitution, and the effect of mutations on 10 positive residues. J Biol Chem *276*, 11499-11506.

Henderson, P.J., and Lardy, H.A. (1970). Bongkrekic acid. An inhibitor of the adenine nucleotide translocase of mitochondria. J Biol Chem *245*, 1319-1326.

Henriquez, F.L., Richards, T.A., Roberts, F., McLeod, R., and Roberts, C.W. (2005). The unusual mitochondrial compartment of *Cryptosporidium parvum.* Trends Parasitol *21*, 68-74.

Herzig, S., Raemy, E., Montessuit, S., Veuthey, J.L., Zamboni, N., Westermann, B., Kunji, E.R., and Martinou, J.C. (2012). Identification and functional expression of the mitochondrial pyruvate carrier. Science *337*, 93-96.

Hirst, J. (2013). Mitochondrial complex I. Annu Rev Biochem *82*, 551-575.

Hirst, J., Kunji, E.R.S., and Walker, J.E. (2019). Comment on "Protein assemblies ejected directly from native membranes yield complexes for mass spectrometry". Science *366*.

Ho, S.N., Hunt, H.D., Horton, R.M., Pullen, J.K., and Pease, L.R. (1989). Site-directed mutagenesis by overlap extension using the polymerase chain reaction. Gene *77*, 51-59.

Hofmann, S., Januliene, D., Mehdipour, A.R., Thomas, C., Stefan, E., Bruchert, S., Kuhn, B.T., Geertsma, E.R., Hummer, G., Tampe, R., and Moeller, A. (2019). Conformation space of a heterodimeric ABC exporter under turnover conditions. Nature *571*, 580-583.

Horvath, S.E., and Daum, G. (2013). Lipids of mitochondria. Prog Lipid Res *52*, 590-614.

Iacobazzi, V., Palmieri, F., Runswick, M.J., and Walker, J.E. (1992). Sequences of the human and bovine genes for the mitochondrial 2-oxoglutarate carrier. DNA Seq *3*, 79-88.

Indiveri, C., Tonazzi, A., and Palmieri, F. (1990). Identification and purification of the carnitine carrier from rat liver mitochondria. Biochim Biophys Acta *1020*, 81-86.

Iwata, S., Lee, J.W., Okada, K., Lee, J.K., Iwata, M., Rasmussen, B., Link, T.A., Ramaswamy, S., and Jap, B.K. (1998). Complete structure of the 11-subunit bovine mitochondrial cytochrome bc1 complex. Science *281*, 64-71.

Jabalameli, M.R., Fitzpatrick, F.M., Colombo, R., Howles, S.A., Leggatt, G., Walker, V., Wiberg, A., Kunji, E.R.S., and Ennis, S. (2021). Exome sequencing identifies a disease variant of the mitochondrial ATP-Mg/Pi carrier SLC25A25 in two families with kidney stones. Mol Genet Genomic Med, e1749.

Jaiquel Baron, S., King, M.S., Kunji, E.R.S., and Schirris, T.J.J. (2021). Characterization of drug-induced human mitochondrial ADP/ATP carrier inhibition. Theranostics *11*, 5077-5091.

Johnson, R.N., and Chappell, J.B. (1973). The transport of inorganic phosphate by the mitochondrial dicarboxylate carrier. Biochem J *134*, 769-774.

Kaplan, R.S., Mayor, J.A., Johnston, N., and Oliveira, D.L. (1990). Purification and characterization of the reconstitutively active tricarboxylate transporter from rat liver mitochondria. J Biol Chem *265*, 13379-13385.

Kaukonen, J., Juselius, J.K., Tiranti, V., Kyttala, A., Zeviani, M., Comi, G.P., Keranen, S., Peltonen, L., and Suomalainen, A. (2000). Role of adenine nucleotide translocator 1 in mtDNA maintenance. Science *289*, 782-785.

Kedrov, A., Hellawell, A.M., Klosin, A., Broadhurst, R.B., Kunji, E.R., and Muller, D.J. (2010). Probing the interactions of carboxy-atractyloside and atractyloside with the yeast mitochondrial ADP/ATP carrier. Structure *18*, 39-46.

Khan, S., Ansar, M., Khan, A.K., Shah, K., Muhammad, N., Shahzad, S., Nickerson, D.A., Bamshad, M.J., Santos-Cortez, R.L.P., Leal, S.M., and Ahmad, W. (2018). A homozygous missense mutation in SLC25A16 associated with autosomal recessive isolated fingernail dysplasia in a Pakistani family. Br J Dermatol *178*, 556-558.

King, M.S., Boes, C., and Kunji, E.R. (2015). Membrane protein expression in Lactococcus lactis. Methods Enzymol *556*, 77-97.

King, M.S., Kerr, M., Crichton, P.G., Springett, R., and Kunji, E.R.S. (2016). Formation of a cytoplasmic salt bridge network in the matrix state is a fundamental step in the transport mechanism of the mitochondrial ADP/ATP carrier. Biochim Biophys Acta *1857*, 14-22.

King, M.S., Tavoulari, S., Mavridou, V., King, A.C., Mifsud, J., and Kunji, E.R.S. (2020). A single cysteine residue in the translocation pathway of the mitosomal ADP/ATP carrier from *Cryptosporidium parvum* confers a broad nucleotide specificity. Int J Mol Sci *21*.

King, M.S., Thompson, K., Hopton, S., He, L., Kunji, E.R.S., Taylor, R.W., and Ortiz-Gonzalez, X.R. (2018). Expanding the phenotype of de novo SLC25A4-linked mitochondrial disease to include mild myopathy. Neurol Genet *4*, e256.

Klingenberg, M. (1989). Molecular aspects of the adenine nucleotide carrier from mitochondria. Arch Biochem Biophys *270*, 1-14.

Klingenberg, M. (2005). Ligand-protein interaction in biomembrane carriers. The induced transition fit of transport catalysis. Biochemistry *44*, 8563-8570.

Klingenberg, M. (2007). Transport viewed as a catalytic process. Biochimie *89*, 1042-1048.

Klingenberg, M. (2008). The ADP and ATP transport in mitochondria and its carrier. Biochim Biophys Acta *1778*, 1978-2021.

Klingenberg, M. (2009). Cardiolipin and mitochondrial carriers. Biochim Biophys Acta *1788*, 2048-2058.

Klingenberg, M., and Buchholz, M. (1973). On the mechanism of bongkrekate effect on the mitochondrial adenine-nucleotide carrier as studied through the binding of ADP. Eur J Biochem *38*, 346-358.

Klingenberg, M., and Nelson, D.R. (1994). Structure-function relationships of the ADP/ATP carrier. Biochim Biophys Acta *1187*, 241-244.

Kokoszka, J.E., Waymire, K.G., Levy, S.E., Sligh, J.E., Cai, J., Jones, D.P., MacGregor, G.R., and Wallace, D.C. (2004). The ADP/ATP translocator is not essential for the mitochondrial permeability transition pore. Nature *427*, 461-465.

Kolarov, J., Kolarova, N., and Nelson, N. (1990). A third ADP/ATP translocator gene in yeast. J Biol Chem *265*, 12711-12716.

Kory, N., Uit de Bos, J., van der Rijt, S., Jankovic, N., Gura, M., Arp, N., Pena, I.A., Prakash, G., Chan, S.H., Kunchok, T., et al. (2020). MCART1/SLC25A51 is required for mitochondrial NAD transport. Sci Adv *6*.

Kory, N., Wyant, G.A., Prakash, G., Uit de Bos, J., Bottanelli, F., Pacold, M.E., Chan, S.H., Lewis, C.A., Wang, T., Keys, H.R., et al. (2018). SFXN1 is a mitochondrial serine transporter required for one-carbon metabolism. Science *362*.

Kramer, R., and Klingenberg, M. (1982). Electrophoretic control of reconstituted adenine nucleotide translocation. Biochemistry *21*, 1082-1089.

Ku, D.H., Kagan, J., Chen, S.T., Chang, C.D., Baserga, R., and Wurzel, J. (1990). The human fibroblast adenine nucleotide translocator gene. Molecular cloning and sequence. J Biol Chem *265*, 16060-16063.

Kumar, S., Tsai, C.J., and Nussinov, R. (2000). Factors enhancing protein thermostability. Protein Eng *13*, 179-191.

Kunji, E.R., Aleksandrova, A., King, M.S., Majd, H., Ashton, V.L., Cerson, E., Springett, R., Kibalchenko, M., Tavoulari, S., Crichton, P.G., and Ruprecht, J.J. (2016). The transport mechanism of the mitochondrial ADP/ATP carrier. Biochim Biophys Acta *1863*, 2379-2393.

Kunji, E.R., Chan, K.W., Slotboom, D.J., Floyd, S., O'Connor, R., and Monné, M. (2005). Eukaryotic membrane protein overproduction in Lactococcus lactis. Curr Opin Biotechnol *16*, 546-551.

Kunji, E.R., and Crichton, P.G. (2010). Mitochondrial carriers function as monomers. Biochim Biophys Acta *1797*, 817-831.

Kunji, E.R., and Harding, M. (2003). Projection structure of the atractyloside-inhibited mitochondrial ADP/ATP carrier of *Saccharomyces cerevisiae*. J Biol Chem *278*, 36985-36988.

Kunji, E.R., Harding, M., Butler, P.J., and Akamine, P. (2008). Determination of the molecular mass and dimensions of membrane proteins by size exclusion chromatography. Methods *46*, 62-72.

Kunji, E.R., and Robinson, A.J. (2006). The conserved substrate binding site of mitochondrial carriers. Biochim Biophys Acta *1757*, 1237-1248.

Kunji, E.R., Slotboom, D.J., and Poolman, B. (2003). Lactococcus lactis as host for overproduction of functional membrane proteins. Biochim Biophys Acta *1610*, 97-108.

Kunji, E.R.S., King, M.S., Ruprecht, J.J., and Thangaratnarajah, C. (2020). The SLC25 carrier family: important transport proteins in mitochondrial physiology and pathology. Physiology (Bethesda) *35*, 302-327.

Kunji, E.R.S., and Ruprecht, J.J. (2020). The mitochondrial ADP/ATP carrier exists and functions as a monomer. Biochem Soc Trans *48*, 1419-1432.

Lawson, J.E., and Douglas, M.G. (1988). Separate genes encode functionally equivalent ADP/ATP carrier proteins in *Saccharomyces cerevisiae*. Isolation and analysis of AAC2. J Biol Chem *263*, 14812-14818.

Lawson, J.E., Gawaz, M., Klingenberg, M., and Douglas, M.G. (1990). Structure-function studies of adenine nucleotide transport in mitochondria. I. Construction and

genetic analysis of yeast mutants encoding the ADP/ATP carrier protein of mitochondria. J Biol Chem *265*, 14195-14201.

Lee, Y., Willers, C., Kunji, E.R., and Crichton, P.G. (2015). Uncoupling protein 1 binds one nucleotide per monomer and is stabilized by tightly bound cardiolipin. Proc Natl Acad Sci U S A *112*, 6973-6978.

Lill, R. (2009). Function and biogenesis of iron-sulphur proteins. Nature *460*, 831-838.

Lindhurst, M.J., Fiermonte, G., Song, S., Struys, E., De Leonardis, F., Schwartzberg, P.L., Chen, A., Castegna, A., Verhoeven, N., Mathews, C.K., et al. (2006). Knockout of Slc25a19 causes mitochondrial thiamine pyrophosphate depletion, embryonic lethality, CNS malformations, and anemia. Proc Natl Acad Sci U S A *103*, 15927-15932.

Lucas, X., Bauza, A., Frontera, A., and Quinonero, D. (2016). A thorough anion-pi interaction study in biomolecules: on the importance of cooperativity effects. Chem Sci *7*, 1038-1050.

Luciani, S., Martini, N., and Santi, R. (1971). Effects of carboxyatractyloside a structural analogue of atractyloside on mitochondrial oxidative phosphorylation. Life Sci II *10*, 961-968.

Lunetti, P., Damiano, F., De Benedetto, G., Siculella, L., Pennetta, A., Muto, L., Paradies, E., Marobbio, C.M., Dolce, V., and Capobianco, L. (2016). Characterization of Human and Yeast Mitochondrial Glycine Carriers with Implications for Heme Biosynthesis and Anemia. J Biol Chem *291*, 19746-19759.

Lunetti, P., Gorgoglione, R., Curcio, R., Marra, F., Pignataro, A., Vozza, A., Riley, C.L., Capobianco, L., Palmieri, L., Dolce, V., and Fiermonte, G. (2022). Drosophila melanogaster Uncoupling Protein-4A (UCP4A) Catalyzes a Unidirectional Transport of Aspartate. Int J Mol Sci *23*.

Luongo, T.S., Eller, J.M., Lu, M.J., Niere, M., Raith, F., Perry, C., Bornstein, M.R., Oliphint, P., Wang, L., McReynolds, M.R., et al. (2020). SLC25A51 is a mammalian mitochondrial NAD(+) transporter. Nature *588*, 174-179.

Madeira, F., Park, Y.M., Lee, J., Buso, N., Gur, T., Madhusoodanan, N., Basutkar, P., Tivey, A.R.N., Potter, S.C., Finn, R.D., and Lopez, R. (2019). The EMBL-EBI search and sequence analysis tools APIs in 2019. Nucleic Acids Res *47*, W636-W641.

Majd, H., King, M.S., Palmer, S.M., Smith, A.C., Elbourne, L.D., Paulsen, I.T., Sharples, D., Henderson, P.J., and Kunji, E.R. (2018a). Screening of candidate substrates and coupling ions of transporters by thermostability shift assays. Elife *7*.

Majd, H., King, M.S., Smith, A.C., and Kunji, E.R.S. (2018b). Pathogenic mutations of the human mitochondrial citrate carrier SLC25A1 lead to impaired citrate export

required for lipid, dolichol, ubiquinone and sterol synthesis. Biochim Biophys Acta Bioenerg *1859*, 1-7.

Majima, E., Yamaguchi, N., Chuman, H., Shinohara, Y., Ishida, M., Goto, S., and Terada, H. (1998). Binding of the fluorescein derivative eosin Y to the mitochondrial ADP/ATP carrier: characterization of the adenine nucleotide binding site. Biochemistry *37*, 424-432.

Makiuchi, T., and Nozaki, T. (2014). Highly divergent mitochondrion-related organelles in anaerobic parasitic protozoa. Biochimie *100*, 3-17.

Martensson, C.U., Doan, K.N., and Becker, T. (2017). Effects of lipids on mitochondrial functions. Biochim Biophys Acta Mol Cell Biol Lipids *1862*, 102-113.

Mayinger, P., Winkler, E., and Klingenberg, M. (1989). The ADP/ATP carrier from yeast (AAC-2) is uniquely suited for the assignment of the binding center by photoaffinity labeling. FEBS Lett *244*, 421-426.

Mehmood, S., Allison, T.M., and Robinson, C.V. (2015). Mass spectrometry of protein complexes: from origins to applications. Annu Rev Phys Chem *66*, 453-474.

Mejia, E.M., and Hatch, G.M. (2016). Mitochondrial phospholipids: role in mitochondrial function. J Bioenerg Biomembr *48*, 99-112.

Mierau, I., and Kleerebezem, M. (2005). 10 years of the nisin-controlled gene expression system (NICE) in Lactococcus lactis. Appl Microbiol Biotechnol *68*, 705-717.

Mifsud, J., Ravaud, S., Krammer, E.M., Chipot, C., Kunji, E.R., Pebay-Peyroula, E., and Dehez, F. (2013). The substrate specificity of the human ADP/ATP carrier AAC1. Mol Membr Biol *30*, 160-168.

Miljus, T., Sykes, D.A., Harwood, C.R., Vuckovic, Z., and Veprintsev, D.B. (2020). GPCR solubilization and quality control. Methods Mol Biol *2127*, 105-127.

Mishra, P., Singh, U., Pandey, C.M., Mishra, P., and Pandey, G. (2019). Application of student's t-test, analysis of variance, and covariance. Ann Card Anaesth *22*, 407-411.

Mitchell, P. (1961). Coupling of phosphorylation to electron and hydrogen transfer by a chemi-osmotic type of mechanism. Nature *191*, 144-148.

Monné, M., Chan, K.W., Slotboom, D.J., and Kunji, E.R. (2005). Functional expression of eukaryotic membrane proteins in *Lactococcus lactis*. Protein Sci *14*, 3048-3056.

Monné, M., Miniero, D.V., Daddabbo, L., Robinson, A.J., Kunji, E.R., and Palmieri, F. (2012). Substrate specificity of the two mitochondrial ornithine carriers can be swapped by single mutation in substrate binding site. J Biol Chem *287*, 7925-7934.

Mracek, T., Drahota, Z., and Houstek, J. (2013). The function and the role of the mitochondrial glycerol-3-phosphate dehydrogenase in mammalian tissues. Biochim Biophys Acta *1827*, 401-410.

Muller, M., Mentel, M., van Hellemond, J.J., Henze, K., Woehle, C., Gould, S.B., Yu, R.Y., van der Giezen, M., Tielens, A.G., and Martin, W.F. (2012). Biochemistry and evolution of anaerobic energy metabolism in eukaryotes. Microbiol Mol Biol Rev *76*, 444-495.

Müller, V., Basset, G., Nelson, D.R., and Klingenberg, M. (1996). Probing the role of positive residues in the ADP/ATP carrier from yeast. The effect of six arginine mutations of oxidative phosphorylation and AAC expression. Biochemistry *35*, 16132-16143.

Neckelmann, N., Li, K., Wade, R.P., Shuster, R., and Wallace, D.C. (1987). cDNA sequence of a human skeletal muscle ADP/ATP translocator: lack of a leader peptide, divergence from a fibroblast translocator cDNA, and coevolution with mitochondrial DNA genes. Proc Natl Acad Sci U S A *84*, 7580-7584.

Nelson, D.R., Felix, C.M., and Swanson, J.M. (1998). Highly conserved charge-pair networks in the mitochondrial carrier family. J Mol Biol *277*, 285-308.

Nelson, D.R., Lawson, J.E., Klingenberg, M., and Douglas, M.G. (1993). Site-directed mutagenesis of the yeast mitochondrial ADP/ATP translocator. Six arginines and one lysine are essential. J Mol Biol *230*, 1159-1170.

Neumann, J., Rose-Sperling, D., and Hellmich, U.A. (2017). Diverse relations between ABC transporters and lipids: An overview. Biochim Biophys Acta Biomembr *1859*, 605-618.

Niesen, F.H., Berglund, H., and Vedadi, M. (2007). The use of differential scanning fluorimetry to detect ligand interactions that promote protein stability. Nat Protoc *2*, 2212-2221.

Nury, H., Dahout-Gonzalez, C., Trezeguet, V., Lauquin, G., Brandolin, G., and Pebay-Peyroula, E. (2005). Structural basis for lipid-mediated interactions between mitochondrial ADP/ATP carrier monomers. FEBS Lett *579*, 6031-6036.

Nury, H., Dahout-Gonzalez, C., Trézéguet, V., Lauquin, G.J., Brandolin, G., and Pebay-Peyroula, E. (2006). Relations between structure and function of the mitochondrial ADP/ATP carrier. Annu Rev Biochem *75*, 713-741.

O'Malley, K., Pratt, P., Robertson, J., Lilly, M., and Douglas, M.G. (1982). Selection of the nuclear gene for the mitochondrial adenine nucleotide translocator by genetic complementation of the op1 mutation in yeast. J Biol Chem *257*, 2097-2103.

Palmieri, F. (1994). Mitochondrial carrier proteins. FEBS Lett *346*, 48-54.

Palmieri, F., and Monne, M. (2016). Discoveries, metabolic roles and diseases of mitochondrial carriers: A review. Biochim Biophys Acta *1863*, 2362-2378.

Palmieri, F., Scarcia, P., and Monné, M. (2020). Diseases caused by mutations in mitochondrial carrier genes. Biomolecules *10*.

Palmieri, L., Alberio, S., Pisano, I., Lodi, T., Meznaric-Petrusa, M., Zidar, J., Santoro, A., Scarcia, P., Fontanesi, F., Lamantea, E., et al. (2005). Complete loss-of-function of the heart/muscle-specific adenine nucleotide translocator is associated with mitochondrial myopathy and cardiomyopathy. Hum Mol Genet *14*, 3079-3088.

Palmieri, L., Pardo, B., Lasorsa, F.M., del Arco, A., Kobayashi, K., Iijima, M., Runswick, M.J., Walker, J.E., Saheki, T., Satrustegui, J., and Palmieri, F. (2001). Citrin and aralar1 are Ca(2+)-stimulated aspartate/glutamate transporters in mitochondria. EMBO J *20*, 5060-5069.

Panja, A.S., Bandopadhyay, B., and Maiti, S. (2015). Protein Thermostability Is Owing to Their Preferences to Non-Polar Smaller Volume Amino Acids, Variations in Residual Physico-Chemical Properties and More Salt-Bridges. PLoS One *10*, e0131495.

Patching, S.G. (2014). Surface plasmon resonance spectroscopy for characterisation of membrane protein-ligand interactions and its potential for drug discovery. Biochim Biophys Acta *1838*, 43-55.

Paumard, P., Vaillier, J., Coulary, B., Schaeffer, J., Soubannier, V., Mueller, D.M., Brethes, D., di Rago, J.P., and Velours, J. (2002). The ATP synthase is involved in generating mitochondrial cristae morphology. EMBO J *21*, 221-230.

Pebay-Peyroula, E., Dahout-Gonzalez, C., Kahn, R., Trézéguet, V., Lauquin, G.J., and Brandolin, G. (2003). Structure of mitochondrial ADP/ATP carrier in complex with carboxyatractyloside. Nature *426*, 39-44.

Pfaff, E., Heldt, H.W., and Klingenberg, M. (1969). Adenine nucleotide translocation of mitochondria. Kinetics of the adenine nucleotide exchange. Eur J Biochem *10*, 484-493.

Pfaff, E., and Klingenberg, M. (1968). Adenine nucleotide translocation of mitochondria. 1. Specificity and control. Eur J Biochem *6*, 66-79.

Pietropaolo, A., Pierri, C.L., Palmieri, F., and Klingenberg, M. (2016). The switching mechanism of the mitochondrial ADP/ATP carrier explored by free-energy landscapes. Biochim Biophys Acta *1857*, 772-781.

Porcelli, V., Fiermonte, G., Longo, A., and Palmieri, F. (2014). The human gene SLC25A29, of solute carrier family 25, encodes a mitochondrial transporter of basic amino acids. J Biol Chem *289*, 13374-13384.

Putignani, L., Tait, A., Smith, H.V., Horner, D., Tovar, J., Tetley, L., and Wastling, J.M. (2004). Characterization of a mitochondrion-like organelle in *Cryptosporidium parvum*. Parasitology *129*, 1-18.

Quick, M., and Javitch, J.A. (2007). Monitoring the function of membrane transport proteins in detergent-solubilized form. Proc Natl Acad Sci U S A *104*, 3603-3608.

Raho, S., Capobianco, L., Malivindi, R., Vozza, A., Piazzolla, C., De Leonardis, F., Gorgoglione, R., Scarcia, P., Pezzuto, F., Agrimi, G., et al. (2020). KRAS-regulated glutamine metabolism requires UCP2-mediated aspartate transport to support pancreatic cancer growth. Nat Metab *2*, 1373-1381.

Rajarathnam, K., and Rosgen, J. (2014). Isothermal titration calorimetry of membrane proteins - progress and challenges. Biochim Biophys Acta *1838*, 69-77.

Ralser, M., Kuhl, H., Ralser, M., Werber, M., Lehrach, H., Breitenbach, M., and Timmermann, B. (2012). The *Saccharomyces cerevisiae* W303-K6001 cross-platform genome sequence: insights into ancestry and physiology of a laboratory mutt. Open Biol *2*, 120093.

Rees, D.M., Leslie, A.G., and Walker, J.E. (2009). The structure of the membrane extrinsic region of bovine ATP synthase. Proc Natl Acad Sci U S A *106*, 21597-21601.

Rial, E., Poustie, A., and Nicholls, D.G. (1983). Brown-adipose-tissue mitochondria: the regulation of the 32000-Mr uncoupling protein by fatty acids and purine nucleotides. Eur J Biochem *137*, 197-203.

Riccio, P., Aquila, H., and Klingenberg, M. (1975). Purification of the carboxy-atractylate binding protein from mitochondria. FEBS Lett *56*, 133-138.

Robinson, A.J., and Kunji, E.R. (2006). Mitochondrial carriers in the cytoplasmic state have a common substrate binding site. Proc Natl Acad Sci U S A *103*, 2617-2622.

Robinson, A.J., Overy, C., and Kunji, E.R. (2008). The mechanism of transport by mitochondrial carriers based on analysis of symmetry. Proc Natl Acad Sci U S A *105*, 17766-17771.

Roger, A.J., Munoz-Gomez, S.A., and Kamikawa, R. (2017). The Origin and Diversification of Mitochondria. Curr Biol *27*, R1177-R1192.

Runswick, M.J., Powell, S.J., Nyren, P., and Walker, J.E. (1987). Sequence of the bovine mitochondrial phosphate carrier protein: structural relationship to ADP/ATP translocase and the brown fat mitochondria uncoupling protein. EMBO J *6*, 1367-1373.

Ruprecht, J.J., Hellawell, A.M., Harding, M., Crichton, P.G., McCoy, A.J., and Kunji, E.R. (2014). Structures of yeast mitochondrial ADP/ATP carriers support a domain-based alternating-access transport mechanism. Proc Natl Acad Sci U S A *111*, E426-434.

Ruprecht, J.J., King, M.S., Zögg, T., Aleksandrova, A.A., Pardon, E., Crichton, P.G., Steyaert, J., and Kunji, E.R.S. (2019). The molecular mechanism of transport by the mitochondrial ADP/ATP carrier. Cell *176*, 435-447.e415.

Ruprecht, J.J., and Kunji, E.R. (2019). Structural changes in the transport cycle of the mitochondrial ADP/ATP carrier. Curr Opin Struct Biol *57*, 135-144.

Ruprecht, J.J., and Kunji, E.R.S. (2020). The SLC25 mitochondrial carrier family: structure and mechanism. Trends Biochem Sci *45*, 244-258.

Ruprecht, J.J., and Kunji, E.R.S. (2021). Structural mechanism of transport of mitochondrial carriers. Annu Rev Biochem.

Sadeghi, M., Naderi-Manesh, H., Zarrabi, M., and Ranjbar, B. (2006). Effective factors in thermostability of thermophilic proteins. Biophys Chem *119*, 256-270.

Saraste, M., and Walker, J.E. (1982). Internal sequence repeats and the path of polypeptide in mitochondrial ADP/ATP translocase. FEBS Lett *144*, 250-254.

Savioli, L., Smith, H., and Thompson, A. (2006). Giardia and Cryptosporidium join the 'Neglected Diseases Initiative'. Trends Parasitol *22*, 203-208.

Schaedler, T.A., Faust, B., Shintre, C.A., Carpenter, E.P., Srinivasan, V., van Veen, H.W., and Balk, J. (2015). Structures and functions of mitochondrial ABC transporters. Biochem Soc Trans *43*, 943-951.

Schenkel, L.C., and Bakovic, M. (2014). Formation and regulation of mitochondrial membranes. Int J Cell Biol *2014*, 709828.

Seeber, F., Limenitakis, J., and Soldati-Favre, D. (2008). Apicomplexan mitochondrial metabolism: a story of gains, losses and retentions. Trends Parasitol *24*, 468-478.

Shaw, G.C., Cope, J.J., Li, L., Corson, K., Hersey, C., Ackermann, G.E., Gwynn, B., Lambert, A.J., Wingert, R.A., Traver, D., et al. (2006). Mitoferrin is essential for erythroid iron assimilation. Nature *440*, 96-100.

Shi, X., Reinstadler, B., Shah, H., To, T.-L., Byrne, K., Summer, L., Calvo, S.E., Goldberger, O., Doench, J.G., Mootha, V.K., and Shen, H. (2021). Combinatorial G x G x E CRISPR screening and functional analysis highlights SLC25A39 in mitochondrial GSH transport. bioRxiv, 2021.2009.2022.461361.

Smith, V.R., Fearnley, I.M., and Walker, J.E. (2003). Altered chromatographic behaviour of mitochondrial ADP/ATP translocase induced by stabilization of the protein by binding of 6'-O-fluorescein-atractyloside. Biochem J *376*, 757-763.

Sousa, J.S., D'Imprima, E., and Vonck, J. (2018). Mitochondrial Respiratory Chain Complexes. Subcell Biochem *87*, 167-227.

Spaan, A.N., Ijlst, L., van Roermund, C.W., Wijburg, F.A., Wanders, R.J., and Waterham, H.R. (2005). Identification of the human mitochondrial FAD transporter and its potential role in multiple acyl-CoA dehydrogenase deficiency. Mol Genet Metab *86*, 441-447.

Sperka-Gottlieb, C.D., Hermetter, A., Paltauf, F., and Daum, G. (1988). Lipid topology and physical properties of the outer mitochondrial membrane of the yeast, *Saccharomyces cerevisiae*. Biochim Biophys Acta *946*, 227-234.

Spikes, T.E., Montgomery, M.G., and Walker, J.E. (2020). Structure of the dimeric ATP synthase from bovine mitochondria. Proc Natl Acad Sci U S A *117*, 23519-23526.

Spikes, T.E., Montgomery, M.G., and Walker, J.E. (2021). Interface mobility between monomers in dimeric bovine ATP synthase participates in the ultrastructure of inner mitochondrial membranes. Proc Natl Acad Sci U S A *118*.

Springett, R., King, M.S., Crichton, P.G., and Kunji, E.R.S. (2017). Modelling the free energy profile of the mitochondrial ADP/ATP carrier. Biochim Biophys Acta Bioenerg *1858*, 906-914.

Sun, F., Huo, X., Zhai, Y., Wang, A., Xu, J., Su, D., Bartlam, M., and Rao, Z. (2005). Crystal structure of mitochondrial respiratory membrane protein complex II. Cell *121*, 1043-1057.

Tamura, K., and Hayashi, S. (2017). Atomistic modeling of alternating access of a mitochondrial ADP/ATP membrane transporter with molecular simulations. PLoS One *12*, e0181489.

Tavoulari, S., Thangaratnarajah, C., Mavridou, V., Harbour, M.E., Martinou, J.C., and Kunji, E.R. (2019). The yeast mitochondrial pyruvate carrier is a hetero-dimer in its functional state. EMBO J *38*.

Thangaratnarajah, C. (2014). The structural and functional characterisation of the mitochondrial aspartate-glutamate carriers. Doctor of Philosophy (University of Cambridge).

Thangaratnarajah, C., Ruprecht, J.J., and Kunji, E.R. (2014). Calcium-induced conformational changes of the regulatory domain of human mitochondrial aspartate/glutamate carriers. Nat Commun *5*, 5491.

Thompson, K., Majd, H., Dallabona, C., Reinson, K., King, M.S., Alston, C.L., He, L., Lodi, T., Jones, S.A., Fattal-Valevski, A., et al. (2016). Recurrent *de novo* dominant mutations in SLC25A4 cause severe early-onset mitochondrial disease and loss of mitochondrial DNA copy number. Am J Hum Genet *99*, 860-876.

Titus, S.A., and Moran, R.G. (2000). Retrovirally mediated complementation of the glyB phenotype. Cloning of a human gene encoding the carrier for entry of folates into mitochondria. J Biol Chem *275*, 36811-36817.

Traba, J., Satrustegui, J., and del Arco, A. (2009). Characterization of SCaMC-3-like/slc25a41, a novel calcium-independent mitochondrial ATP-Mg/Pi carrier. Biochem J *418*, 125-133.

Tsaousis, A.D., Kunji, E.R., Goldberg, A.V., Lucocq, J.M., Hirt, R.P., and Embley, T.M. (2008). A novel route for ATP acquisition by the remnant mitochondria of Encephalitozoon cuniculi. Nature *453*, 553-556.

Tsukihara, T., Aoyama, H., Yamashita, E., Tomizaki, T., Yamaguchi, H., Shinzawa-Itoh, K., Nakashima, R., Yaono, R., and Yoshikawa, S. (1995). Structures of metal sites of oxidized bovine heart cytochrome c oxidase at 2.8 A. Science *269*, 1069-1074.

van der Giezen, M., Slotboom, D.J., Horner, D.S., Dyal, P.L., Harding, M., Xue, G.P., Embley, T.M., and Kunji, E.R. (2002). Conserved properties of hydrogenosomal and mitochondrial ADP/ATP carriers: a common origin for both organelles. EMBO J *21*, 572-579.

Vignais, P.V., Vignais, P.M., and Defaye, G. (1971). Gummiferin, an inhibitor of the adenine-nucleotide translocation. Study of its binding properties to mitochondria. FEBS Lett *17*, 281-288.

Visser, W., van der Baan, A.A., Batenburg-van der Vegte, W., Scheffers, W.A., Krämer, R., and van Dijken, J.P. (1994). Involvement of mitochondria in the assimilatory metabolism of anaerobic *Saccharomyces cerevisiae* cultures. Microbiology *140 (Pt 11)*, 3039-3046.

Visser, W.F., van Roermund, C.W., Waterham, H.R., and Wanders, R.J. (2002). Identification of human PMP34 as a peroxisomal ATP transporter. Biochem Biophys Res Commun *299*, 494-497.

von Renesse, A., Morales-Gonzalez, S., Gill, E., Salomons, G.S., Stenzel, W., and Schuelke, M. (2019). Muscle Weakness, Cardiomyopathy, and L-2-Hydroxyglutaric Aciduria Associated with a Novel Recessive SLC25A4 Mutation. JIMD Rep *43*, 27-35.

Wagner, C.R., and Benkovic, S.J. (1990). Site directed mutagenesis: a tool for enzyme mechanism dissection. Trends Biotechnol *8*, 263-270.

Walker, J.E. (1998). ATP Synthesis by Rotary Catalysis (Nobel lecture). Angew Chem Int Ed Engl *37*, 2308-2319.

Walker, J.E. (2013). The ATP synthase: the understood, the uncertain and the unknown. Biochem Soc Trans *41*, 1-16.

Walse, B., Dufe, V.T., Svensson, B., Fritzson, I., Dahlberg, L., Khairoullina, A., Wellmar, U., and Al-Karadaghi, S. (2008). The structures of human dihydroorotate dehydrogenase with and without inhibitor reveal conformational flexibility in the inhibitor and substrate binding sites. Biochemistry *47*, 8929-8936.

Wang, Y., and Tajkhorshid, E. (2008). Electrostatic funneling of substrate in mitochondrial inner membrane carriers. Proc Natl Acad Sci U S A *105*, 9598-9603.

Wang, Y., Yen, F.S., Zhu, X.G., Timson, R.C., Weber, R., Xing, C., Liu, Y., Allwein, B., Luo, H., Yeh, H.W., et al. (2021). SLC25A39 is necessary for mitochondrial glutathione import in mammalian cells. Nature *599*, 136-140.

Watmough, N.J., and Frerman, F.E. (2010). The electron transfer flavoprotein: ubiquinone oxidoreductases. Biochim Biophys Acta *1797*, 1910-1916.

Watt, I.N., Montgomery, M.G., Runswick, M.J., Leslie, A.G., and Walker, J.E. (2010). Bioenergetic cost of making an adenosine triphosphate molecule in animal mitochondria. Proc Natl Acad Sci U S A *107*, 16823-16827.

Watzke, N., Diekert, K., and Obrdlik, P. (2010). Electrophysiology of respiratory chain complexes and the ADP-ATP exchanger in native mitochondrial membranes. Biochemistry *49*, 10308-10318.

Wienken, C.J., Baaske, P., Rothbauer, U., Braun, D., and Duhr, S. (2010). Protein-binding assays in biological liquids using microscale thermophoresis. Nat Commun *1*, 100.

Wikstrom, M.K. (1977). Proton pump coupled to cytochrome c oxidase in mitochondria. Nature *266*, 271-273.

Wongkittichote, P., Tungpradabkul, S., Wattanasirichaigoon, D., and Jensen, L.T. (2013). Prediction of the functional effect of novel SLC25A13 variants using a *S. cerevisiae* model of AGC2 deficiency. J Inherit Metab Dis *36*, 821-830.

Xia, D., Esser, L., Tang, W.K., Zhou, F., Zhou, Y., Yu, L., and Yu, C.A. (2013). Structural analysis of cytochrome bc1 complexes: implications to the mechanism of function. Biochim Biophys Acta *1827*, 1278-1294.

Yao, S., Yi, Q., Ma, B., Mao, X., Chen, Y., Guan, M.X., and Cang, X. (2021). Structural basis of substrate recognition by the mitochondrial ADP/ATP transporter. bioRxiv.

Yi, Q., Li, Q., Yao, S., Chen, Y., Guan, M.X., and Cang, X. (2019). Molecular dynamics simulations on apo ADP/ATP carrier shed new lights on the featured motif of the mitochondrial carriers. Mitochondrion *47*, 94-102.

Yoneshiro, T., Wang, Q., Tajima, K., Matsushita, M., Maki, H., Igarashi, K., Dai, Z., White, P.J., McGarrah, R.W., Ilkayeva, O.R., et al. (2019). BCAA catabolism in brown fat controls energy homeostasis through SLC25A44. Nature.

Zaltsman, Y., Shachnai, L., Yivgi-Ohana, N., Schwarz, M., Maryanovich, M., Houtkooper, R.H., Vaz, F.M., De Leonardis, F., Fiermonte, G., Palmieri, F., et al. (2010). MTCH2/MIMP is a major facilitator of tBID recruitment to mitochondria. Nat Cell Biol *12*, 553-562.

Zarrilli, R., Oates, E.L., McBride, O.W., Lerman, M.I., Chan, J.Y., Santisteban, P., Ursini, M.V., Notkins, A.L., and Kohn, L.D. (1989). Sequence and chromosomal assignment of a novel cDNA identified by immunoscreening of a thyroid expression library: similarity to a family of mitochondrial solute carrier proteins. Mol Endocrinol *3*, 1498-1505.

Zeman, I., Schwimmer, C., Postis, V., Brandolin, G., David, C., Trézéguet, V., and Lauquin, G.J. (2003). Four mutations in transmembrane domains of the mitochondrial ADP/ATP carrier increase resistance to bongkrekic acid. J Bioenerg Biomembr *35*, 243-256.

Zhang, J., Frerman, F.E., and Kim, J.J. (2006). Structure of electron transfer flavoprotein-ubiquinone oxidoreductase and electron transfer to the mitochondrial ubiquinone pool. Proc Natl Acad Sci U S A *103*, 16212-16217.

Zhou, A., Rohou, A., Schep, D.G., Bason, J.V., Montgomery, M.G., Walker, J.E., Grigorieff, N., and Rubinstein, J.L. (2015). Structure and conformational states of the bovine mitochondrial ATP synthase by cryo-EM. Elife *4*, e10180.

Zhu, J., Vinothkumar, K.R., and Hirst, J. (2016). Structure of mammalian respiratory complex I. Nature *536*, 354-358.